ACOUSTIC TRANSDUCTION – MATERIALS AND DEVICES

Period 31 July 1996 to 31 December 1997

Annual Report

VOLUME II

OFFICE OF NAVAL RESEARCH
Contract No: N00014-96-1-1173

APPROVED FOR PUBLIC RELEASE – DISTRIBUTION UNLIMITED

Kenji Uchino

PENNSTATE

1855

THE MATERIALS RESEARCH LABORATORY
UNIVERSITY PARK, PA

REPORT DOCUMENTATION PAGE

Form Approved
OMB No. 0704-0188

1. AGENCY USE ONLY (Leave blank)	2. REPORT DATE	3. REPORT TYPE AND DATES COVERED
	05/01/98	ANNUAL REPORT 07/31/96-12/31/97

4. TITLE AND SUBTITLE
ACOUSTIC TRANSDUCTION -- MATERIALS AND DEVICES

5. FUNDING NUMBERS
ONR CONTRACT NO:
N00014-96-1-1173

6. AUTHOR(S)
KENJI UCHINO

7. PERFORMING ORGANIZATION NAME(S) AND ADDRESS(ES)
Materials Research Laboratory
The Pennsylvania State University
University Park, PA 16802

8. PERFORMING ORGANIZATION REPORT NUMBER

9. SPONSORING/MONITORING AGENCY NAME(S) AND ADDRESS(ES)
Office of Naval Research
ONR 321SS
Ballston Centre Tower One
800 N Quincy Street
Arlington, VA 22217-5660

Office of Naval Research
Regional Office Chicago
536 S Clark Str., Rm 208
Chicago IL 60605-1588

10. SPONSORING/MONITORING AGENCY REPORT NUMBER

11. SUPPLEMENTARY NOTES

12a. DISTRIBUTION/AVAILABILITY STATEMENT

12b. DISTRIBUTION CODE

13. ABSTRACT (Maximum 200 words)

SEE FOLLOW PAGE

14. SUBJECT TERMS

15. NUMBER OF PAGES

16. PRICE CODE

17. SECURITY CLASSIFICATION OF REPORT	18. SECURITY CLASSIFICATION OF THIS PAGE	19. SECURITY CLASSIFICATION OF ABSTRACT	20. LIMITATION OF ABSTRACT

GENERAL INSTRUCTIONS FOR COMPLETING SF 298

The Report Documentation Page (RDP) is used in announcing and cataloging reports. It is important that this information be consistent with the rest of the report, particularly the cover and title page. Instructions for filling in each block of the form follow. It is important to ***stay within the lines*** to meet ***optical scanning requirements***.

Block 1. Agency Use Only *(Leave blank)*.

Block 2. Report Date. Full publication date including day, month, and year, if available (e.g. 1 Jan 88). Must cite at least the year.

Block 3. Type of Report and Dates Covered. State whether report is interim, final, etc. If applicable, enter inclusive report dates (e.g. 10 Jun 87 - 30 Jun 88).

Block 4. Title and Subtitle. A title is taken from the part of the report that provides the most meaningful and complete information. When a report is prepared in more than one volume, repeat the primary title, add volume number, and include subtitle for the specific volume. On classified documents enter the title classification in parentheses.

Block 5. Funding Numbers. To include contract and grant numbers; may include program element number(s), project number(s), task number(s), and work unit number(s). Use the following labels:

C	- Contract	PR	- Project
G	- Grant	TA	- Task
PE	- Program Element	WU	- Work Unit Accession No.

Block 6. Author(s). Name(s) of person(s) responsible for writing the report, performing the research, or credited with the content of the report. If editor or compiler, this should follow the name(s).

Block 7. Performing Organization Name(s) and Address(es). Self-explanatory

Block 8. Performing Organization Report Number. Enter the unique alphanumeric report number(s) assigned by the organization performing the report.

Block 9. Sponsoring/Monitoring Agency Name(s) and Address(es). Self-explanatory.

Block 10. Sponsoring/Monitoring Agency Report Number. *(If known)*

Block 11. Supplementary Notes. Enter information not included elsewhere such as: Prepared in cooperation with...; Trans. of...; To be published in.... When a report is revised, include a statement whether the new report supersedes or supplements the older report.

Block 12a. Distribution/Availability Statement. Denotes public availability or limitations. Cite any availability to the public. Enter additional limitations or special markings in all capitals (e.g. NOFORN, REL, ITAR).

DOD	- See DoDD 5230.24, "Distribution Statements on Technical Documents."
DOE	- See authorities.
NASA	- See Handbook NHB 2200.2.
NTIS	- Leave blank.

Block 12b. Distribution Code.

DOD	- Leave blank.
DOE	- Enter DOE distribution categories from the Standard Distribution for Unclassified Scientific and Technical Reports.
NASA	- Leave blank.
NTIS	- Leave blank.

Block 13. Abstract. Include a brief *(Maximum 200 words)* factual summary of the most significant information contained in the report.

Block 14. Subject Terms. Keywords or phrases identifying major subjects in the report.

Block 15. Number of Pages. Enter the total number of pages.

Block 16. Price Code. Enter appropriate price code *(NTIS only)*.

Blocks 17. - 19. Security Classifications. Self-explanatory. Enter U.S. Security Classification in accordance with U.S. Security Regulations (i.e., UNCLASSIFIED). If form contains classified information, stamp classification on the top and bottom of the page.

Block 20. Limitation of Abstract. This block must be completed to assign a limitation to the abstract. Enter either UL (unlimited) or SAR (same as report). An entry in this block is necessary if the abstract is to be limited. If blank, the abstract is assumed to be unlimited.

ABSTRACT

The report documents work carried out over the period 31 July 1996 to 31 December 1997 on a Multi-University Research Initiative (MURI) program under Office of Naval Research (ONR) sponsorship. The program couples transducer materials research in the Materials Research Laboratory (MRL), design and testing studies in the Applied Research Laboratory (ARL) and vibration and flow noise control in the Center for Acoustics and Vibration (CAV) at Penn State.

The overarching project objective is the development of acoustic transduction materials and devices of direct relevance to Navy needs and with application in commercial products. The initial focus of studies is upon high performance sensors and high authority high strain actuators. This objective also carries the need for new materials, new device designs, improved drive and control strategies and a continuing emphasis upon reliability under a wide range of operating conditions.

In *Material Studies*, undoubtedly major breakthroughs have occurred in the ultra-high strain relaxor ferroelectric systems. Earlier reports of unusual piezoelectric activity in single crystal perovskite relaxors have been amply confirmed in the lead zinc niobate : lead titanate, and lead magnesium niobate : lead titanate systems for compositions of rhombohedral symmetry close to the Morphotropic Phase Boundary (MPB) in these solid solutions. Analysis of the unique properties of 001 field poled rhombohedral ferroelectric crystals suggests new intrinsic mechanisms for high strain and carries the first hints of how to move from lead based compositions. A major discovery of comparable importance is a new mode of processing to convert PVDF:TrFE copolymer piezoelectric into a relaxor ferroelectric in which electrostrictive strains of 4% have been demonstrated at high fields. Both single crystal and polymer relaxors appear to offer energy densities almost order of magnitude larger than in earlier polycrystal ceramic actuators.

Transducer Studies have continued to exploit the excellent sensitivity and remarkable versatility of the cymbal type flextensional element. Initial studies of a small cymbal arrays show excellent promise in both send and receive modes, and larger arrays are now under construction for tests at ARL. New studies in constrained layer vibration damping and in flow noise reduction are yielding exciting new results.

In *Actuator Studies*, an important advance in piezoelectric generated noise control now permits wider use of acoustic emission as a reliability diagnostic technique. Joint studies with NRL, Washington have developed a completely new d_{15} driven torsional actuator and the CAV program element has designed an exciting high strain high force inchworm.

Finite element analysis continues to be an important tool for understanding the more complex composite structures and their beam forming capability in water. *Thin and Thick Thin Film Studies* are gearing up to provide the material base for micro-tonpilz arrays. New exploitation of ultra sensitive strain and permittivity measurements is providing the first reliable data of electrostriction in simple solids, and suggesting new modes for separating the polarizability contributors in dielectrics and electrostrictors.

APPENDICES

VOLUME I

GENERAL SUMMARY PAPERS

1. Ito, Y. and K. Uchino, Wiley Encyclopedia of Electrical and Electronics Engineering, J. G. Webster, Edit., (Partial Charge "Piezoelectricity"), John Wiley & Sons (1998). [in press].
2. Newnham, R.E., "Molecular Mechanisms in Smart Materials," MRS Bulletin (May 1997).
3. Swartz, S.L., T.R. Shrout, and T. Takenaka, "Electronic Ceramics R&D in the U.S., Japan, Part I: Patent History," The American Ceramic Society Bulletin **76** (8) (1997).

2.0 MATERIALS STUDIES

2.1 Polycrystal Perovskite Ceramics

4. Alberta, E.F., and A.S. Bhalla, "Piezoelectric Properties of $Pb(InNb)_{1/2}O_3$-$PbTiO_3$ Solid Solution Ceramics," J. Korean Phys. Soc. **32**, S1265-S1267 (February 1998).
5. Alberta, E.F. and A.S. Bhalla, "High Strain and Low Mechanical Quality Factor Piezoelectric $Pb[Sc_{1/2}Nb_{1/2})_{0.575}Ti_{0.425}]O_3$ Ceramics" (1997).
6. Zhang, Q.M. and J. Zhao, "Polarization Responses in Lead Magnesium Niobate Based Relaxor Ferroelectrics," Appl. Phys. Lett. **71** (12, 1649-1651 (1997).
7. Glazounov, A.E., J. Zhao, and Q.M. Zhang, "Effect of Nanopolar Regions on Electrostrictive Coefficients of a Relaxor Ferroelectric," Proceedings Williamsburg Meeting, Williamsburg, Virginia (1998).
8. Zhao, J. A.E. Glazounov, Q.M. Zhang, and B. Toby, "Neutron Diffraction Study of Electrostrictive Coefficients of Prototype Cubic Phase of Relaxor Ferroelectric $PbMg_{1/3}Nb_{2/3}O_3$," Appl. Phys. Lett. **72** (9), 1-3 (1998).
9. Park, S.-E., T.R. Shrout, P. Bridenbaugh, J. Rottenberg, and G.M. Loiacono, "Electric Field Induced Anisotropy in Electrostrictive $Pb(Mg_{1/3}Nb_{2/3})O_3$ - $PbTiO_3$ Crystals," Ferroelectrics (1997).
10. You, H. and Q.M. Zhang, "Diffuse X-Ray Scattering Study of Lead Magnesium Niobate Single Crystals," Phys. Rev. Lett. **79** (20), 3950-3953 (1997).
11. Zhao, J., V. Mueller, and Q.M. Zhang, "The Influence of the External Stress on the Electromechanical Response of Electrostrictive $0.9Pb(Mg_{1/3}Nb_{2/3})O_3$–$0.1PbTiO_3$ in the DC Electrical Field Biased State," J. Mat. Res. (1998).

VOLUME II

12. Yoon, S.-J., A. Joshi, and K. Uchino, "Effect of Additives on the Electromechanical Properties of $Pb(Zr,Ti)O_3$–$Pb(Y_{2/3}W_{1/3})O_3$ Ceramics," J. Am. Ceram. Soc **80** (4), 1035-39 (1997).
13. Hackenberger, W., M.-J. Pan, V. Vedula, P. Pertsch, W. Cao, C. Randall, and T. Shrout, "Effect of Grain Size on Actuator Properties of Piezoelectric Ceramics," Proceedings of the SPIE's 5th International Symposium on Smart Structures and Materials, San Diego, CA (March 1-5, 1998).

THIS PAGE LEFT INTENTIONALLY BLANK

Materials Studies–continued

14. Mueller, V. and Q.M. Zhang, "Shear Response of Lead Zirconate Titanate Piezoceramics," J. Appl. Phys. (1998).
15. Park, S.-E., M.-J. Pan, K. Markowski, S. Yoshikawa, and L.E. Cross, "Electric Field Induced Phase Transition of Antiferroelectric Lead Lanthanum Zirconate Titanate Stannate Ceramics," J. Appl. Phys. **82** (4), 1798-1803 (1997).
16. Yoshikawa, S., K. Markowski, S.-E. Park, M.-J. Pan, and L.E. Cross, "Antiferroelectric-to-Ferroelectric Phase Switching Lead Lanthanum Zirconate Stannate Titanate (PLZST) Ceramics)," Proceedings of SPIE's 4th Annual Symposium on Smart Structures and Materials, San Diego, CA (March 3-6, 1997).
17. Pan, M.-J., S.-E. Park, K.A. Markowski, W.S. Hackenberger, S. Yoshikawa, and L.E. Cross, "Electric Field Induced Phase Transition in Lead Lanthanum Stannate Zirconate Titanate (PLSnZT) Antiferroelectrics: Tailoring Properties through Compositional Modification" (1997).
18. Pan, M.-J., P. Pertsch, S. Yoshikawa, T.R. Shrout, and V. Vedula, "Electroactive Actuator Materials: Investigations on Stress and Temperature Characteristics," Proceedings of the SPIE's 5th International Symposium on Smart Structures and Materials, San Diego, CA (March 1-5, 1998).
19. Pan, M.-J. and S. Yoshikawa, "Effect of Grain Size on the Electromechanical Properties of Antiferroelectric-to-Ferroelectric Phase Switching PLSnZT Ceramics" (1997).

2.2 *Relaxor Ferroelectric Single Crystal Systems*

20. Service, R.F., "Shape-Changing Crystals Get Shiftier," Science **275**, 1878 (28 March 1997).
21. Shrout, T.R., S.-E. Park, C.A. Randall, J.P. Shepard, L.B. Hackenberger, "Recent Advances in Piezoelectric Materials" (1997).
22. Park, S.-E. and T.R. Shrout, "Ultrahigh Strain and Piezoelectric Behavior in Relaxor Based Ferroelectric Single Crystals," J. Appl. Phys. **82** (4), 1804-1811 (1997).
23. Park, S.-E. and T. R. Shrout, "Characteristics of Relaxor-Based Piezoelectric Single Crystals for Ultrasonic Transducers," IEEE Transactions, Ferroelectrics, and Frequency Control **44** (5), 1140-1147 (1997).
24. Park, S.-E. and T.R. Shrout, "Relaxor Based Ferroelectric Single Crystals for Electro-Mechanical Actuators," Mat. Res. Innov. **1**, 20-25 (1997).
25. Park, S.-E., M.L. Mulvihill, G. Risch, and T.R. Shrout, "The Effect of Growth Conditions on the Dielectric Properties of $Pb(Zn_{1/3}Nb_{2/3})O_3$ Single Crystals," Jpn. J. Appl. Phys. **36**, 1154-1158 (1997).
26. Mulvihill, M.L., L.E. Cross, W. Cao, and K. Uchino, "Domain-Related Phase Transionlike Behavior in Lead Zinc Niobate Relaxor Ferroelectric Single Crystals," J. Am. Ceram. Soc. **80** (6), 1462-68 (1997).
27. Park, S.-E., P.D. Lopath, K.K. Shung, and T.R. Shrout, "Relaxor-Based Single Crystal materials for Ultrasonic Transducer Applications" (1997).
28. Lopath, P.D., S.-E. Park, K.K. Shung, and T.R. Shrout, "$Pb(Zn_{1/3}Nb_{2/3})O_3/PbTiO_3$ Single Crystal Piezoelectrics for Ultrasonic Transducers" (1997).
29. Lopath, P.D., S-E. Park, K.K. Shung, and T.R. Shrout, "Single Crystal $Pb(Zn_{1/3}Nb_{2/3})O_3/PbTiO_3$ (PZN/PT) in Medical Ultrasonic Transducers" (1997).

Materials Studies–continued

2.3 New High Strain Polymer Materials

30. Su. J., Q.M. Zhang, C.H. Kim, R.Y. Ting, and R. Capps, "Effect of Transitional Phenomena on the Electric Field Induced Strain–Electrostrictive Response of a Segmented Polyurethane Elastomer" (1997).
31. Su, J., Q.M. Zhang, and R.Y. Ting, "Space-Charge-Enhanced Electromechanical Response in Thin-Film Polyurethane Elastomers," Appl. Phys. Lett **71** (3), 386-388 (1997).

VOLUME III

32, Su, J., Q.M. Zhang, P.-C. Wang, A.G. MacDiarmid, K.J. Wynne, "Preparation and Characterization of an Electrostrictive Polyurethane Elastomer with Conductive Polymer Electrodes," Polymers for Adv. Tech. (1998).
33. Zhang, Q.M., V. Bharti, and X. Zhao, "Giant Electrostriction and Relaxor Ferroelectric Behavior in Electron Irradiated Poly(vinylidene Fluoride-Trifluoroethylene) Copolymer," Science (1998).

3.0 TRANSDUCER STUDIES

3.1 Cymbal : Moonie : BB Composites

34. Newnham, R.E., "Composite Sensors and Actuators" (1997).
35. Steele, B.CH., R.E. Newnham, and A.G. Evans, "Ceramics, Composites, and Intergrowth," Current Opinion in Solid State & Materials Science **2**, 563-565 (1997).
36. Tressler, J.F. S. Alkoy, and R.E. Newnham, "Piezoelectric Sensors and Sensor Materials" (1997).
37. Tressler, J.F., S. Alko, A. Dogan, and R.E. Newnham, "Functional Composites for Sensors, Actuators, and Transducers" (1997).
38. Dogan, A., K. Uchino, R.E. Newnham, "Composite Piezoelectric Transducer with Truncated Conical Endcaps 'Cymbal'," IEEE Transactions on Ultrasonics, Ferroelectrics, and Frequency Control **44** (3), 597-605 (1997).
39. Dogan, A., J.F. Fernandez, K. Uchino, and R.E. Newnham, "The 'Cymbal' Electromechanical Actuator" (1997).
40. Tressler, J.F., W. Cao, K. Uchino, and R.E. Newnham, "Ceramic-Metal Composite Transducers for Underwater Acoustic Applications" (1997).
41. Tressler, J.F. and R.E. Newnham, "Doubly Resonant Cymbal-Type Transducers," IEEE Transactions on Ultrasonics, Ferroelectrics, and Frequency Control **44** (5), 1175-1177 (1997).
42. Tressler, J.F., W. Cao, K. Uchino, and R.E. Newnham, "Finite Element Analysis of The Cymbal-Type Transducer" (1997).
43. Tressler, J.F., W.J. Hughes, W. Cao, K. Uchino, and R.E. Newnham, "Capped Ceramic Underwater Sound Projector" (1997).

Transducer Studies–continued

VOLUME IV

44. Alkoy, S., P.D. Lopath, R.E. Newnham, A.-C. Hladky-Hennion, and J.K. Cochran, "Focused Spherical Transducers for Ultrasonic Imaging" (1997).
45. Alkoy, S., A. Dogan, A.-C. Hladky, P. Langlet, J.K. Cochran, and R.E. Newnham, "Miniature Piezoelectric Hollow Sphere Transducers (BBs)" (1997).
46. Zipparo, M.J., K.K. Shung, and T.R. Shrout, "Piezoceramics for High-Frequency (20 to 100 MHz) Single-Element Imaging Transducers," IEEE Transactions on Ultrasonics, Ferroelectrics, and Frequency Control **44** (5), 1038-1048 (1997).

3.2 Frequency Agile Transducers

47. Davis, C. and G.A. Lesieutre, "An Actively-Tuned Solid State Piezoelectric Vibration Absorber" (1997).
48. Davis, C.L., G.A. Lesieutre, and J. Dosch, "A Tunable Electrically Shunted Piezoceramic Vibration Absorber" (1997).
49. Lesieutre, G.A. and U. Lee, "A Finite Element for Beams Having Segmented Active Constrained Layers with Frequency-Dependent Viscoelastic Material Properties" (1997).
50. Hebert, C.A. and G.A. Lesieutre, "Rotocraft Blade Lag Damping Using Highly Distributed Tuned Vibration Absorbers," American Institute of Aeronautics and Astronautics (AIAA 98-2001).
51. Lesieutre, G.A. and C.L. Davis, "Can a Coupling Coefficient of a Piezoelectric Device be Higher than Those of its Active Material?," SPIE 4th Annual Symposium on Smart Structures and Materials, San Diego, CA (March 1997).

3.3 3-D Acoustic Intensity Probes

52. Lauchle, G.C., J.R. MacGillivray, and D.C. Swanson, "Active Control of Axial-flow Fan Noise," J. Acoust. Soc. Am 101 (1), 341-349 (1997).
53. McGuinn, R.S., G.C. Lauchle, and D.C. Swanson, "Low Flow-Noise Microphone for Active Noise Control Applications," AIAA Journal **35** (1), 29-34 (1997).
54. McGuinn, R.S., G.C. Lauchle, and D.C. Swanson, "Low Flow-Noise Pressure Measurements Using a "Hot-Mic," AIAA -97-1665-CP.
55. Capone, D.E., and G.C. Lauchle, "Designing a Virtual Sound-Level Meter in LabVIEW," Education/Acoustics, LabVIEW, National Instruments.

VOLUME V

4.0 ACTUATOR STUDIES

4.1 Materials : Designs : Reliability

56. Uchino, K., "Piezoelectric Actuators" (1997).
57. Uchino, K., "Overview: Materials Issues in Design and Performance of Piezoelectric Actuators," SPIE Mtg. (1997).
58. Uchino, K., "Shape Memory Ceramics," Chapter 8 (1997).

Actuator Studies–continued

59. Aburatani, H., S. Yoshikawa, K. Uchino, and J.W.C. deVries, "A Study of Acoustic Emission in Piezoelectric Multilayer Ceramic Actuator," Jpn. J. Appl. Phys. **37**, 204-209 (1998).
60. Aburatani, H. and K. Uchino, "Acoustic Emission (AE) Measurement in Piezoelectric Ceramics" (1997).
61. Aburatani, H. and K. Uchino, "The Application of Acoustic Emission (AE) Method for Ferroelectric Devices and Materials," 8th US-Japan Seminar (1997).
62. Uchino, K., "Reliability of Ceramic Actuators" (1997).

4.2 Photostrictive Actuators

63. Tonooka, K. P. Poosanaas, and K. Uchino, "Mechanism of the Bulk Photovoltaic Effect in Ferroelectrics," Proceedings of the 5th SPIE Mtg., San Diego, CA (1998).
64. Poosanass, P. A. Dogan, S. Thakoor, and K. Uchino, "Dependence of Photostriction on Sample Thickness and Surface Roughness for PLZT Ceramics," Proceedings of the 1997 IEEE Ultrasonics Symposium, Toronto, Ontario, Canada (October 1997).
65. Poosanaas, P. A. Dogan, A.V. Prasadarao, S. Komarneni, and K. Uchino, "Photostriction of Sol-Gel Processed PLZT Ceramics," J. Electroceramics **1** (1), 105-111 (1997).

VOLUME VI

66. Poosanaas, P., A. Dogan, A.V. Prasadarao, S. Komarneni, and K. Uchino, "Effect of Ceramic Processing Methods on Photostrictive Ceramics," J. Adv. Perf. Mat. (1997).
67. Thakoor, S., P. Poosanaas, J.M. Morookian, A. Yavrovian, L. Lowry, N. Marzwell, J. Nelson, R.R. Neurgaonkar, and K. Uchino, "Optical Microactuation in Piezoceramics" (1997).

4.3 New Torsional Amplifier/Actuators

68. Glazounov, A.E., Q.M. Zhang, and C. Kim, "Piezoelectric Actuator Generating Torsional Displacement from Piezoelectric d_{15} Shear Response," Appl Phys. Lett. (1997).
69. Glazounov, A.E., Q.M. Zhang, and C. Kim, "A New Torsional Actuator Based on Shear Piezoelectric Response," Proceedings of SPIE Smart Materials, San Diego, CA (March 1998).

4.4 High Force Amplifiers and Inchworms

70. Uchino, K., J. Zheng, A. Joshi, S. Yoshikawa, S. Hirose, S. Takahashi, and J.W.C. deVries, "High Power Characterization of Piezoelectric Materials" (1997).
71. Uchino, K., "High Electromechanical Coupling Piezoelectrics - How High Energy Conversion Rate is Possible," Mat. Res. Soc. Symp. Proc. **459**, 3-14 (1997).
72. Park, S.-E., V. Vedula, M.-J. Pan, W.S. Hackenberger, P. Pertsch, and T.R. Shrout, "Relaxor Based Ferroelectric Single Crystals for Electromechanical Actuators," Proceedings of the SPIE's 5th International Symposium on Smart Structures and Materials, San Diego, CA (March 1998).

Actuator Studies–continued

73. Koopmann, G.H. G.A. Lesieutre, B.R. Dershem, W. Chen, and S. Yoshikawa, "Embeddable Induced Strain Actuators Using Framed 3-3 Piezoceramic Stacks: Modeling and Characterization," Proceedings of the SPIE's 4th Annual International Symposium on Smart Structures and Materials, San Diego, CA (March 1997).
74. Driesch, P.L., G.H. Koopmann, J. Dosch, and H. Iwata, "Development of a Surface Intensity Probe for Active Control Applications," IMECE, Dallas, Texas (November 1997).
75. Galante, T., J. Frank, J. Bernard, W. Chen, G.A. Lesieutre, and G.H. Koopmann, "Design, Modeling, and Performance of a High Force Piezoelectric Inchworm Motor" (1997).
76. Galante, T.P., "Design and Fabrication of a High Authority Linear Piezoceramic Actuator: The PSU H3 Inchworm," Master of Science Thesis, The Pennsylvania State University (August 1997).
77. Lesyna, M.W., "Shape Optimization of a Mechanical Amplifier for Use in a Piezoceramic Actuator," Master of Science Thesis, The Pennsylvania State University (May 1998).

VOLUME VII

78, Uchino, K., "Piezoelectric Ultrasonic Motors: Overview," J. Smart Materials and Structures–Special Issue (1997).
79. Uchino, K., "Compact Piezoelectric Ultrasonic Motors," J. Medical Ultrasonics 24 (9), 1191-92 (1997).

5.0 MODELING and CHARACTERIZATION

5.1 Finite Element Methods

80. Qi, W. and W. Cao, "Finite Element Analysis and Experimental Studies on the Thickness Resonance of Piezocomposite Transducer," Ultrasonic Imaging **18**, 1-9 (1996).
81. Qi, W. and W. Cao, "Finite Element Study on Random Design of 2-2 Composite Transducer," SPIE **3037**, 176-180 (1997).
82. Geng, X. and Q.M. Zhang, "Evaluation of Piezocomposites of Ultrasonic Transducer Applications–Influence of the Unit Cell Dimensions and the Properties of Constituents on the Performance of 2-2 Piezocomposites," IEEE Transactions on Ultrasonics, Ferroelectrics, and Frequency Control **44** (4), 857-872 (1997).
83. Zhang, Q. and X. Geng, "Acoustic Properties of the Interface of a Uniform Medium-2-2 Piezocomposite and the Field Distributions in the Composite," Jpn. J. Appl. Phys. **36**, 6853-6861 (1997).
84. Geng, X. and Q.M. Zhang, "Analysis of the Resonance Modes and Losses in 1-3 Composites for Ultrasonic Transducer Applications," IEEE UFFC (1997).

APPENDIX 12

journal

J. Am. Ceram. Soc., 80 [4] 1035–39 (1997)

Effect of Additives on the Electromechanical Properties of $Pb(Zr,Ti)O_3$–$Pb(Y_{2/3}W_{1/3})O_3$ Ceramics

Seok-Jin Yoon

Division of Ceramics, Korea Institute of Science and Technology, Seoul, 130-650, Korea

Amod Joshi and Kenji Uchino*

Material Research Laboratory, The Pennsylvania State University, University Park, Pennsylvania 16802

Dielectric and piezoelectric properties of $0.02Pb(Y_{2/3}W_{1/3})O_3$·$0.98Pb(Zr_{0.52}Ti_{0.48})O_3$ ceramics doped with additives (Nb_2O_5, La_2O_3, MnO_2, and Fe_2O_3) were investigated. The grain sizes of these ceramics decreased with increasing amounts of additives. For additions of MnO_2 and Fe_2O_3, dielectric losses decreased, while for Nb_2O_5 and La_2O_3, these values increased. The maximum values of the mechanical quality factor Q_m were found to be 956 and 975 for additions of 0.9 wt% Fe_2O_3 and 0.7 wt% MnO_2, respectively, but donor dopants (Nb_2O_5 and La_2O_3) did not change the values of Q_m. On the other hand, the piezoelectric constant d_{33} and the electromechanical coupling factor k_p decreased with additions of MnO_2 and Fe_2O_3, but improved with additions of Nb_2O_5 and La_2O_3.

I. Introduction

$Pb(Zr,Ti)O_3$-based solid solution systems have been investigated by the addition of various additives or by incorporation with other ABO_3-type perovskites for improving sinterability, dielectric, and piezoelectric properties. After the report of superior properties at the phase boundary in PZT by Jaffe *et al.*,[1] many researchers have tried to improve the properties of these materials using various techniques.[2,3]

The effect of dopants is a complex matter, but a number of important generalizations have been made regarding aliovalent substituents in perovskites. Donor dopants (e.g., La^{3+},[2] Nb^{5+},[3] and Sb^{5+}), those of higher charge than that of the ions they replace, are compensated by cation vacancies, whereas acceptor dopants (Fe^{3+}, Cr^{3+},[3] and Mn^{3+}), ions of lower charge than that of replaced ions, are compensated by oxygen vacancies. Cations and cation vacancies tend to be separated by oxygen ions so that there is a considerable energy barrier to be overcome before the ion and its vacancy can be interchanged. Oxygen, however, forms a continuous lattice structure so that oxygen vacancies have oxygen ion neighbors with which they can easily exchange. Typical concentrations of dopants (0.05–5 at.%) must result in the formation of dipolar pairs between an appreciable fraction of the dopants and associated vacancies: e.g., $2La^{3+}$:$[D^{\cdot}] = 2[V_m'']$ or $2Fe^{3+}$:$[A'] = 2[V_O^{\cdot\cdot}]$. Donor doping in PZT could be expected to reduce the concentration of oxygen vacancies, especially rare-earth substituents such as La^{3+}, Nd^{3+}, etc., leading to a reduction in the concentration of domain-stabilizing defect pairs. The resulting increase in wall mobility causes an observed increase in dielectric constant and loss, piezoelectric coefficients and coupling factors, and reduction in mechanical quality factor Q_m and coercive field. The introduction of oxygen vacancies through acceptor doping increases the Q_m.[4]

Nb_2O_5 and the WO_3-doped PZT system or the PMN–PZT system are not adequate for applications such as various kinds of transducers or actuators because of the low values of Q_m.[5] The desirable features in these applications are low mechanical loss and high piezoelectric properties (d and k). In the case of low Q_m, heat generation during operation is the main reason for degradation of piezoelectricity, while high d is required for large mechanical displacement under a certain electric input.

In previous work,[6,7] a ternary solid solution system consisting of $Pb(Zr_{0.52}Ti_{0.48})O_3$ (PZT) and a complex perovskite-type compound $Pb(Y_{2/3}W_{1/3})O_3$ (PYW) was developed. Although the solubility of $Pb(Y_{2/3}W_{1/3})O_3$ in $Pb(Zr_{0.52}Ti_{0.48})O_3$ was as low as 2 mol% of PYW, superior piezoelectric properties were observed in the 0.02PYW·0.98PZT composition: values of d_{33} and k_p were 365×10^{-12} C/N and 54%, respectively. The present paper has investigated the effect of various additives on the dielectric and piezoelectric properties in 0.02PYW·0.98PZT ceramics.

II. Experimental Procedure

Reagent-grade PbO, ZrO_2, TiO_2, Y_2O_3, WO_3, La_2O_3, Nb_2O_5, Fe_2O_3, and MnO_2 were used as starting materials. Mixtures of the desired composition were ball-milled with zirconia balls as grinding media and deionized water as a lubricant for 12 h. After mixing and milling, the powders were dried for 12 h, which were later crushed and then calcined at 850°C for 1 h. Following dispersion of a binder 5 wt% poly(vinyl alcohol) (PVA) to aid the pressing process, the resulting powders were cold pressed into cylindrical form at a pressure of 1000 kg/cm^2. The pressed pellets were covered with powders of the same composition, placed in a double-alumina crucible arrangement, and sintered at 1200°C for 1 h. The sintered pellets were ground to a thickness of 1 mm, electroded using silver paste, and heat-treated at 600°C for 10 min. The electroded samples were poled at 120°C at 35 kV/cm for 30 min in silicone oil. After 24 h of aging at room temperature, dielectric and piezoelectric properties were measured using a HP impedance/gain-phase analyzer. The piezoelectric properties were determined by the resonance methods.[8]

III. Results and Discussion

Selected SEM photographs of compositions are shown in Fig. 1. The grain size in the 0.02PYW·0.98PZT sample fired at 1200°C for 1 h was about 8 μm, but grain size remarkably decreased with increasing additive additions. The addition of Nb_2O_5 to the PZT solid solution inhibited grain growth. This limited grain growth is probably due to the solid solution impurity drag mechanism.[9] Okazaki and Nagata[10] have reported that dielectric and piezoelectric-related properties increase with

T. R. Gururaja—contributing editor

Manuscript No. 191599. Received August 19, 1996; approved February 14, 1997.
*Member, American Ceramic Society.

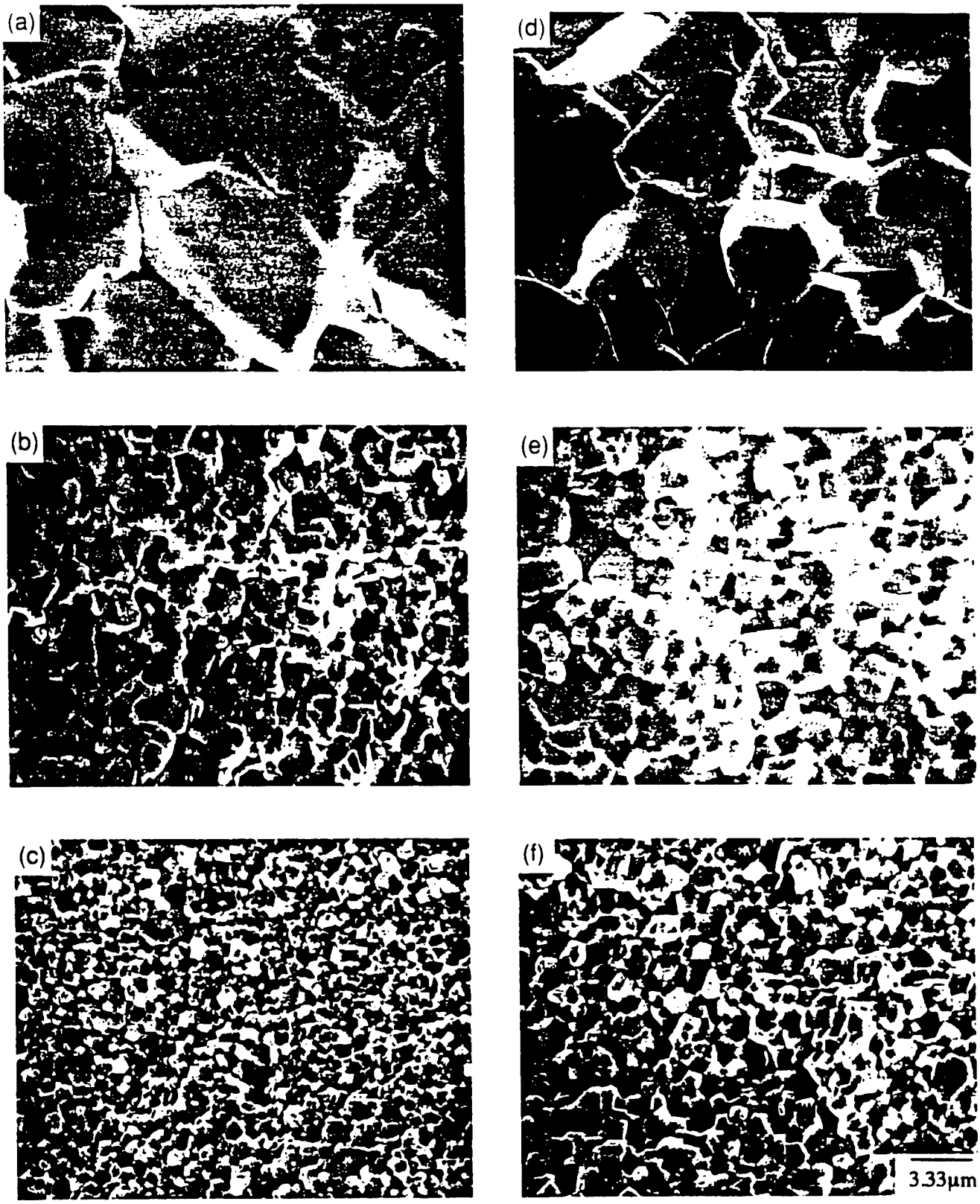

Fig. 1. SEM photographs of $0.02Pb(Y_{2/3}W_{1/3})O_3$-$0.98Pb(Zr_{1-x}Ti_x)O_3$ containing Fe_2O_3 and Nb_2O_5 sintered at 1200°C for 1 h: (a) none, (b) 0.5 wt% Fe_2O_3, (c) 0.9 wt% Fe_2O_3, (d) 0.1 wt% Nb_2O_5, (e) 0.5 wt% Nb_2O_5, (f) 0.9 wt% Nb_2O_5.

increasing grain size. In their model, as grain size decreases, the grain boundary phases, which are directly related to the volume of space charge regions, get larger and finally result in lowering the dielectric constant. In a review of grain size effects on dielectric and piezoelectric properties in the PZT system, there are insufficient works from which to draw conclusions. However, the piezoelectric and related properties have been consistently reported to decrease with decreased grain size. It is believed that the observed piezoelectric behavior is due to a "clamping" of domain walls.

Lattice parameters and tetragonal distortion for Fe-doped 0.02PYW-0.98PZT ceramics are plotted in Fig. 2. The lattice distortion along the tetragonal c-axis was more strongly renormalized by the decreasing grain size than was the distortion along the a-axis. The tetragonal distortion c/a was also found to decrease with decreasing grain size, resulting in a decrease of

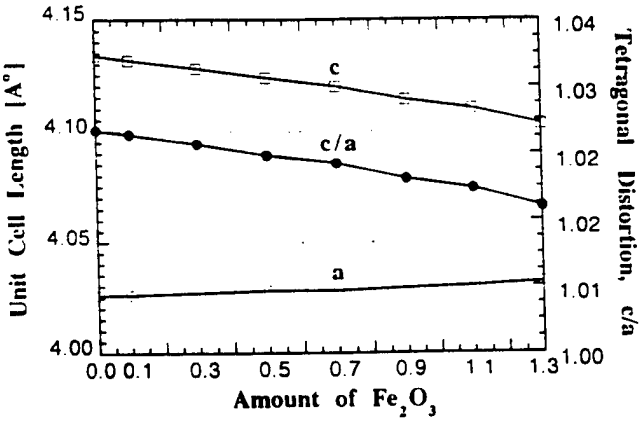

Fig. 2. Unit cell distortion at room temperature for Fe-doped 0.02PYW-0.98PZT ceramics.

the averaged unit cell volume similiar to the decrease observed in $BaTiO_3$ ceramics.[11]

Figure 3 shows the polarization vs field hysteresis loops for Fe-doped 0.02PYW-0.98PZT ceramics. The Fe-doped samples exhibited a type of "pinched" or "propeller-shaped" curve. The Mn-doped samples also had similar shapes. This behavior was more like conventionally sintered samples and was found to be stronger in tetragonal compositions than in the rhombohedral ones.

The Nb-doped ceramics exhibited typical square P–E hysteresis loops shown in Fig. 4. The remanent polarization (P_r) was found to have a minimum value at about 0.3 wt% Nb_2O_5 additives, but the P_r values increased with additional Nb_2O_5 doping. The decrease of P_r is believed to be due to the clamping of domains exhibited by neighboring grain and grain boundaries and also due to relatively free domain reversal processes just after the removal of field.[12] The maximum value of P_r was obtained at 0.9 wt% Nb_2O_5 and the value was about 35 $\mu C/cm^2$.

Acceptor dopants (Fe^{3+}, Mn^{3+}, etc.) create oxygen vacancies for ionic charge compensation and tend to pin the domain wall, which is evident by an increase in the internal bias field. Like acceptor-doped PZT ceramics, undoped PZT ceramics are also known to have oxygen vacancies due to superoxidation, which is the result of excess Pb-site vacancies due to the PbO volatility over oxygen vacancies,[13] resulting in an increase of the internal bias field and thus the stabilization of domain structure. Hysteresis measurements indicate that donor dopants (La^{3+}, Nb^{5+}) increase the domain wall mobility and create very small internal bias fields. Takahashi[12] has studied space-charge effects in PZT ceramics with impurities. Experimental results show that the space-charge field (internal bias field) increases in undoped and acceptor-doped PZT ceramics in comparison with donor-doped PZT ceramics. In the tetragonal compositions, it appears that domain wall pinning, which is caused by a structural factor (tetragonality), was coupled with the defect dipoles, resulting in a relatively strong pinched hysteresis loop. This kind of pinched loop was found to diminish under severe electrical excitation or after a heat treatment above the Curie temperature (T_c) with slow cooling in an oxygen atmosphere.

Dielectric constants of various compositions are shown in Fig. 5. Donor-doped (Nb_2O_5 and La_2O_3) PYW–PZT has higher dielectric constants than the acceptor-doped (MnO_2, Fe_2O_3) compositions. For substitutions of a lower valence for Pb^{2+} or for $(Ti,Zr)^{4+}$, the unit cell actually shrank[13] because of the creation of oxygen vacancies. The shrinking and distortion of the cells are thought to contribute to an increase in Q_m, the coercive field, E_c, but a slightly lowered dielectric constant. This behavior is believed to be due to the difficulty of the domain reversal process (clamping) and/or to the reduced number of twinned domains. With decreasing grain size, the twinned domains were assumed to be greatly clamped by neighboring grains and boundaries under the electric field, resulting in an increase of an internal bias field (E_i), i.e., coercive field (E_c).[12]

Figure 6 shows the dielectric loss change with various additives for 0.02PYW-0.98PZT ceramics. The acceptor dopants (MnO_2 and Fe_2O_3) reduce dielectric losses, while donor dopants (Nb_2O_5 and La_2O_3) increase dielectric losses. All dopant ions that reduce the losses are characterized by a lower valence state than that of the substituted host lattice ions (e.g., Mn^{3+}, Fe^{3+} at $(Zr,Ti)^{4+}$ site). Consequently, they possess acceptor characteristics, with the charge deficiency being compensated by vacancies in the oxygen lattice. The acceptor-dopant ions pin the domain wall and thus reduce the loss of domain wall motion. Conversely, donor dopants increase the mobility of the domain wall motion, and thus reorientation of the twinned domain walls actively occurs. It is interesting that the dielectric loss is lowered at 1 kHz, even though the conductivity is significantly higher, again pointing out the predominance of domain wall mobility in causing dielectric losses at ordinary temperatures and frequencies. As shown in Fig. 1, the grain size decreased with increasing amounts of additives. The increase in dielectric losses with decreasing grain size that is observed in Nb-doped ceramics is probably due to the accumulation of space charge at the grain boundary phases, similar to that found in $BaTiO_3$ ceramics.[14]

It is well known that additions of MnO_2 and Fe_2O_3 acting as acceptor ions improve the value of Q_m, whereas La_2O_3 and

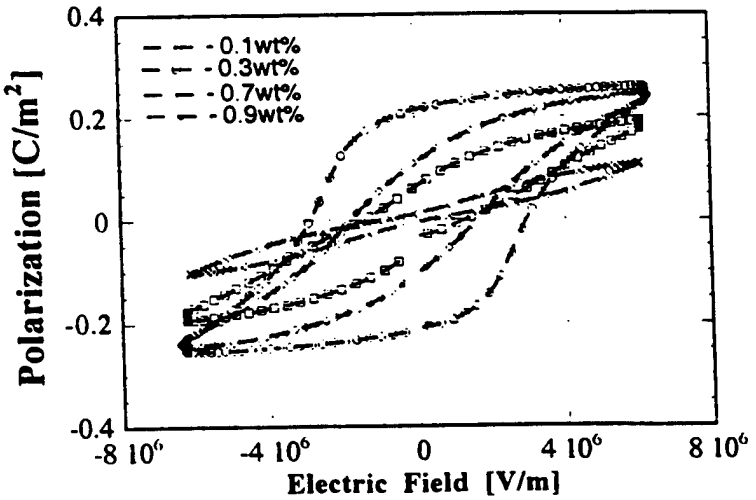

Fig. 3. P–E hysteresis loop change in Fe-doped $0.02Pb(Y_{2/3}W_{1/3})O_3$-$0.98Pb(Zr_{0.52}Ti_{0.48})O_3$ ceramics.

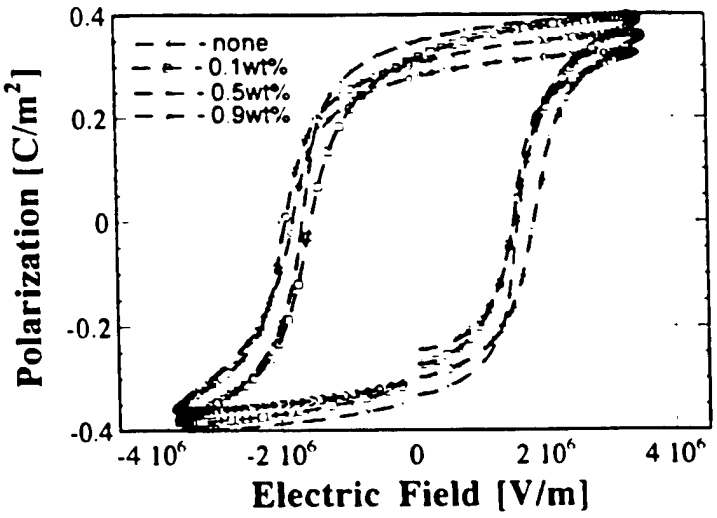

Fig. 4. P–E hysteresis loop change in Nb-doped $0.02Pb(Y_{2/3}W_{1/3})O_3$–$0.98Pb(Zr_{0.52}Ti_{0.48})O_3$ ceramics.

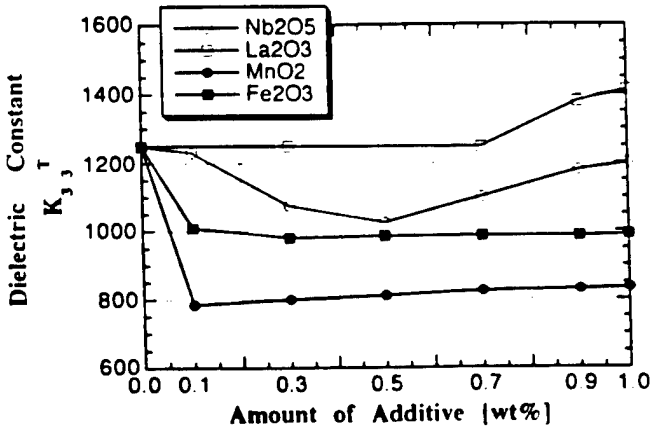

Fig. 5. Dielectric constant change in doped-$0.02Pb(Y_{2/3}W_{1/3})O_3$–$0.98Pb(Zr_{0.52}Ti_{0.48})O_3$ ceramics.

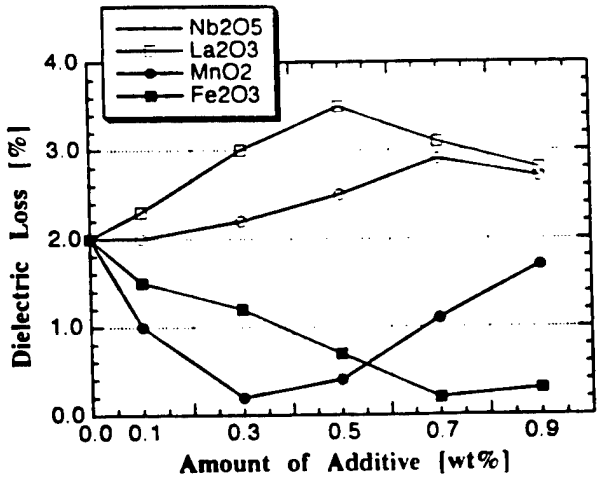

Fig. 6. Dielectric loss change in doped-$0.02Pb(Y_{2/3}W_{1/3})O_3$–$0.98Pb(Zr_{0.52}Ti_{0.48})O_3$ ceramics.

Nb_2O_5 acting as donor ions to ferroelectric materials with perovskite structure enhance the values of d_{33} and k_p while degrading Q_m, as shown in Figs. 7, 8, and 9. The values of d_{33} and k_p exhibit maximum values of 428×10^{-12} C/N and 60%, respectively, at 0.1 wt% La_2O_3, and then decrease gradually with the above additions. The largest values of d_{33} and k_p (d_{33} = 418×10^{-12} C/N and k_p = 61%) were observed at 0.1 wt% Nb_2O_5. On the other hand, as the amount of MnO_2 increases from 0.1 to 0.7 wt%, the values of Q_m increase remarkably from 72 to 975. In addition, the values of d_{33} and k_p are 310×10^{-12} C/N and 51%, respectively, for 0.5 wt% MnO_2 additives. For Fe_2O_3 addition, the maximum values of d_{33} and k_p (d_{33} = 289×10^{-12} C/N, k_p = 49%) were observed at 0.9 wt%. Moreover, the maximum value of Q_m (Q_m = 956) in Fe_2O_3 additions was observed at an addition of 0.9 wt%. As mentioned above, donor doping in PZT is expected to reduce the concentration of oxygen vacancies, especially rare-earth substituents such as La^{3+}, Nd^{3+}, etc., leading to reduction in the concentration of domain-stabilizing defect pairs and thus to lower aging rates. The resulting increase in wall mobility causes an observable increase in dielectric constant and loss, elastic compliance, piezoelectric coefficients, and coupling factors, and a reduction in Q_m and E_c. The introduction of oxygen vacancies through acceptor doping leads to a slight reduction in unit cell size, which tends to reinforce these effects.

IV. Conclusion

The dielectric and piezoelectric properties of additive-doped $0.02Pb(Y_{2/3}W_{1/3})O_3$–$0.98Pb(Zr_{0.52}Ti_{0.48})O_3$ ceramics were investigated. Doping of MnO_2 and Fe_2O_3 in 0.02PYW–0.98PZT ceramics decreased the dielectric loss, dielectric constant, and piezoelectric properties, but enhanced the mechanical quality factor. The maximum Q_m values of MnO_2 and Fe_2O_3 additions were 975 and 956, respectively. In contrast, the additions of

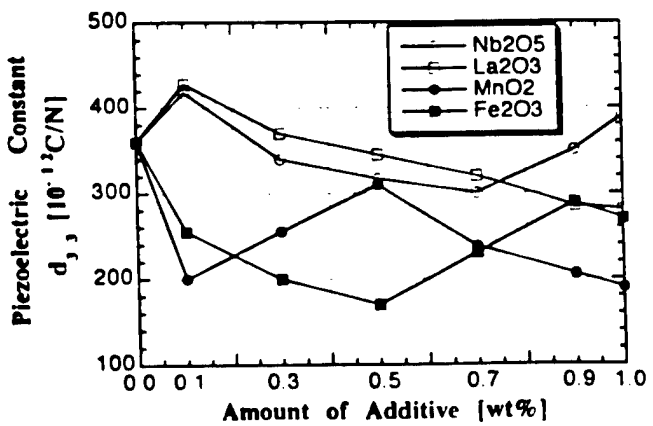

Fig. 7. Piezoelectric constant change in doped-$0.02Pb(Y_{2/3}W_{1/3})O_3$–$0.98Pb(Zr_{0.52}Ti_{0.48})O_3$ ceramics.

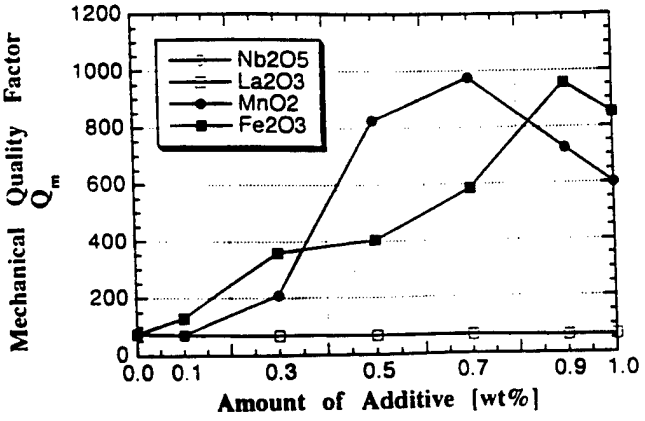

Fig. 8. Mechanical quality factor change in doped-0.02Pb-$(Y_{2/3}W_{1/3})O_3$·0.98Pb$(Zr_{0.52}Ti_{0.48})O_3$ ceramics.

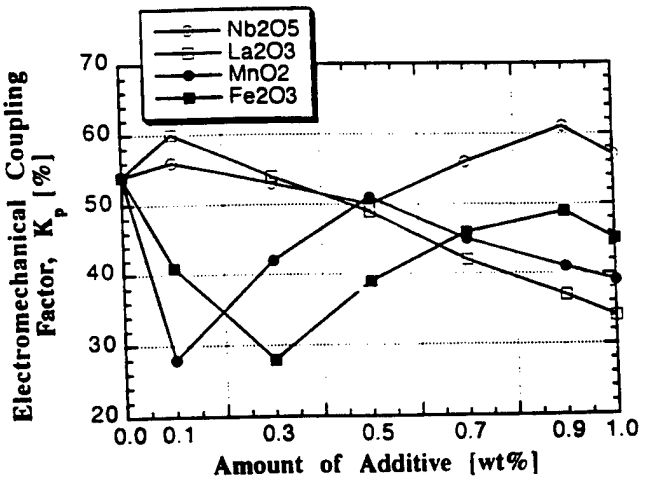

Fig. 9. Electromechanical coupling factor change in doped-0.02Pb$(Y_{2/3}W_{1/3})O_3$·0.98Pb$(Zr_{0.52}Ti_{0.48})O_3$ ceramics.

La_2O_3 and Nb_2O_5 increased the piezoelectric properties. The maximum values of d_{33} and k_p were 428 × 10^{-12} C/N and 60% for the addition of 0.1 wt% La_2O_3, and for the addition of 0.1 wt% Nb_2O_5 the largest values were 418 × 10^{-12} C/N and 61%, respectively.

References

[1]B. Jaffe, R. S. Roth, and S. Marzullo, "Properties of Piezoelectric Ceramics in the Solid-Solutions Series Lead Titanate–Lead Zirconate–Lead Oxide:Tin Oxide, and Lead Titanate–Lead Hafnate," *J. Res. Natl. Bur. Stand. (U.S.)*, **55** [5] 239–54 (1955).

[2]G. H. Haertling and C. E. Land, "Hot-Pressed (Pb,La)(Zr,Ti)O, Ferroelectric Ceramics for Electrooptic Applications," *J. Am. Ceram. Soc.*, **54**, 1–11 (1974).

[3]F. Kulskar, "Electromechanical Properties of Lead Titanate Zirconate Ceramics Modified with Certain Three- or Five-Valent Additions," *J. Am. Ceram. Soc.*, **42**, 343–49 (1959).

[4]R. S. Atkin and R. M. Fulrath, "Point Defects and Sintering of Lead Zirconate-Titanate," *J. Am. Ceram. Soc.*, **54** [5] 265–70 (1971).

[5]H. Ouchi, M. Nishida, and S. Hayakawa, "Piezoelectric Properties of $Pb(Mg_{1/3}Nb_{2/3})O_3$–$PbTiO_3$–$PbZrO_3$ Ceramics Modified with Certain Additives," *J. Am. Ceram. Soc.*, **49** [11] (1966).

[6]S. J. Yoon, H. J. Kim, H. J. Jung, and C. Y. Park, "Dielectric and Piezoelectric Properties of $xPb(Y_{2/3}W_{1/3})O_3$–$(1-x)Pb(Zr_{0.52}Ti_{0.48})O_3$ Ceramics," *Ferroelectrics*, **145**, 1–7 (1993).

[7]S. J. Yoon, S. Y. Yoo, J. H. Moon, H. J. Jung, and H. J. Kim, "Effects of La_2O_3 and MnO_2 on the Piezoelectric Properties of 0.02Pb$(Y_{2/3}W_{1/3})O_3$–0.98Pb$(Zr_{0.52}Ti_{0.48})O_3$," *J. Mater. Res.*, **11** [2] 348–52 (1996).

[8]IEEE Standard on Piezoelectricity, IEEE Su-31, Vol. 2, American National Standard, New York, 1982.

[9]R. A. Langman, R. B. Runt, and S. R. Butler, "Isothermal Grain Growth of Pressure-Sintered PLZT Ceramics," *J. Am. Ceram. Soc.*, **56** [9] 486–88 (1973).

[10]K. Okazaki and K. Nagata, "Effects of Grain Size and Porosity on Electrical and Optical Properties of PLZT Ceramics," *J. Am. Ceram. Soc.*, **56**, 82–86 (1973).

[11]G. Arlt, D. Hennings, and G. de With, "Dielectric Properties of Fine-Grained Barium Titanate Ceramics," *J. Appl. Phys.*, **58** [4] 1619 (1985).

[12]M. Takahashi, "Space Charge Effect in Lead Zirconate Titanate Ceramics Caused by Addition of Impurities," *Jpn. J. Appl. Phys.*, **9** [10] 1236–46 (1970).

[13]B. Jaffe, W. R. Cook, and H. Jaffe, *Piezoelectric Ceramics*, Academic Press, London, U.K., 1971.

[14]L. Egerton and S. E. Kooncw, "Effect of Firing Cycle on Structure and Some Dielectric and Piezoelectric Properties of Barium Titanate Ceramics," *J. Am. Ceram. Soc.*, **38**, 412–18 (1955). □

APPENDIX 13

Submitted to the proceedings of the SPIE's 5th International Symposium on Smart Structures and Materials, March 1-5, 1998, San Diego, CA.

Effect of Grain Size on Actuator Properties of Piezoelectric Ceramics

Wesley Hackenberger[a], Ming-Jen Pan[b], Venkata Vedula[b], Patrick Pertsch* , Wen-wu Cao[b], Clive Randall[b], and Thomas Shrout[a]

[a]TRS Ceramics, Inc., 2820 E. College Ave., State College, PA 16801
[b]Materials Research Laboratory, The Pennsylvania State University, University Park, PA 16802

ABSTRACT

Properties of piezoelectric ceramics important for actuator applications have been measured as a function of grain size. Fine grain piezoelectrics (≤ 1 μm) have been found to exhibit improved machinability and increased mechanical strength over conventional materials. Actuators made from fine grain ceramic are, therefore, expected to have improved reliability, higher driving fields, and lower driving voltages (from thinner layers in stacked or co-fired actuators) over devices fabricated from conventional materials. TRS Ceramics in collaboration with the Pennsylvania State University's Materials Research Laboratory, has developed fine grain piezoelectric ceramics with minimal or no reduction in piezoactivity. New chemical doping strategies designed to compensate ferroelectric domain clamping effects from grain boundaries have been successful in yielding submicron grain sized ceramics with both low and high field properties equivalent to conventional materials. In the case of Type II ceramics, reduced grain size results in a very stable domain state with respect to both electric field and compressive prestress. Work is in progress to develop both epoxy bonded stack and co-fired actuators from fine grain piezoelectrics.

Keywords: fine grain piezoelectrics, actuators, prestress, mechanical strength, grain size

1. INTRODUCTION

For ceramic materials used in mechanical load bearing applications, many benefits result from grain sizes that are less than 1 μm. For example mechanical strength and resistance to fatigue under cyclic loading are both known to increase with decreasing grain size[1]. In the case of piezoelectric ceramic actuators, poor mechanical strength and fatigue characteristics of conventional materials has lead to short service lifetimes limiting the widespread use of these devices. However, reducing the average grain size of piezoelectric ceramics is complicated by the fact that severe degradation of piezoelectric properties is observed in ceramics with grain sizes < 1 μm (see figure 1)[2]. Cryogenic property measurements and transmission electron microscopy studies (TEM) have shown that grain size affects the extrinsic contributions to piezoelectricity (*i.e.*, ferroelectric domain wall motion)[3]. Once extrinsic effects are "frozen out", no grain size dependence is observed for the remaining intrinsic piezoelectricity (a crystallographic property). Extrinsic piezoelectricity in ceramics such as $Pb(Zr,Ti)O_3$ (PZT) is highly dependent on chemical composition, particularly the types and amounts of modifying dopants. At TRS Ceramics, we have developed new PZT compositions in which the normal degradation in piezoelectricity with grain size has been compensated. Processes have also been developed to produce fine grain PZT's with conventional mixed oxide methods and normal sintering conditions at atmospheric pressure. The fine grained ceramics can thus be produced at about the same cost as conventional materials.

In this paper we will present comparisons of property measurements for conventional and fine grain PZT's commonly used in actuator applications. The materials studied were TRS200 (a PZT-5A or DOD Type II equivalent material) and TRS600 (a PZT-5H or DOD Type VI equivalent material) and their fine grain counterparts. Figures 2 trough 5 are micrographs showing the grain sizes of the materials studied. Initial investigations of these materials have focused on properties useful for transducer applications such as bio-medical ultrasound probes, but it will be shown that fine grain ceramics also have high field properties similar or equivalent to conventional materials. Thus, fine grain PZT's show great promise for a new generation of high reliability piezoelectric actuators. Specific measurements that will be discussed include low field properties measured by IEEE standard techniques[4], mechanical strength, machinability, strain *vs.* electric field, and strain and polarization *vs.* electric field and compressive prestress.

---

* Visiting Scientist from Fraunhofer Institute for Applied Optics and Precision Engineering, D-07745 Jena, Germany

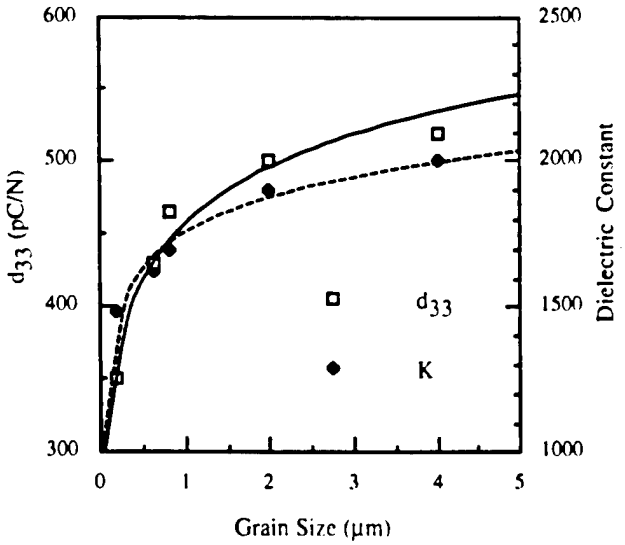

Figure 1: Piezoelectric coefficient (d_{33}) and dielectric constant *vs.* grain size for a conventional Type II PZT composition.

Figure 2: Micrograph for TRS200 (Type II PZT). Scale bar = 5 μm and grain size ~ 5 μm.

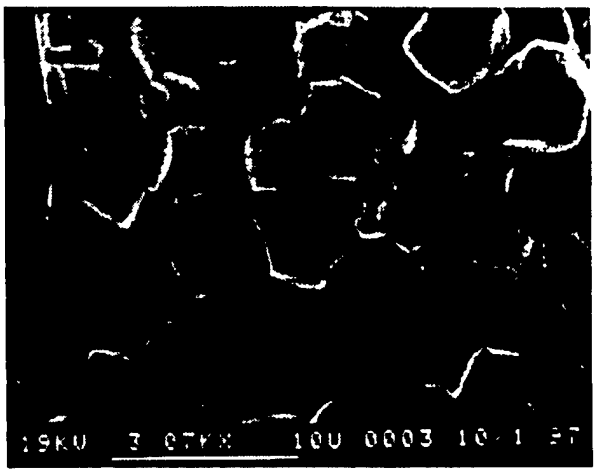

Figure 4: Micrograph for TRS600 (Type VI PZT). Scale bar = 10 μm and grain size ~ 5 μm.

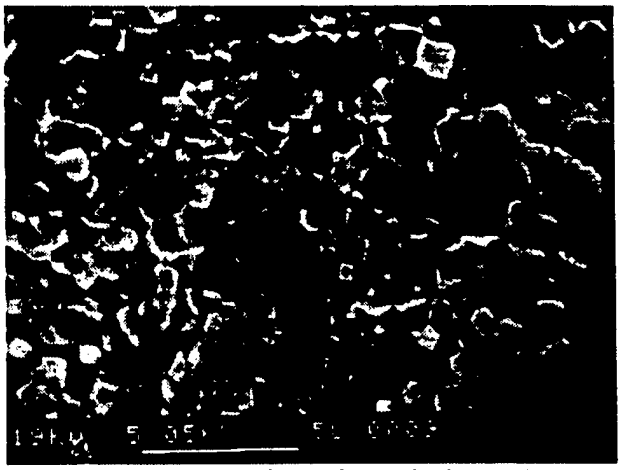

Figure 3: Micrograph for TRS200FG (fine grain Type II). Scale bar = 5 μm and grain size ~ 0.8 μm.

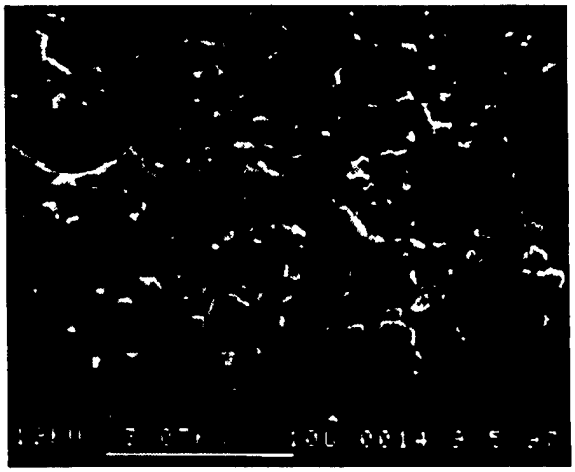

Figure 5: Micrograph for TRS600FG (fine grain Type VI). Scale bar = 10 μm and grain size ~ 0.9 μm.

2. LOW FIELD PROPERTIES OF FINE GRAIN PZT'S

Piezoelectric and dielectric properties of conventional and fine grain PZT's are shown in tables I and II. The properties were measured using a combination of impedance spectroscopy and pulse-echo ultrasonics for elastic coefficients. For Type II ceramic, chemical compensation of the grain size effect resulted in higher low field properties for fine grain material compared to conventional ceramic. Both course and fine grain Type II ceramics have about the same elastic properties, indicating that the mechanical performance of actuators made from fine grain ceramic will not be significantly different from conventional material. For the Type VI ceramic the situation was reversed with the properties of fine grain ceramic being somewhat lower than those of conventional coarse grained material. This indicates that more compensation of grain size effects may be necessary; however, as will be explained later, high field behavior of fine grain Type VI ceramic indicates that there may be fundamental differences in the domain-grain size interactions for fine grain Type II and VI ceramic. Ultrasonic transducer arrays have been constructed from the fine grain Type II material. These include high frequency transducers (10 MHz single element 1-3 composite and 66 MHz single plate transducer) in which the fine grain ceramic demonstrated performance equivalent to or better than the conventional materials.

Table I: Properties of Type II Conventional and Fine Grain Ceramics Determined from Impedance and Pulse-Echo Ultrasonic Measurements

Property	TRS200	TRS200FG
K @ 1 kHz	1650	1900
Loss	0.015	0.015
d_{33} (pC/N)	350	400
d_{31} (pC/N)	-170	-190
k_{33}	0.69	0.73
k_{31}	0.34	0.39
k_p	0.57	0.60
k_t	0.51	0.47
$1/s_{33}$ (GPa)	56	56
$1/s_{11}$ (GPa)	61	68
T_c (°C)	360	325

Table II: Properties of Type VI Conventional and Fine Grain Ceramics

Property	TRS600	TRS600FG
K @ 1 kHz	3725	3700
Loss	0.02	0.02
d_{33} (pC/N)	720	650
k_p	0.67	0.61
T_c (°C)	190	190

3. MECHANICAL STRENGTH AND MACHINING BEHAVIOR

The mechanical strength of fine grain ceramic was evaluated using 4-point bend tests. Bars 45 mm x 4 mm x 3 mm were prepared from both fine grain and conventional Type II ceramic and tested according to ASTM standard procedures[5]. The PZT bars were unpoled. A Weibull distribution of the results is shown in figure 6. Average strengths were 70 MPa and 85 MPa for TRS200 and 200FG, respectively. The fine grain material exhibited a 20% higher bending strength than the conventional ceramic. Upon poling the mechanical strength of PZT increases to > 110 MPa perpendicular to the poling direction[6]. Thus, the strength of poled fine grain ceramic is expected to be > 130 MPa. The distribution of strength data was also much narrower for the fine grain ceramic (Weibull modulus of 21 compared to 14 for conventional material) indicating a more uniform microstructure. Work is in progress to identify the strength limiting flaws in the fine grain PZT and to further increase strength through process refinements.

The improved microstructural homogeneity of fine grain PZT leads to improved machinability. This has been demonstrated for the Type II material with dicing studies as a prelude to ultrasonic array fabrication. In a side by side dicing comparison with all parameters the same (test performed on a Kulicke and Soffa precision dicing saw), the fine grain material could be diced into posts with a considerably larger aspect ratio than similar material from two other piezoelectric ceramic vendors (see Table III). Figures 7 and 8 show cross sections of diced arrays for the fine grain TRS200 and material from vendor #1. The fine grain ceramic had a considerably more uniform microstructure compared to the scale of the diced posts.

For actuators, improved mechanical strength will lead directly to improved reliability. Better machinability is also a benefit as it allows fabrication of epoxy bonded stack actuators with thinner layers obtained from either lapping or slicing. Improved mechanical strength is important here as well to provide adequate handlability for thin plates.

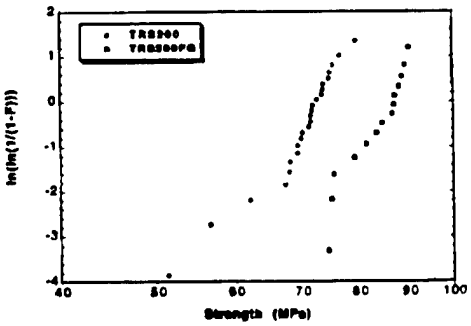

Figure 6: Weibull plot of 4-point bend strengths for TRS200 and 200FG

Table III: Results of Ultrasonic Array Dicing Study for Type II Materials. Minimum Achievable Post Sizes.

Material	Cut Depth (μm)	Kerf (μm)	Width (μm)	Aspect Ratio
TRS200FG	380	23	18	21:1
Vendor 1	380	23	28	15:1
Vendor 2	380	23	38	10:1

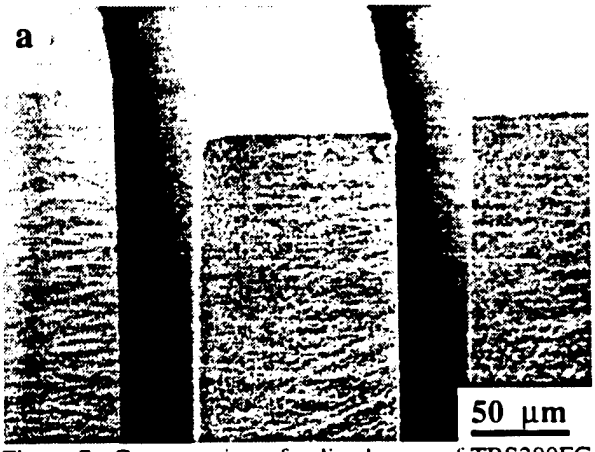

Figure 7: Cross section of a diced array of TRS200FG.

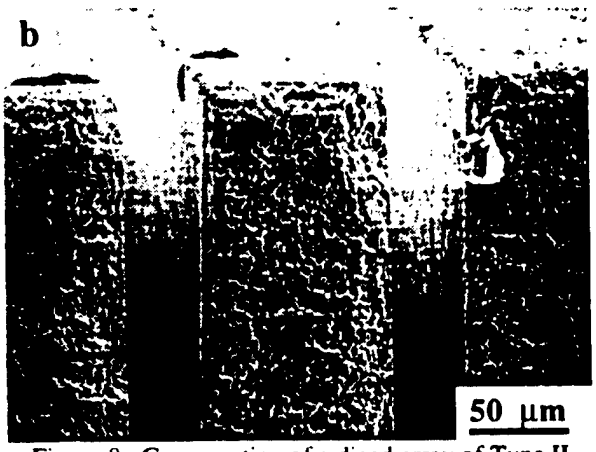

Figure 8: Cross section of a diced array of Type II ceramic from vendor 1.

4. HIGH ELECTRIC FIELD BEHAVIOR

To characterize the grain size effect on high field behavior (the operation domain of piezoelectric actuators), field induced strain in monolithic test pellets (10 mm diameter x 1 mm thick) was measured with a linear variable differential transformer (LVDT) and a programmable power supply. Samples were driven at ± 2.5 and ± 5 kV/cm with a sinusoidal varying electric field and to + 30 kV/cm with a linearly ramped electric field (unipolar drive). Results are shown in figures 9 through 11 for TRS200 and 200FG and in figures 12 through 13 for TRS600 and 600FG. For the Type II materials, despite the higher low field properties of the fine grain ceramics, the high field strain of these samples was slightly lower than that of the conventional ceramic. High field strain can be enhanced by reorientation of ferroelectric domains for which the field-aligned state is not stable. Thus, removal of the electric field causes these unstable domains to switch back to their unaligned state. The material is, therefore, partially repoled and depoled every time it is cycled. Though strain can be large in such a situation, hysteresis also tends to be large leading to detrimental effects such as heat generation and fatigue.

For the Type II materials studied, conventional coarse grained ceramic had a less stable domain state in the zero field condition as evidenced by its higher hysteresis and strain. This is especially evident during bipolar drive. The fine grain ceramic has higher low field properties because its domains remain more completely aligned after removal of the electric field. However, this also means there is less strain at high fields due to fewer contributions from domain reorientation. TEM studies suggest fine grain piezoelectrics have fewer domain orientation variants than coarse grained ceramic[3]. Therefore, it may be that the unstable domain orientations in conventional material do not exist in fine grain ceramic. With a more stable domain state and a smaller grain size to impede crack growth, the fine grain Type II material should be less susceptible to mechanical fatigue during cyclic driving. Work is in progress to see if this is the case.

Once again the situation is reversed for the Type VI material. Fine grain samples had reduced low field properties compared to conventional material, but the strain was higher for fine grain ceramic during high field unipolar drive. Thus, for the piezoelectrically "soft" Type VI materials, there is more domain instability in the fine grain ceramic than in the coarse grained material. TEM has not yet been done on these materials to see if grain size has the same effect on domain orientation variants as it does in Type II ceramic. A very high electric field is required to observe the domain instability in Type VI ceramic. For bipolar drive at both ± 2.5 and ± 5 kV/cm, the strain and hysteresis are lower for fine grain ceramic than for

coarse material. Only during unipolar driving at 30 kV/cm does the strain for fine grain Type VI ceramic increase above that of coarse grained material. It may be that for Type VI material, the grain size that causes a reduction in domain orientation variants is smaller than it is in Type II material. Thus, Type VI grain size would need to be further reduced before it behaves like the Type II ceramic.

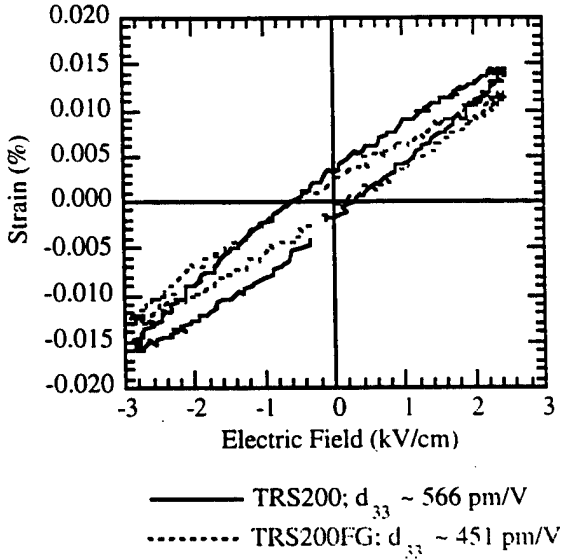

Figure 9: Strain for TRS200 and 200FG during bipolar drive at ± 2.5 kV/cm. d33's calculated from linear regression are shown.

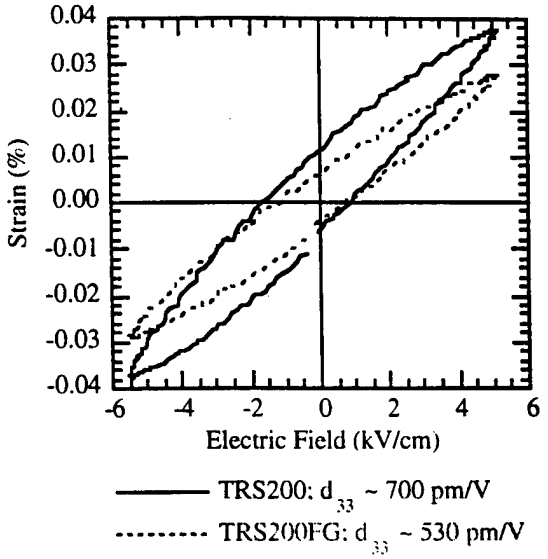

Figure 10: Strain for TRS200 and 200FG during bipolar drive at ± 5 kV/cm. d33's calculated from linear regression are shown.

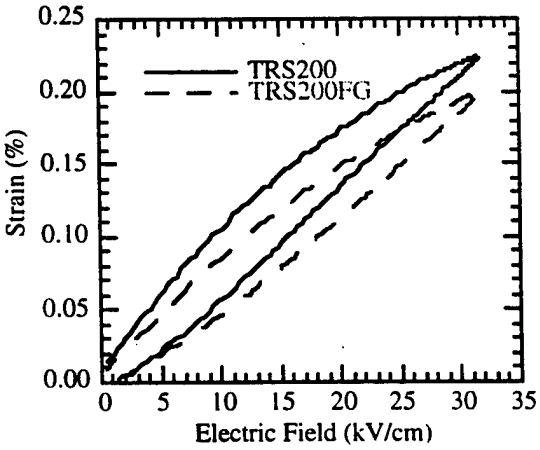

Figure 11: Strain for TRS200 and 200FG during unipolar driving to + 30 kV/cm.

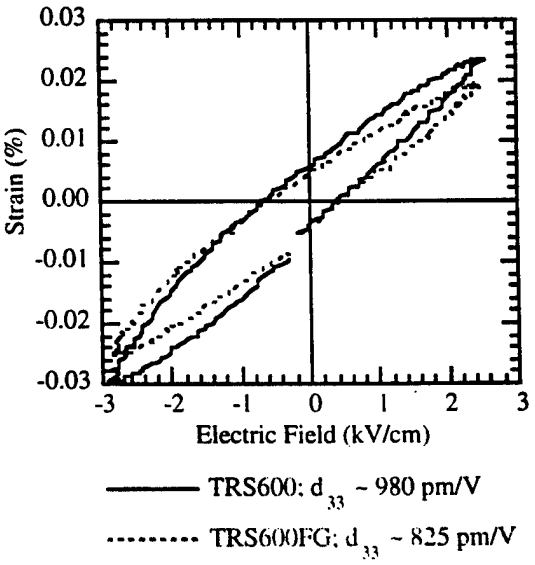

Figure 12: Strain for TRS600 and 600FG during bipolar drive at ± 2.5 kV/cm.

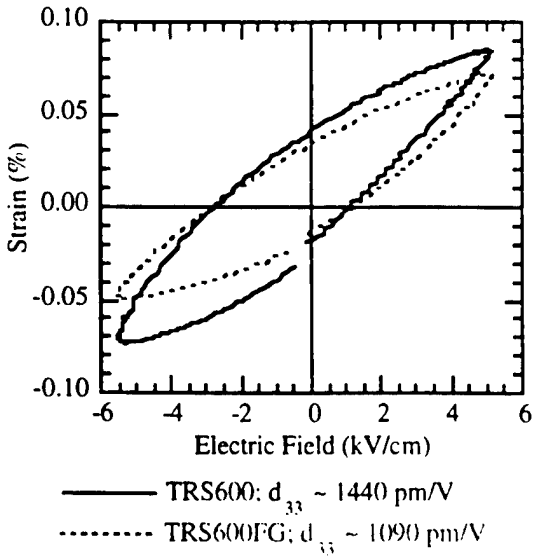

Figure 13: Strain for TRS600 and 600FG during bipolar drive at ± 5 kV/cm.

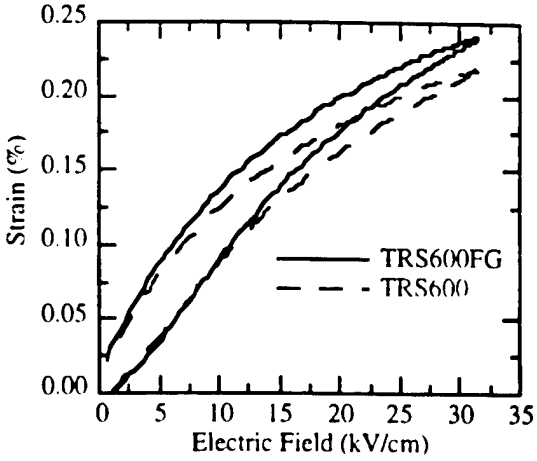

Figure 14: Strain for TRS600 and 600FG during unipolar drive at 30 kV/cm.

5. BEHAVIOR UNDER ELECTRICAL AND MECHANICAL BIAS

Many benefits can result from driving piezoelectric actuators with the AC electric field superimposed on a DC bias. Reduced hysteresis and higher driving fields without depoling are two examples. Comparisons of bipolar drive at ± 5 kV/cm with no bias and bipolar drive with a 10 kV/cm bias are shown in figure 15 for TRS600FG. There is a dramatic reduction in hysteresis for only a very slight decrease in strain. The bias field stabilizes the domain structure, while for normal bipolar driving the negative electric field portion of the cycle partially depoles the material leading to high hysteresis and heat generation. Mechanical bias or compressive prestress is also commonly applied to piezoelectric actuators to prevent the ceramic from being stressed in tension. The behavior of materials under prestress is an important factor in actuator design. Strain from fine grain and conventional ceramics was measured under prestress levels from 0 to 100 MPa using a load frame to apply the stress and strain gauges for the strain measurements. AC electric fields were applied with a period of 1 second. The AC fields were superimposed on DC bias's fields of 5 or 10 kV/cm. An example of the resulting strain data for TRS600FG is shown in figure 16, and figure 17 is a schematic of the load frame. In all cases compressive stress was applied before the samples were subjected to an electric field.

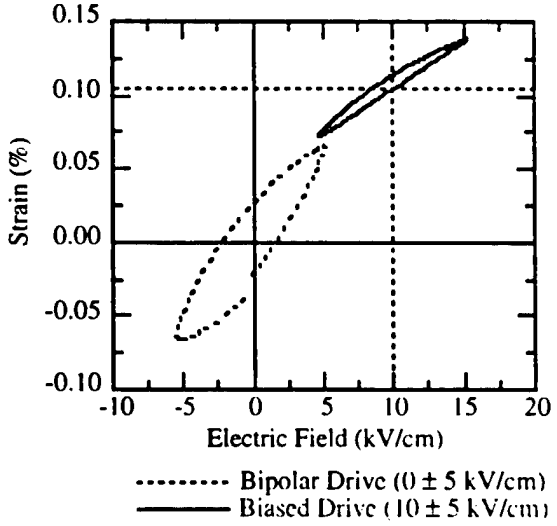

Figure 15: Comparison of biased and unbiased driving for TRS600FG.

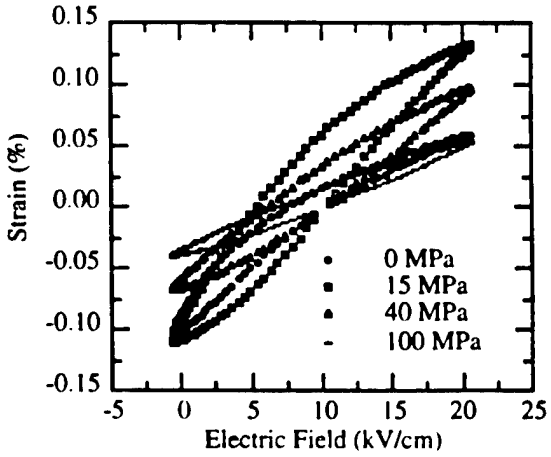

Figure 16: Strain resulting from driving TRS600FG with an AC field of ± 10 kV/cm superimposed on a DC bias of 10 kV/cm and with applied compressive stress from 0 to 100 MPa.

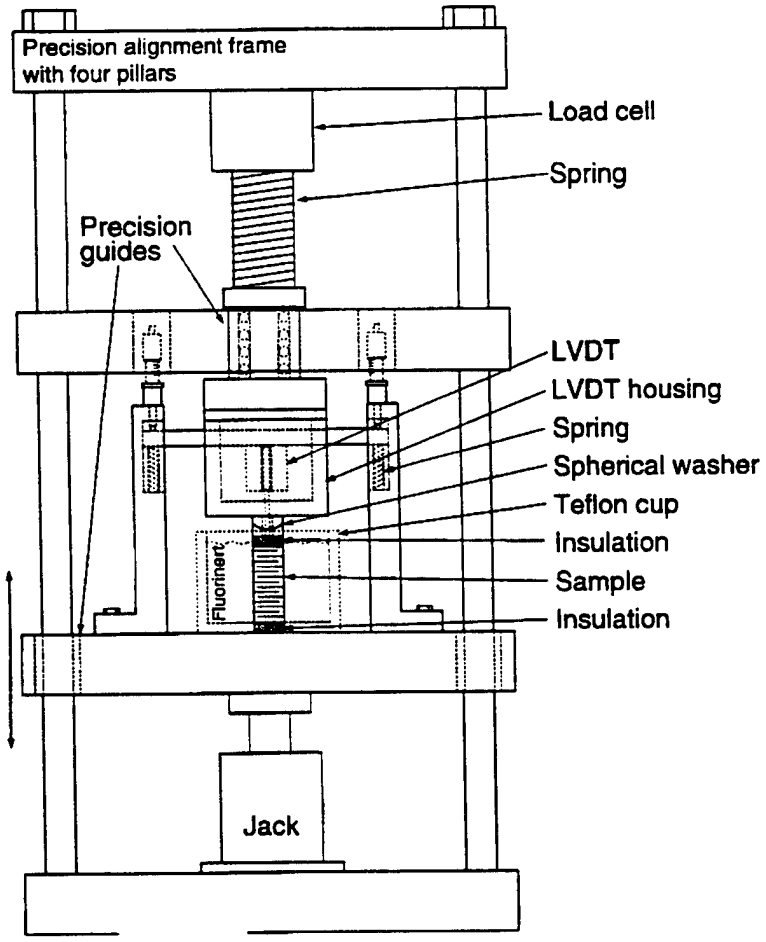

Figure 17: Load frame used to perform the prestress measurements.

Strain *vs.* driving conditions and prestress level for the four materials is shown in figures 18 through 21. There is very little dependence of strain behavior on bias field. For Type VI ceramic, the small increase in strain at low bias fields and stress levels results from reduced clamping of domain wall motion compared to higher bias levels (*i.e.* the 10 kV/cm bias is closer to the saturation region of the material's strain *vs.* field curve than the lower bias field). The Type VI materials exhibited increases in strain as prestress was increased from 0 to about 20 MPa. Above 20 MPa field induced strain decreased with stress. Type VI materials become depoled as compressive stress is applied, but application of a electric field repolarizes the material. This can be seen in figure 22, a comparison of polarization induced during driving under compressive prestress at ± 10 kV/cm around a 10 kV/cm bias. Since the bias field prevents depolarization from an electric field opposite in polarity to the ceramic, the observed effects in figure 22 are all due to the applied stress.

For the Type VI material, induced polarization continually increases with increasing stress until about 20 MPa where the polarization levels off. For the 600FG material, polarization decreases again above 40 MPa. These data further support the premise that there is a domain instability in the Type VI fine grain material. For the conventional ceramic, applying prestress above 20 MPa does not cause more depolarization than can be made up by the applied field. Strain then decreases above this stress level because the generative force of the piezoelectric effect at the applied field levels is not enough to completely counteract the applied stress. Since the polarization is constant above a prestress of 20 MPa, the reduction in strain above that level is not caused by depolariztion. The situation is different for the Type VI fine grain. Here polarization increases up to 20 MPa as in the previous case, but above 40 MPa induced polarization decreases causing a more rapid decrease in strain with stress than is observed in the conventional material. This behavior could be explained by a partial depolarization of an unstable domain state which can not be reoriented at stresses above 40 MPa with the fields applied in the experiment.

In the case of the Type II material, the data further support an extremely stable domain state in the fine grain ceramic. Stress causes the strain to continually decrease in the Type II fine grain material, but the polarization data indicate that none of this is due to depolarization. Induced polarization shows no dependence on applied stress. The decrease in strain is simply due to the balance between piezoelectric generative force and the applied compressive force. This is a particularly attractive feature for an actuator material, as excessive domain reorientation can lead to heating and fatigue, limiting device lifetime. Some depolarization with stress is observed in the conventional Type II material although it is still much less than the Type VI ceramic.

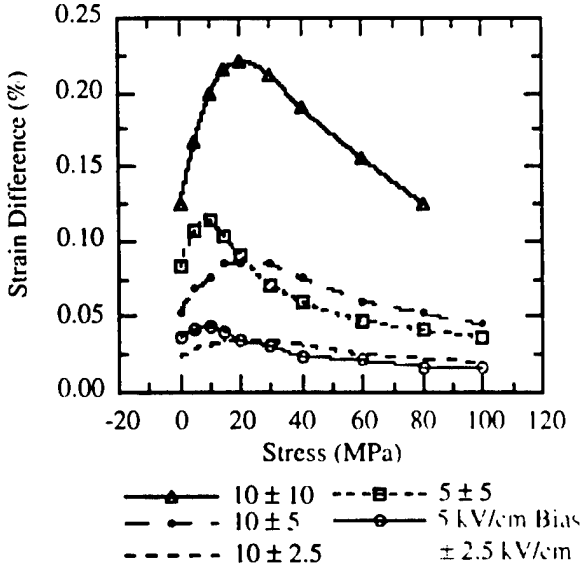

Figure 18: Total strain *vs.* prestress and driving conditions for TRS600.

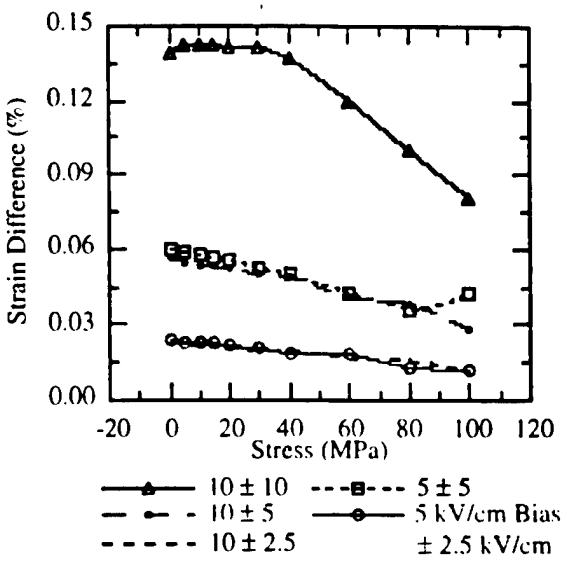

Figure 20: Total strain *vs.* prestress and driving conditions for TRS200.

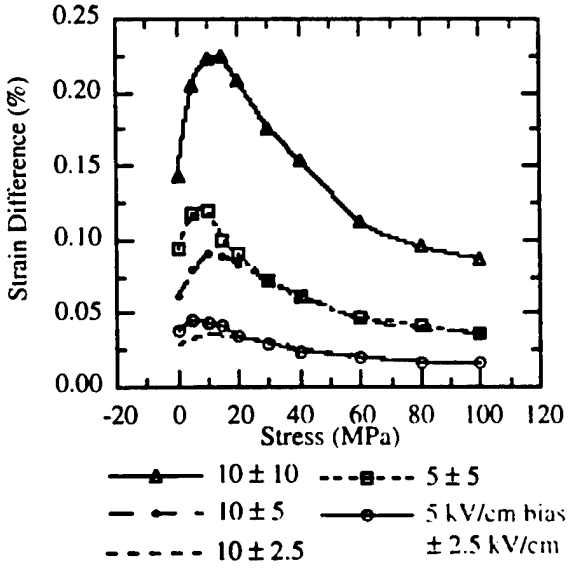

Figure 19: Total strain *vs.* prestress and driving condition for TRS600FG.

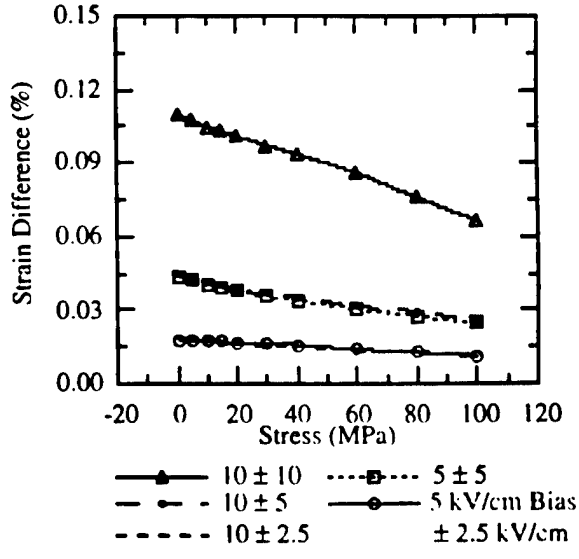

Figure 21: Total strain *vs.* prestress and driving condition for TRS200FG

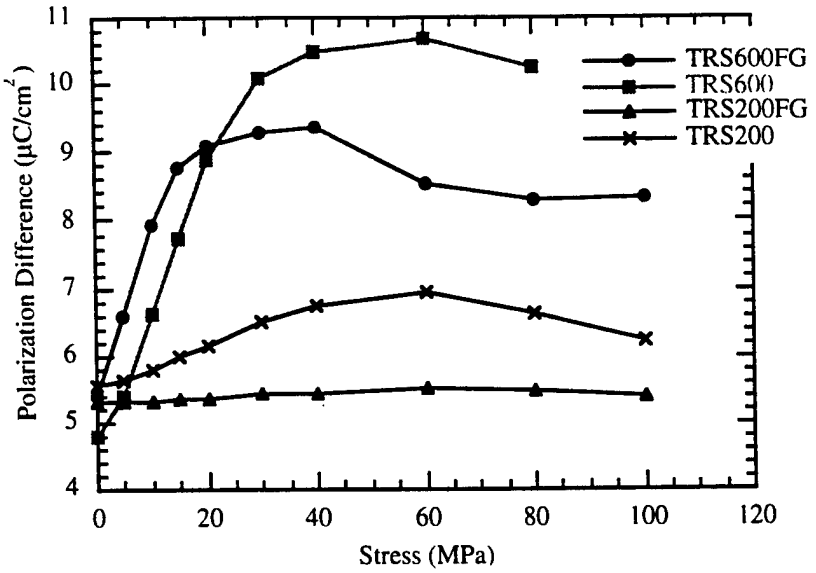

Figure 22: Induced polarization *vs.* compressive stress during driving at ± 10 kV/cm around a bias of 10 kV/cm.

6. CONCLUSION

The effect of grain size on piezoelectric properties important for actuator applications was investigated for Type II and VI ceramics. Chemical compensation of property degradation with grain size successfully resulted in Type II ceramics with higher low field piezoelectric and dielectric properties than conventional material. Fine grain ceramics have been shown to exhibit at least a 20% improvement in mechanical strength over coarse grained material, and in precision dicing studies, fine grain ceramics have been shown to be more machinable. High field measurements and response to compressive prestress have shown that fine grain Type VI ceramics have a domain instability which results in higher field induced strain than is achievable with conventional material. Prestress measurements of fine grain Type II ceramic revealed that this material has an extremely stable domain structure making it a promising candidate for high reliability piezoelectric actuators.

ACKNOWLEDGMENTS

The authors would like to thank the Office of Naval Research and the Defense Advanced Projects Research Agency for funding this work. We would also like to acknowledge Tim Ritter of Blatek, Inc. for performing the precision dicing study.

REFERENCES

1. C. S. Lynch, "Fracture of Ferroelectric and Relaxor Electro-Ceramics: Influence of Electric Field", accepted for publication in *J. Am. Ceram. Soc.*

2. N. Kim, Ph.D. Thesis, "Grain Size Effects on the Dielectric and Piezoelectric Properties in Compositions near the Morphotropic Phase Boundary of Lead Zirconate-Titanate Based Ceramics", The Pennsylvania State University, 1994.

3. W. Cao and C. A. Randall, "Grain Size and Domain Size Relations in Bulk Ceramic Ferroelectric Materials", *J. Phys. Chem. Solids*, **57** [10], pp. 1499-1505, 1996.

4. *IRE Standards on Piezoelectric Crystals: Measurements of Piezoelectric Ceramics, 1961*, IEEE, New York, NY, 1961.

5. ASTM Standard C1161-94, "Standard Test Method for Flexural Strength of Advanced Ceramics at Ambient Temperature", 1994.

6. T. Yamamoto, H. Igarashi, and K. Okazaki, *Ceramics International*, **11**, p. 75, 1985.

APPENDIX 14

J. Appl. Phys. (in press 1998).

SHEAR RESPONSE OF LEAD ZIRCONATE TITANATE PIEZOCERAMICS

VOLKMAR MUELLER* and Q.M. ZHANG
Materials Research Laboratory, Pennsylvania State University, University Park, PA 16802, USA

*present address: FB Physik, Universität Halle, F.-Bach-Platz 6, D-06108 Halle, Germany

The piezoelectric shear strain S_5 of several commercially available lead zirconate titanate (PZT) piezoceramics was evaluated under non resonant conditions in a sinusoidal ac-field $E_1(t)$ directed perpendicular to the poling direction. Results obtained on donor doped (soft PZT) and acceptor doped (hard PZT) ceramics are compared. At fields sufficiently below the limiting field E_{lim} necessary to electrically depole the sample, we find a linear, nonhysteretic relationship between S_5 and the polarization P_1. In soft PZT ceramics, the effective piezoelectric shear coefficient $d_{15}=S_5/E_1$ shows a pronounced ac-field dependence which was fitted according to $d_{15}(E_1)=d_{lin}[1+(d_{nl}E_1)^{\alpha}]$ with $\alpha\approx1.2$. The results indicate that irreversible motion of non-180° walls causes the nonlinearity of PZT and the contribution of 180° walls to the linear and nonlinear coefficients is negligible. The analysis of the relationship between linear and nonlinear coefficients obtained at different ceramic systems leads us to the suggestion that another extrinsic contribution to the permittivity exists in PZT which may not be attributed to domain wall motion but related to the dielectric dispersion at microwave frequencies.

PACS No.: 77.80.Dj,64.70.Rh

Introduction

Several ferroelectric materials have gained a considerable importance for industrial applications due to their unique piezoelectric properties.[1] Among them, poled lead zirconate titanate (PZT, $Pb(Zr_xTi_{(1-x)}O_3)$ and related piezoceramics are of particular interest because this material system is widely used for actuators, sensors and transducers.[2] In most actuators produced up to now, the electric field is applied parallel to the polar axis of the piezoceramic in order to obtain displacements u_3 and u_1 parallel and perpendicular to this axis, respectively. Accordingly, a large number of experimental work was conducted[1] to investigate various features related to the corresponding piezocoefficients d_{33} and d_{31} and to separate intrinsic properties (of a hypothetic ceramic consisting of single domain grains) from extrinsic contributions to these coefficients which are assumed to be due to domain wall and phase boundary motion.[1,3-12] It was found that both piezoelectric and dielectric coefficients of PZT can be adjusted in a wide range by tuning the defect chemistry of the ceramic.[1,2] This was attributed to dopants influencing the activity of domain walls in the piezoceramics. Generally speaking, donor doped PZTs have an exceptionally high domain wall mobility whereas acceptor dopants supress the domain wall response.[1,3] In what follows we refer to donor (acceptor) doped PZT as soft (hard) PZT.

Much less is known about the piezoelectric coefficient d_{15} related to the shear strain S_5 which will be induced if the electric field is applied perpendicular to the polar axis. However, new generations of piezoelectric actuators, for example torsional actuators, may make use of the piezoelectric shear response of piezoceramics. The data available indicates that dopants effect d_{15} in a similar way as d_{33} and d_{31} which is in agreement with theoretical considerations[12,13] which show that contributions to S_5 occur due to field induced displacements of (ferroelastic) non-180° walls. Most of the d_{15} data, however, were obtained using resonance techniques at frequencies much higher than the operating frequency range of typical actuators. More important, due to dielectric heating at high driving levels, resonance methods are not well suited for studying the ac-field dependence of piezoelectric properties. On the other hand, a first measurement of d_{15} at low frequencies revealed a pronounced increase of d_{15} with increasing amplitude of the ac-field.[8] Obviously, the actuator performance will be enhanced due to this nonlinearity if the device is driven in high fields. In a previous paper, we found indication that a threshold for the onset of piezoelectric nonlinearity exists in soft PZT at $E_c \approx 100V/cm$.[14] Above threshold, the ac-field dependence of piezoelectric and dielectric coefficients obeys a non-analytic scaling law which seems to reflect a universal behavior of soft PZT. This scaling behavior of PZT may be useful in finding a limited set of nonlinear coefficients which characterize the ac-field dependence of piezoelectric properties of a given ceramic completely.

Another problem which has to be addressed for future actuator applications is the depoling of the ceramic due to the driving field which sets in at a limiting field E_{lim}. Clearly, E_{lim} determines besides the linear and nonlinear piezocoefficients the maximum attainable strain S_5^{max}.

In this paper, the piezoelectric shear strain S_5 of several commercially available soft and hard PZT-ceramics was investigated. The frequency of the measuring ac-field was $f=100Hz$ which is within the operating range of most actuator applications. The amplitude $E_1^{(ac)}$ of the ac-field oriented perpendicular to the poling direction was gradually increased until the sample was depoled electrically. We present data describing both the dependence $S_5(P_1)$ between shear strain and polarization and $d_{15}(E_1^{(ac)})$ between the effective

piezocoefficient $d_{15}=S_5/E_1^{(ac)}$ and the ac-field amplitude. Note that both 180° and non-180° walls contribute to the permittivity of the material whereas the piezocoefficient is influenced by the motion of non 180° walls only. For this reason, both the piezoelectric and the dielectric nonlinearity of the piezoceramics was analyzed and related to the corresponding small signal coefficients. From the results, we will argue that several extrinsic mechanisms contribute to the small signal permittivity both in soft and hard PZT whereas irreversible motion of non-180° domain walls seems to be the only major source of nonlinearity in PZT-piezoceramics.

2. Experimental

The material systems under investigation were exclusively commercially available piezoceramics. We considered both soft PZT (Tokin N-10, N-21; Motorola 3203HD; Morgan Matroc PZT-5H and PZT-5A and EDO PZT-5A) and hard PZT (Morgan Matroc PZT-4D and PZT-8). The Curie temperatures of the ceramics examined cover a wide temperature range $145K<T_c<365K$.[15] Samples were cut as parallelepipeds (typical dimension $5\times5\times8mm^3$ for soft PZT and $1.5\times5\times8mm^3$ for hard PZT) and polished. After that they were cleaned first in acetone and then in deionized water followed by drying to eliminate residual water. Au-electrodes were sputtered on the major faces in such a way that the harmonic measuring field (f=100Hz) was directed perpendicular to the poling direction.

The sample was glued with its bottom electrode on a stage and a mirror was placed on the top electrode of the sample from which the shear displacement was measured by an optical displacement sensor (MTI 2000). The output signal of the optical fiber sensor was fed both to a lock-in amplifier to detect the first harmonic component $S_5^{(1f)}$ and, for sufficiently large signals, to a digital oscilloscope which displayed the whole $S_5(E_1)$ relationship. From these data, the effective piezoelectric coefficient $d_{15}=S_5^{(1f)}/E_1^{(ac)}$ was obtained, where $E_1^{(ac)}$ is the amplitude of the measuring field. Before each measurement was performed, the whole setup was calibrated by measuring the signal due to the static sample displacement controlled by a micrometer screw.

The field dependence $D_1(E_1)$ of the dielectric displacement measured by a Sawyer-Tower circuit[16] was displayed simultaneously on the second channel of the oscilloscope and analyzed in its fundamental harmonic $D_1^{(1f)}$ by another lock-in amplifier. This yields information about the effective dielectric coefficient $\varepsilon_{11}=D_1^{(1f)}/E_1^{(ac)}$.

All measurements were performed at room temperature. In order to estimate the effect of dielectric heating, measurements were additionally performed in the tone burst mode were the sample was excited by pulses containing ten 100Hz sinusoidal waves with a 3 second dead time and the results were compared with those obtained in the continous wave mode.

3. Results and Discussion

For all PZTs examined, the piezoelectric shear strain S_5 exhibits a very similar behavior, i.e. it increases non-linearly with the amplitude of the ac-field until the electrical depoling of the sample sets in at E_{lim} (Fig. 1). Therefore, in addition to the weak signal piezoelectric coefficient, the depoling behavior and the piezoelectric nonlinearity clearly also determine the suitability of a piezoceramic in actuators. In what follows, both of these issues will be

addressed in detail.

3.1 Electrically depoling in fields perpendicular to the poling direction

Electrically depoling involves all field induced processes which lead to a total or partial loss of the preferable orientation of the polarization vector of the grains which was attained during the poling of the ceramic. Depoling processes occur in our measuring geometry at lower fields because external field and poling direction are not parallel as in other piezoelectric devices using longitudinal strain S_1 and S_3. Roughly speaking, the mean polarization vector of the ceramic has to be distorted by 90° only instead of 180° to depole the sample.

As the poling process itself, electrically depoling is strongly related to irreversible changes of the domain structure and depends on a variety of experimental conditions such as temperature, amplitude and frequency of the external field, time, sample history and electrodes. At fields sufficiently smaller than E_{lim}, the data obtained in the continous wave and tone burst mode are almost identical indicating that dielectric heating of the sample can be neglected. During depoling, however, a strong temperature increase was observed. Additionally, electrical depoling was preceded by a time dependent relaxation of both piezoelectric and dielectric coefficients, that is, for a given amplitude of the electric field, the corresponding values of polarization and strain are not constant but vary with time. This relaxation seems not to be attributed exclusively to the change of the sample temperature due to dielectric and mechanical heating. At a field just below the depoling field, this relaxation leads to an increase of the polarization and the strain. As the field is increased further, the polarization will remain to increase with time whereas the shear strain starts to decrease, indicating the onset of depoling.

For some of the samples, the experiment carried out in the continous wave mode was terminated right at this point and then the measurement was continued in the tone burst mode. In this mode, the measurement could be extended to considerably higher field strengths before the sample was totally depoled. In Table I, we consider the depoling field E_{lim} to be that at which depoling starts within a few seconds after adjusting a higher field level in the continous wave and tone burst mode, respectively. It should be noted that the sample history may influence the result and fatigue and electrical depoling processes may be related. Nevertheless, it is obvious from the data presented in Table I that it is neither the softest nor the hardest materials which have the highest strain response available at E_{lim} despite they show the highest piezocoefficient and depoling field, respectively.

In addition to a loss of piezoelectricity in the sample, depoling is also accompanied by the creation of sparks at the edges of the sample. This is unique to the depoling by a field E_1 perpendicular to the original poling direction and is related to charges on the unelectroded faces of the sample which were initially compensated by the bound domain charge of the poled sample and are released when the orientation of these domains is changed during electrical driving. Changes in the domain structure manifest itself at fields close below E_{lim} by a steep increase of the ratio ε_{11}/d_{15} indicating a corresponding increase of the ratio between 180° and non-180° walls (Fig. 2). At the same time, the strain-polarization dependence which is linear and nonhysteretic in lower fields becomes hysteretic and nonlinear. Apparently, new 180° walls are created temporarily in some grains as depoling field is approached before the polarization vector is reoriented irreversibly at E_{lim}.

3.2 Nonlinear piezoelectric behavior

We analyze now the piezoelectric behavior at ac-fields well below E_{lim}. Although the field dependence $P_1(E_1)$ and $S_5(E_1)$ of polarization and shear strain is nonlinear and hysteretic which indicates the contribution of non-180° domain wall and phase boundary motion in this field range, the strain-polarization relationship is nonhysteretic and linear. Accordingly, the relationship between shear strain and polarization amplitude induced in the ceramic by the harmonic ac-field can be fitted according to

$$S_5^{(1f)} = g_{15} [P_1^{(1f)}]^c \qquad (1)$$

which results in an exponent $c \approx 1$ (Fig. 3 and Table II) for both soft and hard materials. Apparently, the ratio between dielectric active 180° and dielectric and piezoelectric active non-180° walls in the piezoceramics remains approximately constant and mainly dielectric loss mechanisms contribute to the piezoelectric loss at the measuring frequency.

The effective piezocoefficient g_{15} defined in eq.(1) exhibits a significant material dependence (Table II). Generally speaking, g_{15} decreases with increasing permittivity and piezocoefficient, respectively, of the particular piezoceramic. Due to the centrosymmetric paraelectric phase of the PZT-ceramics, g_{15} can be reduced to an effective electrostrictive coefficient

$$Q_{135} = g_{15} / 2P_3 \qquad (2)$$

where $P_3 \approx P_{spont}$ is the polarization induced in 3-direction during poling of the ceramic. In a single domain single crystal with a second order phase transition, g_{15} would obey therefore the same temperature dependence $g_{15} \sim (T_c-T)^{1/2}$ as the spontaneous polarization of the crystal, where T_c is the Curie-temperature. The double logarithmic plot of g_{15} versus T_c, taken from the data sheets of the manufacturer, results in a straight line with a slope $n=0.44$ for all soft PZT ceramics examined except for Tokin N-21 (Fig. 4). We conclude that different g_{15} values obtained in this group of ceramics result mainly from differences in T_c due to the different dopant level in the materials and all ceramics have approximately the same nearly temperature independent Q_{135} coefficient.

We consider now the ac-field dependence of effective coefficients ε_{11} and d_{15} defined above which should not be mistaken with the small signal values $\varepsilon_{11}^{(0)} = \partial D_1/\partial E_1$ and $d_{15}^{(0)} = \partial S_5/\partial E_1$ of permittivity and piezomodul, respectively. In a soft PZT-piezoceramic, we find qualitatively the same ac-field dependence for dielectric and piezoelectric data (Fig. 5) which is in agreement with previous findings.[8] On the other hand, the nonlinearity is more pronounced for the coefficients ε_{11} and d_{15} which were obtained in fields perpendicular to the poling direction than for the longitudinal coefficients ε_{33} and d_{33}. Most important, the data clearly shows that the nonlinear contribution to the total strain response in soft PZT plays a major role already at fields well below the depoling field. Clearly, the linear piezoelectric coefficients determined at a low measuring voltage are insufficient to describe the performance of a PZTpiezoceramic in an actuator application. In order to evaluate ceramic materials of various kind, it is therefore highly desirable to find a limited number of nonlinear coefficients which enable one to describe the $S_5(E)$ dependence of a given ceramic material as simply as possible.

Apparently, the nonlinear behavior of PZT is related to the activity of domain walls in PZT since the intrinsic nonlinearity of the material should be negligibly small at temperatures far below T_c. Though the specific mechanism leading to the nonlinear domain wall response is unknown, it was suggested that it is attributed to the potential energy of the wall.[8] This can be described phenomenologically assuming an anharmonic potential $U(\Delta x)$ of a wall displaced by the distance Δx from its equilibrium position. Accordingly, it should be possible to expand the domain wall contribution to piezoelectric shear strain and dielectric displacement in a Taylor expansion in terms of E_1 and the higher order coefficients may be used to characterize the nonlinear behavior of the piezoceramic. For symmetry reasons, the Taylor expansion of $S_5(E_1)$ and $D_1(E_1)$

$$S_5(E_1) = S_5^{(0)} + d_{15}^{(0)} E_1 + d_{1115} E_1^3 + \ldots$$
$$D_1(E_1) = D_1^{(0)} + \epsilon_{11}^{(0)} E_1 + \epsilon_{1111} E_1^3 + \ldots \qquad (3)$$

will contain only odd order terms of E_1 because these coefficients describe the response in a field perpendicular to the poling direction of the ceramic. If a harmonic field $E_1 = E_1^{(ac)}\cos(\omega t)$ is applied, we find from the fundamental harmonic of the Fourier-series of strain and polarization, respectively, the effective coefficients

$$d_{15} = d_{15}^{(0)} + \frac{3}{4} d_{1115} (E_1^{(ac)})^2 + \ldots$$
$$\epsilon_{11} = \epsilon_{11}^{(0)} + \frac{3}{4} \epsilon_{1111} (E_1^{(ac)})^2 + \ldots \qquad (4)$$

The double logarithmic plot of the nonlinear part of the effective coefficients $\Delta\varepsilon_{11} = \varepsilon_{11}(E_1^{(ac)}) - \varepsilon_{11}^{(0)}$ and $\Delta d_{15} = d_{15}(E_1^{(ac)}) - d_{15}^{(0)}$, respectively, versus the ac-field amplitude provides straight lines for $E > 100$V/cm (Fig. 6) as it might be expected from eq.(3) assuming that higher order than quadratic terms can be neglected. The slope of the lines $n \approx 1.2$, however, is much smaller than it follows from eq.(4) and can also not be explained if a reasonable number of higher order terms would be taken into account in the Taylor-expansion (eq.(3)).

In a previous paper, we have shown that the experimental data obtained at various soft PZT piezoceramics are consistent with the assumption that a threshold for the onset of nonlinearity in these materials exists at $E_{c1} \approx 100$V/cm.[14] Above threshold, a non-analytic scaling behavior according to

$$\Delta d_{15} = B(E_1^{(ac)} - E_{c1})^{\phi}$$
$$\Delta \epsilon_{11} = A(E_1^{(ac)} - E_{c1})^{\phi} \qquad (5)$$

characterized by effective coefficients $\phi \approx 1.2$ was observed. This behavior was found in very different ceramic systems with respect to the type and level of dopants and its Curie temperature and seems to be therefore a universal property of soft PZT piezoceramics.

Apparently, the threshold at E_{c1} is connected with the onset of irreversible domain wall motion in the PZT piezoceramic. Though the reason for the nonlinearity is not clear yet, we can exclude from the experimental results mechanisms which will influence the potential energy of the wall. Instead we like to point out that theoretical models[17,18] treating the depinning threshold of elastic interfaces as a dynamical critical phenomena predict a critical behavior of the interface velocity according to

$$v\,(F-F_c)^{\xi} \qquad (6)$$

where F is the driving force, F_c the critical force necessary to depin the interface and ξ a critical exponent depending on the dimension of the system. No experimental data are available for fields within the critical regions in the sense of the theoretical models mentioned above. Nevertheless it is amazing that the effective exponents characterizing the piezoelectric and dielectric nonlinearity of soft PZT piezoceramics seem to be consistent with the mean field result $\xi = 1.5$ of the theoretical considerations.[17]

More theoretical and experimental work is necessary to clarify whether the dynamics of domain walls moving in a random pinning medium causes the peculiar nonlinear behavior of soft PZT. On the other hand, the nonlinearity of dielectric and piezoelectric coefficients is practically the same which indicates that exclusively non-180° wall motion is involved. As we have shown at the beginning of this paper on the basis of the linear $S_5^{(1f)}(P_1^{(1f)})$ dependence, the ratio between active 180° and non-180° walls does not change with the ac-field amplitude. Considering the large difference in the wall energy between the 180° and the non-180° wall,[16] it seems unlikely that both types of walls exhibit the same threshold behavior and the ratio between them remains constant above threshold. Therefore, it seems to be reasonable to conclude that very few dielectrically active 180° walls remain in the piezoceramic after poling which is in agreement with results of other studies.[19-21]

It should be pointed out that it is quite difficult to determine the threshold field E_{c1} in eq.(5) accurately because of deaging phenomena which result in a poorly defined $\varepsilon_{11}^{(0)}$ and $d_{15}^{(0)}$ and the existence of another threshold at lower fields $E_{c2} \approx 1$V/cm.[14] For data at fields $E_1^{(ac)} > 100$V/cm in soft PZT, the data are described reasonably well by

$$d_{15} = d_{lin}\,[1 + (d_{nl} E_1^{(ac)})^{b}]$$
$$\epsilon_{11} = \epsilon_{lin}\,[1 + (\epsilon_{nl} E_1^{(ac)})^{a}] \qquad (7)$$

The additional parameters ε_{nl}, d_{nl} and the exponents a,b are sufficient to describe the nonlinear behavior of soft PZT piezoceramics above E_c completely (Fig. 7).

The nonlinear behavior of hard PZT-ceramics, however, is different (Fig. 8). First, the dielectric and piezoelectric coefficients increase steeply, which may be related to deaging effects.[22] Only above a threshold field $E_c^{hard} \approx 1000$-2000V/cm which is much higher than that in soft PZT, the nonlinearity can be fitted according to eq.(7).

Apparently, domain wall pinning is more efficient in hard PZT which may be due to the presence of extended defects. Moreover, no single threshold field for the onset of irreversible motion of *all* walls seems to exist but every wall has apparently an individual threshold depending on its individual defect environment. Consequently, the domain walls are gradually released with increasing ac-field. The steep increase of the piezoelectric activity for $E_1^{(ac)} < E_c^{hard}$ may be attributed to the increasing number of active domain walls. The apparent threshold E_c^{hard} may therefore mark the field for which nearly all domain walls are released and the number of active walls does not increase further. Consequently, hard PZT piezoceramic exhibit for $E_1^{(ac)} > E_c^{hard}$ qualitatively the same nonlinear behavior as soft PZT.

The fitting parameter obtained at $E_1^{(ac)} > 100$V/cm and $E_1^{(ac)} > E_c^{hard}$ in soft and hard PZT, respectively, are listed in Table II. Apparently, the influence of dopants on the linear and nonlinear piezoelectric coefficients is similar whereas no significant influence is discernible on the value of the exponent b. In order to compare the nonlinearity of different

materials, it is more convenient to deal with fixed exponents a = 1.2 and b = 1.2, respectively, even if this makes the accuracy of the fit worse for some materials. For the materials examined, a nearly linear relationship exists between nonlinear dielectric and piezoelectric coefficients determined in this manner (Fig. 9). Particularly, the linear fit crosses the origin of the coordinate system. Therefore, there seems to be no dielectric nonlinearity without corresponding piezoelectric nonlinearity. This provides another indication that it is exclusively the non-180° walls which cause the nonlinear dielectric behavior of PZT-piezoceramics.

Moreover, there seems to be a relationship betweeen the linear and nonlinear dielectric coefficients (Fig. 10) obtained on several ceramics. Tentatively, a linear relationship is assumed here for the sake of simplicity. In this scenario, the linear fit of the data presented in Fig. 10 intersects the horizontal axis at a value $\varepsilon^{(nd)} \approx 1100$ which is close to the permittivity of the hardest ceramic (PZT-8) investigated. The assumption of a similar relationship between the corresponding piezoelectric coefficients leads to a value $d_{15}^{(nd)} \approx$ 400pC/N.

Clearly, the small signal dielectric response of the ceramic depends strongly on the dopants. Starting from $\varepsilon^{(nd)}$, which is quite close to the permittivity of the hardest ceramic examined, the permittivity can be increased by $\Delta\varepsilon^{(dom)}$ in dependence on the amount and type of dopants introduced. In parallel, the nonlinear coefficient which is negligibly small in the hardest ceramic increases in a similar way. Apparently, the increased activity of non-180° domain walls which is believed to be the reason for the enhanced permittivity of donor doped ceramics leads also to an increase of the nonlinear coefficient due to the irreversible motion of these walls above threshold.

On the other hand, the very small nonlinearity of the hardest PZT ceramic indicates a small domain wall activity and it may be argued that the domain contribution to the small signal permittivity in this material is negligible as well. Indeed, despite the very different Curie temperatures of the materials examined, all ceramics have apparently almost the same background permittivity $\varepsilon^{(nd)} \approx 1100$ for which domain wall related nonlinearity vanishes. We are aware that $\varepsilon^{(nd)}$ is not well defined because the assumption of a proportionality $\varepsilon_{nl} \sim \Delta\varepsilon^{(dom)}$ may be oversimplified and data obtained at soft and hard PZT should be analyzed separately. However, any reasonable extrapolation of the experimental data seems to give a value $\varepsilon^{(nd)}$ which is significantly higher than the intrinsic contribution $\varepsilon^{(int)} \approx 400$.[7,23] Apparently, besides the intrinsic contribution to the permittivity and the normal domain wall motion related dielectric contribution considered up to now, a second extrinsic mechanism exists which contributes at room temperature to the permittivity in all the materials examined and seems to be nearly independent on the doping level of the ceramic. Note that this mechanism may freeze in at low temperatures in a similar way as the dielectric domain wall contribution. Therefore, our assumption is not in contradiction with a former study[7] in which was shown that the permittivity of PZT measured at low temperatures does not depend on dopants.

The value of $\varepsilon^{(nd)}$ determined from the present data is close to the relaxor strength of a non-Debye relaxation found in an undoped PZT composition near the morphotropic phase boundary.[23] Due to its temperature independent relaxation frequency $f_r \approx 700$MHz, it was argued that neither the soft mode nor domain wall motion causes this dielectric contribution. In an alternative model, Arlt and coworkers[24] proposed that ferroelastic domains may contribute to the permittivity up to microwave frequencies. Due to the fact that every increase of the domain wall mobility in PZT achieved by doping apparently manifests itself in an increase of the small signal permittivity *and* of the nonlinear dielectric coefficient, we

conclude that the contribution $\Delta\varepsilon^{(nd)}=\varepsilon^{(nd)}-\varepsilon^{(int)}$ of the second extrinsic mechanism leading to the high frequency dispersion of PZT is not necessarily related to the motion of domain walls. At least it is unlikely that classical non-180° walls, which activity depends strongly on the doping level and which we have shown to cause nonlinearity above threshold, are related to this mechanism. Because high frequency data of piezoelectric coefficients are not available, it remains unclear whether this second extrinsic mechanism influences also the piezoelectric activity.

4. Conclusions

Commercial available PZT-piezoceramics with different doping level were examined with respect to their suitability in future shear actuator applications. The results show that it is neither the softest nor the hardest materials which produces the highest piezoelectric shear strain. In the field range well below the depoling field, a linear, nonhysteretic strain polarization relationship was observed which may be of importance for high accuracy positioning control. We conclude, that in these field range no domains are nucleated or annihilated but movements of existing domain walls contribute to S_5.

The unique scaling behavior above threshold for the onset of nonlinearity in PZT enabled us to define two additional nonlinear piezoelectric and dielectric parameters, respectively, which characterize the piezoelectric and dielectric nonlinearity of the material completely. The comparison of parameters obtained on different ceramic systems shows a strong correlation between the piezoelectric and dielectric nonlinearity in PZT which gives another indication that the nonlinearity is exclusively caused by the onset of irreversible non-180° wall motion. The data seems also to indicate a relationship between domain wall related linear and nonlinear contributions. We note that ceramics in which the nonlinearity and therefore also the domain wall contribution to the linear coefficient is negligibly small have nevertheless a small signal permittivity much higher than the intrinsic value. It may be concluded, that a second extrinsic mechanism contributes to the permittivity of PZT which is not necessarily related to domain wall motion but is connected with the non-Debye relaxation at microwave frequencies.

5. Acknowledgement

The authors gratefully acknowledge stimulating discussions with Dr. Jan Fousek and Dr. Eric Cross. This work was supported by the Office of Naval Research.

References

1 B. Jaffe, J. Cook, H. Jaffe, Piezoelectric Ceramics , (Academic Press, London 1971).

2 L.E. Cross, Ferroelectric Ceramics: Tailoring Properties for Specific Applications in Ferroelectric Ceramics , edited by N. Setter and E.L. Colla (Birkhaeuser Verlag, Basel 1993).

3 V. A. Isupov, Ferroelectrics, **46**, 217 (1983).

4 G. Arlt, Ferroelectrics, **76**, 451 (1987).

5 G. Arlt, H. Dederichs, and R. Herbiet, Ferroelectrics **74**, 37 (1987).

6 R. Herbiet, U. Robels, H. Dederichs, and G. Arlt, Ferroelectrics **98**, 189 (1989).

7 X.L. Zhang, Z.X. Chen, L.E. Cross, and W.A. Schulze, J. Mater. Sci. **18**, 968 (1983).

8 S. Li, W. Cao, and L.E. Cross, J. Appl. Phys. **69**, 7219 (1991).

9 Q.M. Zhang, W. Y. Pan, S.J. Jang and L.E. Cross, J. Appl. Phys. **64**, 6445 (1988).

10 D. Damjanovic and M. Demartin, J. Phys. C **9**, 4943 (1997).

11 D. Damjanovic, Phys. Rev. B **55**, R649 (1997).

12 Q.M. Zhang, H. Wang, N. Kim and L.E. Cross, J. Appl. Phys. **75**, 454 (1994).

12 V. I. Aleshin, Sov. Phys. - Techn. Phys. **35**, 107 (1990).

13 G. Arlt and N. A. Pertsev, J. Appl. Phys. **70**, 2283 (1991).

14 V. Mueller and Q. M. Zhang, to be published.

15 Curie-temperatures were taken from the technical information sheet of Morgan Matroc Inc., Tokin Inc. and Motorola Inc., respectively.

16 M. E. Lines and A.M. Glass, Principles and Applications of Ferroelectrics and Related Materials , (Clarendon Press, Oxford, 1977).

17 D. S. Fisher, Phys. Rev. B **31**, 1396 (1985).

18 P.B. Littlewood, in Charge Density Waves in Solids , edited by L.P. Gorkov and G. Gruner (Elsevier, Amsterdam, 1989).

19 W. L. Zhong, Y. G. Wang, S. B. Yue, and P. L. Zhang, Sol. State Comm. **90**, (1994).

20 Y. S. Ng and A. D. McDonald, Ferroelectrics **62**, 167 (1985).

21 L. Wu, C.-C. Wei, T.-S. Wu, and H.-C. Liu, J. Phys. C **16**, 2813 (1983).

22 U. Robels and G. Arlt, J. Appl. Phys. **73**, 3454 (1993).

23 O. Kersten and G. Schmidt, Ferroelectrics **67**, 191 (1986).

24 G. Arlt, U. Boettger, and S. Witte, Appl. Phys. Lett. **63**, 602 (1993).

Table I: Limiting field E_{lim} and limiting field strain S_5^{max}.

material	E_{lim} [kV/cm] (continous wave)	$S_5^{max} \times 10^3$ (continous wave)	E_{lim} [kV/cm] (tone burst)	$S_5^{max} \times 10^3$ (tone burst)
PZT-8	11	0.4	19.8	0.75
PZT-4D	9	0.7	14.4	1.4
PZT-5A	6.5	1.0	-	-
N-21	6.2	1.2	9.3	2.75
EDO-5A	4.8	1.2	-	-
PZT-5H	4.9	1.1	8.9	2.5
3203HD	3.8	0.85	-	-
N-10	3.0	0.75	-	-

Table II: Fitting coefficients according to eqs.(1) and (7), respectively.

material	g_{15} $\times 10^2$ [m^2/C]	c	d_{lin} [pC/N]	d_{nl} $\times 10^4$ [m/V]	b
PZT-8	3.77	0.981	410	0.14	1.4
PZT-4D	3.72	0.981	500	0.45	1.5
PZT-5A	3.98	0.996	565	4.7	1.2
N-21	3.77	0.970	770	6.8	1.2
EDO-5A	4.22	1.000	700	2.0	1.1
PZT-5H	3.47	0.982	775	6.4	1.25
3203HD	2.89	0.985	950	13	1.2
N-10	2.43	0.983	1000	13	0.9

Captions

FIG.1: AC-field dependence of the piezoelectric shear strain S_5 determined at a soft PZT piezoceramic (Motorola 3203HD). Dashed lines indicate the onset of electrical depoling at $E=E_{lim}$ and the maximum attainable strain S_{max}, respectively.

FIG.2: Ratio of effective dielectric and piezoelectric coefficients ε_{11} and d_{15} in dependence on the amplitude $E_1^{(ac)}$ of the ac-field. Data are obtained at PZT-8.

FIG.3: Shear strain-polarization relationship $S_5(P_1)$ of the PZT piezoceramics examined.

FIG.4: Piezoelectric coefficient g_{15} determined for several PZT piezoceramics in dependence on the temperature difference $\Delta T=T_c-T_m$ with $T_m=295K$. T_c is the Curie temperature of the particular piezoceramic.

FIG.5: AC-field dependence of a) - effective dielectric and b) - effective piezoelectric coefficients of a soft PZT piezoceramic (Motorola 3203HD). The coefficients are normalized to its small signal value $\varepsilon^{(0)}$ and $d^{(0)}$, respectively. Open circles represent coefficients measured parallel to the poling direction (ε_{33} and d_{33}, respectively), full circles represent coefficients obtained perpendicular to the poling direction (ε_{11} and d_{15}, respectively).

FIG.6: AC-field dependence of the field dependent part $\Delta\varepsilon_{11}$ and Δd_{15} of effective dielectric and piezoelectric coefficients, respectively, of soft PZT (Motorola 3203HD). The lines represent least square fits according to eq.(7) of data obtained for $E_1 > 100V/cm$.

FIG.7: AC-field dependence of the effective piezoelectric coefficient d_{15} obtained at the soft PZT piezoceramics examined: 1 - N-10; 2 - 3203HD; 3- EDO-5A; 4 - PZT-5H; 5 - N-21; 6 - PZT-5A. The lines represent fits according to eq.(7) of data measured for $E_1 > 100V/cm$.

FIG.8: AC-field dependence of the effective piezoelectric coefficient d_{15} of a hard PZT piezoceramic (PZT-4D). The lines represent fits according to eq.(7) of data measured for $E_1 > 1000V/cm$.

FIG.9: Nonlinear piezoelectric coefficients d_{nl} of the PZT piezoceramics examined plotted versus the corresponding nonlinear dielectric coefficients ε_{nl}.

FIG.10: Nonlinear dielectric coefficients ε_{nl} of the PZT piezoceramics examined plotted versus the corresponding linear dielectric coefficients ε_{lin}.

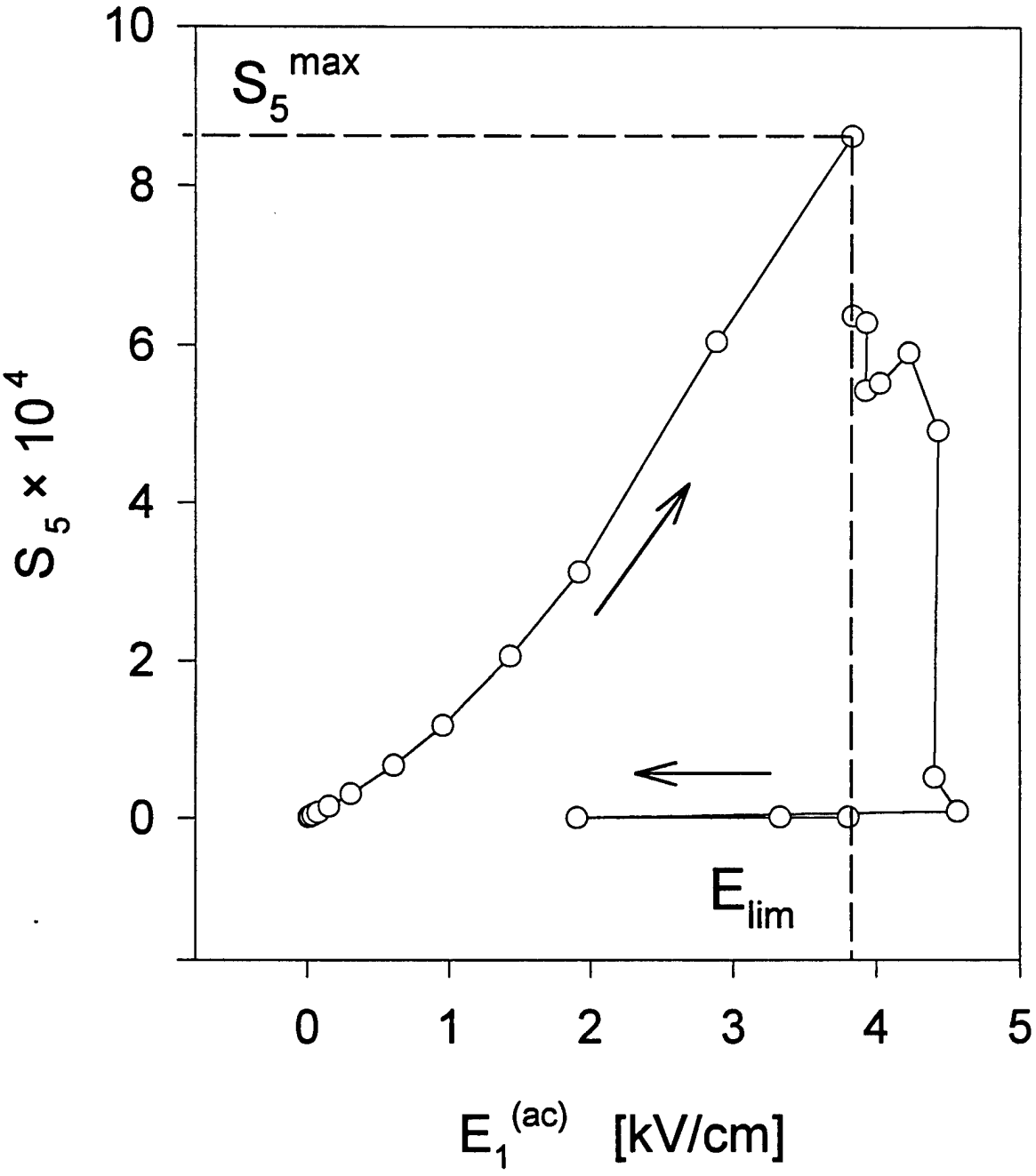
10
8
6
4
2
0
S_5^{max}
$S_5 \times 10^4$
E_{lim}
0
1
2
3
4
5
$E_1^{(ac)}$ [kV/cm]

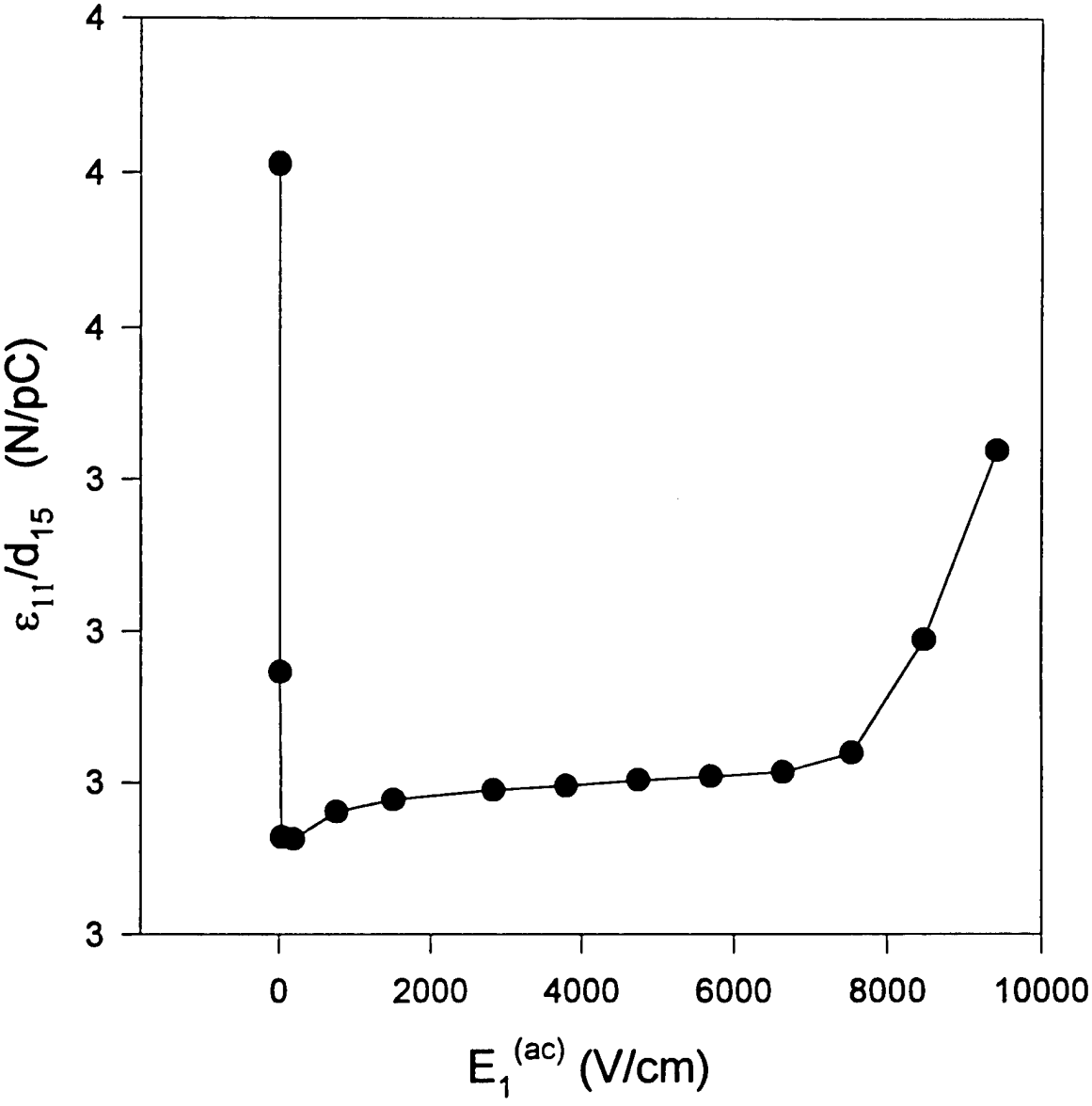
4
4
4
3
3
3
ε_{11}/d_{15} (N/pC)
0
2000
4000
6000
8000
10000
$E_1^{(ac)}$ (V/cm)

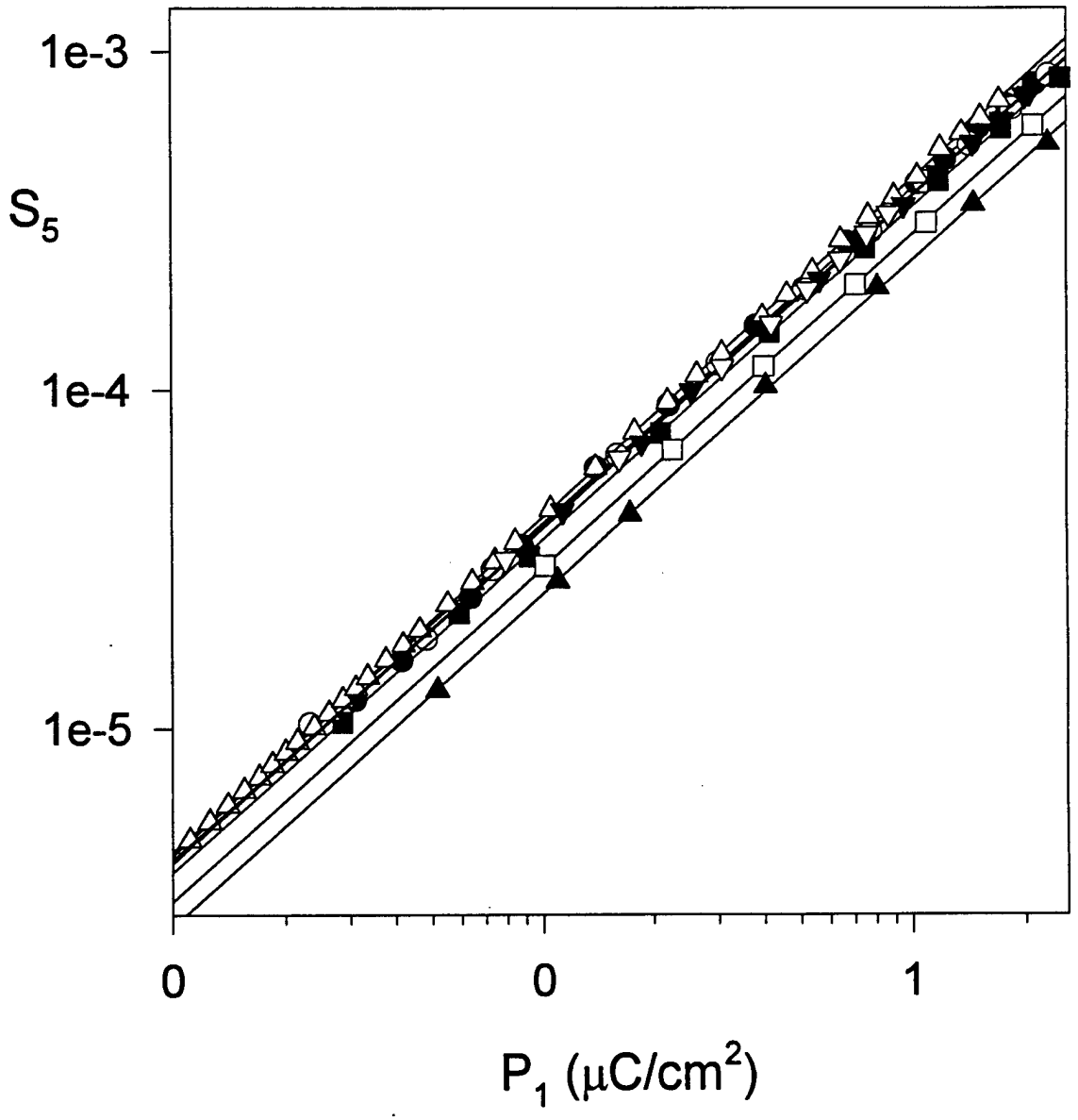
1e-3
1e-4
1e-5
S_5
0
0
1
P_1 (μC/cm^2)

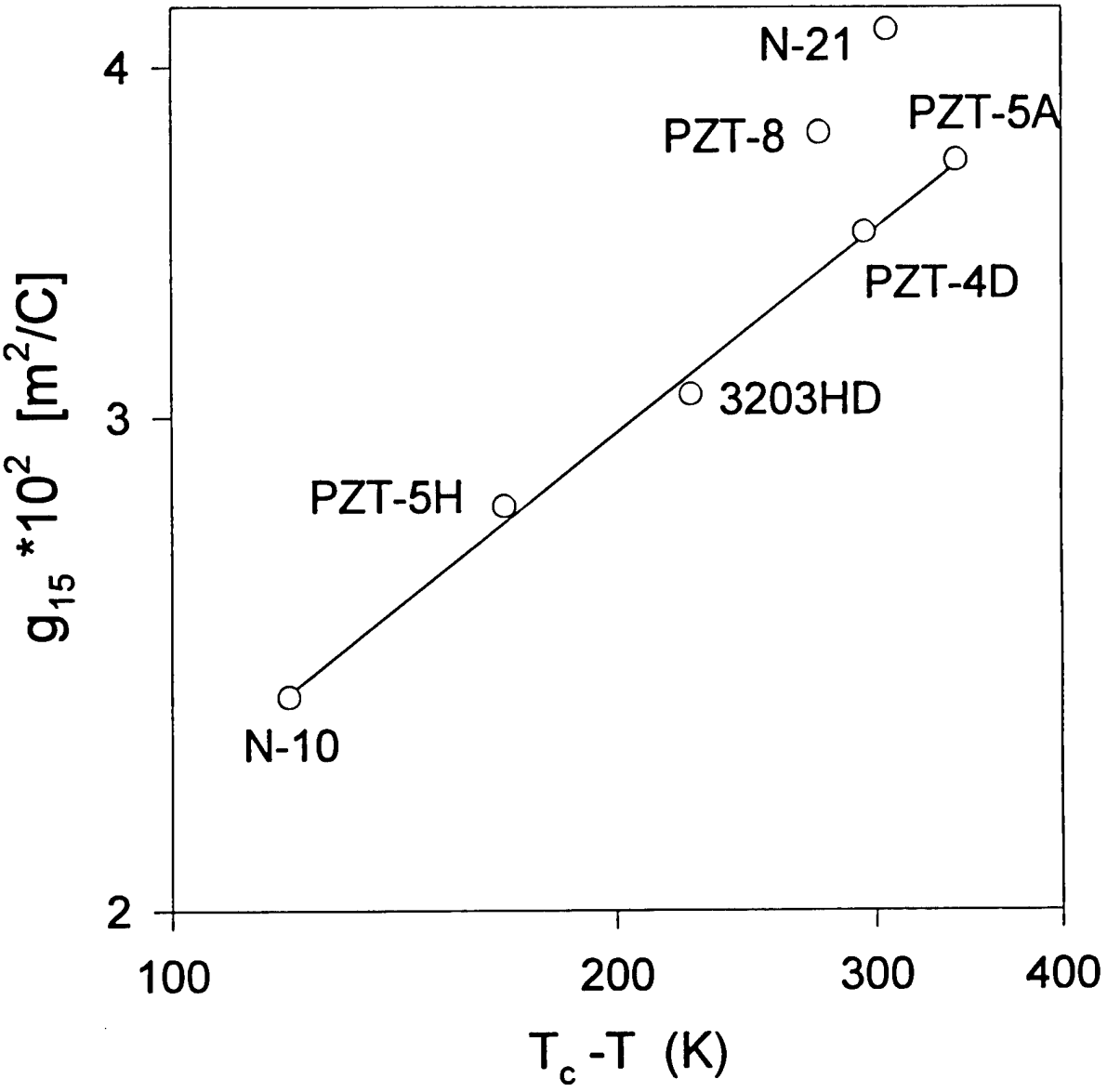
N-21
PZT-8
PZT-5A
PZT-4D
3203HD
PZT-5H
N-10
4
3
2
100
200
300
400
g_{15} *10^2 [m^2/C]
T_c -T (K)

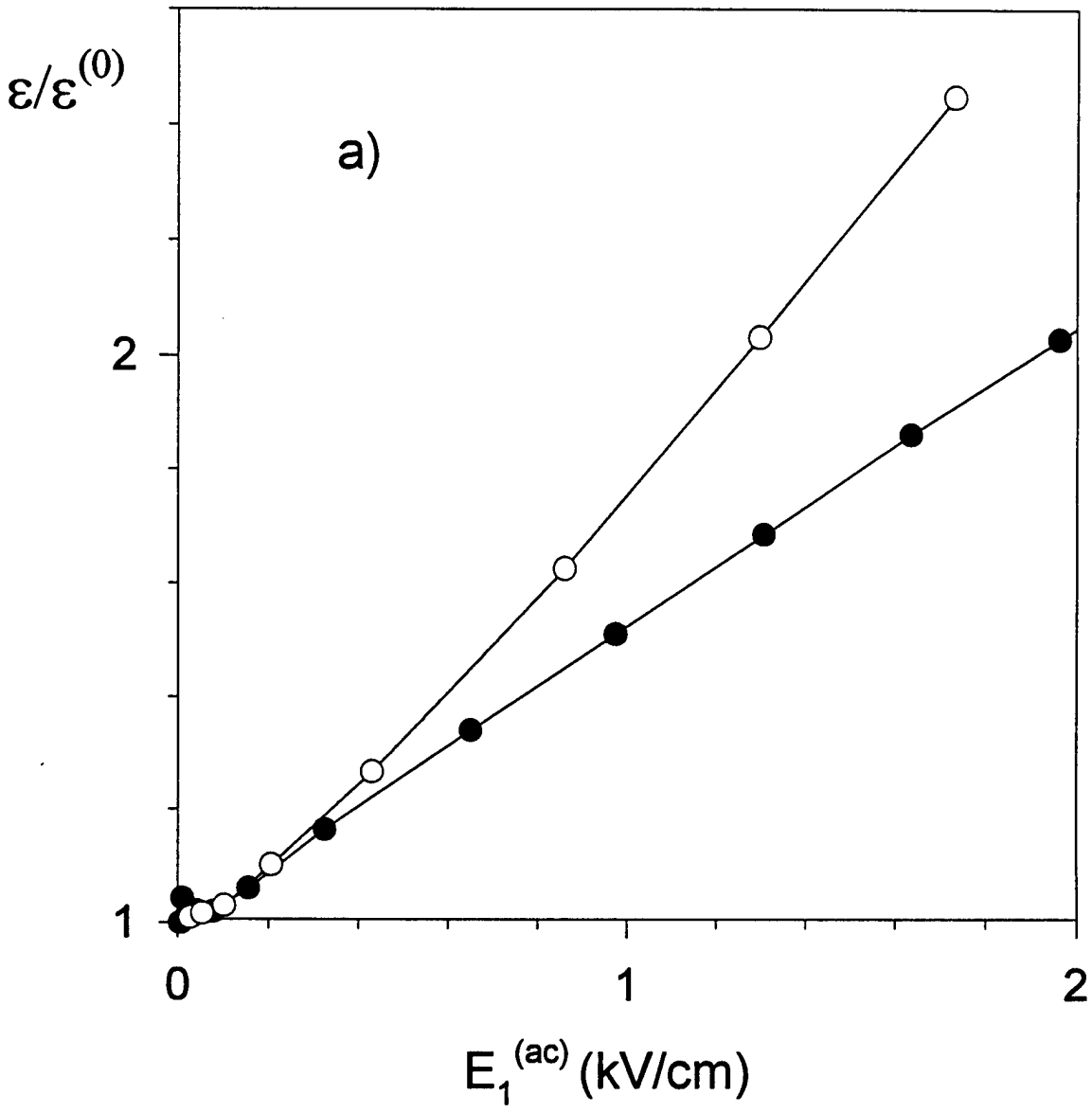
ε/ε(0)
a)
2
1
0
1
2
E1(ac) (kV/cm)

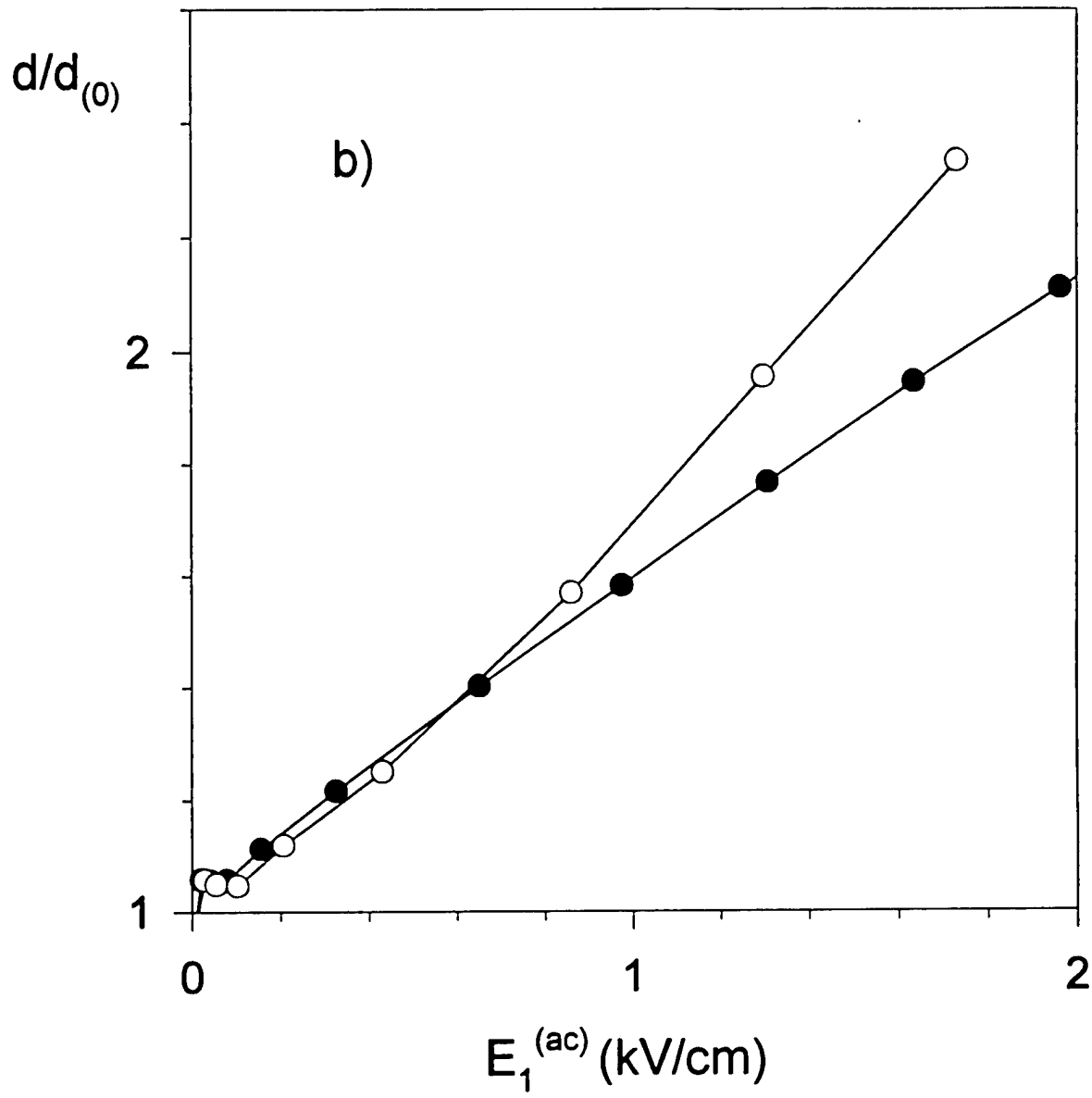
d/d(0)
b)
2
1
0
1
2
E1(ac) (kV/cm)

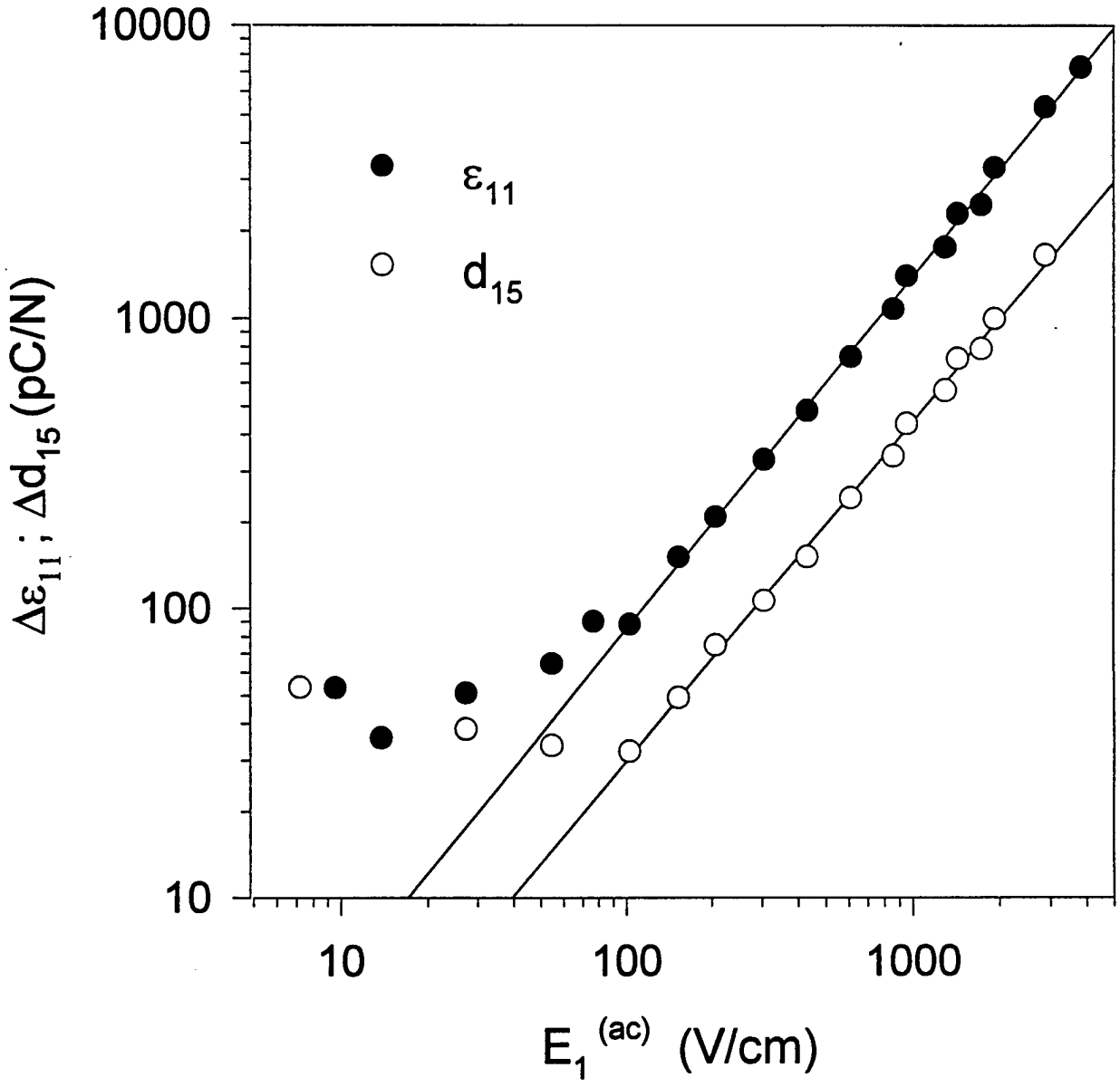
10000
1000
100
10
10
100
1000
$\Delta\varepsilon_{11}$; Δd_{15} (pC/N)
ε_{11}
d_{15}
$E_1^{(ac)}$ (V/cm)

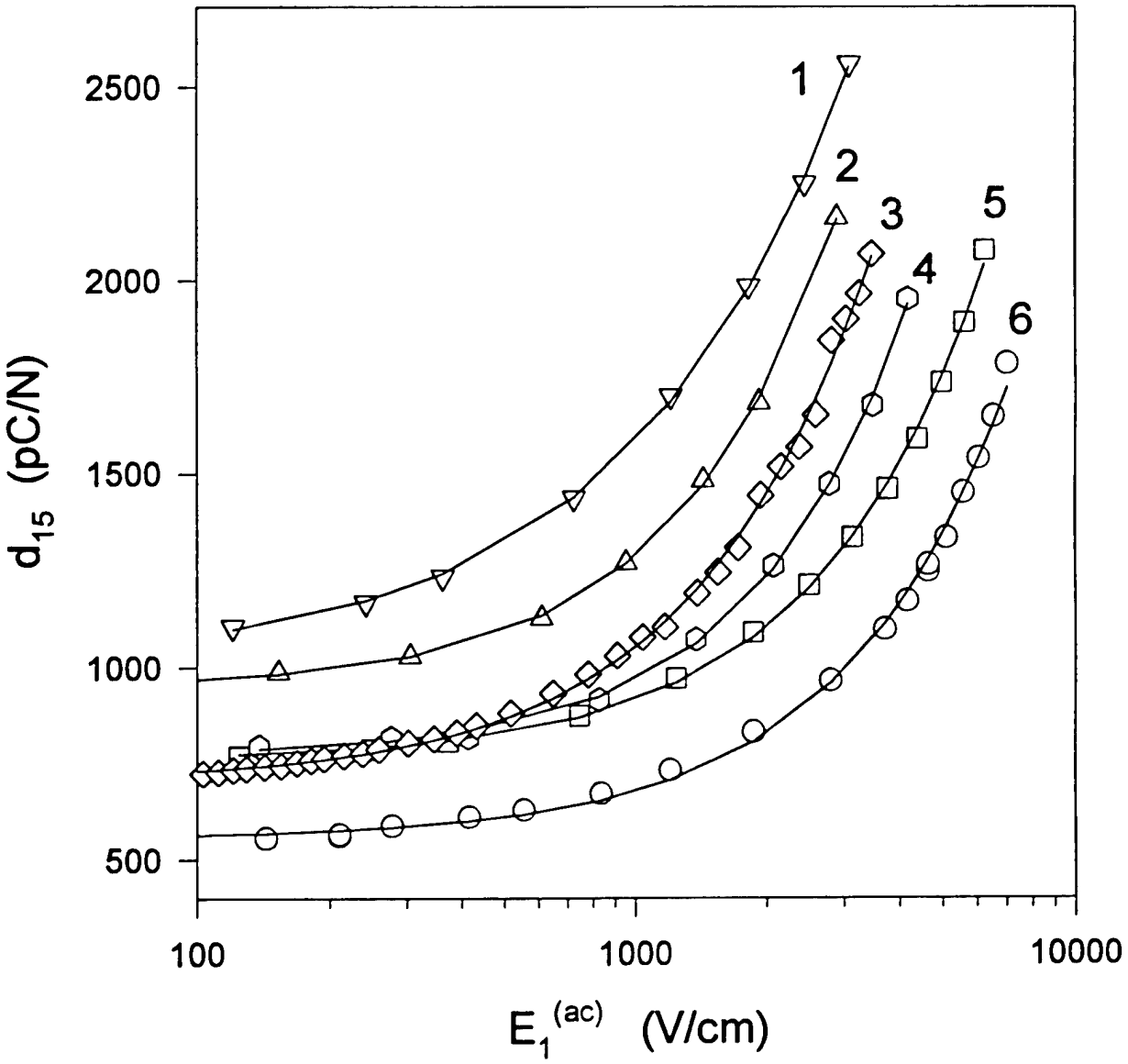
2500
2000
1500
1000
500
100
1000
10000
d_{15} (pC/N)
$E_1^{(ac)}$ (V/cm)
1
2
3
4
5
6

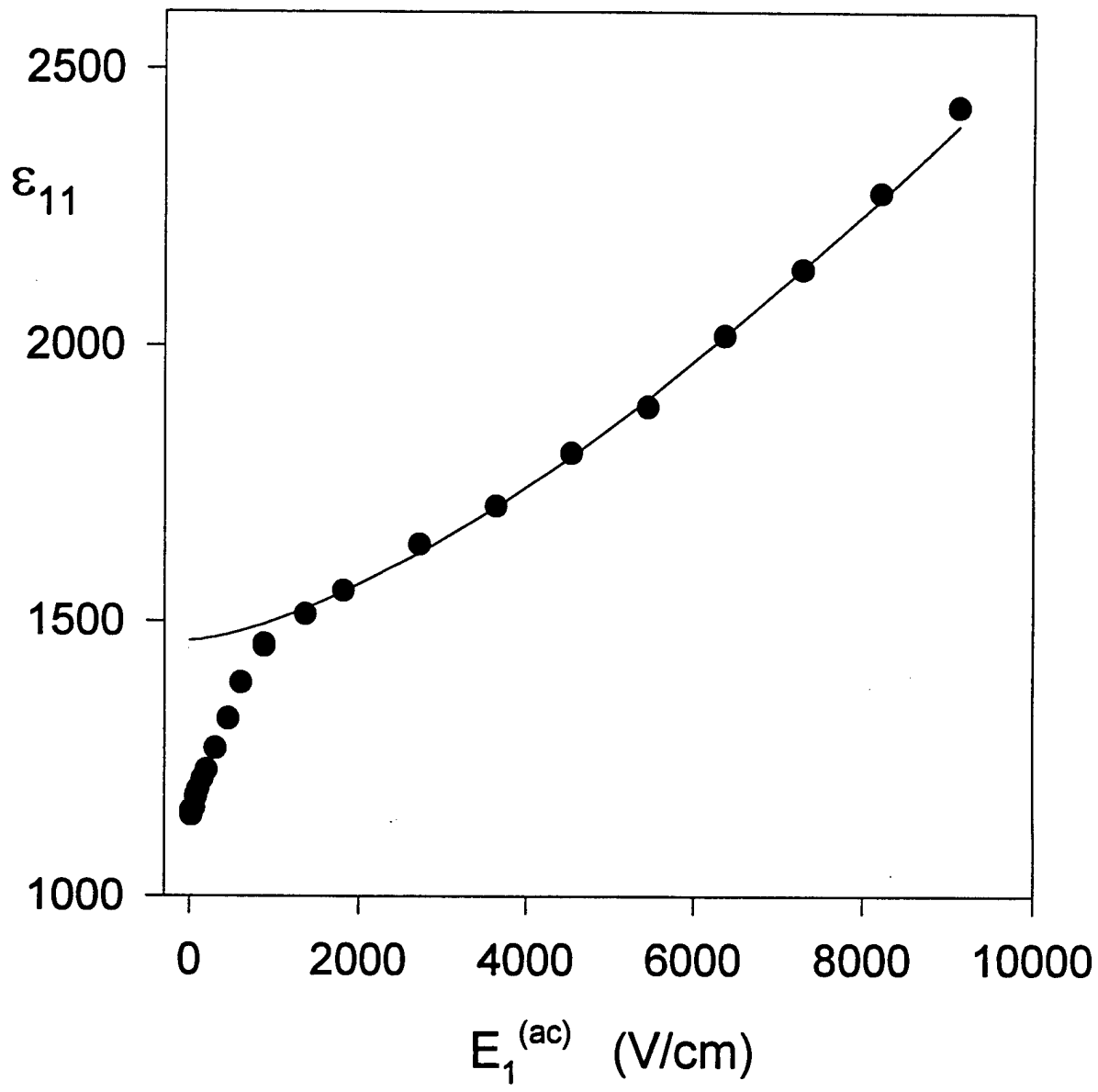
2500
2000
1500
1000
ε_{11}
0
2000
4000
6000
8000
10000
$E_1^{(ac)}$ (V/cm)

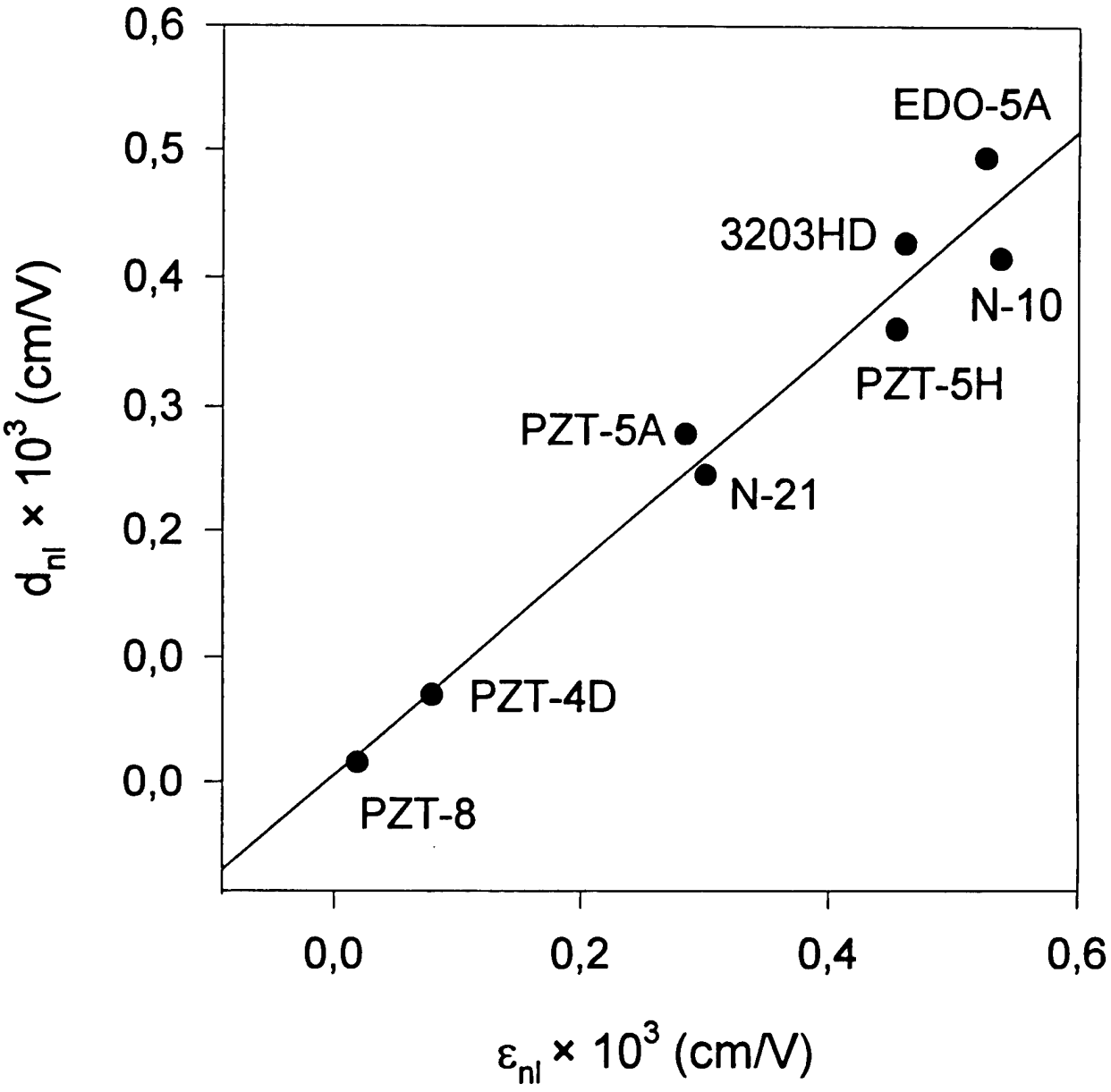
0,6
0,5
0,4
0,3
0,2
0,0
0,0
0,0
0,2
0,4
0,6
EDO-5A
3203HD
N-10
PZT-5H
PZT-5A
N-21
PZT-4D
PZT-8
$d_{nl} \times 10^3$ (cm/V)
$\varepsilon_{nl} \times 10^3$ (cm/V)

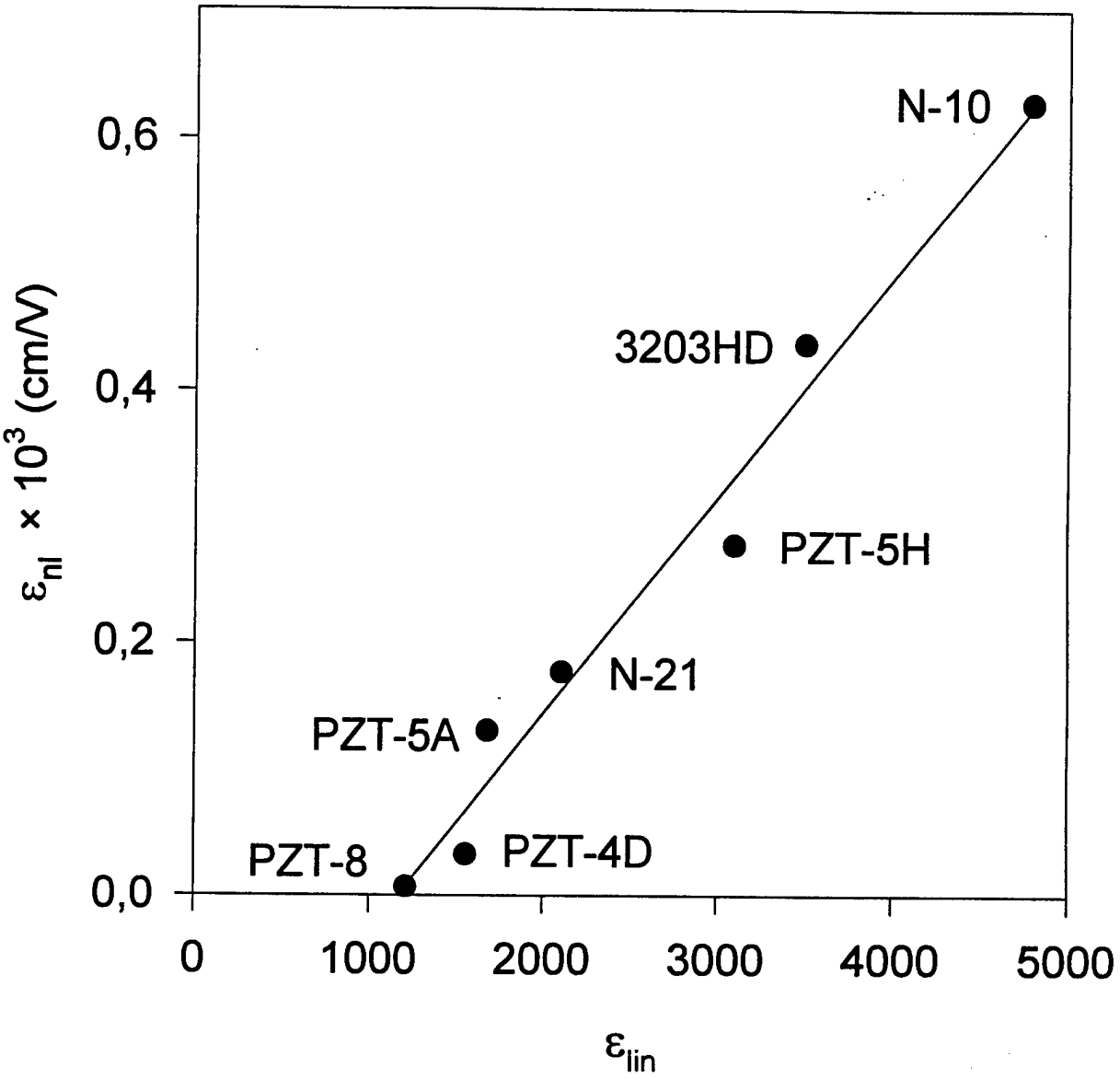
N-10
3203HD
PZT-5H
N-21
PZT-5A
PZT-4D
PZT-8
0,6
0,4
0,2
0,0
0
1000
2000
3000
4000
5000
$\varepsilon_{nl} \times 10^3$ (cm/V)
ε_{lin}

APPENDIX 15

Electric field induced phase transition of antiferroelectric lead lanthanum zirconate titanate stannate ceramics

Seung-Eek Park,[a] Ming-Jen Pan, Kelley Markowski,[b] Shoko Yoshikawa, and L. Eric Cross
Materials Research Laboratory, The Pennsylvania State University, University Park, Pennsylvania 16802

(Received 22 April 1997; accepted for publication 6 May 1997)

The electric field induced phase transition behavior of lead lanthanum zirconate titanate stannate (PLZTS) ceramics was investigated. PLZTS undergoes a tetragonal antiferroelectric (AFE_{Tet}) to rhombohedral ferroelectric (FE_{Rh}) phase transition with the application of an electric field. The volume increase associated with this antiferroelectric (AFE)–ferroelectric (FE) phase transition plays an important role with respect to actuator applications. This volume increase involves an increase in both transverse and longitudinal strains. The E field at which the transverse strain increases is accompanied by an abrupt jump in polarization. The longitudinal strain, however, lags behind this polarization jump exhibiting a slight decrease at the onset of phase switching. This decoupling was related to the preferentially oriented AFE domain configuration, with its tetragonal c-axis perpendicular to the applied electric field. It is suggested that phase switching involves multiple steps involving both structural transformation and domain reorientation. © *1997 American Institute of Physics.* [S0021-8979(97)02016-1]

I. INTRODUCTION

Antiferroelectric (AFE) lead lanthanum zirconate titanate stannate (PLZTS) switches to a ferroelectric (FE) phase with the application of an electric field (E field).[1] This phase switching is accompanied by a large volume expansion, therefore, this material has been investigated for various actuator applications.[2–4] This volume expansion is due to a structural change, that is, change in unit cell parameters.[1,5,6] Although the evidence has been suggested of incommensurate modulation in the PLZTS structure,[7–9] it is believed that the strain caused by phase switching is primarily based on the change in the primitive perovskite cell.[1,5,6,10] The ability to tailor the phase transition behavior and associated properties such as switching field (E_{AF}:AFE to FE switching field, E_{FA} : FE to AFE switching field) and hysteresis ($\Delta E = E_{AF} - E_{FA}$) through compositional modifications,[11,12] is also significant for practical applications.

The composition $Pb_{0.98}La_{0.02}(Zr_{0.66}Ti_{0.10}Sn_{0.24})_{0.995}O_3$ (PLZTS) was chosen to characterize AFE-FE phase switching behavior. This composition is located near the boundary between the tetragonal AFE (AFE_{tet}) and rhombohedral FE (FE_{Rh}) phases, as shown in Fig. 1.[10] It is known that the AFE_{tet} phase (with a primitive cell of tetragonal symmetry) switches to a FE_{Rh} phase on the application of an E field.[5,6] Primitive perovskite cell parameters of both AFE and FE phases of PLZTS have been reported as presented in Table I. The primitive cell of the AFE phase has a c/a ratio less than 1. Note that a_{Rh} of the FE phase is larger than c_{Tet} although it is smaller than a_{Tet} of the AFE phase. This implies that, when E-field is in c-direction, a PLZTS single crystal should show increased strain along the applied E-field direction (longitudinal strain) whereas the strain along the direction normal to the E field (transverse strain) should decrease during phase switching. The overall volume increases because the ratio of a_{Rh}/c_{Tet} is larger than the ratio of a_{Tet}/a_{Rh}. In polycrystalline ceramics, however, a more complicated situation is expected due to randomly oriented grains. Although the overall stress can be compensated by randomly oriented grains, each grain containing AFE/FE domains experiences different expansion/contraction, depending on the orientation of adjacent domains. In spite of several reports[5–9] on the structure of PLZTS ceramics, few studies on the behavior of longitudinal/transverse/volume strains associated with phase switching have been reported, especially from the view point of structural change. The AFE-FE transition includes not only the structural phase transformation but also the couplings among domains, resulting in complicated phenomenological interactions during this transformation. The first pioneering observations on the E-field induced strain behavior for AFE materials,[1,10] and additional observations[13] involving the discontinuity of E-field induced strains during this AFE-FE phase transition suggest a two stage model for the phase transformation.

It is the objective of this study to investigate and understand the behavior of AFE domains and polarization(P)/strain associated with E-field induced phase switching. These behaviors include preferentially oriented AFE domains, change in sample dimensions, polarization, and longitudinal/transverse/volume strain associated with phase switching. Hereafter, the structural transition will be discussed on the basis of the change in the primitive perovskite cell, to which the strain caused by the applied E-field induced phase transition is primarily attributed. A possible switching mechanism based on this work will be discussed.

[a]Electronic mail: sxp37@email.psu.edu
[b]Current address: Materials System, Inc., 521 Great Road, Littleton, MA 01460.

 0021-8979/97/82(4)/1798/6/$10.00

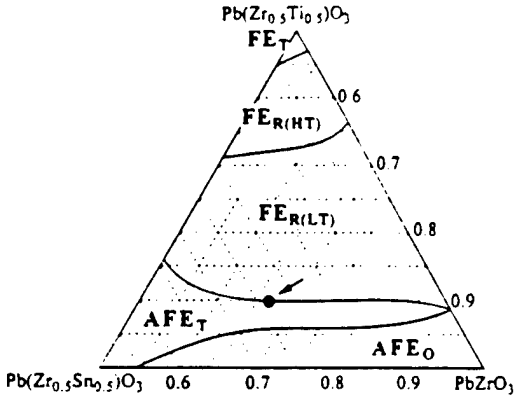

FIG. 1. Ternary phase diagram for the system $Pb_{0.98}La_{0.02}(Zr,Ti,Sn)O_3$ (Ref. 10).

II. EXPERIMENTAL PROCEDURE

A. Sample preparation

Polycrystalline ceramic materials investigated in this study were prepared by solid state reaction using the following reagent grade raw materials: lead carbonate [$2PbCO_3 \cdot Pb(OH)_2$] (Hammond Lead Products, Inc., Hammond, IN), lanthanum oxide (La_2O_3, Alpha Products Co., Danvers, MA), zirconium dioxide (ZrO_2, Harshaw Chemical Co., Cleveland, OH), titanium dioxide (TiO_2, Whitaker, Clark and Daniels Co., Plainfield, NJ), and tin oxide (SnO_2, Alpha, Ward Hill, MA). The chemical purity of each was greater than 99%. The sintering process was carried out in a lead rich environment in order to minimize lead volatilization. After sintering the samples experienced about 2% weight loss. The samples were pale yellow after sintering and remained this color throughout processing. After sintering the samples were 97% dense and the average grain size, observed using scanning electron microscopy (SEM), was 4–5 μm. Disk samples (with diameter 11 mm and thickness 0.3 mm) were then prepared by polishing with silicon carbide and alumina polishing powders to achieve flat and parallel surfaces onto which gold was sputtered as an electrode.

B. Phase and microstructure

Calcined and sintered powders were examined by x-ray diffraction (XRD) to insure phase purity and to identify the crystal structure. Typically the samples showed a single tetragonal structure within the detection limit of XRD (<2%). Powder XRD was obtained by scanning a 2θ range of 20°–80° with 0.01° step and a count time of 3 s.

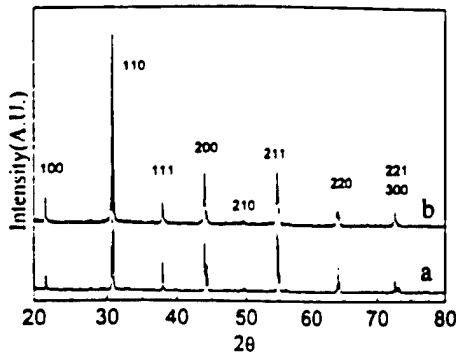

FIG. 2. XRD patterns of PLZTS when $E = 0$ kV/cm. (a) as-sintered sample and (b) E-field exposed sample.

C. Polarization and strain

High-field measurements included polarization and strain hysteresis using a computer-controlled Sawyer Tower circuit and a linear variable displacement transducer (LVDT) sensor driven by a lock-in amplifier (Stanford Research Systems, Model SR830). The voltage was supplied using a Trek 609C-6 high voltage dc amplifier. Through the LVDT sensor the strain of the samples can be measured with the application of an applied field. Electric fields as high as ~80 kV/cm were applied using a 0.2 Hz amplified sine wave form and 0.05 Hz quarter sine wave form for better resolution.

III. RESULTS AND DISCUSSION

A. Preferred orientation of AFE domains

Figure 2(a) shows the XRD pattern of an as-sintered sample. No superlattice reflections associated with multicell or an incommensurately modulated structure were detected in the XRD pattern. This is attributed to the low intensity of superlattice peaks, indicating that the supercell has large modulation wavelength.[9] All diffraction peaks in Fig. 2(a) could be fitted to a single tetragonal phase with cell parameters of $a = 4.118$ Å and $c = 4.090$ Å. The P vs E curve in Fig. 3 shows AFE_{Tet} to FE_{Rh} transition at 37 kV/cm with abrupt increase of polarization. The reverse transition into AFE_{Tet} occurred at 8 kV/cm with an associated decrease in the E field. Figure 2(b) shows XRD patterns of an AFE sample where the E field is removed after sample experienced the E field (50 kV/cm) induced transition. Although all peaks could be indexed as a tetragonal phase, a difference between the diffraction patterns of the virgin sample and that of the E-field exposed sample could be observed through changes in both peak intensity and width. Figure 4 shows

TABLE I. Parameters of primitive unit cell for AFE and FE phases.

	AFE tetragonal		FE rhombohedral		
Composition	a_{Tet}(Å)	c_{Tet}(Å)	a_{Rh}(Å)	α_{Rh}	Ref.
$Pb_{0.97}La_{0.02}(Zr_{0.66}Ti_{0.11}Sn_{0.23})O_3$	4.119	4.095	4.118	89.8°	5
$Pb_{0.97}La_{0.02}(Zr_{0.55}Ti_{0.33}Sn_{0.12})O_3$	4.107	4.081	4.105	89.85°	6

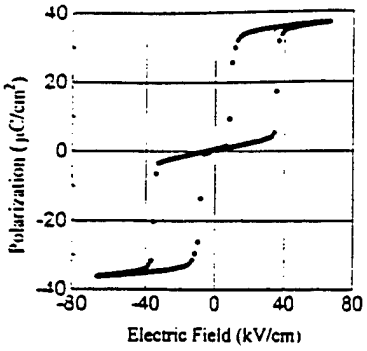

FIG. 3. Polarization vs E-field curves of PLZTS.

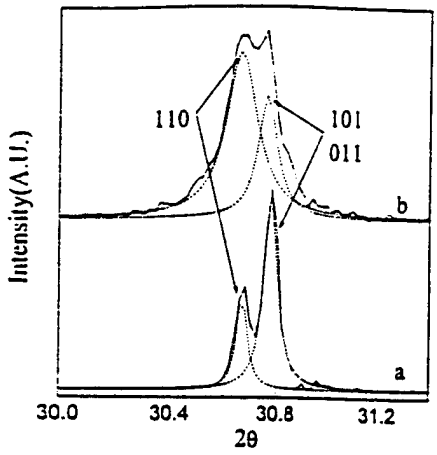

FIG. 5. {110} peaks in XRD patterns of PLZTS when $E=0$ kV/cm. (a) as-sintered sample and (b) E-field exposed sample (α_2 contributions are eliminated).

{200} peaks of both a virgin sample [Fig. 4(a)] and an E-field exposed sample [Fig. 4(b)] at $E=0$ kV/cm. Decreased intensity of the (002) peak can be found in Fig. 4(b) associated with increased peak width, resulting in unclear α_2 contributions [α_2 contributions were quite distinct for virgin samples as shown in Fig. 4(a)]. The {110} peaks in Fig. 5 show the same change in intensity, that is, decreased intensity of the peak attributed to (101) and (011) reflections. The peak broadening for the sample, after experiencing the phase transition, can be observed more clearly through analysis of the {111} peak in Fig. 6. Note that tetragonal symmetry does not cause the {111} peak to split. The virgin sample showed a sharp single {111} peak with a distinct α_2 contribution [Fig. 6(a)] whereas the E-field exposed sample shows peak broadening, resulting in unclear α_2 contribution [Fig. 6(b)]. These XRD results imply that AFE domains, which had random orientation before E-field exposure, are preferentially oriented after experiencing the E-field induced phase transition. With respect to the grains which contribute to the intensity of {200} or {110} peaks in a polycrystalline samples, a schematic diagram of this preferred domain orientation is suggested in Fig. 7. It is obvious that the c axis of each domain has a tendency to orient normal to E-field direction (parallel to the sample surface) after E-field exposure. This preferred orientation of AFE domains results not only in an intensity change but also the change in sample dimensions, as report by Berlincourt *et al.*[10] The c/a is less than 1 for AFE tetragonal primitive cells and, consequently, this preferred domain configuration must result in the sample increase in size along longitudinal direction. This also indicates the converse, i.e., the sample decrease in size along the transverse direction. An increased dielectric constant after E-field exposure (840 and 1050 before and after E-field exposure at 1 kHz, respectively) might be related to this preferred AFE domain orientation.[11]

Peak broadening in Figs. 4–6 is possibly due to nonuniform strains in the lattice caused by preferred orientation. As a result of the incompatibility among preferentially oriented grains, complex strain distribution and resulting compensations are expected to exist in the sample. An elastically frozen state coupled with lattice distortions were suggested as the origin of preferred AFE domain orientation.[13,14] Although it may explain the peak broadening caused by nonuniform strain as a result of preferred orientation, however, this elastic point of view cannot explain the origin of preferred AFE domain configuration. A recent report[15] focused on the increased incommensurate superlattice peak

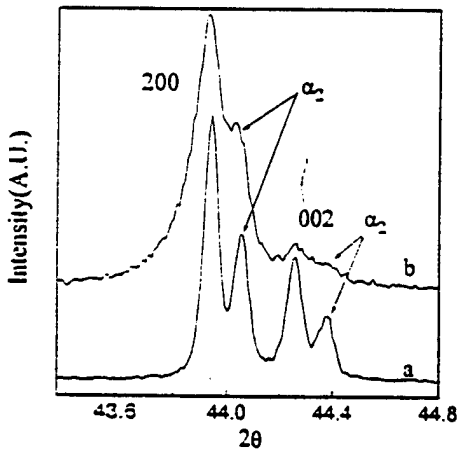

FIG. 4. {200} peaks in XRD patterns of PLZTS when $E=0$ kV/cm. (a) as-sintered sample and (b) E-field exposed sample.

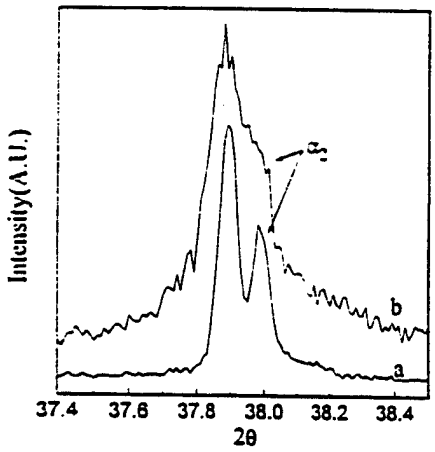

FIG. 6. {111} peaks in XRD patterns of PLZTS when $E=0$ kV/cm. (a) as-sintered sample and (b) E-field exposed sample.

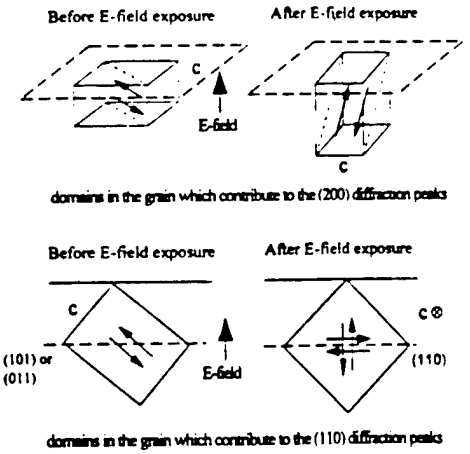

FIG. 7. Schematic of preferentially oriented AFE domains after E-field exposure.

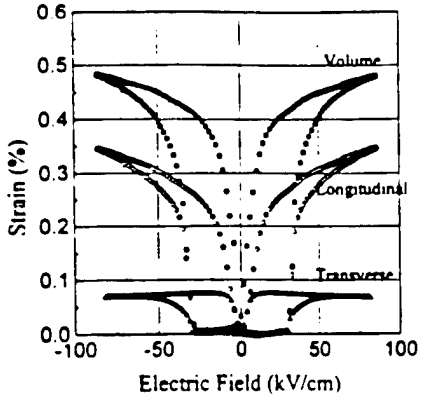

FIG. 8. Longitudinal/transverse/volume strain as a function of E field (0.2 Hz).

caused by preferred AFE domain orientation with $Pb_{0.98}La_{0.02}(Zr_{0.95}Ti_{0.05})_{0.995}O_3$ indicates that the preferred orientation of the AFE domain is strongly connected with incommensuration associated with a disrupted oxygen framework. This origin is subject to more study from a crystallographic point of view in the future.

B. Strain behavior associated with E-field induced AFE-FE transition

Figure 8 shows the strain behavior during the E-field induced AFE-FE transition using a 0.2 Hz sine wave input signal. At a switching field of 37 kV/cm, 0.2% longitudinal strain and 0.3% volume strain were achieved. It was noted that there is a decoupling between polarization and longitudinal strain, i.e., longitudinal and volume strains continue to significantly increase even after polarization saturates.[16] Similar observations have been made in other works.[14] An incommensurately modulated polar structure is suggested as a possible explanation for this behavior because the symmetry of the FE phase may continue to be orthorhombic if the incommensurate modulation remains during phase transition. Although the overall symmetry can appear orthorhombic due to the incommensurate modulation, longitudinal strain caused by the change in unit cell parameter (tetragonal ⇔rhombohedral) may not be compensated only by incommensurate modulation. Specifically, over 0.5% of volume change associated with phase transition was expected in previous studies.[5,6] Therefore, phase switching behavior can be neither investigated nor understood sufficiently through the consideration of longitudinal strain behavior alone. Pan *et al.*[17] experimentally suggested that commensurate AFE PLZTS should also show this type of decoupling, supporting that incommensurate modulation is not an origin to explain the decoupling behavior.

Figure 9 shows the polarization and longitudinal/transverse strain as a function of the E field using one quarter of a sine wave (0.05 Hz) as the input signal, for better resolution. It is found in Fig. 9(b) that the transverse strain increases abruptly at the same E field where polarization shows an abrupt jump. The fact that transverse strain does not show decoupling between polarization and strain is consistent with the general electromechanical coupling behavior. Therefore, in the case of transverse strain, it is not necessary to employ a new explanation. On the other hand, as shown in Fig. 9(a), longitudinal strain lags behind the polarization jump during phase switching. In spite of the abrupt increase

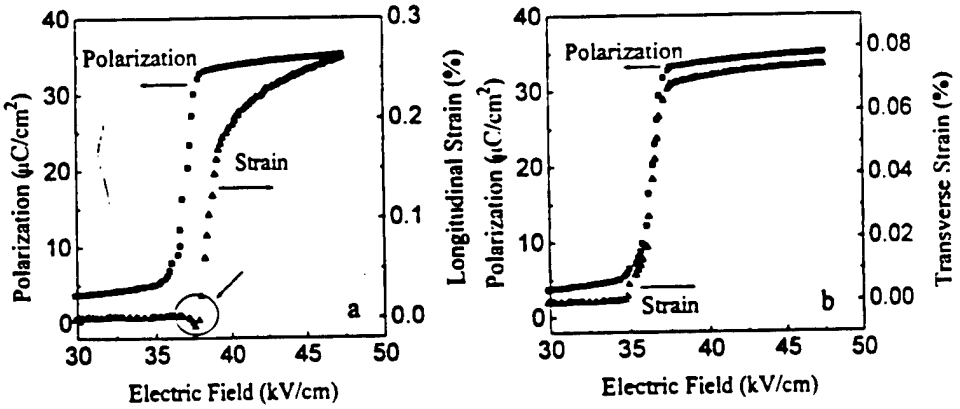

FIG. 9. (a) Polarization and longitudinal strain, (b) polarization and transverse strain as a function of E field using quarter sine wave (0.05 Hz) as an input signal.

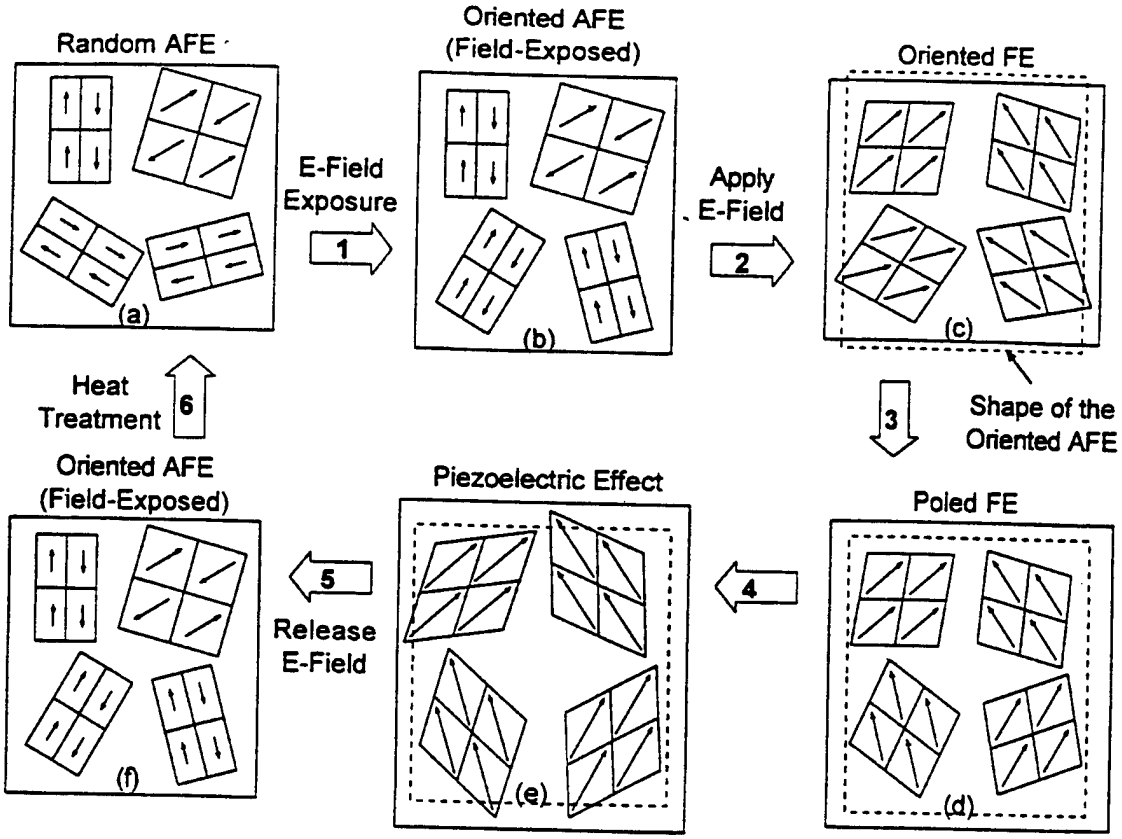

FIG. 10. Schematic diagram of AFE-FE phase switching procedure.

in polarization, longitudinal strain showed a small decrease at the starting point of phase switching [marked by a circle in Fig. 9(a)]. Decoupling is observed only with longitudinal strain.

C. Phase switching sequence

Though a combination of strain behaviors and preferred orientation of AFE domains discussed in previous sections, it is possible to construct an AFE-FE switching sequence as shown in Fig. 10. A step-by step sequence is presented as follows:

(i) Random AFE to oriented AFE after field exposure (oriented AFE): A virgin sample with randomly oriented AFE domains [Fig. 10(a)] becomes preferentially oriented AFE with its c axes perpendicular to the field direction [Fig. 10(b)] after E-field exposure. At this state, increased size along longitudinal direction is observed because $c/a<1$. The size subsequently decreases along the transverse direction. Once the sample is exposed to an E field large enough to induce the AFE-FE transition, it does not return to the virgin state, unless it is heated above its paraelectric temperature range.

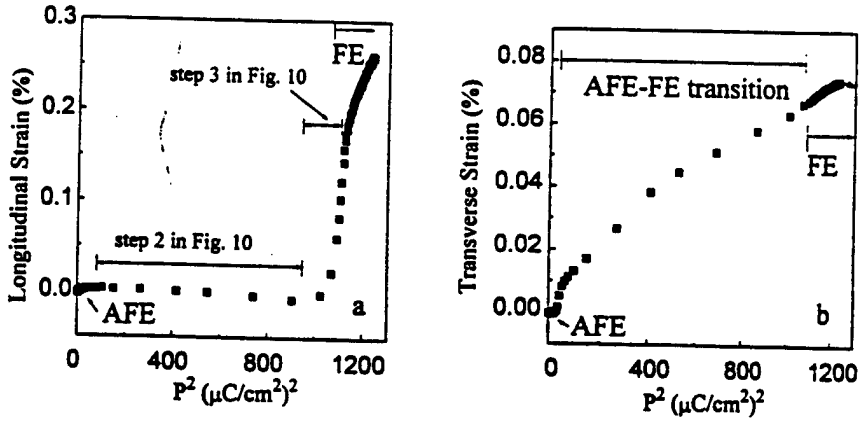

FIG. 11. Strain vs square of the polarization curves for (a) longitudinal strain and (b) transverse strain.

(ii) Oriented AFE to oriented FE, at the switching field: When an E field is applied, AFE cells become FE with their polarization directions trying to align along the E-field direction in order to minimize free energy [Fig. 10(c)]. A sudden increase of polarization is expected due to the switching of the antipolar state to a polar state. However, perfect alignment of polarization vectors may not be achieved at this point, due to factors such as stresses induced by volume expansion. When an AFE tetragonal primitive cell switches to rhombohedral FE with c-axis expansion, it is associated with a slight decrease in the a axis as referred to in the Introduction. As the c axes of most unit cells are perpendicular to the E field prior to the phase switching, there is a slight decrease in the longitudinal dimension and a large increase in the transverse direction in comparison to an E-field exposed sample [dashed line in Fig. 10(c)]. This is consistent with the observations in Fig. 9 and has been confirmed by statistical calculation.[18]

(iii) Oriented FE to poled FE at an applied E field larger than the switching field: With further application of the E field, some FE domains will try to align more closely to the E-field direction through 109° domain reorientation [Fig. 10(d)]. At this stage, polarization continues to increase. With the alignment of the domains and increase in polarization, the ceramic exhibits an increase in longitudinal strain. This dimensional increase falls behind the polarization increase caused by the AFE-FE transition.

(iv) Piezoelectric region: If an even higher E field is applied, the longitudinal strain continues to increase whereas transverse strain begins to decrease as a result of the piezoelectric effect (d_{31}) as shown in a previous report[15] [Fig. 10(e)].

(v) When the E field is removed, the FE phase returns to an oriented AFE state [Fig. 10(f)]. If the ceramic is heated to temperatures significantly above its AFE-paraelectric transition temperature (T_{max}), it recovers the random AFE state corresponding to the virgin sample.

E-field induced AFE-FE transition behavior appears to be time dependent because the associated stress caused by abrupt and large change in electrical/elastic state should be compensated for. In other words, if a very low frequency input signal is employed, the lag of longitudinal strain will not be observed. However, complete coupling between longitudinal strain and polarization was not observed even when the longest period the equipment was capable of producing was measured (100 s). The change in phase transition behavior with respect to the frequency of the input signal will be studied in the future. It also seems that nonuniform internal stress caused by a preferentially oriented AFE domain state plays a role in several steps during the phase transition. These steps are more obvious if strain is plotted as a function of the square of the polarization as shown in Fig. 11. In the case of transverse strain [Fig. 11(b)], the strain is dependent upon the square of polarization with a varied slope. In Fig. 11(a) the longitudinal strain shows a negative slope [Fig. 11(a)], indicating that strain decreases with increased polarization. It should be noted that the increase in transverse strain is primarily associated with volume increase at the starting point of the transition and the polarization/strain can apparently deviate from electrostrictive phenomenology. ($X = QP^2$, x:strain, Q:electrostrictive coefficient, P: polarization). Based on this understanding, steps during the AFE-FE transition discussed above are suggested in Fig. 11(a).

IV. CONCLUSION

AFE domain and strain behavior of PLZTS ceramics, as a function of applied E field, were investigated using XRD and polarization/strain versus E-field curves. AFE samples which were exposed to an E field inducing an AFE-FE transition showed preferred orientation of domains, where the c axis is perpendicular to the E-field direction, which results in both decreased intensities of (001) peaks and increased peak width caused by nonuniform strain. Transverse strain increased abruptly at the E field where polarization shows a sudden increase, whereas longitudinal strain lags behind the polarization jump with a slight decrease at the initiation of phase switching. It is found that phase switching involves more than one domain reorientation step.

ACKNOWLEDGMENTS

This study has been supported by DARPA and Boeing SSRC Consortium. The authors would like to thank Joe Kearns for his help with the preparation of samples, and T. Shrout and C. Randall for their helpful suggestions in this research.

[1] D. Berlincourt, H. H. A. Krueger, and B. Jaffe, J. Phys. Chem. Solids **25**, 659 (1964).
[2] K. Uchino, and S. Nomura, Ferroelectrics **50**, 191 (1983).
[3] W. Y. Pan, C. Q. Dam, Q. M. Zhang, and L. E. Cross, J. Appl. Phys. **66**, 6014 (1989).
[4] W. Y. Pan, Q. Zhang, A. Bhalla, and L. E. Cross, J. Am. Ceram. Soc. **72**, 571 (1989).
[5] L. Shevanov, M. Kusnetsov, and A. Sternberg, J. Appl. Phys. **76**, 4301 (1994).
[6] C. T. Blue, C. T. Hicks, S.-E. Park, S. Yoshikawa, and L. E. Cross, Appl. Phys. Lett. **68**, 2942 (1996).
[7] Z. Xu, D. Viehland, P. Yang, and D. A. Payne, J. Appl. Phys. **74**, 3406 (1993).
[8] Y. J. Chang, J. Y. Lian, and Y. L. Wang, Appl. Phys. A **36**, 221 (1985).
[9] D. Viehland, D. Forst, Z. Xu, and J. F. Li, J. Am. Ceram. Soc. **78**, 2101 (1995).
[10] D. Berlincourt, IEEE Trans. Sonics Ultrason. **SU-13**, 116 (1966).
[11] K. Markowski, S.-E. Park, S. Yoshikawa, and L. E. Cross, J. Am. Ceram. Soc. **79**, 2397 (1997).
[12] S.-E. Park, K. Markowski, S. Yoshikawa, and L. E. Cross, J. Am. Ceram. Soc. **80**, 407 (1997).
[13] K. Uchino, Jpn. J. Appl. Phys. 1 **24**, Suppl. 24-2, 460 (1985).
[14] A. Furuta, K. Oh, and K. Uchino, Sensors Mater. **3**, 205 (1992).
[15] K. W. Gachigi, Ph.D. thesis, The Pennsylvania State University, University Park, PA, 1996.
[16] S. Yoshikawa, N. Kim, T. Shrout, Q. Zhang, P. Moses, and L. E. Cross, Proc. SPIE **2441**, 223 (1995).
[17] M.-J. Pan (unpublished).
[18] A. Kachaturian (private communication).

APPENDIX 16

To be presented at SPIE's 4th Annual Symposium on Smart Structures and Materials
3-6 March 1997, San Diego, CA

Antiferroelectric-to-Ferroelectric Phase Switching Lead Lanthanum Zirconate Stannate Titanate (PLZST) Ceramics

Shoko Yoshikawa[a] , Kelley Markowski[b] , Seung-Eek Park,
Ming-Jen Pan, L. Eric Cross

Materials Research Laboratory, The Pennsylvania State University,
University Park, PA 16802

ABSTRACT

Electric field induced antiferroelectric (AFE) to ferroelectric (FE) phase transformations are accompanied by large strain and significant hysteresis. The properties of these materials can be tailored to fit specific applications such as high strain actuators and charge capacitors. As an attempt to reduce hysteresis, Barium and Strontium A-site substitution of the phase transformation behavior of $(Pb_{0.98-\delta}La_{0.02}A_{\delta})(Zr_xSn_yTi_z)O_3$ (A=Ba, Sr) ceramics have been investigated. The ceramic samples in this study produced 0.2% to 0.3% strain level. Barium proved to be a strong FE stabilizer with decreasing both switching field and hysteresis, while Strontium proved to be a strong AFE stabilizer. Some practical data, including temperature stability and current requirements, are also to be discussed.

Keywords: lead zirconate stannate titanate ceramics, antiferroelectric-to-ferroelectric phase switching ceramics, field induced strain, field induced polarization

1. INTRODUCTION

Lead zirconate ($PbZrO_3$) and lead titanate ($PbTiO_3$) form a complete solid-solution series (lead zirconate titanate, or PZT) of great technological importance. It is used in various Zr:Ti ratios and with numerous dopants to manufacture a vast array of electronic and electromechanical devices.

The effects of pressure-enforced ferroelectric (FE) to antiferroelectric (AFE) in modified $PbZrO_3$ was originally studied by Berlincourt et al. for an application of shock-actuated power supplies[1,2]. The relatively recent work on the same ceramics are published from Sandia National Laboratories[3,4].

Triaxial phase diagram introducing lead stannate ($PbSnO_3$) for both Niobium (Nb) and Lanthanum (La) doped system have been developed from the large amount of compositional study pursued at Clevite Corporation[1,2] in 1960s.

[a] Shoko Yoshikawa: Correspondence: e-mail: sxy3@psuvm.psu.edu; Phone: (814) 863-1096; Fax: (814) 865-2326
[b] Kelley Markowski: Current address: Materials Systems Inc., Littleton, MA 01460

Our interest in these families of materials lies in their ability to produce large strain at the electric (E)-field induced tetragonal AFE (AFE_T) to rhombohedral FE transformation (FE_R)[5,6]. Depending on the compositional adjustments, the materials can exhibit shape memory effect as described by Uchino, et al.[7].

Our compositions, unlike the above example of FE-to-AFE transformation to release energy upon application of pressure, start from AFE_T phase and switches to FE phase upon application of E-field. For actuator application, it is, therefore, important to optimize the compositions to exhibit following characteristics:

1. Larger strain, thus larger displacement,
2. Lower hysteresis, thus less heat generation, and
3. Lower switching field, thus less E-field requirement.

We have shown previously[8,9] that the B-site compositional modification controls switching field, though hysteresis behavior has little influence.

The objective in this study, therefore, is to attempt to produce compositions with less hysteresis without sacrificing too much strain while maintaining relatively low switching E-field. A-site modifications were accomplished by the addition of Ba and Sr.

2. EXPERIMENTAL PROCEDURE

2.1 Sample preparation

The five compositions described as A, A1, A2, B, and C in Table 1 were prepared according to the formula. Figure 1 shows the location of these compositions in the PLZST ternary phase diagram. Polycrystalline ceramic materials investigated in this study were prepared by solid state reaction, using the appropriate amount of reagent grade raw materials of lead carbonate ($PbCO_3$), lanthanum oxide (La_2O_3), zirconium dioxide (ZrO_2), titanium dioxide (TiO_2), and tin oxide (SnO_2). The chemical purity of each of the raw materials was greater than 99%. Barium and strontium additions were made using the appropriate amounts of strontium carbonate ($SrCO_3$) and barium carbonate ($BaCO_3$), respectively. The sintering process was carried out in a lead rich environment in order to minimize lead volatilization. To further enhance densification and increase the electric field where dielectric breakdown occurs, the sintered specimens were hot isostatically pressed for 2 hours at 1200°C in an air atmosphere under a pressure of 20MPa. Disk samples were then prepared by polishing with silicon carbide and alumina polishing powders to achieve a flat and parallel surface onto which gold was sputtered as an electrode.

Table 1. PLZT compositions.

	COMPOSITION	Comments
A	$(Pb_{0.88}La_{0.02})(Zr_{0.66}Ti_{0.26})_{0.995}O_3$	0% Ba, Zr:Ti:Sn 66:8:26
A1	$(Pb_{0.93}Ba_{0.05}La_{0.02})(Zr_{0.66}Ti_{0.08}Sn_{0.26})_{0.995}O_3$	5%Ba,Sr:Ti:Sn 66:8:26
A2	$(Pb_{0.88}Ba_{0.10}La_{0.02})(Zr_{0.66}Ti_{0.08}Sn_{0.26})_{0.995}O_3$	10%Ba,Zr:Ti:Sn 66:8:26
B	$(Pb0.93Sr0.05La0.02)(Zr_{0.55}Ti_{0.15}Sn_{0.30})_{0.995}O_3$	5% Sr, FE region of phase diagram
C	$(Pb0.93Ba0.05La0.02)(Zr_{0.55}Ti_{0.15}Sn_{0.30})_{0.995}O_3$	5% Ba, FE region of phase diagram

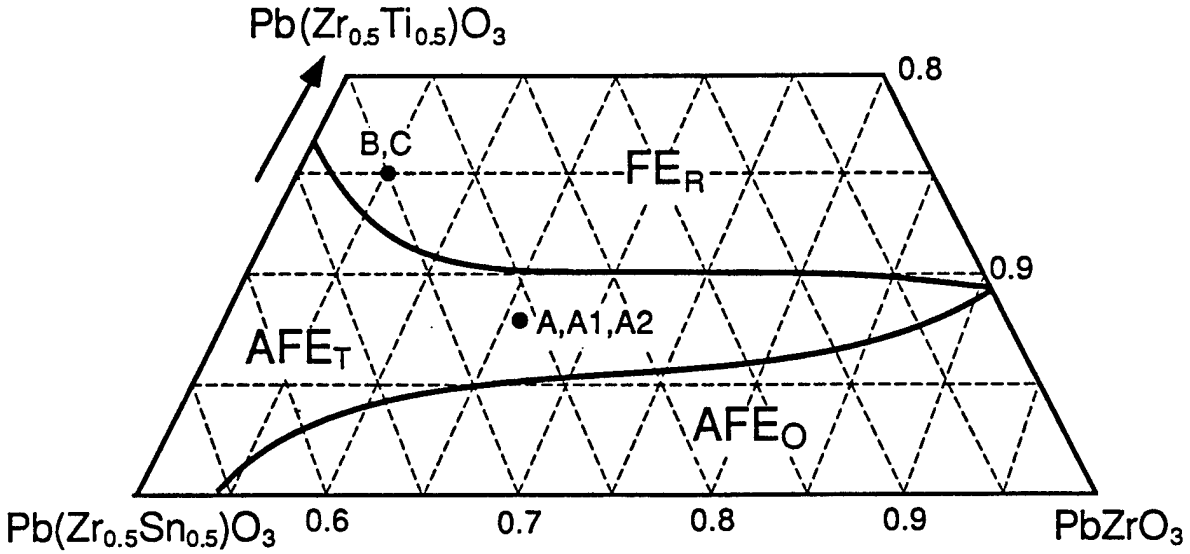

Figure 1: PLZST phase diagram and investigated compositions.

2.2 Characterization techniques

(a) Phase and microstructure

Calcined and sintered powders were examined by x-ray diffraction to insure phase purity and to identify the crystal structure. Typically, the samples showed a single phase within the detection limit of XRD (< 2%).

(b) Dielectric properties

Multifrequency meters (Hewlett Packard 4274A and 4275A LCR meters) were used in conjunction with a computer controlled temperature chamber (Delta Design Inc., Model MK 2300) to measure capacitance as a function of temperature and frequency. Capacitance was converted to dielectric permittivity using the sample geometry and permittivity of air. Measurements were taken from 100 Hz to 100 kHz at temperatures from -150°C to 250°C.

(c) Polarization and strain

High field measurements included polarization and strain hysteresis using a computer controlled modified Sawyer Tower system with a National Instruments Input Output card and linear variable displacement transducer (LVDT) sensor driven by a lock in amplifier (Stanford Research Systems, Model SR830). The voltage was supplied using a Trek 609C-6 high voltage DC amplifier. Through the LVDT sensor the strain of the samples can be measured with the applications of an applied field. Electric fields as high as ~ 100kV/cm were applied using an amplified sine waveform at 0.2 Hz. During testing the samples were submerged in Fluorinert (FC-40, 3M), an insulating liquid, to prevent arcing.

3. RESULTS AND DISCUSSION

3.1 A-Site Modification

A-site modifications were based on tolerance factor, which can be described for perovskites with the general formula ABX_3 by:

$$t = (R_A + R_X) / (\sqrt{2})(R_B + R_X)$$

where R_A = radius of A, R_B = radius of B and R_X = radius of X. Ba^{2+} (1.48Å) is larger than Pb^{2+} (1.32Å), and Sr^{2+} (1.27Å) is smaller than Pb^{2+}. When $t > 1$ the FE phase is stabilized when $t < 1$ the AFE phase is stabilized[10]. For Pb based compounds, however, only trends need to be considered because of the high polarizability of the Pb. Both Ba and Sr were considered as A-site additions only in this study. Ba being a FE stabilizer and Sr being a AFE stabilizer both potentially lowering T_{max} and subsequently suppressing hysteresis.

Figure 2 shows E-field induced polarization (a) and strains (b) for compositions A, A1, and A2. As anticipated, increased Ba^{2+} content clearly lowered switching field, and decreased hysteresis. It is important to note that the maximum strain is a function of applied electric field after the switching. The dielectric data is shown in Figure 3. This data showed a decrease T_{max} (associated with decreased hysteresis), increased K_{max} and increased $T_{FE\text{-}AFE}$ (associated with decreased switching field) with increased Ba^{2+} content, though $T_{FE\text{-}AFE}$ is not obvious in virgin sample. This also indicates that the operating temperature range is narrower as Ba^{2+} content increased (to be discussed below).

Figures 4 to 7 show the results of compositions B and C. The original location of the composition is in rhombohedral ferroelectric region (FE_R); therefore, the composition without Ba or Sr addition is ferroelectric. As anticipated from Sr being AFE stabilizer, as sintered composition B with 5% Sr addition showed antiferroelectric, and underwent AFE-to-FE transformation upon application of E-field (Figure 4). The switching field was approximately 50 kV/cm, and hysteresis was relatively small.

On the contrary, the same composition with Ba^{2+} addition instead of Sr^{2+} showed stable ferroelectric behavior, as shown in Figure 6. Dielectric data in Figure 7 showed a transition from FE to PE (paraelectric) without any AFE stable temperature range. It is determined from the fact that the cooling run (sample depoled by exposing temperature above T_{max}) showing higher dielectric constant than heating (E-field exposed sample) run, unlike the data in Figure 5.

3.2. Temperature stability

Low field dielectric data, as discussed above, are important tools to determine temperature stability of each composition without actually measuring the strain in different temperature conditions. At very low temperature all of the compositions discussed in this study are ferroelectric. There are temperature regions in which compositions show AFE phase, which can be transformed to FE by E-field. Above T_{max}, the phase is PE so that only electrostrictive strain behavior can be observed.

General temperature behavior of this family of ceramics is shown in Figure 8 of temperature and E-field phase diagram. The shaded areas describe hysteresis. As the figure indicates, it is possible to decrease hysteresis by operating at a higher temperature, though strain level will be reduced.

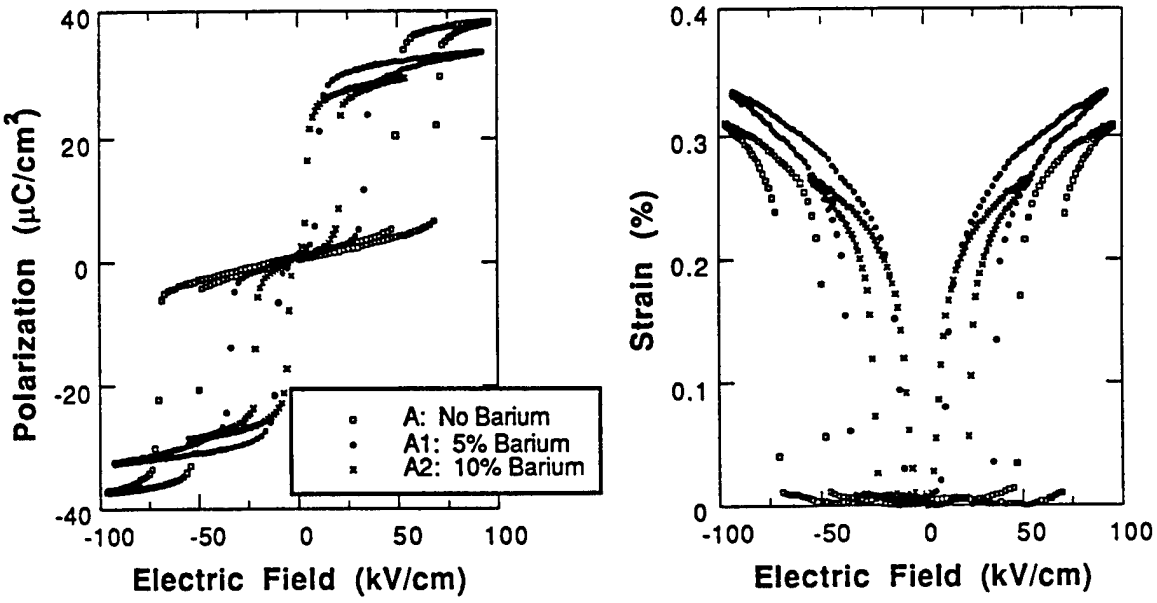

(a) (b)

Figure 2: Electrically induced polarization (a) and strain (b) for compositions A, A1, and A2.

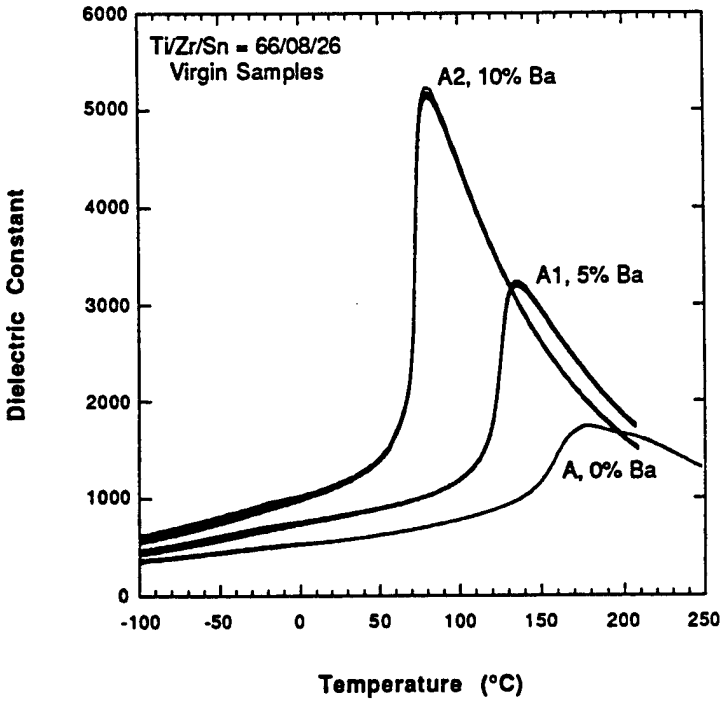

Figure 3: Temperature dependence of dielectric constant for the compositions A, A1, and A2; (cooling) virgin sample.

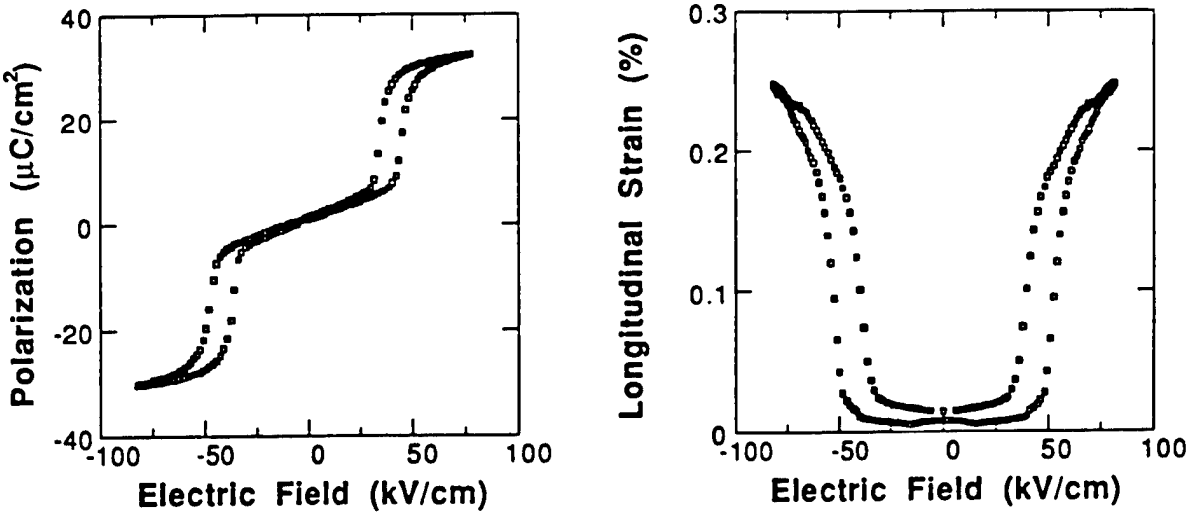

Figure 4: Electrically induced polarization and strain for composition B.

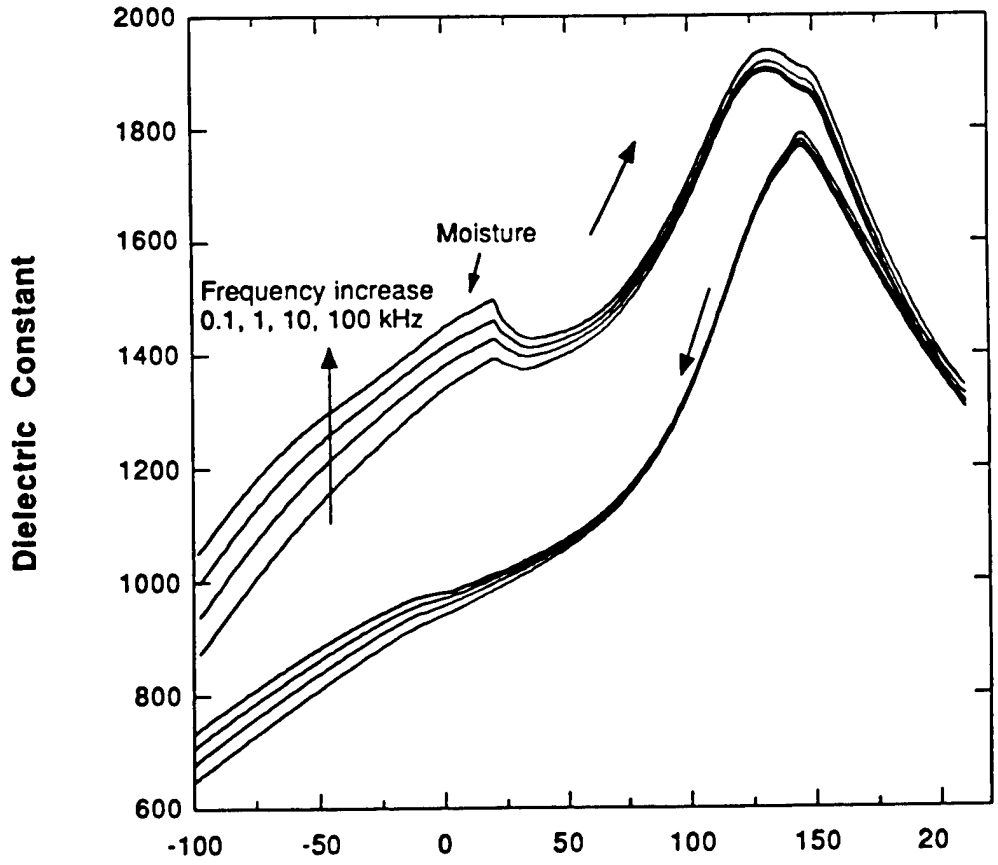

Figure 5: Temperature dependence of dielectric constant for the composition B; poled sample, heating first, then cooling

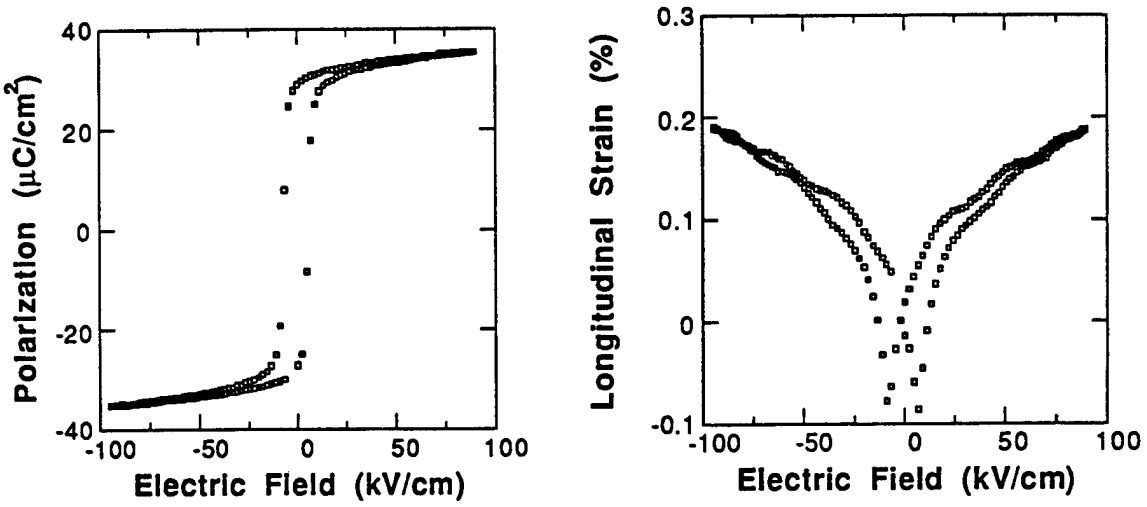

Figure 6: Electrically induced polarization and strain for composition C.

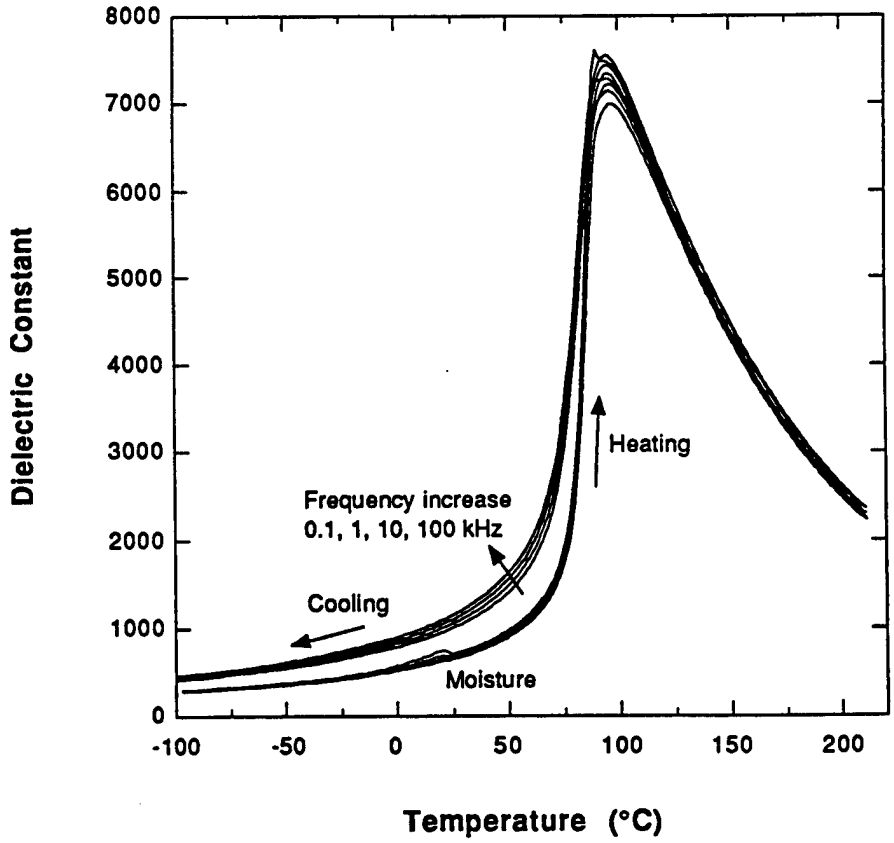

Figure 7: Temperature dependence of dielectric constant for the composition C; poled sample, heating first, then cooling

The above study of A-site modification showed that it is possible to decrease hysteresis and switching field at room temperature with, unfortunately, narrowing AFE temperature range. It is, therefore, critical to determine optimum composition based upon the requirements of a specific application and tailor the properties of the phase change materials.

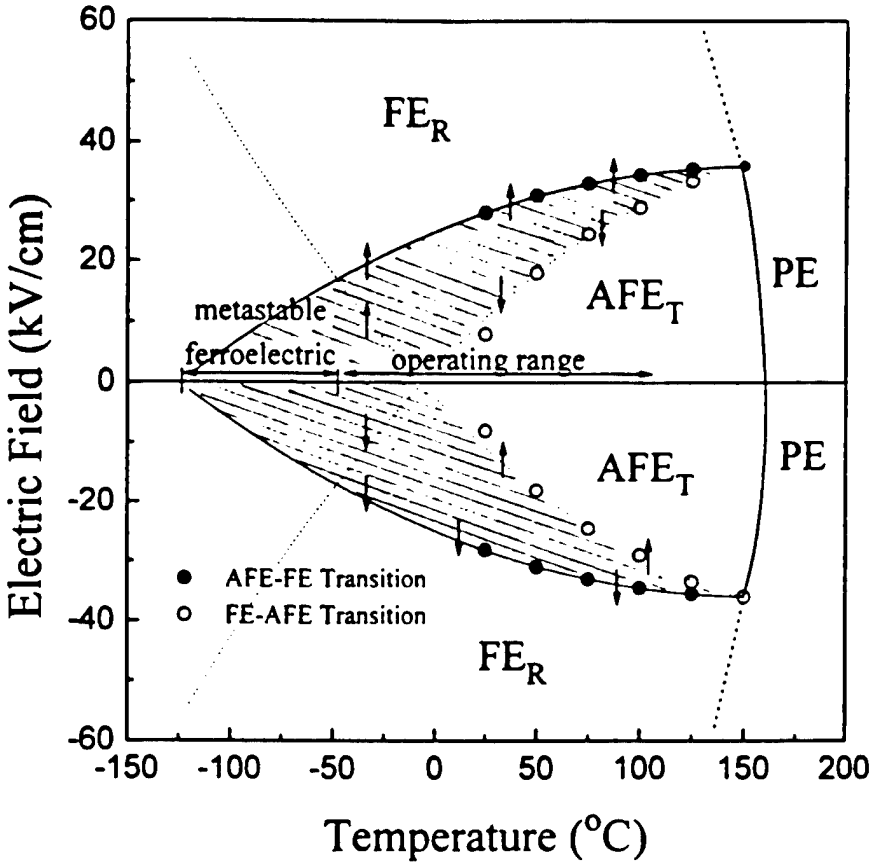

Figure 8: Temperature-electric field phase diagram. Shaded area indicates hysteresis.

3.3. Current requirement

Previous study[5] on compositional modification on the B-site also showed high field dielectric constants and loss by using DC bias field. As sharp increase and decrease in polarization hysteresis loop indicate, charge requirement to drive these ceramics as actuators can be quite high. Figure 9 shows the AC current required when one of the samples undergoes a phase transition from AFE-FE and subsequent switching back into the AFE phase by increasing and decreasing E-field. These measurements were completed at a low frequency (0.2 Hz) and represent relatively low current requirements. The current required at a higher frequency would be substantially higher and should be taken into account when the operating circuit for this material is designed. Current is lost in the time required to complete a measurement cycle (5 sec in this case), which accounts for the lack of symmetry in Figure 9.

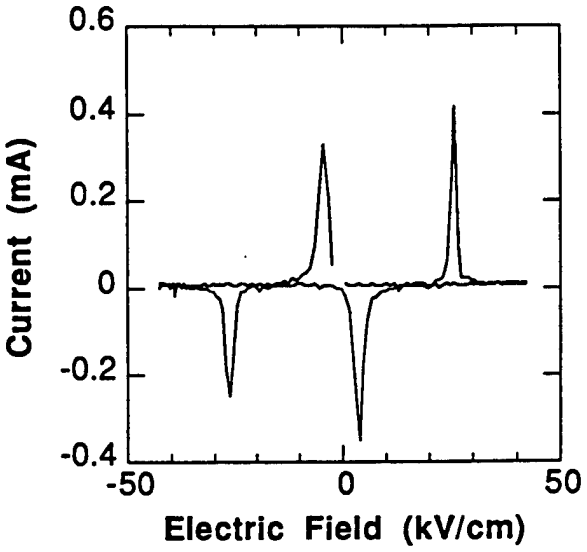

Figure 9: Current requirements on phase switching (0.2 Hz).

4. CONCLUSIONS

A-site compositional modification can be used along with B-site Ti:Sn ratio changes to modify the properties of phase switching ceramics, for example decreasing hysteresis. Sr additions have limited merit alone because they cause increases in the switching field and, therefore, increases in the field necessary to obtain maximum strain levels. Sr addition, however, suppressed hysteresis.

Ba additions proved to be a FE phase stabilizer, lowering both the amount of hysteresis and the switching field. It should be noted, however, that these changes also make the AFE temperature range smaller. The operation temperature and current requirement for this family of ceramics were also summarized. Ideally, with respect to application, a balance should be maintained between switching field, hysteresis and operating temperature range.

ACKNOWLEDGEMENTS

This work was sponsored by DARPA contract through Boeing SSRC (Smart Structure Rotor Control) Consortium, program monitor being Drs. Robert Crowe and Spencer Wu. The authors would like to thank Profs. Thomas Shrout and Clive Randall for their stimulating discussions, and Joe Kearns for his help on sample preparations.

REFERENCES

1. D. Berlincourt, H.H.A. Krueger, and B. Jaffe, "Stability of Phases in Modified Lead Zirconate with Variation in Pressure, Electric Field, Temperature, and Composition," *J. Phys. Chem. Solids*, **Vol. 25**, 659–674 (1964).

2. B. Jaffe, "Antiferroelectric Ceramics with Field-Enforced Transitions: A New Nonlinear Circuit Element," *The Proceedings of the IRE*, **Vol. 49**[8], 1264–1267 (1961).

3. D.H. Zeuch, S.T. Montgomery, J.D. Keck, "Hydrostatic and triaxial compression experiments on unpoled PZT 95/5-2Nb ceramic: The effects of shear stress on the F_{R1} to A_O polymorphic phase transformation," *J. Mater. Res.*, **7**, pp. 3314–3332 (1992).

4. D.H. Zeuch, S.T. Montgomery, J.D. Keck, "Further observation on the effect of nonhydrostatic compression on F_{R1} to A_O polymorphic phase transformation in niobium doped, lead-zirconate-titanate ceramic," *J. Mater. Res.*, **9**, pp. 1322–1327 (1994).

5. K. Uchino and S. Nomura, "Electrostriction in PZT-Family Antiferroelectrics," *Ferroelectrics*, **Vol. 50**, 191–196 (1983).

6. W.Y. Pan, Q. Zhang, A. Bhalla, and L.E. Cross, "Field-Forced Antiferroelectric-to-Ferroelectric Switching in Modified Lead Zirconate Titanate Ceramics," *J. Am. Ceram. Soc.*, **Vol.[4]**, 571–578 (1989).

7. A. Furuta, K-Y Oh, and K. Uchino, "Shape Memory Ceramics and Their Application to Latching Relays," *Sensors and Materials*, **3.4**, 205–215 (1992).

8. S. Yoshikawa, N. Kim, T. Shrout, Q. Zhang, P. Moses, L.E Cross, "Field-Induced Lead Zirconate Titanate Stannate Antiferroelectric-to-Ferroelectric Phase Switching Ceramics, SPIE North American Conference on Smart Structure and Materials, *SPIE* **Vol. 2441**, p. 223–232.

9. K. Markowski, S-E. Park, S. Yoshikawa, L.E. Cross, "The Effect of Compositional Variations in the Lead Lanthanum Zirconate Stannate Titanate System on Electrical Properties," to be published in J. *Am. Ceram. Soc.*

10. K.J. Rao, C.N.R. Rao, Phase Transition in Soleds: An approach to the Study of the Chemistry and Physics of Solids," McGraw-Hill, New York (1978).

APPENDIX 17

Electric Field Induced Phase Transition in Lead Lanthanum Stannate Zirconate Titanate (PLSnZT) Antiferroelectrics: Tailoring Properties through Compositional Modification

Ming-Jen Pan, Seung-Eek Park, Kelley A. Markowski*, Wesley S. Hackenberger, Shoko Yoshikawa†, and L. Eric Cross
Materials Research Laboratory
The Pennsylvania State University
University Park, PA 16802

Abstract

In this study, we investigated the effects of dopants on the antiferroelectric-to-ferroelectric (AFE-FE) phase transition behavior of lead lanthanum stannate zirconate titanate (PLSnZT) family of ceramics. In particular, the possibility to lower both the switching field and hysteresis by compositional modification was sought. Based on tolerance factor considerations, barium (Ba) and strontium (Sr) were chosen as modifiers to stabilize ferroelectric and antiferroelectric phases, respectively. With the right starting composition and proper amount of dopant, we demonstrated that the properties of PLSnZT can be tailored to fit the needs of specific applications. It was also observed that the temperature dependence of dielectric constants, such as the ferroelectric-to-antiferroelectric transition temperature ($T_{FE\text{-}AFE}$) and the temperature of the maximum dielectric constant (T_{MAX}), is strongly related to the phase switching behavior. The influence of dopants on the operating temperature range was also examined.

Keywords: antiferroelectrics, phase switching ceramics, compositional modification, lead lanthanum stannate zirconate titanate (PLSnZT)

---

* Now with Materials Systems Inc., Littleton, MA.

† Now with Active Control eXperts, Inc, Cambridge, MA.

I. Introduction

Lead lanthanum stannate zirconate titanate (PLSnZT) family of ceramics was first investigated by Berlincourt [1] and has been widely studied since then. The ternary phase diagram is shown in Figure 1. It was established that the antiferroelectric tetragonal (AFE_{tet}) phase can be readily switched to ferroelectric rhombohedral (FE_{rh}) phase with the application of an electric field. This antiferroelectric-to-ferroelectric (AFE-FE) phase transition is accompanied by a large volume strain, which is a result of the larger FE_{rh} cell as compared to the AFE_{tet}. In particular, the high longitudinal strain (in the electric field direction) has been of interest for high performance actuators and transducers. Previous studies reported strain as high as 0.85% [2,3], although other crystallographic analyses based on X-ray diffraction have shown that 0.5% is the maximum strain possible for an ideal single crystal in this system [4,5]. Our previous study [6] showed that 0.2% strain is readily achieved at the AFE-FE switching field for polycrystalline PLSnZT ceramics. Subsequent increase in electric field beyond switching yields further increase in strain, a result of the piezoelectric effect of the FE_{rh} phase.

For the application of AFE ceramics, it is desirable to have low switching field coupled with high strain. In particular, large hysteresis is an undesirable characteristic as the generated heat is difficult to dissipate in an encapsulated environment during service. Efforts have been made in the past to search for compositions with both low switching field and hysteresis. [6] The effect of varying Zr:Sn and Ti:Sn ratios near the AFE_{tet}-FE_{rh} morphotropic phase boundary (MPB) in the phase diagram (Figure 1) was investigated and reported. It was found that on decreasing the Ti:Sn ratio (top to bottom) along a line perpendicular to the MPB, the switching field increased and the hysteresis remained constant. On the other hand, increasing the Zr:Sn ratio (left to right) along the MPB caused the switching field to decrease and the hysteresis to increase. Apparently, although one can modify the switching field and hysteresis with B-site variation, it is not possible to produce

the desired decrease in both switching field and hysteresis. These variations at best produce compositions with lowered switching field and constant hysteresis (Ti:Sn ratio variation).

Alternatively, A-site modifications based on tolerance factor consideration and phase stability can be used for tailoring PLSnZT properties. The tolerance factor (t) for perovskites can be described with the general formula ABO_3 by:

$$t = \frac{R_A + R_O}{\sqrt{2}(R_B + R_O)}$$

where R_A= radius of A
R_B= radius of B
R_O= radius of O.

In general, when t > 1 the FE phase is stabilized and when t < 1 the AFE phase is stabilized.[7] For Pb-based compounds, however, only trends needed to be considered, i.e., the size of the substitute ions relative to Pb ions, because of the high polarizability of lead ions. In this study, barium (Ba) and strontium (Sr) were chosen for the A-site modification. Their ionic radii (valence=2+ and coordination=12) are 1.48Å and 1.27Å, respectively, comparing to 1.32Å for Pb^{2+}. Therefore, it was suggested that both barium and strontium can be used to modify the switching behavior: Ba being a FE stabilizer and Sr being a AFE stabilizer. [8] Note that both Ba and Sr were considered as A-site additions due to their valence.

In this study, the effect of A-site substitution on the AFE-FE phase transition behavior of PLSnZT was investigated. Specifically, we examined the possibility of "fine-tuning" both switching field and hysteresis with Ba and Sr modifications. Most of the compositional modifications were made adjacent to a well-studied PLSnZT, $Pb_{0.98}La_{0.02}(Sn_{0.33}Zr_{0.55}Ti_{0.12})_{0.995}O_3$ (composition A), whose phase switching behavior is shown in Figure 2. Various combinations of starting composition and dopant

were attempted. Their electric field-induced polarization, strain, and dielectric properties were characterized and the implications of the results were discussed.

II. Experimental Procedure

One composition in the AFE_{tet} region $((Pb_{0.98}La_{0.02})(Sn_{0.35}Zr_{0.55}Ti_{0.10})_{0.995}O_3$, designated R0) and another in the FE_{rh} region $((Pb_{0.98}La_{0.02})(Sn_{0.27}Zr_{0.55}Ti_{0.18})_{0.995}O_3$, designated S0) were selected as the primary compositions for this study. Various amounts of Ba and Sr, respectively, were added to these and neighboring compositions. Note that the compositions have a Zr content (on B-site) of either 55% or 66% while varying Ti:Sn ratio. This was based on our previous observation that constant Zr is correlated to constant hysteresis. [6] In this way, the effects of dopants on different compositions can be compared on the same basis. All the compositions and their designations were tabulated in Table I. Polycrystalline samples were made by solid state reaction using reagent grade raw powders.

Calcined powders were examined by X-ray diffraction (XRD) to insure phase purity and to identify crystal structure. Typical samples showed a single phase within the detection limit of XRD. Ceramic pellets were sintered at 1300°C for 6 hours in a lead-rich environment to suppress lead volatilization. Dimensional density and lead loss of sintered samples were measured and listed in Table II. Grain size of samples was examined by scanning electron microscopy (SEM). Typical grain size was between 5 and 8 μm. Sintered pellets were ground and polished to achieve flat and parallel surfaces onto which gold electrodes were sputtered.

The polarization and strain under high electric field were measured using an integrated, computer-controlled system. Electric fields as high as 100 kV/cm were applied

to the sample using a high voltage amplifier†. All measurements were conducted at 0.2Hz. During measurement, samples were immersed in Fluorinert*, an insulating liquid, to prevent arcing. Polarization induced by the applied field was measured by using a Sawyer-Tower circuit. In the meantime, strain in the field direction was monitored by a linear variable displacement transducer (LVDT) driven by a lock-in amplifier¶. LCR meters¥ were used in conjunction with a computer controlled temperature chamber‡ to measure sample capacitance as a function of temperature and frequency. Measurements were taken at 100, 1k, 10k, and 100kHz at temperatures from -100°C to 200°C.

III. Results and Discussion

(1) Strontium Modification

(a) Constant (5%) Sr Addition and Varying Ti:Sn Ratios

As Strontium is an AFE stabilizer, composition S0 (Zr:Ti:Sn=55:18:27), located in the FE_{rh} region of the PLSnZT phase diagram, was chosen for the modification. It exhibited the typical polarization and strain behaviors of ferroelectric materials, as summarized in Table II.

Three compositions (S1, S2, and S3) with varying Ti:Sn ratios, i.e., different distance from the MPB, were modified with 5% Sr. It has been shown that varying Ti:Sn ratio while maintaining the same Zr content does not affect the hysteresis of PLSnZT.[6] Their polarization and strain behaviors are shown in Figure 3 and summarized in Table II. Since Sr^{2+} ion is smaller than Pb^{2+} ion (1.27Å and 1.32 Å respectively for coordination=12), it increases the tolerance factor upon substitution, and thus stabilizes the antiferroelectric phase. As a result, compositions S1 and S2 have become antiferroelectric,

---

† Trek 609C-6, Trek Incorporated, Medina, New York

* Fluorinert™ FC-40, 3M, St. Paul, Minnesota

¶ Model SR830, Stanford Research Systems,

¥ Model 4274A and 4275A, Hewlett Packard,

although they are located in the FE region (Figure 3). The strain at the switching field for both S1 and S2 was about 0.2%, which was comparable to that of S0. The hysteresis was slightly reduced comparing to composition A. Moving farther away from the morphotropic phase boundary, the material would become ferroelectric, as in the case of composition S3.

The addition of Sr produced a dramatic decrease in maximum dielectric constant and diffuse dielectric behavior as a function of temperature, as shown in Figure 4. This can be attributed to the smaller size of Sr^{2+} ion, which decreases the space where B-site cation can "rattle" and thus decreases polarizability. Sr addition also slightly decreased the T_{MAX}, indicating further stabilization of the paraelectric phase along with the antiferroelectric phase.

(b) Varying Sr Addition and Constant Ti:Sn (18:55) Ratios

Various amounts of Sr (5%, 8%, and 10% for compositions S4, S5, and S6, respectively) were added to composition S0 to further observe the effects of varying Sr addition. The polarization and strain behaviors are shown in Figure 5 and also summarized in Table II. Polarization data showed that increasing Sr content to 8% and 10% resulted in very narrow hysteresis loops, diffuse phase transition, and compromised strain level. Note that as Sr is an antiferroelectric phase stabilizer, the required electric field for phase switching increased with increasing Sr content. This makes Sr somewhat cumbersome to be used as a compositional modifier. As a result, property-tailoring would require a perfect combination of modifier quantity and starting composition on the phase diagram.

As mentioned in the previous section, the addition of Sr causes a decrease in polarizability and dielectric constant. This became more obvious as more Sr was added to the system. As shown in Figure 6, not only did the maximum dielectric constant decrease dramatically, but the dielectric behavior also became very diffuse as a function of

---

‡ Model MK 2300, Delta Design Inc.,

temperature. Note that T_{MAX} shifted to lower temperatures with increasing Sr content. This was consistent with our previous study [6] on this ternary system which had also correlated T_{MAX} with hysteresis.

A discrepancy in the hysteresis loops of polarization and strain was observed. The hysteresis of strain loops is apparently larger than that of polarization loops. The origin of this decoupling of polarization and strain is not known. Similar decoupling behavior, however, has also been observed elsewhere. [9,10] An attempt to explain the decoupling phenomenon has recently been made [10] and will not be elaborated here. The reason for the observed decoupling is subjected to further study.

(2) Barium Modification

Composition R0 (Zr:Ti:Sn=55:10:35) located in the AFE_{tet} region of the PLSnZT phase diagram was chosen for the barium modification. Additions of 5%, 10%, and 12% of Ba (compositions R1, R2, and R3, respectively) were attempted. Their polarization and strain behaviors are shown in Figure 7. The switching field, polarization, and strain data are summarized in Table II. It was clear that the addition of Ba induced a shift in the AFE_{tet}-FE_{rh} morphotropic phase boundary towards composition R0, as shown by the decrease in both the switching field and hysteresis. This was consistent with the fact that Ba is an FE phase stabilizer. Increasing Ba content further reduced the switching field and hysteresis with a small decrease in generated strain. Like Sr additions, the phase transition also became more diffuse.

One interesting result was the behavior of composition R3 (12% Ba). Both the polarization and strain, while maintaining their antiferroelectric characteristic, showed a relaxor-type behavior with little hysteresis. Its antiferroelectric characteristics can still be seen in the form of the narrow double-hysteresis loop. Nevertheless, the strain is much smaller than what can be achieved in other compositions. The temperature dependence of composition R3 will be discussed later.

The dielectric data of R0, R1, R2, and R3 are shown in Figure 8. The addition of Ba obviously produced an increase in the maximum dielectric constants. This can be described by the tolerance factor considerations. Since Ba^{2+} ion is larger than Pb^{2+} (1.48Å and 1.32Å for respectively for coordination=12), it increases the space in which the B-site cation can "rattle," and thus the increase in polarizability. Ba additions also decreased the T_{MAX}, indicating stabilization of the paraelectric phase along with the antiferroelectric phase. Although this decrease in T_{MAX} can be correlated to the reduction in hysteresis, it also means that the usable temperature range of Ba-doped materials is reduced.

(3) Comparison of Results in other AFE Region (Zr=66% on B-Site)

To check the validity of the above doping strategy in different regions of the phase diagram, further modifications were made in the vicinity of composition B (Zr=66%). Specifically, compositions R4 and R5 with 5% and 10% barium, respectively, which have the same distance to the MPB as compositions R1 and R2, which were also 5% and 10%. On the other hand, 5% strontium was added in composition S7, which also has the same distance to the MPB as composition S2. In this way, the comparisons could be made on the same basis. As shown in Figure 9 and Table II, both dopants have similar effects as in the previous region. Compositions C2 and C3 showed decreased hysteresis with strain levels comparable to that of composition B. Composition S7, which was modified with 5% Sr, became an "metastable" antiferroelectric material. Coincidentally, its counterpart with Zr=55% also showed a "metastable" switching behavior.

It was interesting to see the effectiveness of Ba and Sr in reducing hysteresis in these regions. Shown in Figure 10 is the percentage reduction of hysteresis for various conditions. Clearly barium was a better hysteresis suppresser when added in compositions with lower Zr content, i.e., away from the $PbZrO_3$ corner of the phase diagram. In

contrast, strontium has roughly the same effects in suppressing hysteresis regardless of the Zr content.

(4) Temperature Effect

As mentioned earlier, the addition of Ba can be used to tailor a material's dielectric properties. It, however, also reduces T_{MAX} and stabilizes ferroelectric phase. As a result, the temperature range under which a composition can be operated was also limited. To illustrate this reduction of operating temperature range, we measured the electrical behavior of composition R3 at a different temperature. As shown in Figure 11, it became ferroelectric at 0°C and lost the advantageous narrow hysteresis. Thus, although R3 had excellent characteristics at room temperature, it also had an extremely narrow operating temperature range, which severely limit its value as an actuator material. In comparison, the addition of Sr reduces T_{MAX} but stabilizes AFE phase and therefore the operating temperature is less affected. Strontium doping, however, increased the switching field, which required a starting FE composition deep into the FE region. As a result, it was disadvantageous to be used as a modifier.

IV. Conclusions

Based on tolerance factor considerations, we have successfully demonstrated that both Ba and Sr are effective dopants for reducing hysteresis and controlling switching fields in different regions of the PLSnZT ternary phase diagram. We further exemplified the capability of this system to be tailored to fit specific applications through a combination of A- and B-site modifications. Barium proved to be an FE stabilizer, lowering both the hysteresis and switching field. On the other hand, strontium was an AFE stabilizer,

lowering the hysteresis while increasing the switching field, which made strontium somewhat cumbersome to be used as a composition modifier.

The ability to tailor materials' electrical properties, however, does come at the price of reduced strain level. For this reason, it is important to make compositional modification on starting compositions with high strain. In addition, the Ba and Sr modifiers also alter the phase stability of materials at different temperatures, and thus limit the operating temperature range of the materials. Therefore, a balance must be maintained among switching field, hysteresis, and operating temperature according to the needs of specific applications.

References

1. D. Berlincourt, IEEE Transactions on Sonics and Ultrasonics, Vol. SU-13 [4] 116-125 (1966).
2. W. Pan, Q. Zhang, A. Bhalla, and L.E. Cross, *J. Am. Ceram. Soc.*, **72** [4] 571-78 (1989).
3. W.Y. Pan, C.Q. Dam, Q.M. Zhang, and L.E. Cross, *J. Appl. Phys.*, **66** [12] 6014-23 (1989).
4. C.T. Blue, J.C. Hicks, S.-E. Park, S. Yoshikawa, and L.E. Cross, *Appl. Phys. Lett.*, **68** [21] 2942-44 (1996).
5. L. Shebanov, M. Kusnetsov, and A. Sternberg, *J. Appl. Phys.*, **76** [7] 4301-4 (1994).
6. K.A. Markowski, S.-E. Park, S. Yoshikawa, and L.E. Cross, *J. Am. Ceram. Soc.*, **79** [12] 3297-304 (1996).
7. K.J. Rao and C.N.R. Rao, *Phase Transitions in Solids: An Approach to the Study of the Chemistry and Physics of Solids*, McGraw-Hill, New York, 1978.
8. S.-E. Park, K.A. Markowski, S. Yoshikawa, and L.E. Cross, *J. Am. Ceram. Soc.*, **80** [2] 407-12 (1997).
9. D. Vieland, D. Forst, Z. Xu, and J.-F. Li, *J. Am. Ceram. Soc.*, **78** [8] 2101-12 (1995).
10. S.-E. Park, M.-J. Pan, K.A. Markowski, S. Yoshikawa, and L.E. Cross, ," *J. Appl. Phys.*, **82** [4] 1798-803 (1997).

Table I List of compositions and their designations

Designation	Composition
A	$Pb_{0.98}La_{0.02}(Sn_{0.33}Zr_{0.55}Ti_{0.12})_{0.995}O_3$
B	$Pb_{0.98}La_{0.02}(Sn_{0.24}Zr_{0.66}Ti_{0.10})_{0.995}O_3$
R0	$Pb_{0.98}La_{0.02}(Sn_{0.35}Zr_{0.55}Ti_{0.10})_{0.995}O_3$
R1	$Pb_{0.93}Ba_{0.05}La_{0.02}(Sn_{0.35}Zr_{0.55}Ti_{0.10})_{0.995}O_3$
R2	$Pb_{0.88}Ba_{0.10}La_{0.02}(Sn_{0.35}Zr_{0.55}Ti_{0.10})_{0.995}O_3$
R3	$Pb_{0.86}Ba_{0.12}La_{0.02}(Sn_{0.35}Zr_{0.55}Ti_{0.10})_{0.995}O_3$
R4	$Pb_{0.93}Ba_{0.05}La_{0.02}(Sn_{0.26}Zr_{0.66}Ti_{0.08})_{0.995}O_3$
R5	$Pb_{0.93}Ba_{0.10}La_{0.02}(Sn_{0.26}Zr_{0.66}Ti_{0.08})_{0.995}O_3$
S0	$Pb_{0.98}La_{0.02}(Sn_{0.27}Zr_{0.55}Ti_{0.18})_{0.995}O_3$
S1	$Pb_{0.93}Sr_{0.05}La_{0.02}(Sn_{0.28}Zr_{0.55}Ti_{0.17})_{0.995}O_3$
S2	$Pb_{0.93}Sr_{0.05}La_{0.02}(Sn_{0.27}Zr_{0.55}Ti_{0.18})_{0.995}O_3$
S3	$Pb_{0.93}Sr_{0.05}La_{0.02}(Sn_{0.26}Zr_{0.55}Ti_{0.19})_{0.995}O_3$
S4	$Pb_{0.93}Sr_{0.05}La_{0.02}(Sn_{0.27}Zr_{0.55}Ti_{0.18})_{0.995}O_3$
S5	$Pb_{0.90}Sr_{0.08}La_{0.02}(Sn_{0.27}Zr_{0.55}Ti_{0.18})_{0.995}O_3$
S6	$Pb_{0.88}Sr_{0.10}La_{0.02}(Sn_{0.27}Zr_{0.55}Ti_{0.18})_{0.995}O_3$
S7	$Pb_{0.93}Sr_{0.05}La_{0.02}(Sn_{0.26}Zr_{0.66}Ti_{0.08})_{0.995}O_3$

Table 2 Summary of polarization and strain for the compositions in this study

	Electric-Field Induced Polarization and Strain							Contents	
	At Switching Field				At Maximum Applied Field				
	E_{AF} (kV/cm)	$\Delta E = E_{AF} - E_{FA}$ (kV/cm)	P_S ($\mu C/cm^2$)	S_3 (%)	$E_{app.}$	$P_{app.}$ ($\mu C/cm^2$)	S_3 (%)	Dopant	Zr Content
A	28	22	30	0.16	84	34	0.34	no Ba	55%
B	37	25	32	0.18	111	38	0.42	no Ba	66%
R0	60	15	27	0.19	73	32	0.26	no Ba	55%
R1	30	12.8	23	0.18	89	31	0.29	5% Ba	55%
R2	14.5	7.6	20	0.16	90	29	0.26	10% Ba	55%
R3	13	1.8	20	0.08	68	27	0.16	12% Ba	55%
R4	39	24	24	0.20	92	34	0.34	5% Ba	66%
R5	27	15	24	0.17	54	29	0.27	10% Ba	66%
S0	FE	13	---	---	61	35	0.24	no Sr	55%
S1	32	18	20	0.18	86	30	0.27	5% Sr	55%
S2	16	18	24	0.17	78	32	0.28	5% Sr	55%
S3	FE	15	---	---	69	32	0.24	5% Sr	55%
S4	16	18	24	0.17	72	32	0.27	5% Sr	55%
S5	42	8	22	0.12	82	29	0.18	8% Sr	55%
S6	50	3	19	0.10	82	25	0.16	10% Sr	55%
S7	16	21	24	0.19	61	34	0.30	5% Sr	66%

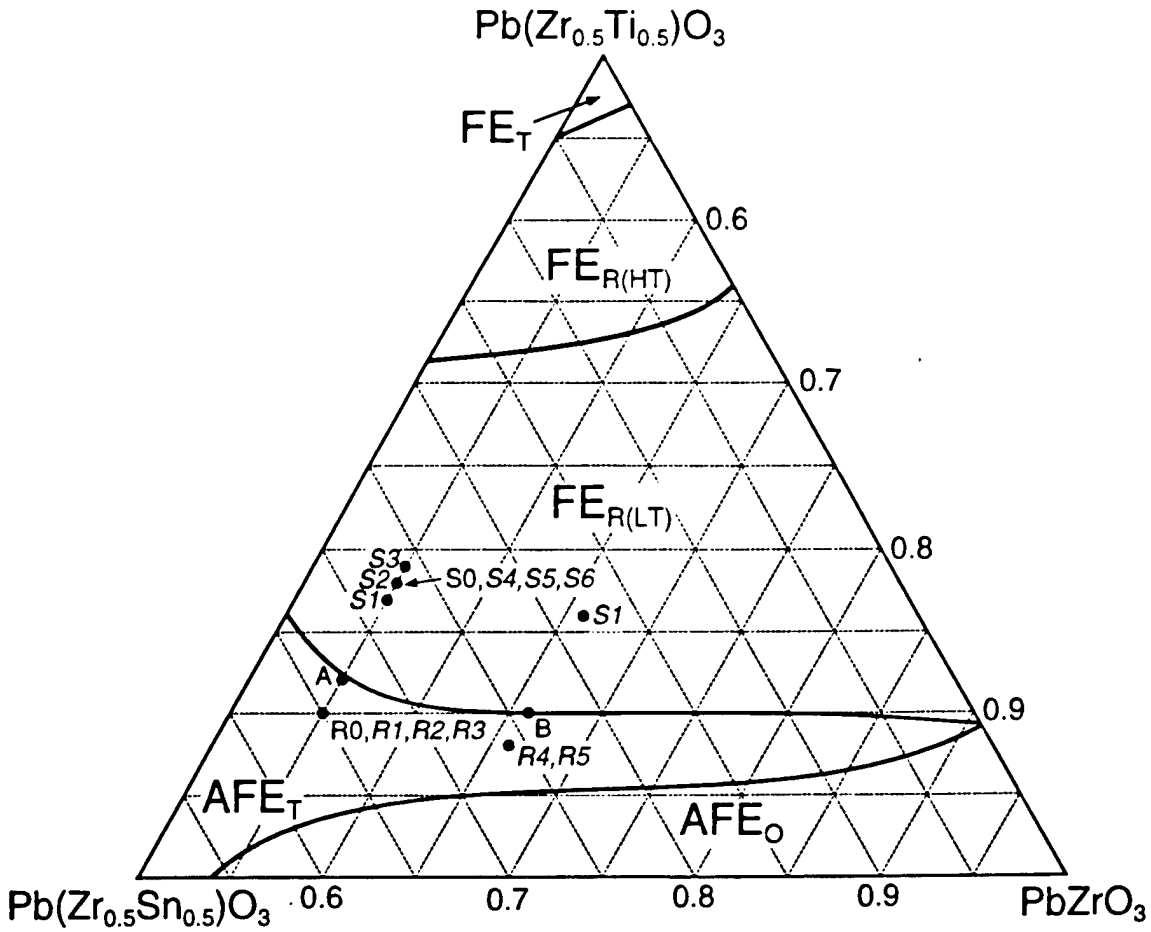

Figure 1 The ternary phase diagram of lead stannate zirconate titanate (with 2% lanthanum) family of ceramics and the compositions used in this study. Note that most compositions were doped with either barium or strontium, as indicated in Table I.

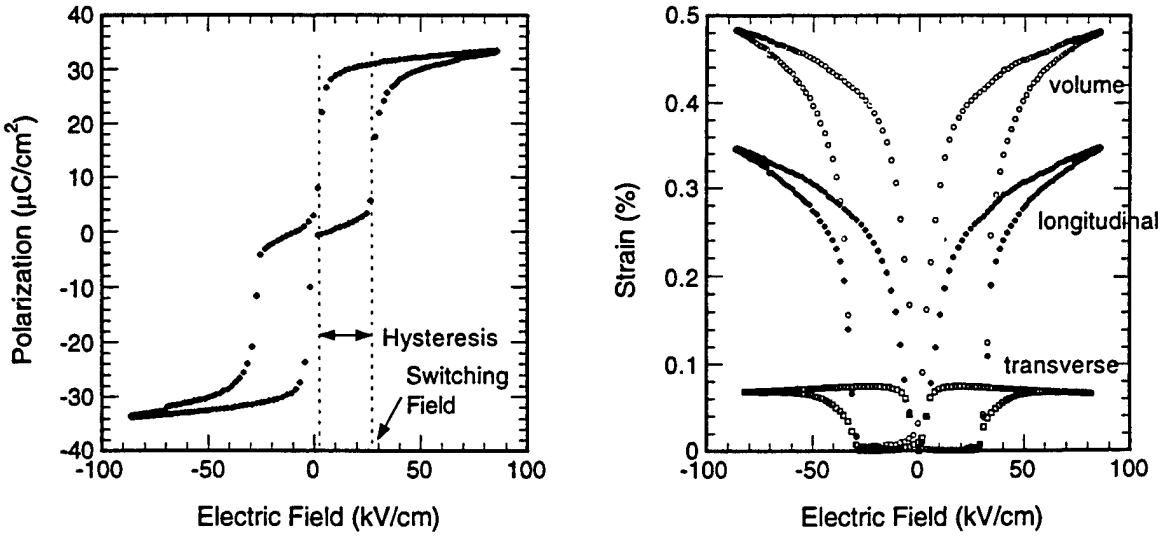

Figure 2 Electric field-induced polarization and strain for composition A

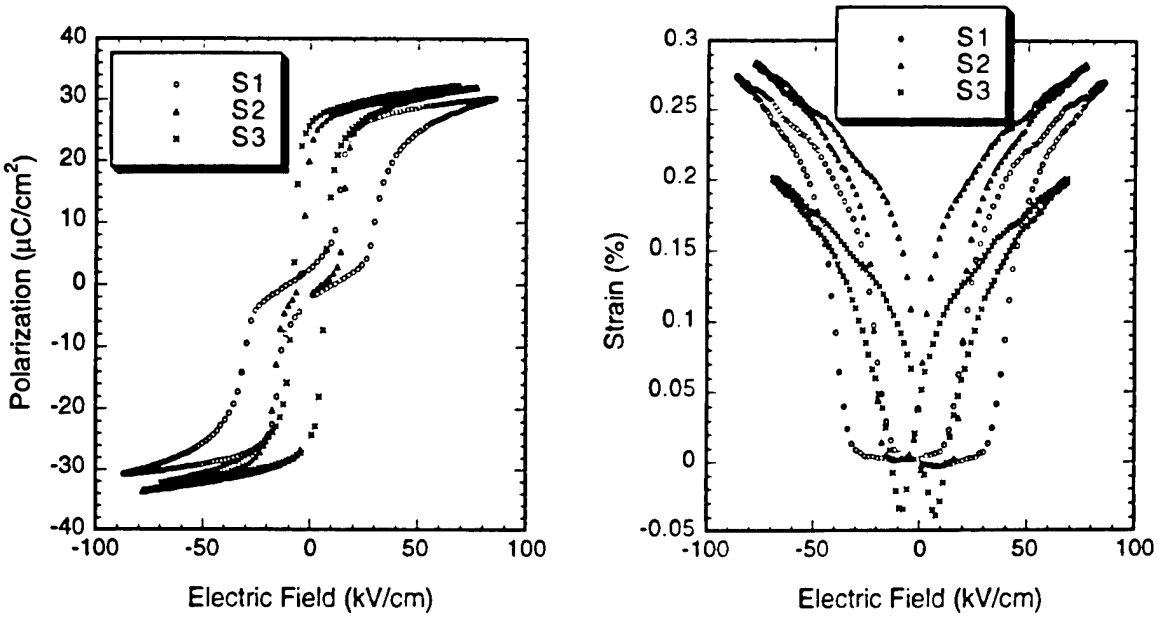

Figure 3 Electric field-induced polarization and strain for compositions S1, S2, and S3

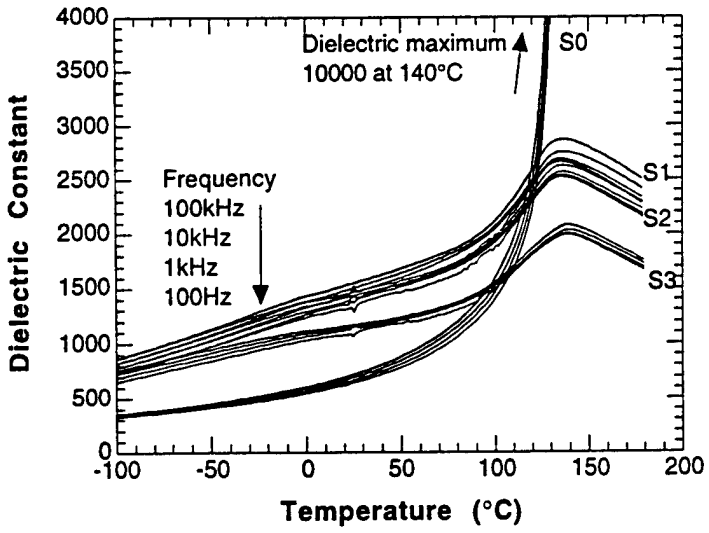

Figure 4 Dielectric constant as a function of temperature for compositions S0, S1, S2, and S3

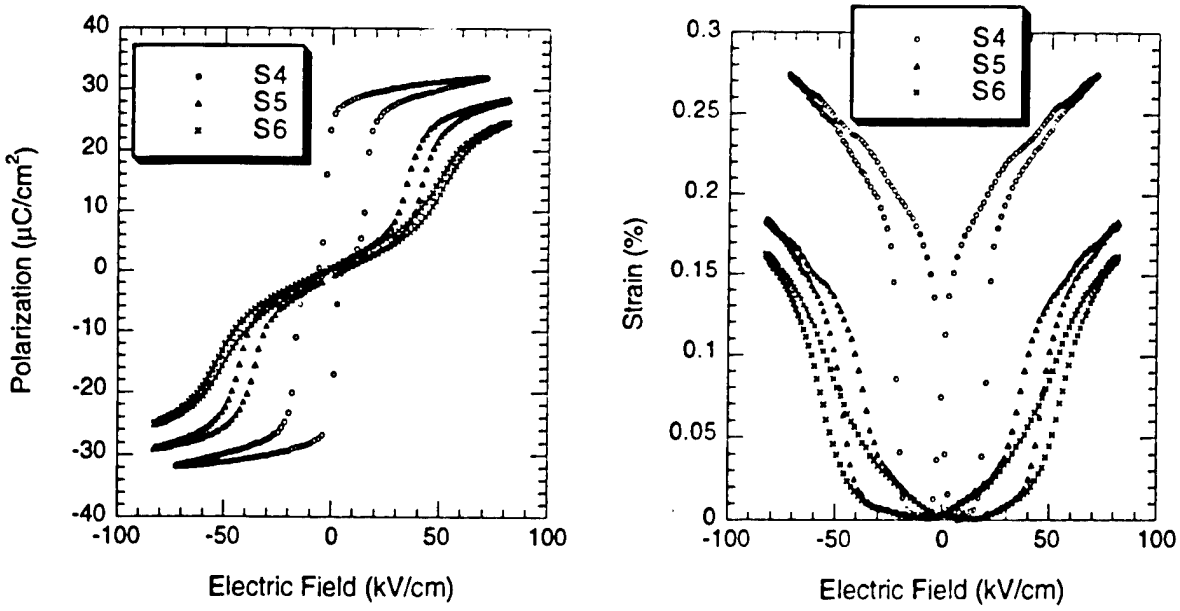

Figure 5 Electric field-induced polarization and strain for compositions S4, S5, and S6

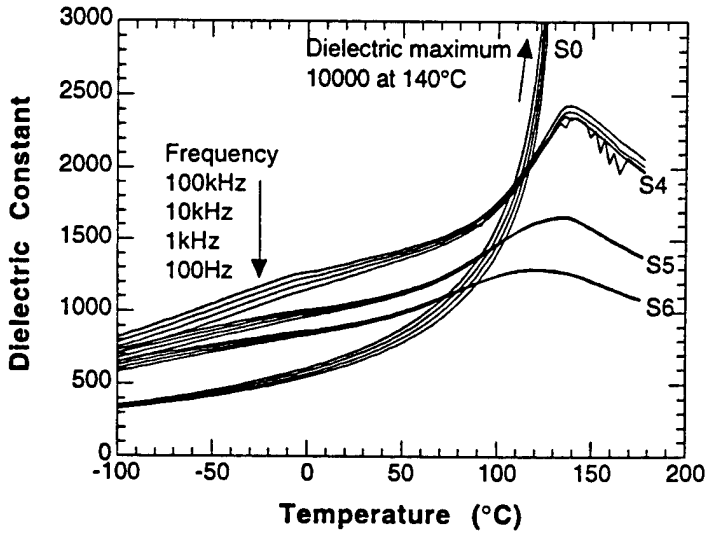

Figure 6 Dielectric constant as a function of temperature for compositions S0, S4, S5, and S6

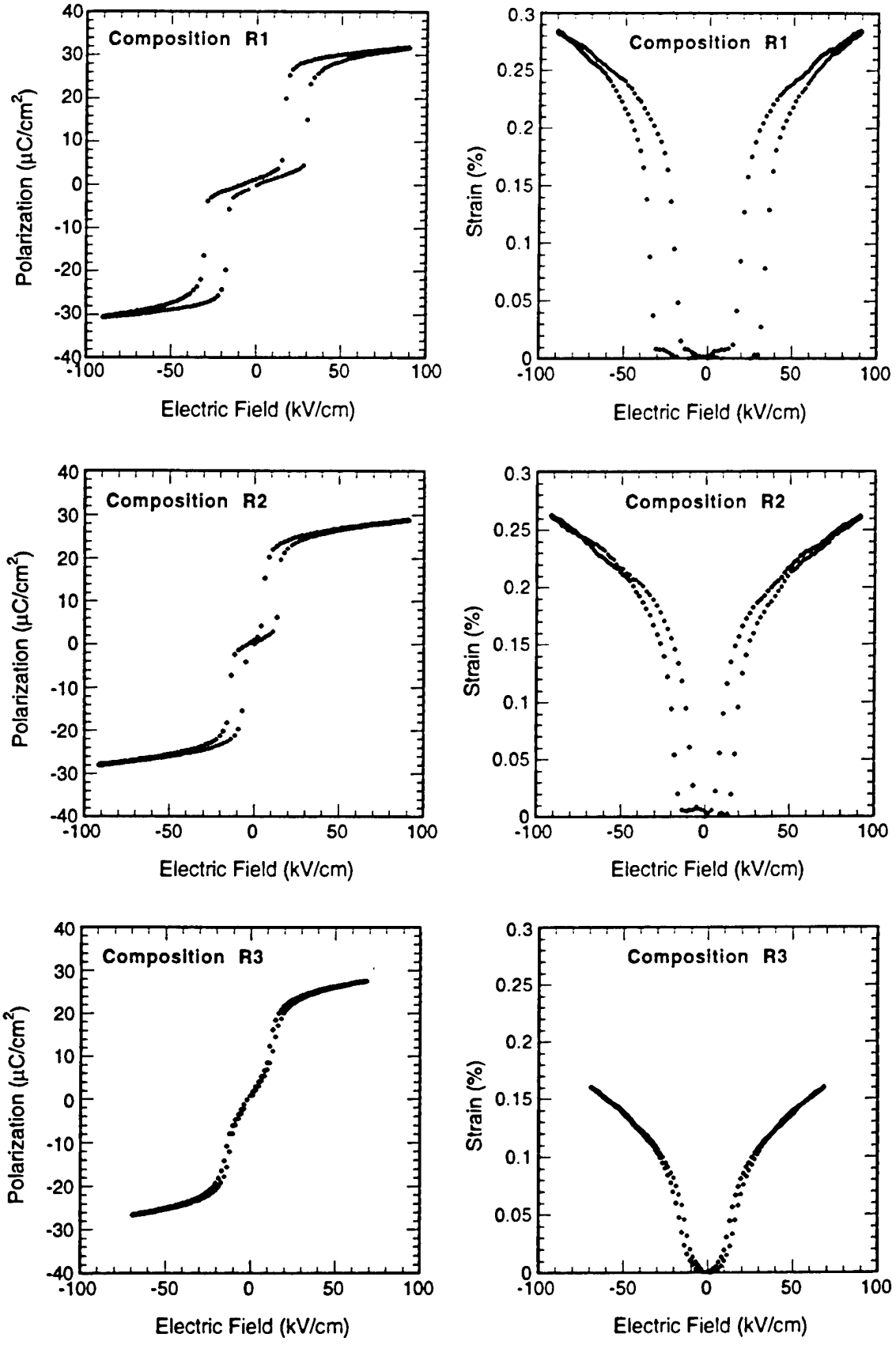

gure 7 Electric field-induced polarization and strain for compositions R1, R2, R3

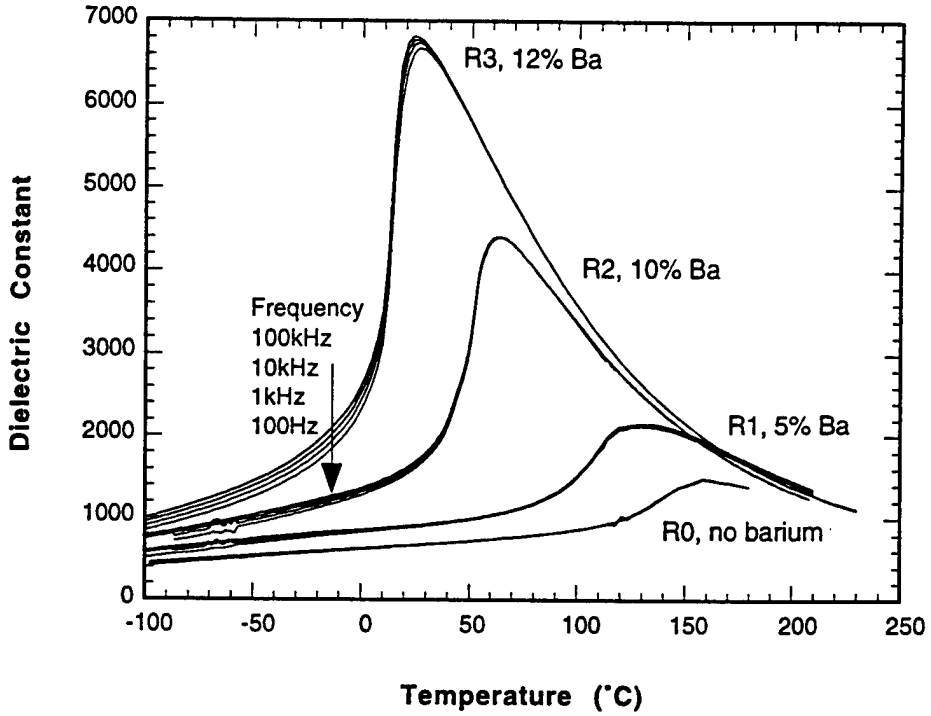

Figure 8 Dielectric constant as a function of temperature for compositions R0, R1, R2, and R3

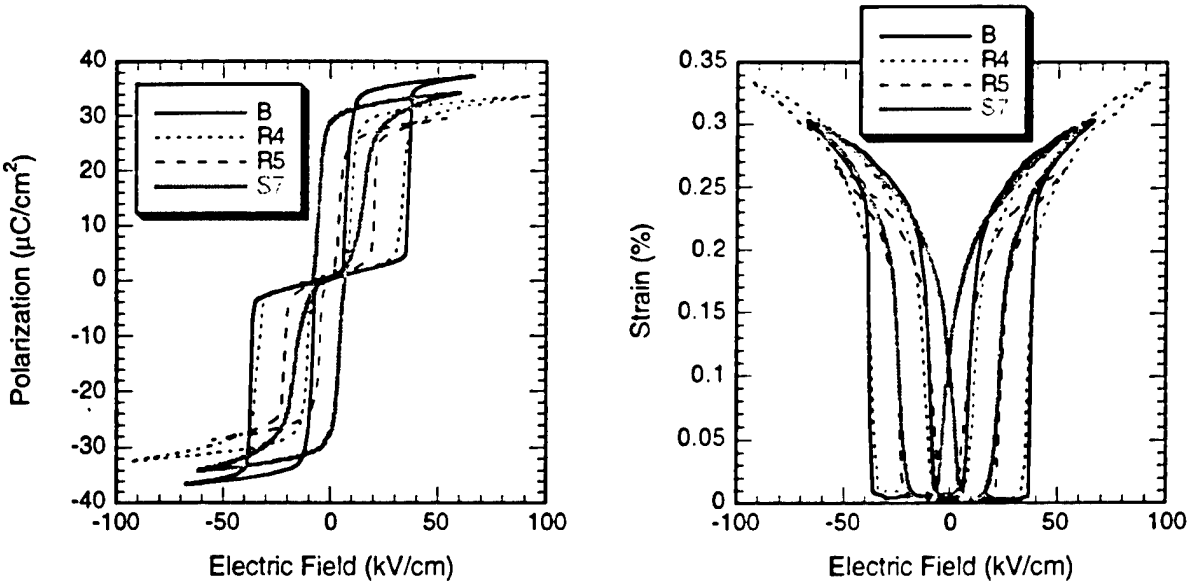

Figure 9 Electric field-induced polarization and strain for compositions B, R4, R5, and S7, all of which contain 66% Zr on B-site, comparing to 55% in previous compositions.

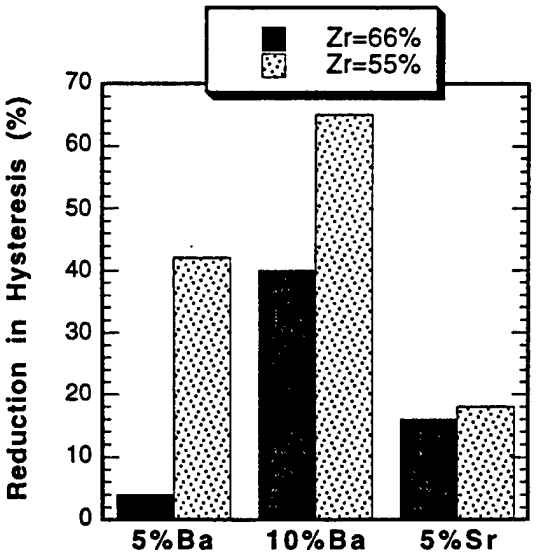

Figure 10 A comparison of the effectiveness of dopants in reducing hysteresis in two different regions of the phase diagram.

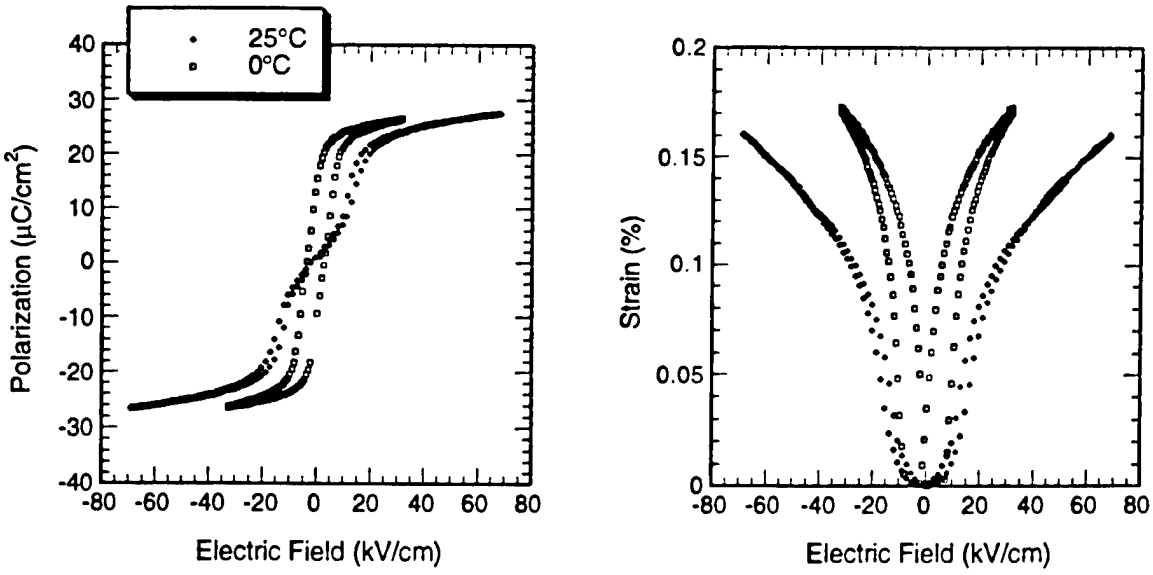

Figure 11 Electric field-induced polarization and strain for composition R3 at 25°C and 0°C. Note that the material has become ferroelectric at 0°C.

List of Figure Captions

Figure 1 The ternary phase diagram of lead stannate zirconate titanate (with 2% lanthanum) family of ceramics and the compositions used in this study. Note that most compositions were doped with either barium or strontium, as indicated in Table I.

Figure 2 Electric field-induced polarization and strain for composition A

Figure 3 Electric field-induced polarization and strain for compositions S1, S2, and S3

Figure 4 Dielectric constant as a function of temperature for compositions S0, S1, S2, and S3

Figure 5 Electric field-induced polarization and strain for compositions S4, S5, and S6

Figure 6 Dielectric constant as a function of temperature for compositions S0, S4, S5, and S6

Figure 7 Electric field-induced polarization and strain for compositions R1, R2, R3

Figure 8 Dielectric constant as a function of temperature for compositions R0, R1, R2, and R3

Figure 9 Electric field-induced polarization and strain for compositions B, R4, R5, and S7, all of which contain 66% Zr on B-site, comparing to 55% in previous compositions.

Figure 10 A comparison of the effectiveness of dopants in reducing hysteresis in two different regions of the phase diagram.

Figure 11 Electric field-induced polarization and strain for composition R3 at 25°C and 0°C. Note that the material has become ferroelectric at 0°C.

APPENDIX 18

Submitted to the proceedings of the SPIE's 5th International Symposium on Smart Structures and Materials, March 1-5, 1998, San Diego, CA.

Electroactive Actuator Materials: Investigations on Stress and Temperature Characteristics

Ming-Jen Pan,† Patrick Pertsch,* Shoko Yoshikawa,
Thomas R. Shrout, and Venkata Vedula

Materials Research Laboratory
The Pennsylvania State University
University Park, PA 16802

ABSTRACT

The quasistatic electromechanical and dielectric behaviors of different electroactive actuator materials are investigated under the simultaneous influence of uniaxial stress and temperature at high driving field. An experimental setup capable of applying 9000 newtons of uniaxial force was carefully designed, based on a precisely guided steel frame. Extra caution was taken to minimize the effects of mis-alignment and contact surface clamping. The materials examined in this study include a prospective PLSnZT antiferroelectric ceramics which is currently under development, as well as electrostrictive ceramics, namely PMN-PT 90/10 and PMN-PT 76/24. To assess the applicability of these materials in real systems, multilayer stacks were assembled and their response to stress and temperature was examined. The overall strain of the PLSnZT composition showed increases with increasing uniaxial stress. This might be the result of re-orientation of antiferroelectric domains under pre-stress. It also showed excellent stability in strain over the temperature range 20 to 75°C under stress as high as 100 MPa. In contrast, the electrostrictive ceramics are less dependent on stress than antiferroelectrics but more susceptible to temperature changes.

Keywords: actuators, phase switching ceramics, antiferroelectrics, electrostrictive ceramics, lead magnesium niobate, pre-stress, temperature effect

1. INTRODUCTION

Ceramic actuators offer many characteristics that are attractive to smart structures applications, such as large generative force, fast response, low power consumption, and high volume efficiency. They are often used under large mechanical load or placed in pre-stressed conditions to maintain their integrity during service. In addition, actuators are often used in encapsulated environment where heat dissipation might cause local temperature increase. As a result, there has been a lot of interest in studying actuator response under pre-stress and temperature. Previous studies mostly have focused on the piezoelectric properties of various ferroelectrics.[1-4] In this study, we investigated two types of non-piezoelectric ceramics, namely electrostrictive and phase switching ceramics. Unlike piezoelectric materials which only involve ferroelectric domain reorientation, antiferroelectric materials also undergo a phase transition and change in unit cell dimensions. In contrast, lead magnesium niobate-lead titanate (PMN-PT) relaxors do not have ferroelectric domains before the application of an electric field.

Electrostrictive PMN-PT ceramics belong to a class of relaxor ferroelectrics which exhibit no macroscopic polarization. Upon the application of an electric field, dimensional change which is proportional to the square of the field-induced polarization can be observed. Because of the little hysteresis it exhibits and consequently little heat generation and excellent position repeatability, PMN-PT is attractive for precision submicron control. The most common composition is 90% PMN-10% PT (90-10) for room temperature applications. Also, a composition with higher PT content (76-24) and thus higher field-induced ferroelectricity has been identified for use at 85°C.[5] The dielectric constant versus temperature data for these two materials are plotted in Figure 1.

---

† Corresponding author: email: mjpan@psu.edu; Phone: (814) 863-2639; Fax: (814) 865-2326
* Visiting scientist from Fraunhofer-Institute for Applied Optics and Precision Engineering, D-07745 Jena, Germany.

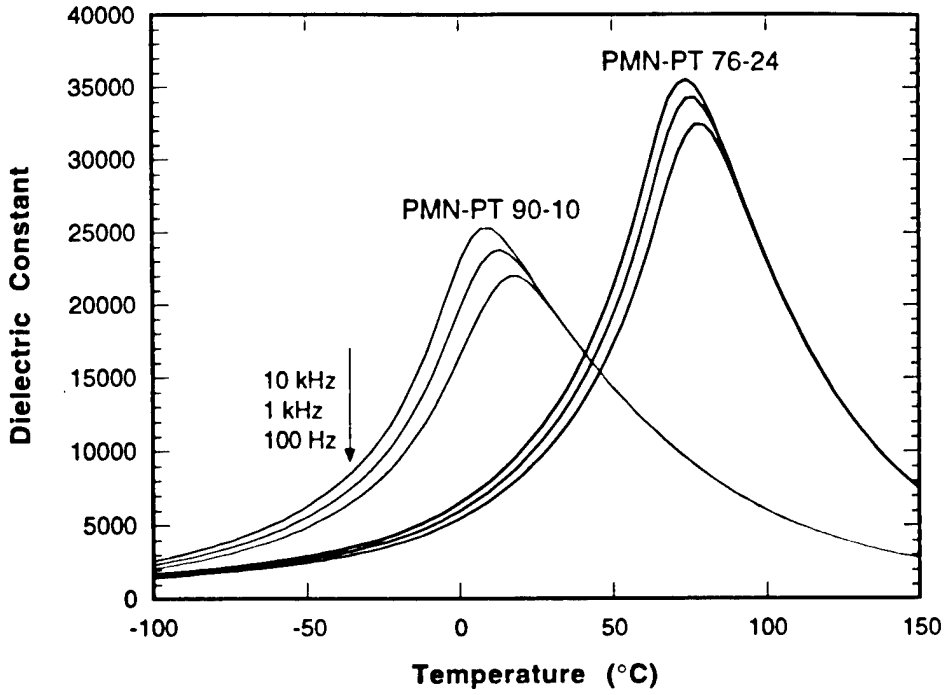

Figure 1 Temperature dependence of dielectric constant for PMN-PT 90-10 and 76-24.

The lead lanthanum stannate zirconate titanate (PLSnZT) system (Figure 2) has been widely studied for actuator applications due to its potential of producing high strain. In this family of ceramics, the antiferroelectric tetragonal (AFE_{tet}) phase can be readily switched to its neighboring ferroelectric rhombohedral (FE_{rh}) phase with the application of an electric field. This phase transition is accompanied by a large change in volume associated with high longitudinal strain (in the field direction). Crystallographic analyses based on X-ray diffraction have shown that 0.5% is the maximum strain possible for an ideal single

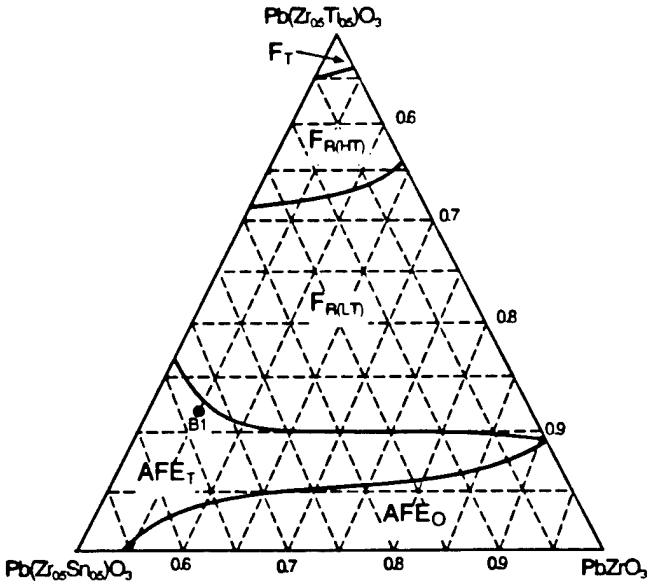

Figure 2 PLSnZT ternary phase diagram

crystal in this system.[6,7] For polycrystalline samples, a strain of 0.2% can be readily achievable at the antiferroelectric-to-ferroelectric (AFE-FE) switching field.[8] This study investigates the influence of pre-stress and temperature on the AFE-FE phase switching. A composition in the AFE_{tet} region, $(Pb_{0.98}La_{0.02})(Sn_{0.33}Zr_{0.55}Ti_{0.12})_{0.995}O_3$, was chosen for this study.

2. EXPERIMENTAL SETUP AND SAMPLE PREPARATION

An experimental setup was designed to measure the material and actuator response under both uniaxial stress and temperature (Figure 3). A rigid, precisely guided steel frame provides true uniaxial stress during loading. The spherical washer on top of the upper contact plate further minimizes transverse force and bending moment caused by non-parallel sample surfaces. A soft spring is used in the load train (3000 N maximum force with 160 N/mm stiffness or 9000 N with 480 N/mm stiffness) to provide relative constant load when the sample expands under an electric field. Due to the spring and some heavy mechanical parts, only quasi-static measurements can be performed on this setup (< 1 Hz).

During measurements, a desired pre-stress is first applied to the sample and then an electric field is applied. The field-induced polarization is measured using a Sawyer-Tower circuit. The displacement of the sample is monitored by a linear variable differential transformer (LVDT), which is driven by a lock-in amplifier. By using a lock-in amplifier, the LVDT resolution is in the range of 10 nanometers. Note that the LVDT assembly is not part of the load train, but part of the steel frame. The LVDT is attached to a pair of micrometer-controlled positioning fixtures, which are fastened onto the steel frame. So when a sample strains under an electric field, the LVDT senses the relative motion between the frame and the top of the sample. During measurement, the sample is immersed in an insulating liquid, Fluorinert™ (3M, St. Paul, MN, USA), to prevent arcing. A heating ribbon assembly, which can be inserted into the liquid-filled Teflon™ cup, allows the sample temperature to reach as high as 165°C (Figure 4).

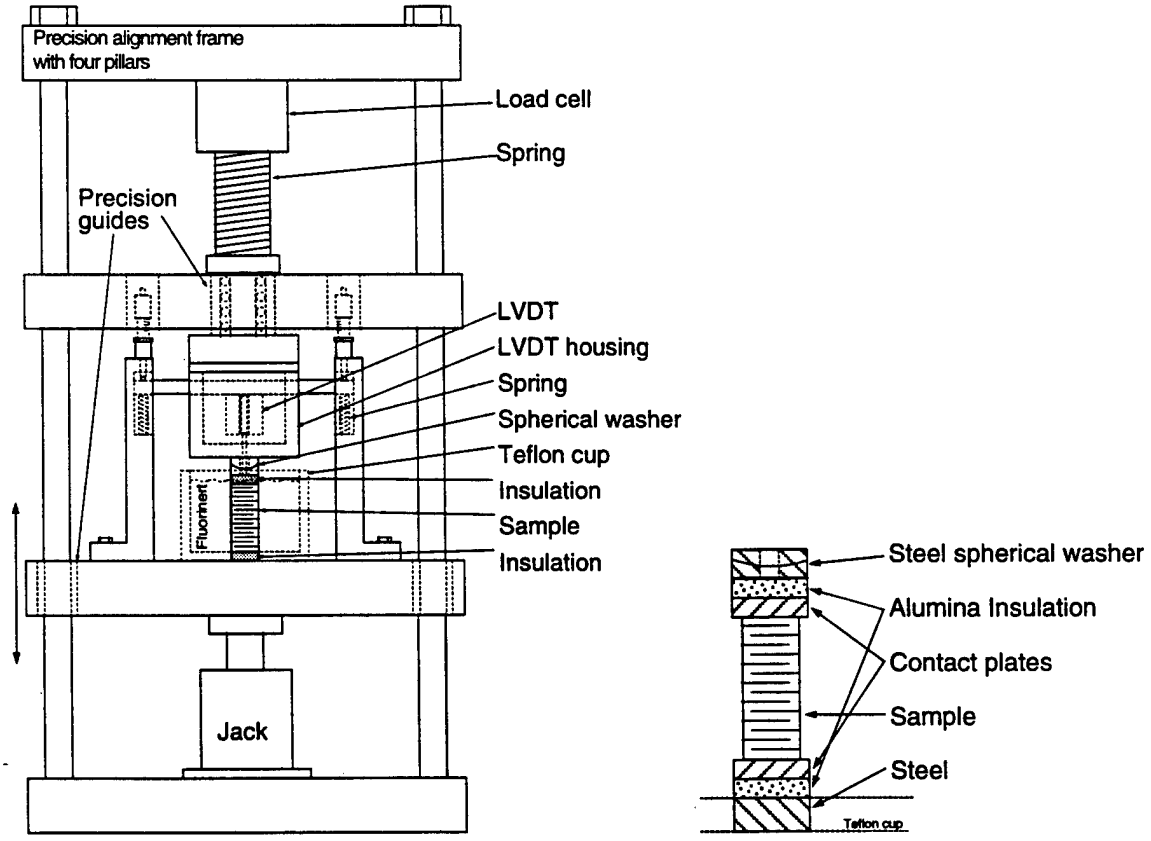

Figure 3 A schematic of the experimental setup for pre-stress measurements

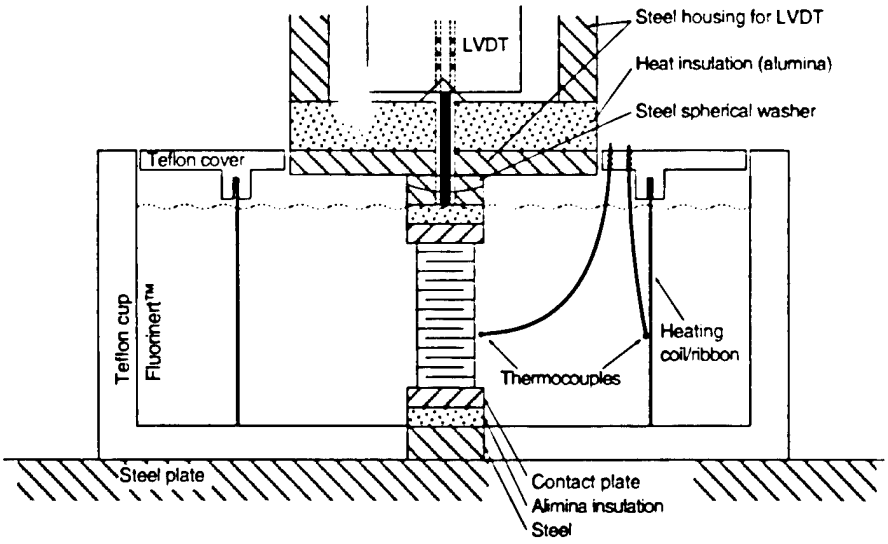

Figure 4 A schematic of the Teflon™ heating bath

A major concern in this type of measurement is the friction at sample/fixture surfaces. Therefore, efforts were made to reduce the effects of frictional clamping. The contacts plates have a mirror finish with an average surface roughness of R_a = 5 nm. The clamping effect can be further reduced by using samples with high aspect ratio. In this study multilayer stacks with 10.0 mm diameter and 10.7 mm in height are built for the measurements. Each stack has 16 active layers which have a thickness of 0.5 mm. Two passive endcaps at the top and bottom of the stack are made of the same material and were polished to R_a = 75 nm on the outer surfaces. The electrical contact of the discs is realized by 50 μm thick metal shims between the active layers.

3. ELECTROSTRICTIVE CERAMICS

Uniaxial stress up to 100 MPa was applied to various samples. During the measurements, pre-stressed samples expand under the applied electric field and the corresponding polarization and displacement were measured simultaneously. Shown in Figures 5(a) and 5(b) is the stress dependence of PMN-PT 90-10. Only small changes in polarization and strain were observed. At 100 MPa, the material still retains 85% and 68% of its stress-free polarization and strain, respectively. The hysteresis remained virtually unchanged for all stresses. Moreover, the strain versus polarization curves showed perfect parabolic shapes for all stresses (Figure 5c), indicating that the electrostrictive coefficient, Q_{111}, was independent of the applied stress. By using least square regression, the above coefficient was determined to be 0.0178 m^4/C^2.

PMN-PT 76-24 material, which has a higher dielectric maximum temperature due to its higher PT content, was tested at its operating temperature, 85°C. As shown in Figures 5(d) to 5(f), it had the same characteristics as PMN-PT 90-10, although its strain level was almost 50% higher than that of 90-10. This was not surprising because 76-24 is simply the high temperature version of 90-10. The electrostrictive coefficient Q_{111}, which was determined to be 0.0210 m^4/C^2, was also independent of stress.

Both materials were also subjected to various combinations of temperature and stress. For each condition, a unipolar (half sine wave) electric field with a 20 kV/cm maximum was applied to the sample. The results for PMN-PT 90-10 are plotted in figures 6(a) and 6(b). This shows that the field-induced polarization and strain decreased monotonically with increasing temperature as it moves away from its dielectric maximum and into the paraelectric region. The stress dependence of 90-10 remained similar for all temperatures. PMN-PT 76-24 displays the same behavior at temperatures higher than 85°C. At room temperature, however, a stress dependence typical of a normal "soft" ferroelectric material was seen. The observed

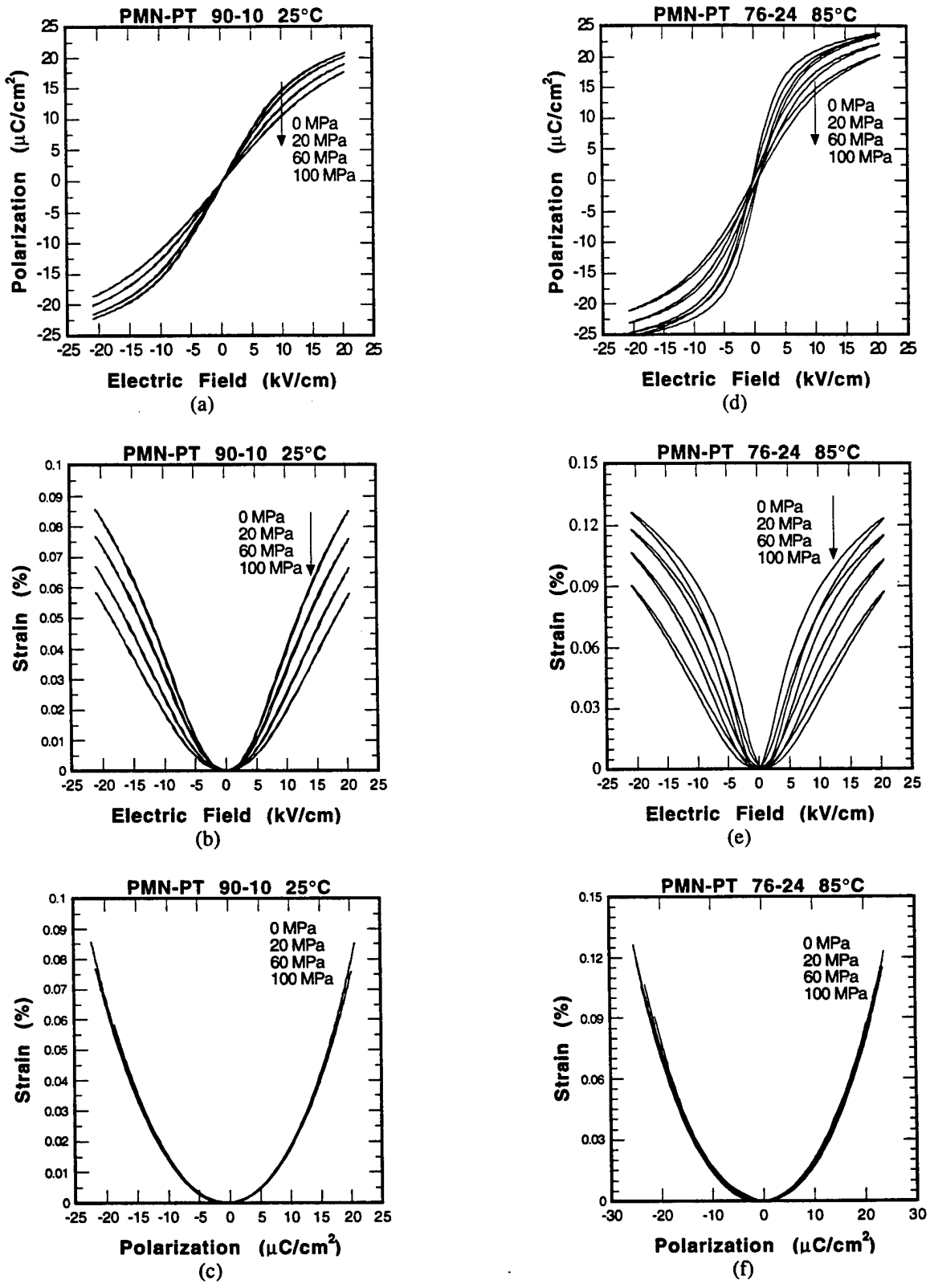

Figure 5 The polarization and strain behaviors of PMN-PT 90-10 ((a)-(c)) and 76-24 ((d)-(e))

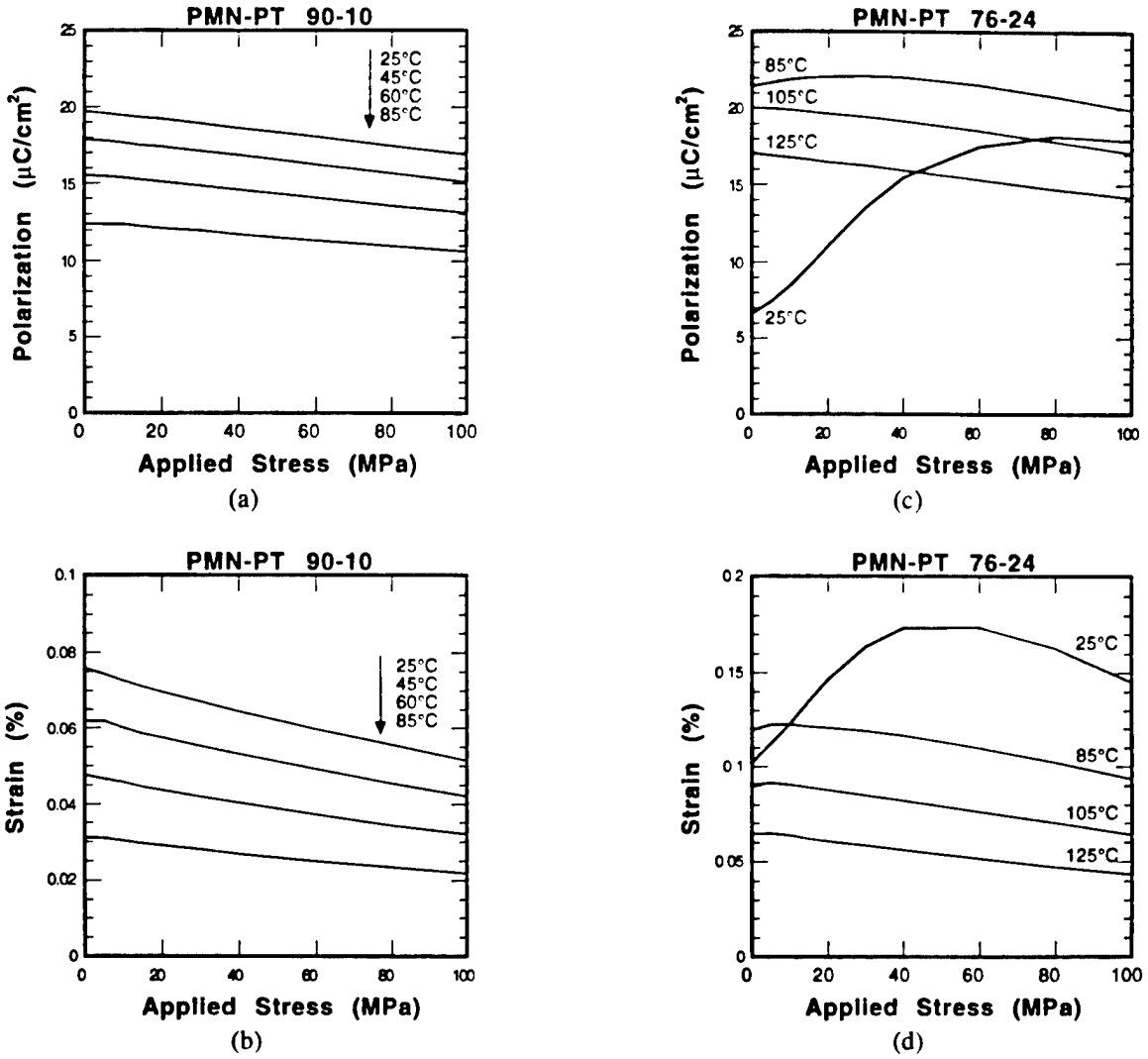

Figure 6 The polarization and strain of PMN-PT 90-10 and 76-24 under various combination of temperature and stress

behavior was the result of two competing processes: domain flipping due to stress (polar direction perpendicular to stress) and electric field (polar direction align with field). Similar behavior of soft piezoelectrics has been reported in the past.

4. PHASE SWITCHING CERAMICS

Like the electrostrictive materials, uniaxial stress up to 100 MPa was applied to the phase switching material. Some of the results are shown in Figure 7. It is interesting to observe that the overall strain increases with increasing pre-stress. As shown in Figure 8a, the strain at stresses greater than 80 MPa can be twice as high as that without pre-stress. At the same time, however, the polarization remained relatively unchanged, indicating that the AFE-to-FE phase switching was complete. Apparently, there was a decoupling between the polarization and strain. The pre-stress also increased the switching fields as shown in Figure 8b. Both the forward and backward switching fields have equivalent slopes of 0.11 kV/cm per MPa. The hysteresis (the difference between the forward and backward switching fields) remained constant at about 20 kV/cm.

To explain the above observations of phase switching behavior under uniaxial stress, we propose an addition to the switching sequence in Reference 9, as illustrated in Figure 9. It is possible that the AFE domains of a typical electric field-exposed sample (b) collapse under applied stress (b'). This makes the sample smaller in the stress direction. As a result, the

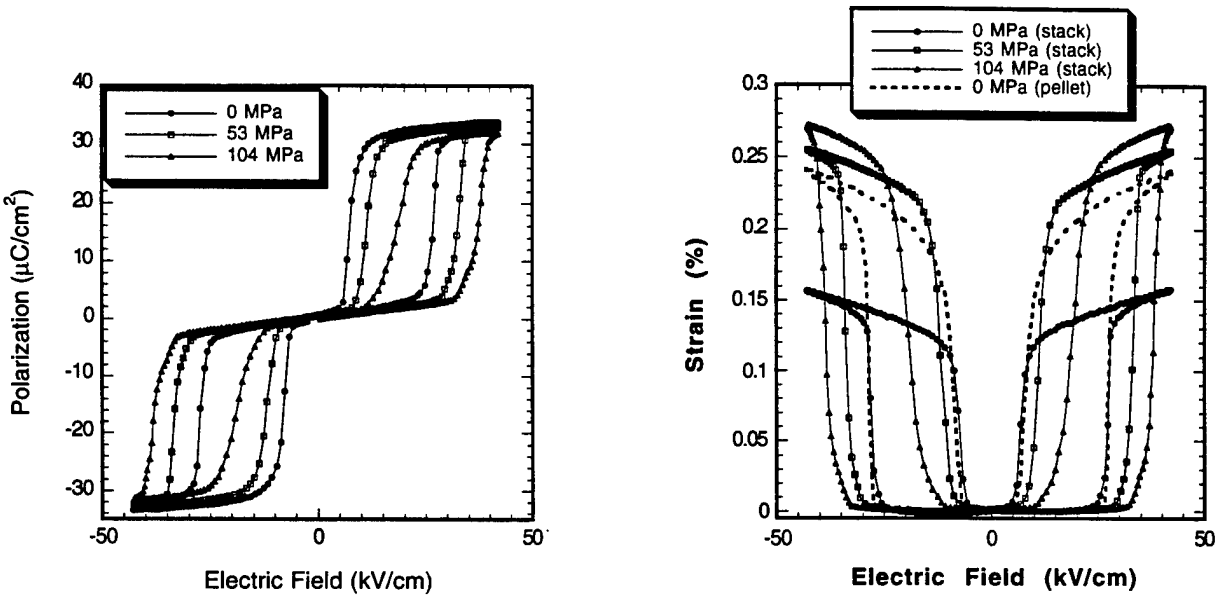

Figure 7 (a) Polarization and (b) strain behaviors under various pre-stresses

dimensional change in E-field direction between the AFE and FE states (b' to e) of a stressed sample is larger than that of a stress-free sample (b to e). The collapsed AFE domain state also implies that additional energy is needed during phase transformation when a sample stretches against the applied stress, which explains why the increased switching field under stress. Experimental confirmation of the proposed explanation, however, is still needed.

Finally, it was noted that the strain of multilayer samples, even without external stress, is more than 30% smaller than that of a single pellet (Fig. 8a). This reduction in performance was likely due to the multilayer structure. Specifically, the passive endcaps, shims and epoxy used for assembling the multilayer stacks constrain the active ceramic layers expansion in the transverse directions and caused a reduction of the longitudinal strain.

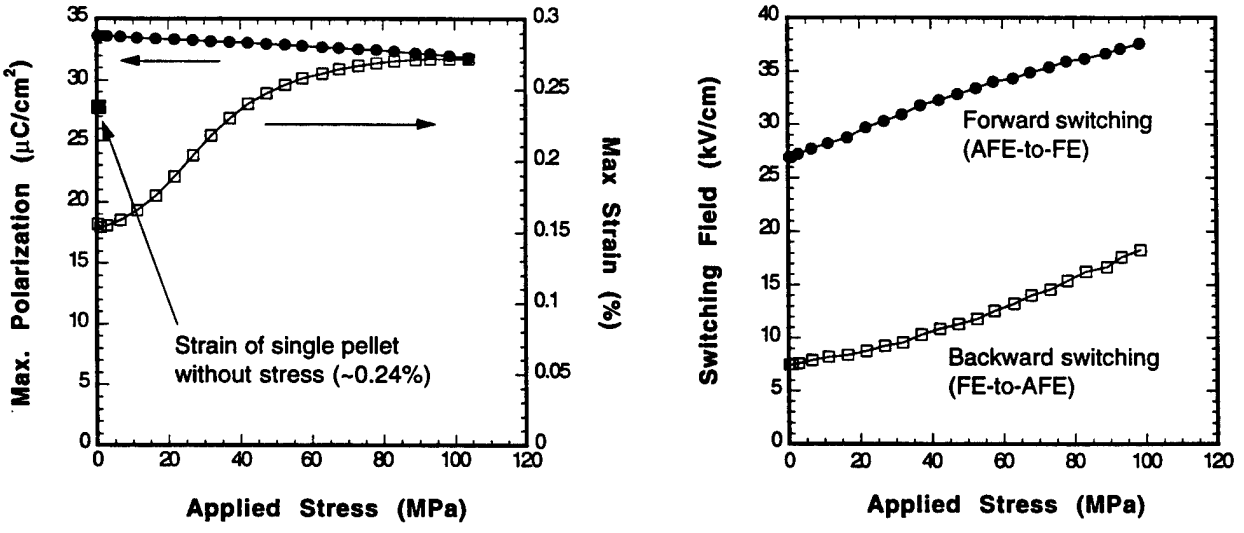

Figure 8 (a) Maximum polarization and strain and (b) switching fields as a function of pre-stress

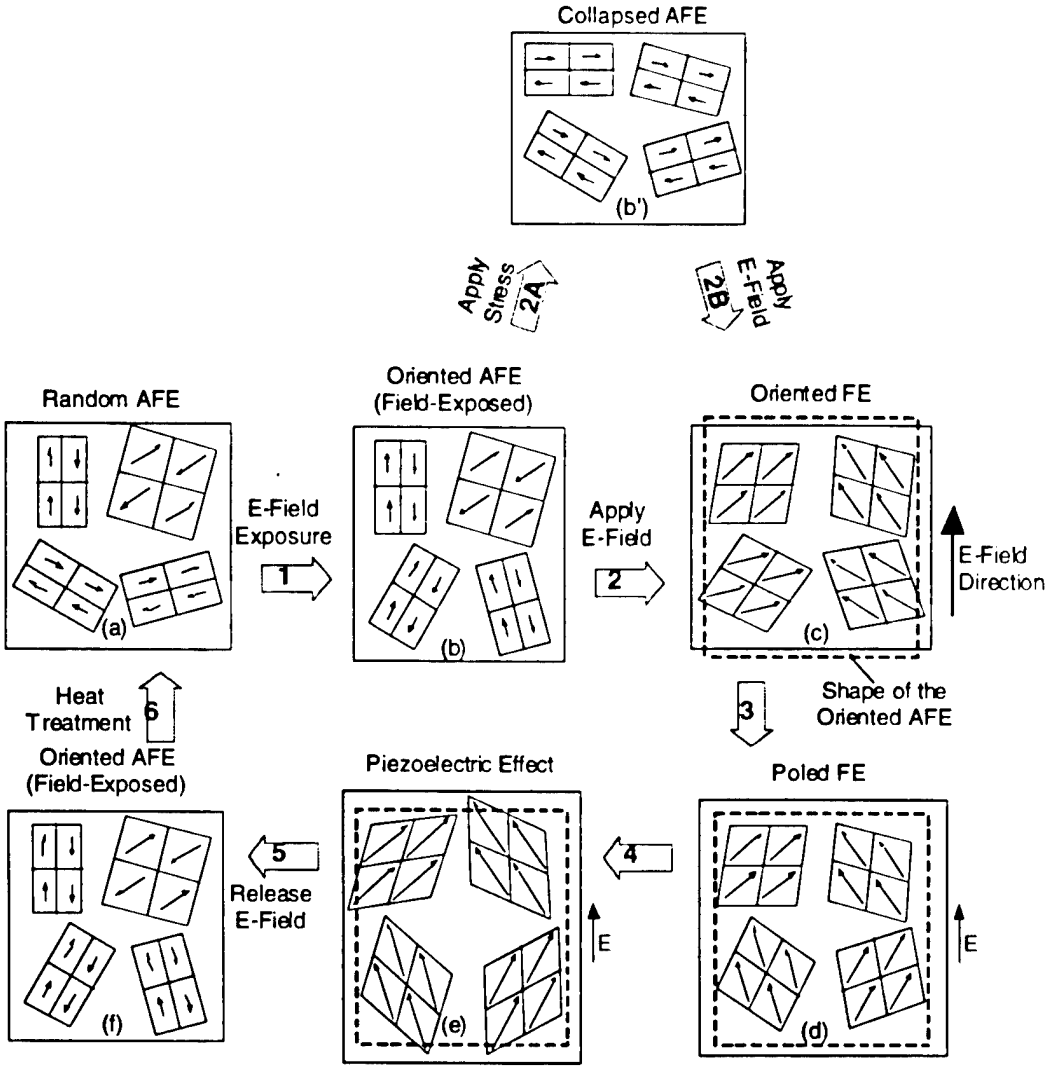

Figure 9 A schematic of the AFE-FE phase switching steps. The proposed extra steps 2A and 2B are caused by the uniaxial stress.

The effects of temperature on phase switching were also examined. Because the epoxy used for assembling the antiferroelectric multilayer stacks does not have high temperature capability, the measurements were performed only at 50 and 75 °C. Table I is the summary of the strain and hysteresis under various stresses and temperatures. The strain showed a remarkable stability for the temperature range 20 to 75°C. At 60 MPa, the strain at 75°C retained more than 75% of the strain at 21°C. This composition also displayed reduced hysteresis at higher temperatures.

5. SUMMARY

An experimental setup that applies up to 9000 N of uniaxial force was designed and built. Extra caution was taken to prevent any transverse movement or bending on samples. The clamping effect at contact surfaces was minimized by using mirror finish contact plates and high aspect ratio samples, i.e., multilayer stacks. Two types of electroactive ceramics were investigated in this study: electrostrictive and antiferroelectric materials.

Table I The strain and hysteresis at various stresses and temperatures of the antiferroelectric material in this study

	Strain (%)		Hysteresis (kV/cm)	
	0 MPa	60 MPa	0 MPa	60 MPa
21°C	0.144	0.252	21.3	21.0
50°C	0.137	0.230	14.3	15.0
75°C	0.124	0.191	9.1	9.5

For electrostrictive ceramics, PMN-PT 90-10 and its high temperature (85°C) counterpart 76-24, were tested. It was shown that neither electrostrictive PMN-PT is sensitive to external stress, while 76-24 showed superior electromechanical properties to 90-10. The electrostrictive coefficients for both materials were independent of stress. PMN-PT, nevertheless, was very sensitive to temperature change, because it was mostly operated at temperatures near its dielectric maximum. For the antiferroelectric material in this study, the strain at high pre-stress (>80 MPa) was almost twice as high as the strain without pre-stress. This is likely due to the AFE domain re-orientation process under load. The material also showed excellent stability in performance for the temperature range 20 to 75°C under various pre-stresses.

6. ACKNOWLEDGMENTS

The original effort was supported by DARPA Smart Structure for Rotorcraft Consortium (SSRC). The authors would like to thank Dr. Wes Hackenberger for his technical insight and TRS Ceramics, Inc. for providing the technical expertise and the ceramic materials used in this study.

7. REFERENCES

1. H.H. Krueger, "Stress Sensitivity of Piezoelectric Ceramics: Part 1. Sensitivity to Compressive Stress Parallel to the Polar Axis," *J. Acoust. Soc. Am.*, **42** [3] 636-645 (1967).
2. S.W. Meeks and R.W. Timme, "Effects of One-Dimensional Stress on Piezoelectric Ceramics," *J. Appl. Phys.*, **46** [10] 4334-38 (1975).
3. T. Inoue and S. Takahashi, "Measurements for Piezoelectric Ceramic Properties Applied Compressive Stress Parallel to the Polar Axis," *Trans. IECE Japan*, vol. E69, 1180-1187 (1986).
4. M. Kondo, K. Ohya, and S. Shimizu, "Effects of One-Dimensional Compressive Stress on the Properties of Multilayer Piezoelectric Ceramic Actuator," IEEE ISAF'90 pp.530-534.
5. W.S. Hackenberger, TRS Ceramics, Inc., private communication, 1997.
6. C.T. Blue, J.C. Hicks, S.-E. Park, S. Yoshikawa, and L.E. Cross, "*In situ* X-Ray Diffraction Study of the Antiferroelectric-ferroelectric Phase Transition in PLSnZT," *Appl. Phys. Lett.*, **68** [21] 2942-44 (1996).
7. L. Shebanov, M. Kusnetsov, and A. Sternberg, "Electric Field-Induced Antiferroelectric-to-Ferroelectric Phase Transition in Lead Zirconate Titanate Stannate Ceramics Modified with Lanthanum," *J. Appl. Phys.*, **76** [7] 4301-4 (1994).
8. K.A. Markowski, S.-E. Park, S. Yoshikawa, and L.E. Cross, "Effect of Compositional Variations in Lead Lanthanum Zirconate Stannate Titanate System on Electrical Properties," *J. Am. Ceram. Soc.*, **79** [12] 3297-304 (1996).
9. S.-E. Park, M.-J. Pan, K. Markowski, S. Yoshikawa, and L.E. Cross, "Electric Field Induced Phase Transition of Antiferroelectric Lead Lanthanum Zirconate Titanate Stannate Ceramics," *J. Appl. Phys.*, **82** [4] 1798 (1997).

APPENDIX 19

Effect of Grain Size on the Electromechanical Properties of Antiferroelectric-to-Ferroelectric Phase Switching PLSnZT Ceramics

Ming-Jen Pan and Shoko Yoshikawa
Materials Research Laboratory
The Pennsylvania State University
University Park, PA 16802 USA

Abstract—In this study, the effect of processing on the phase transformation behavior of antiferroelectric lead lanthanum stannate zirconate titanate (PLSnZT) ceramics was investigated. Specifically, the effects of sintering condition, and consequently grain size, were examined in order to address some practical issues. Sub-micron PLSnZT powder was made by using conventional solid state reaction and additional attrition milling. Samples were sintered at different temperature and dwell time to produce different grain sizes ranging from approximately 15 to 0.5 μm. It was found that the sintering temperature for producing fully dense samples can be as low as 950°C with attrition-milled powder. The electrical properties of the samples were the same when the sintering temperature is higher than 1000°C. Below 1000°C, sample performance begins to deteriorate, possibly because of either excess lead remaining in the samples or the lack of domain formation in sub-micron grains. It was also found that decreased grain size can increase mechanical strength by 30%.

I. Introduction

The high electric field-induced strain in lead lanthanum stannate zirconate titanate (PLSnZT) family of ceramics has been of interest for high performance actuators and transducers. It was established by Berlincourt [1] that the antiferroelectric tetragonal (AFE_{tet}) phase can be readily switched to ferroelectric rhombohedral (FE_{rh}) phase with the application of an electric field. This antiferroelectric-to-ferroelectric (AFE-FE) phase transition is accompanied by a large volume strain, which is a result of the larger FE_{rh} cell as compared to the AFE_{tet}. Previous studies reported strain as high as 0.85% [2,3], although other crystallographic analyses based on X-ray diffraction have shown that 0.5% is the maximum strain possible for an ideal single crystal in this system [4,5]. For polycrystalline samples, strain of 0.2% should be readily achievable at the AFE-FE switching field [6,7].

Because of their high tin content, PLSnZT ceramics are usually sintered at temperatures higher than 1300°C, where lead volatility can cause serious quality control problems. In order to alleviate such problems, attempts were made to improve the material production process, especially the possibility of using sub-micron powder to improve the reactivity during sintering. In this way, the sintering temperature can be lowered, thus improving consistency during production. More importantly, the ability to alter the sintering condition, and consequently grain size, provided an effective means to optimize material properties. As PLSnZT ceramics have been extensively studied in previous reports [6,7], the composition $Pb_{0.98}La_{0.02}(Sn_{0.33}Zr_{0.55}Ti_{0.12})_{0.995}O_3$ which offers reasonable strain and hysteresis was chosen for this study.

II. Experimental Procedure

A. Sample Preparation

The composition (B1) used in this study is shown in Fig. 1. Stoichiometric ceramic powder was prepared by solid state reaction, using the appropriate amounts of reagent grade raw materials. Calcined powders were examined by X-ray diffraction (XRD) to insure phase purity. Typically, the samples showed a tetragonal structure within the detection limit of XRD. Calcined powder was then attrition-milled for 8 hours to reduce the particle size. The milled powder was

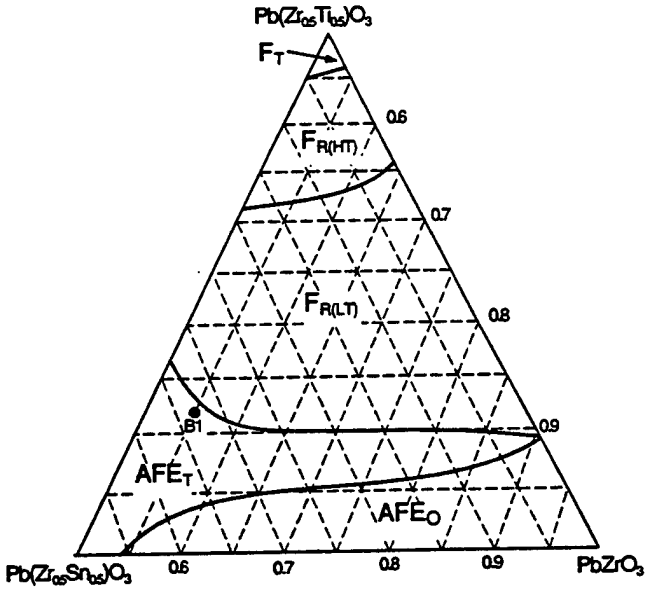

Fig. 1 PLSnZT ternary phase diagram

dried and then re-calcined at a lower temperature to improve its homogeneity. Finally, the powder was attrition-milled again and dried. The finished particle surface area was 9.1 m^2/gram.

The sintering process was carried out in a lead rich environment in order to minimize lead volatilization. Samples were sintered at different temperatures and dwell times to produce different grain sizes. Table I shows a list of conditions and the resulted density and grain size. The samples were pale yellow after sintering and remained this color throughout processing.

For electrical measurements, disk samples (with diameter 11 mm and thickness 0.3 mm) were then prepared by polishing to achieve flat and parallel surfaces onto which gold was sputtered. For mechanical strength, bar samples (30 mm x 2 mm x 2 mm) were prepared and the edges were slightly chamfered to eliminate machining defects.

TABLE I
LIST OF SINTERING CONDITIONS AND RESULTS

Sintering Condition	Density (g/cm^3)	Weight Loss (%)	Grain Size (μm)
A. 1300°C/10hrs	8.12	1.72	10-20
B. 1300°C/2hrs	8.15	1.42	5-10
C. 1200°C/2hrs	8.22	1.32	3-5
D. 1150°C/2hrs	8.23	1.33	1.5-3
E. 1100°C/2hrs	8.28	1.20	1-2
F. 1000°C/2hrs	8.20	0.78	0.8-1.5
G. 975°C/4hrs	8.04	0.69	0.5-1
H. 950°C/6hrs	8.18	0.78	0.5-1
J. 975°C/2hrs	7.76	0.51	0.5-1

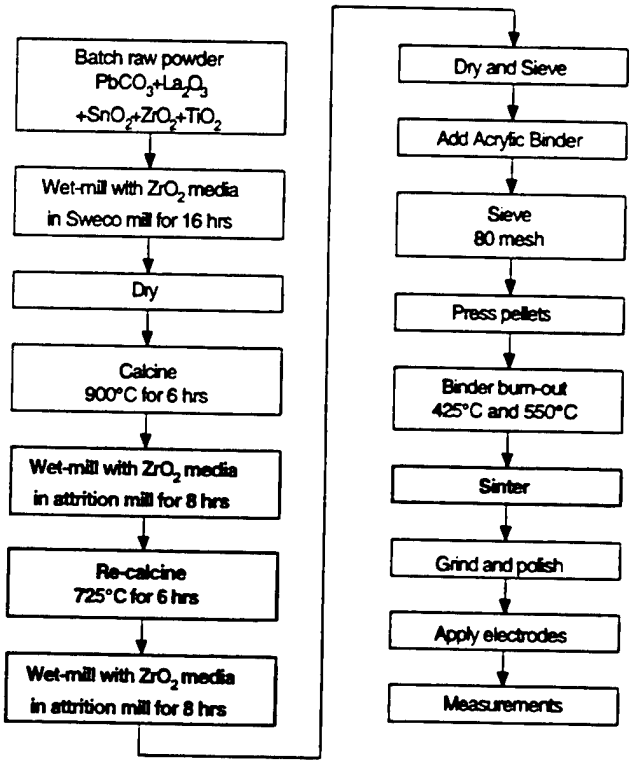

Fig. 2 Processing flow chart

B. Characterization

High-field measurements included polarization and strain hysteresis using a computer-controlled modified Sawyer Tower circuit and a linear variable displacement transformer (LVDT) driven by a lock-in amplifier (Stanford Research Systems, Model SR830). The voltage was supplied using a Trek 609C-6 high voltage DC amplifier. Through the LVDT, the strain of the samples can be measured with the application of an applied field. Electric fields as high as 70 kV/cm were applied using an amplified sine waveform at 0.2 Hz. During testing the samples were submerged in Fluorinert (FC-40, 3M, St. Paul, MN), an insulating liquid, to prevent arcing. For mechanical strength, the samples were subjected to three-point bend test on an Instron machine (Model 4212, Instron Corp., Canton, MA).

III. Results and Discussion

A. Microstructure

As shown in Table I, fully dense ceramics can be achieved at temperature as low as 950°C, with the exception of condition J. The weight loss due to lead volatilization decreases with decreasing sintering temperature. Depending on sintering conditions, the grain size varies from 15 μm to 0.5 μm. Some of the microstructures obtained under different conditions are shown in figure 3. Fully dense, well-defined microstructures are clearly visible.

B. Electrical Properties

The polarization and strain behaviors of these samples are shown in Figure 4. There is no difference in their properties when sintered at temperatures higher than 1000°C. Nevertheless, below 1000°C (conditions F, G, and H) the properties begin to deteriorate. The AFE-FE phase switching becomes more diffuse and both the polarization and strain level decrease. In particular, condition J (Figure 5a) shows only lossy hysteresis loops and no antiferroelectric characteristics.

This observation is attributed to two possible reasons. First is the existence of excess lead oxide along grain boundaries. This is partially evidenced by the decreasing weight loss with decreasing sintering temperature. Because of the low sintering temperatures, excess lead oxide did not have enough vapor pressure to escape completely. The excess lead residing along grain boundaries contributes to space charge and thus reduces the electric field that the grains actually

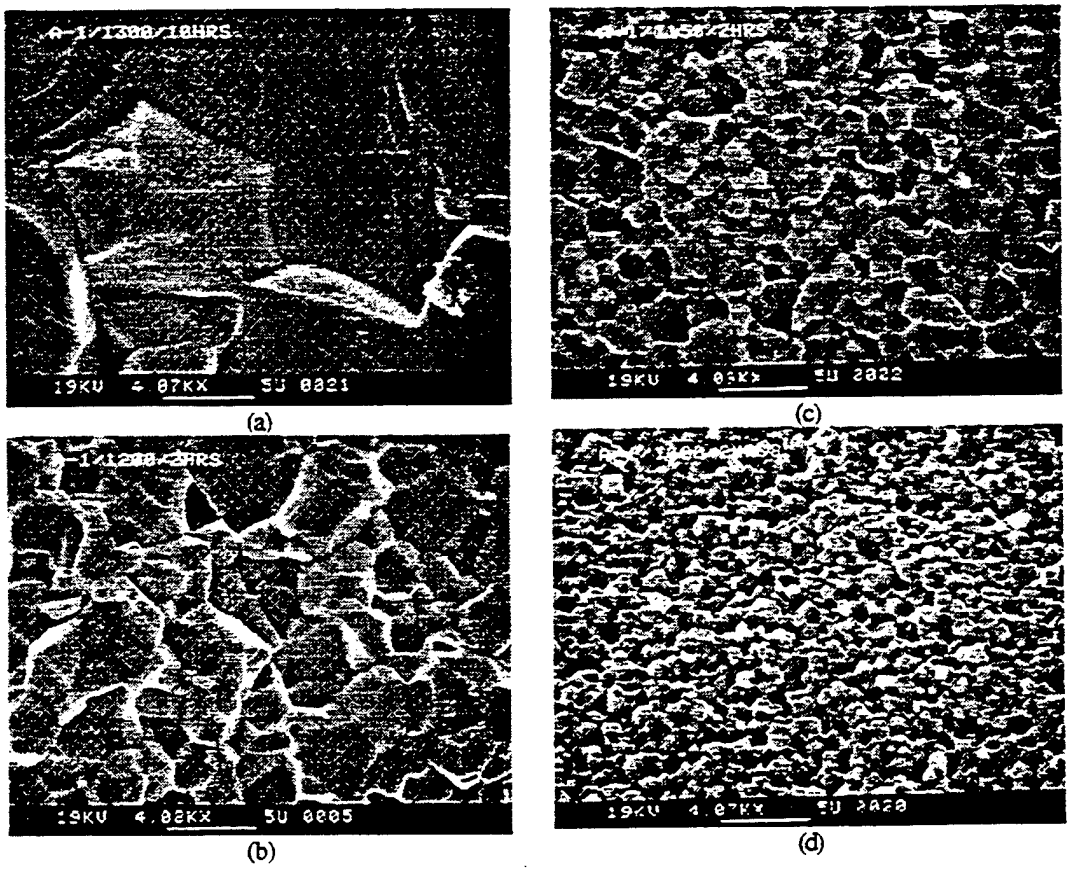

Fig. 3 Microstructures of some sintered samples: (a) 1300°C/10hrs, (b) 1200°C/2hrs, (c) 1150°C/2hrs, and (d) 1000°C/2hrs.

experience. If one takes a sample sintered under condition J and anneal it at 850°C for 12 hours in oxygen to remove excess lead, the hysteresis loops will shift towards those of the high-fired samples (Figure 5b).

Second possibility is the reduced tetragonality/crystallinity, which could be the result of the lack of domain formation or the low sintering temperature and thus low energy state. As shown in Figure 6, the X-ray diffraction patterns of {002} peaks clearly shows the trend of shifting tetragonality.

C. Flexural Strength

As shown in Table II, the flexural strengths of these materials are comparable to those of conventional PZTs. But more importantly, the samples sintered at 1100°C/2hrs show remarkable improvement in strength compared to other conditions. The 30% higher strength is very favorable for actuator applications as most actuators are meant to carry some form of mechanical load.

IV. Conclusions

Sub-micron ceramic powder can be produced by adding attrition-milling, re-calcining, and a second attrition-milling to a normal solid state reaction process. Powder surface area can reach 9 m^2/gram. Using this powder, samples of different grain sizes were made by adjusting sintering temperature and dwell time. It was found that fully dense ceramics with good electrical properties and superior mechanical properties can be sintered at temperatures as low as 1000°C. More importantly, this low sintering temperature implies that silver:palladium electrodes, instead of platinum, can be used for co-fired multilayer actuators to reduce production cost.

TABLE I

MECHANCAL STRENGTHS OF SAMPLES SINTERED UNCER VARIOUS CONDITIONS

Sintering Condition	Mechanical Strength (MPa)	Standard Deviation (MPa)
A. 1300°C/10hrs	101	5
B. 1300°C/2hrs	103	5
C. 1200°C/2hrs	113	4
D. 1150°C/2hrs	120	5
E. 1100°C/2hrs	131	8
F. 1000°C/2hrs	103	9
G. 975°C/4hrs	98	7
H. 950°C/6hrs	89	8

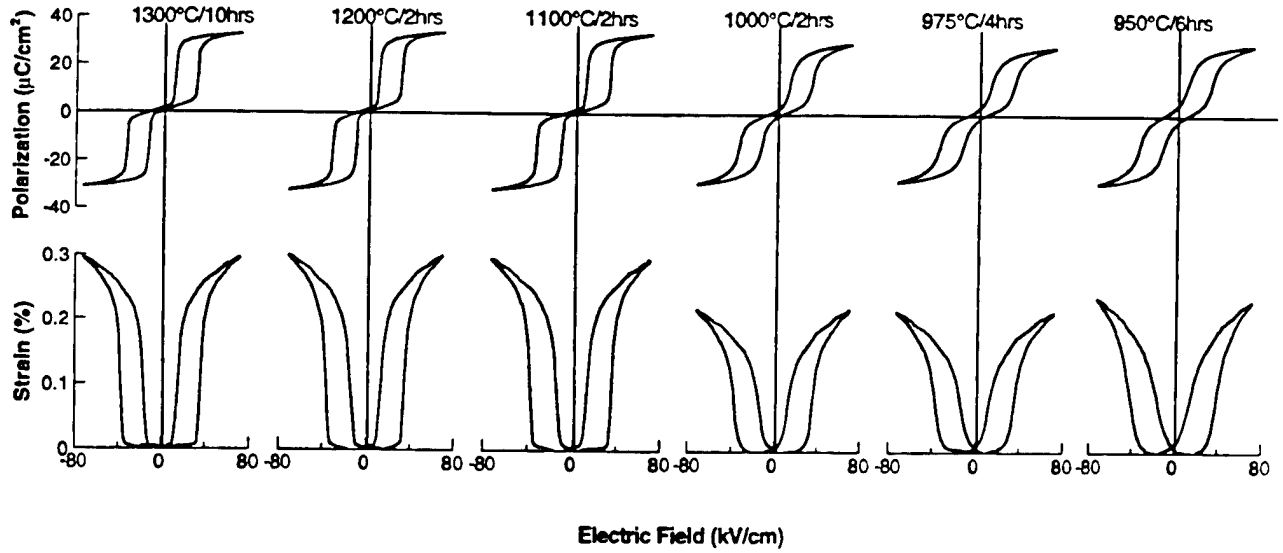

Fig. 4 The polarization and strain behaviors of samples sintered under various conditions

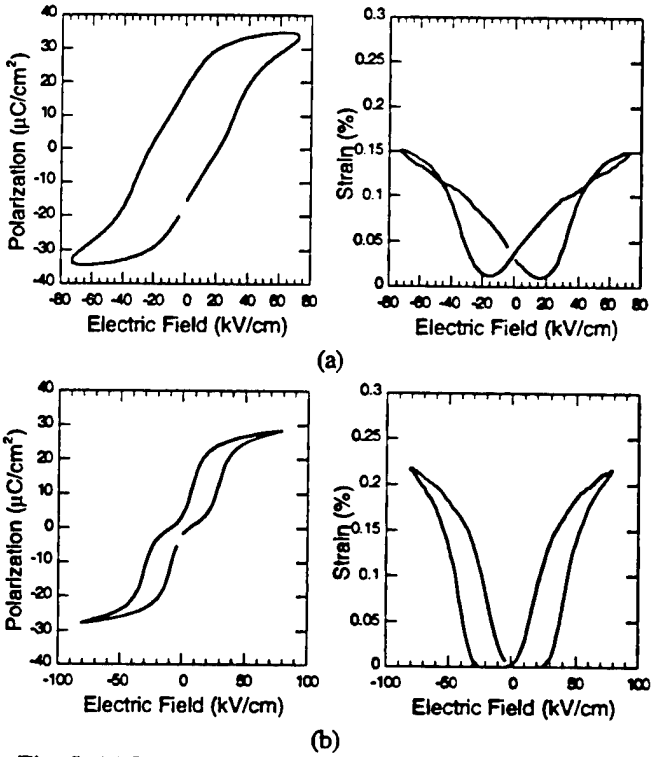

Fig. 5 (a) Lossy polarization and strain loops of samples sintered at 975°C/2hrs and (b) after being annealed at 850°C/12hrs in oxygen.

REFERENCES

[1] D. Berlincourt, "Transducers Using Forced Transitions between Ferroelectric and Antiferroelectric States," IEEE Transactions on Sonics and Ultrasonics, Vol. SU-13 [4] 116-125 (1966).

[2] W. Pan, Q. Zhang, A. Bhalla, and L.E. Cross, "Field-Forced Antiferroelectric-to-Ferroelectric Switching in Modified Lead Zirconate Titanate Stannate Ceramics," *J. Am. Ceram. Soc.*, **72** [4] 571-78 (1989).

[3] W.Y. Pan, C.Q. Dam, Q.M. Zhang, and L.E. Cross, "Large Displacement Transducers Based on Electric Field Forced Phase Transition in the Tetragonal $(Pb_{0.97}La_{0.02})(Ti,Zr,Sn)O_3$ Family of Ceramics," *J. Appl. Phys.*, **66** [12] 6014-23 (1989).

[4] C.T. Blue, J.C. Hicks, S.-E. Park, S. Yoshikawa, and L.E. Cross, "*In situ* X-Ray Diffraction Study of the Antiferroelectric-ferroelectric Phase Transition in PLSnZT," *Appl. Phys. Lett.*, **68** [21] 2942-44 (1996).

[5] L. Shebanov, M. Kusnetsov, and A. Sternberg, "Electric Field-Induced Antiferroelectric-to-Ferroelectric Phase Transition in Lead Zirconate Titanate Stannate Ceramics Modified with Lanthanum," *J. Appl. Phys.*, **76** [7] 4301-4 (1994).

[6] K.A. Markowski, S.-E Park, S. Yoshikawa, and L.E. Cross, "Effect of Compositional Variations in the Lead Lanthanum Zirconate Stannate Titanate System on Electrical Properties," *J. Am. Ceram. Soc.*, **79** [12] 3297-304 (1996).

[7] S.-E Park, K.A. Markowski, S. Yoshikawa, and L.E. Cross, "Effect on Electrical Properties of Barium and Strontium Additions in the Lead Lanthanum Zirconate Stannate Titanate System," *J. Am. Ceram. Soc.*, **80** [2] 407-12 (1997).

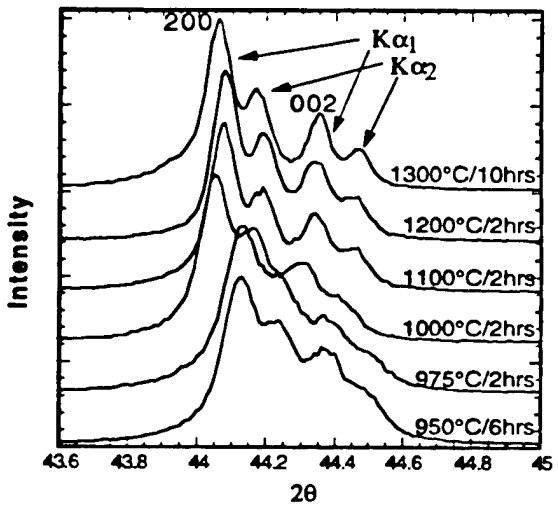

Fig. 6 XRD patterns show decreased crystallinity with decreasing sintering temperature

Relaxor Ferroelectric Single Crystal Systems

APPENDIX 20

Shape-Changing Crystals Get Shiftier

talented family of materials has gained me even more gifted members. So-called ezoelectric crystals have the unique ability swell or shrink when zapped with electric-, as well as give off a jolt of juice themlves when compressed or pulled apart. Enneers have exploited this trait for decades convert mechanical energy to electricity d back again in applications ranging from onograph needles to telephone speakers.

Now, a pair of researchers from Pennsylva-a State University has bred new piezoelectric nderkinds, some of which display an effect times greater than that of current family mbers. A paper by the researchers, materials entists Thomas Shrout and Seung-Eek Park, cheduled to appear this spring in the inaugu- issue of the journal *Materials Research Innoions*, but early word of the new work is aldy turning a few heads. "It's an exciting akthrough," says Eric Cross, another piezoctric materials expert at Penn State, who is affiliated with the project. "Improvements a factor of 10 are not easy to come by in a d that's 50 years old and considered mature."

he materials are commercial-l, as Cross and others believe y will be, they could usher in ew generation of piezoelectric ices that would improve evthing from the resolution of asound machines to the range onar listening devices.

Piezoelectric materials owe ir abilities largely to the asymrical arrangement of posily and negatively charged ns in their crystal structure. The positive and negative charges balance out in each of the crystal's unit cells—its basic repeating units—but the positive charges, for instance, may be weighted toward the top of each cell. An electric field can displace the charges even farther, which distorts the overall shape of the unit cell and of the crystal as a whole. The process can also run in reverse: Squeezing or stretching the material shifts the charges relative to each other, redistributing electric charge around the surface of the crystal, which can produce a small electric current.

The usual showcase for these properties is a cheap ceramic material called PZT, containing millions of crystalline grains in different orientations. PZT, which is composed primarily of lead, zirconium, titanium, and oxygen, can deform by as much as 0.17% in a strong applied field. To boost this shape-shifting ability, researchers have tried to grow single crystals of PZT, in which all the unit cells would line up in the same direction. Their contributions to the piezoelectric effect would also line up, enhancing it. But because PZT's components tend to separate during processing, the ceramic is extremely difficult to grow as a single crystal, says Shrout.

To coax the material into forming single crystals, Shrout and Park tried varying its composition. They settled on a couple of different mixtures, such as a combination of lead, zinc, and niobium spiked with varying amounts of lead-titanate (PT). The researchers found that a small admixture of PT—less than 9%—yielded materials that not only grew into single crystals, but also ended up with piezoelectric abilities that are enhanced more than they expected.

Just why that is, "we still don't know for sure," says Shrout. But he and Park believe that at least part of the enhancement is due to the fact that an electric field applied to the new materials does more than just shift a few atoms around in the unit cell, as in PZT: "We think it causes the whole crystalline lattice structure to change from one form to another," says Shrout. The changed crystal structure, in turn, frees individual atoms to respond more strongly to the field, increasing the overall distortion of the material. Likewise, a mechanical distortion probably produces a similar lattice shift, enabling the material to generate more current than standard PZT.

Whatever the reason for the effect, it's likely to be very useful, says Robert Newnham, another piezoelectricity expert at Penn State. The new crystals will undoubtedly cost more than ceramics like PZT, says Park, because growing single crystals is a slow and painstaking process. But he adds that he and Shrout are working on ways to speed it up. If they succeed, the new piezoelectric wunderkinds could grow up to live expansive lives indeed.

–Robert F. Service

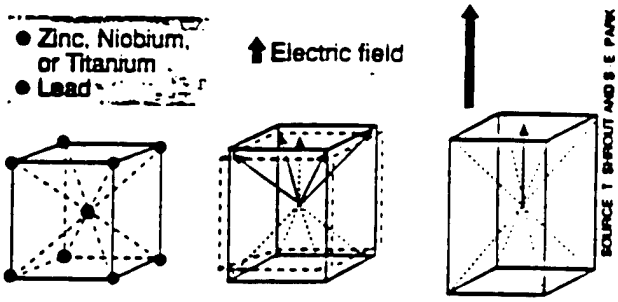

Crystal growth. A weak field dislocates atoms toward the corners of the unit cells, but a stronger field rearranges the lattice.

APPENDIX 21

Recent Advances in Piezoelectric Materials

T.R. Shrout[a], S.E. Park[a], C.A. Randall[a], J.P. Shepard[a],
L.B. Hackenberger[b], D. Pickrell[b], and W.S. Hackenberger[b]

[a]Materials Research Laboratory, The Pennsylvania State University
University Park, PA 16802

[b]TRS Ceramics, Inc., 2820 East College Avenue
State College, PA 16801

ABSTRACT

Recent developments in piezoelectric materials include submicron grain size ceramics and single crystals. $Pb(Zr,Ti)O_3$ (PZT) ceramics with submicron grain sizes (~ 0.5 μm) have been produced with properties comparable to conventional, coarse grained (~ 3 to 5 μm) ceramics. The fine grain ceramics exhibit improved machinability over conventional materials. Ultrasonic transducer arrays with post widths less than 15 μm have been fabricated as well as thin plates with thicknesses as low as 10 μm. The yields and performance of such operations are expected to be much greater with fine grain ceramic than with conventional material.

The single crystal piezoelectrics developed offer field induced strain an order of magnitude higher than what can be achieved in piezoelectric ceramic actuators (> 1%). Furthermore, the strain electric field hysteresis and dielectric losses are very low for these materials and electromechanical coupling factors (k_{33}) are greater than 90%. Applications which may benefit from the recent developments include smart materials and structures and MEMS.

1. INTRODUCTION

Piezoelectric ceramics are currently the material of choice for transducer and actuator applications, offering relatively high electromechanical coupling (k_{ij}), piezoelectric coefficients (d_{ij}), and a wide range of dielectric constants (K) with low dielectric loss. For transducer applications, these key merits of piezoelectric ceramics translate into enhanced performance in the form of high sensitivity, broad bandwidth, electrical impedance matching, and minimal thermal heating. For actuators, the piezoelectric coefficient (d_{ij}), determining the level of induced strain at a given electric field, and the maximum achievable strain level are the most widely used parameters describing actuator performance.

In this paper we review recent developments in piezoelectric materials from submicron polycrystalline ceramics to domain engineered single crystals. The impact of these new materials on device fabrication and performance will be presented, including the potential for micro-electromechanical systems (MEMS).

1.1 Piezoelectric ceramics

$Pb(Zr_{1-x},Ti_x)O_3$ (PZT) ceramics have been the mainstay for transducer and actuator applications. Compositionally, PZT ceramics lie near the morphotropic phase boundary (MPB) between the tetragonal and rhombohedral phases, as shown in Figure 1. MPB compositions exhibit anomalously high dielectric and piezoelectric properties as a result of enhanced polarizability arising from the coupling between two equivalent energy states, i.e. the tetragonal and rhombohedral phases, allowing optimum domain reorientation during the poling process.

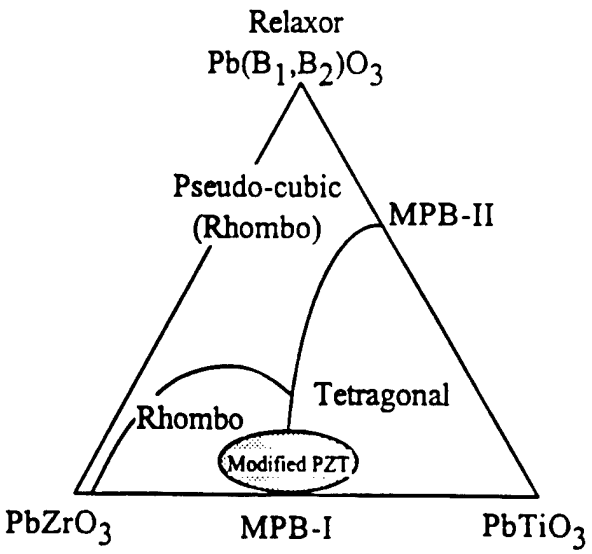

Figure 1. Ternary diagram depicting MPBs in PZT and Relaxor-PT systems for piezoelectric ceramics. [3]

Alternate MPB systems can be found in Relaxor-$PbTiO_3$, also shown in Figure 1. Lead based relaxor materials are complex perovskites with the general formula $Pb(B_1B_2)O_3$, (B_1=Mg^{2+},Zn^{2+},Ni^{2+},Sc^{3+}..., B_2=Nb^{5+}, Ta^{5+}, W^{6+}...). Characteristic of relaxors is a broad and frequency dispersive dielectric maxima [1].

To achieve a high piezoelectric coefficient, MPB-based ceramics are further engineered by compositionally adjusting the Curie temperature (T_c) downward toward room temperature. The effect of transition temperature (T_c) on the piezoelectric properties is clearly evident in Figures 2 and 3. As shown, the room temperature values of dielectric constant (K) and piezoelectric coefficient (d_{33}) are plotted as a function of T_c for a variety of modified PZT ceramics, including Relaxor-PT systems. Enhanced piezoelectric activity of MPB-based ceramics,

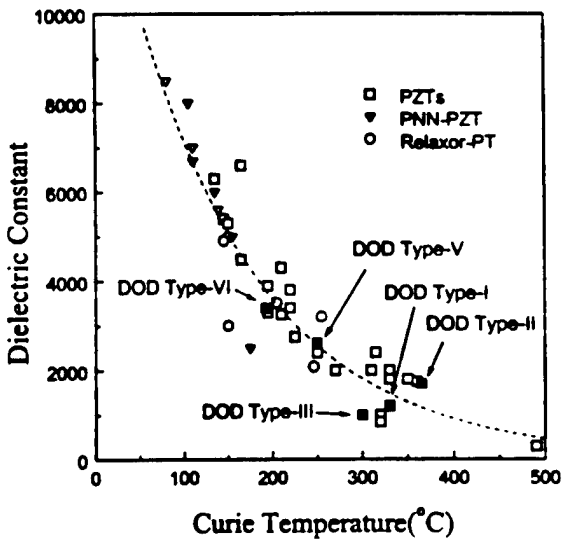

Fig. 2. Dielectric constant as a function transition temperature (T_c) for piezoelectric ceramics, including PZT, modified PZTs, and Relaxor-PT systems.

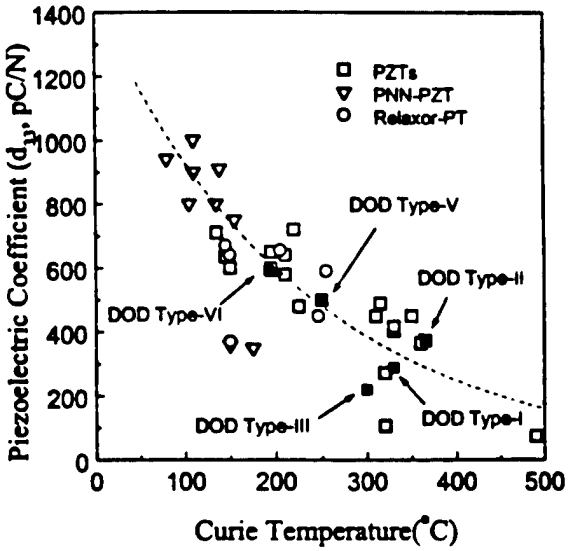

Figure 3. Piezoelectric Coefficient (d_{33}) as a function transition temperature (T_c) for piezoelectric ceramics, including PZT, modified PZTs, and Relaxor-PT systems.

achieved by compositionally adjusting T_c downward relative to room temperature, results in 'soft' piezoelectric ceramics. This enhanced piezoelectric effect, therefore, comes at the expense of more temperature dependent properties, and less polarization stability, i.e. aging and loss of piezoelectric activity. For electromechanical coupling, such as k_{33}, no relationship with T_c is evident, as presented in Figure 4. Further details on the relationship between dielectric/piezoelectric properties and Curie temperature (T_c) can be found in the article by S.-E. Park et al. [2].

2.0 FINE GRAIN PIEZOELECTRIC CERAMICS

Submicron grain size piezoelectric ceramics offer many advantages for both ultrasonic transducers and high driving field actuators. Reduced grain sizes leads to improved machinability for finer feature sizes in high frequency arrays (> 10 MHz), reduced yield loss for array fabrication, increased mechanical strength for high reliability actuators, and reduced layer thicknesses in tape cast multilayers for low driving voltage actuators [5]. A major problem with reducing grain sizes in piezoelectric ceramics has been a corresponding reduction in properties (see Figure 6). TEM studies and cryogenic property measurements have revealed that reducing grain sizes effects the extrinsic contributions to piezoelectricity in PZT ceramics [6]. Domain observations indicate that in grains less than 1 μm in size, there is a reduction in the number of domain orientation variants [7], which effectively must result in a reduction of poling efficiency.

The effect of grain size minimization may be overcome by modifying traditional dopant strategies to promote domain wall mobility [8]. This increases the extrinsic piezoelectric effect in fine grain ceramics to the extent that properties are equivalent to conventional materials, while employing conventional mixed oxide processing. The material is, therefore, cost competitive with conventional ceramics. To date, materials that have been made in fine grain form include DOD Types II, III, and VI. A grain size comparison of commercially available conventional and fine grain Type II material is shown in Figure 7.

2.1 Transducer applications

A number of studies have been conducted using the fine grain Type II ceramic (PZT-5) to demonstrate its potential benefit for a variety of applications. Dicing studies have been performed to compare the composite fabrication behavior of submicron grain ceramics directly to conventional material. Very fine scale arrays have been fabricated to test the benefits of submicron ceramic for high frequency ultrasonic arrays. And finally, the benefits of fine grain ceramic for actuators have been investigated.

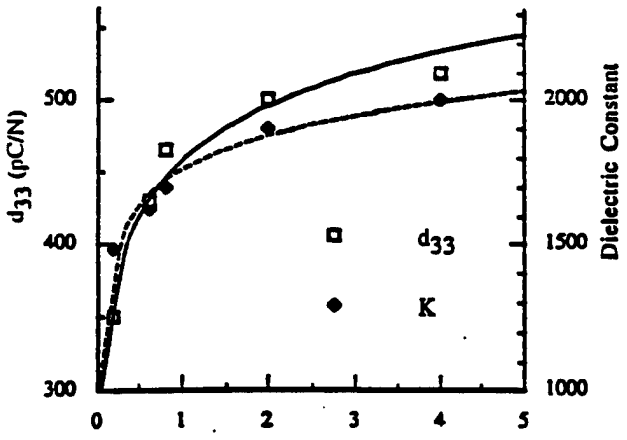

Figure 6. Piezoelectric coefficient and dielectric constant as a function of grain size for a DOD Type II ceramic [6].

Table 1. Comparison of Fine Grain and Conventional PZT Ceramic Properties.

	PZT-5 "Soft"		PZT-8 "Hard"		PZT-5H "Soft"	
Property	Type II	Type IIFG	Type III	Type IIIFG	Type VI	Type VIFG
K	1900	1900	1150	1125	4500	4400
Loss	0.018	0.017	0.002	0.003	0.02	0.025
d_{33}	425	415	260	260	785	730
k_p	0.65	0.62	0.51	0.49	0.70	0.68
T_c	350	325	—	—	185	185

2.1.1 Dicing and 1-3 composite studies

A dicing study was performed for a side-by-side comparison of machinability for Type II fine grain ceramic (TRS200FG), and two conventional materials (Edo EC65 and Motorola 3195HD).. Dicing conditions (blade rpm, travel speed, coolant flow and direction, dressing conditions, etc.)

As a general rule of thumb, piezoelectric materials can be safely used to approximately 1/2 T_c, without significant reduction in piezoelectric activity. This can restrict the working range of the device or limit fabrication techniques. During the fabrication process of transducers, the piezoelectric material may experience excessive temperature due to cutting/dicing, polymer curing, or the attachment of acoustic matching/backing materials. It is noted that the most widely used material in the ultrasonic imaging industry has a T_c ~ 210°C owing to the material's relatively high dielectric constant and coupling coefficient while providing good temperature stability.

In regard to actuator applications, a consequence of increased piezoelectric activity for piezoelectrically "soft" ceramics is large hysteresis in the strain vs. E-field behavior as a result of domain motion. Strain vs. E-field behavior for PZT-5H (Navy type-VI) is shown in Figure 5 as an example. Though the piezoelectric coefficient (d_{33}) of PZT-5H ceramics is in the range of ~ 600 to 700 pC/N [4] (implying ~ 0.06 to 0.07% strain at 10 kV/cm), actual strain levels as high as 0.1% are observed at 10 kV/cm. This enhanced nonlinear strain is a result of domain motion, and, therefore, accompanied by significant hysteresis, which results in poor positioning accuracy. The area within the strain vs. E-field curve also results in significant heat generation during operation. Heat generation combined with a decreased temperature usage range, results in poor temperature stability and may limit these ceramics to low frequency applications.

Polarization instability and strain vs. E-field hysteresis can be minimized with the use of "hard" piezoelectric ceramics. Hard piezoelectric ceramics such as PZT-8 (Navy type III) offer very low hysteresis, as shown in Figure 5. However, the reduction in hysteresis and loss comes at the expense of k_{33} (~ 60% vs. ~ 75%) and d_{33} (~ 200 vs. ~ 700 pC/N) for PZT-8 and PZT-5H, respectively.

Among electrostrictors, another category of electromechanical ceramics, a few materials such as PMN and its solid solution with PT exhibit significant electrostrictive strain (> 0.1%) with virtually no hysteresis, as shown in Figure 5. Effective d_{33}'s > ~ 800 pC/N calculated directly from the strain vs. E-field curve can be achieved, but only over a very narrow range of E-field and temperature.

In general, the polycrystalline materials presented above are made up of multidomain crystals on the order of a few microns to tens of microns. This microstructural scale, however, limits the applicability of these materials for high frequency transducers, ultra low voltage actuators, and MEMS structures, where the device scale approaches that of the individual grain size.

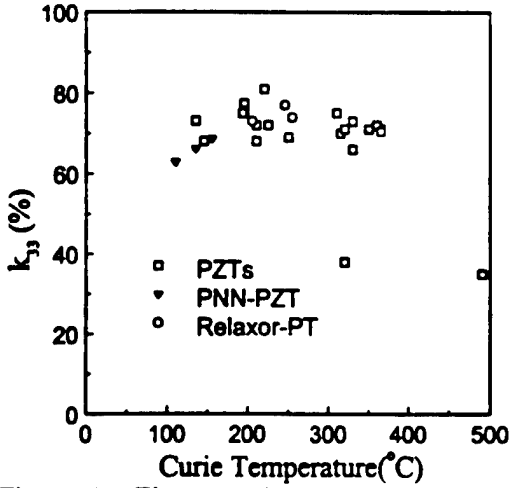

Figure 4. Electromechanical coupling (k_{33}) as a function transition temperature (Tc) for piezoelectric ceramics, including PZT, modified PZTs, and Relaxor-PT systems.

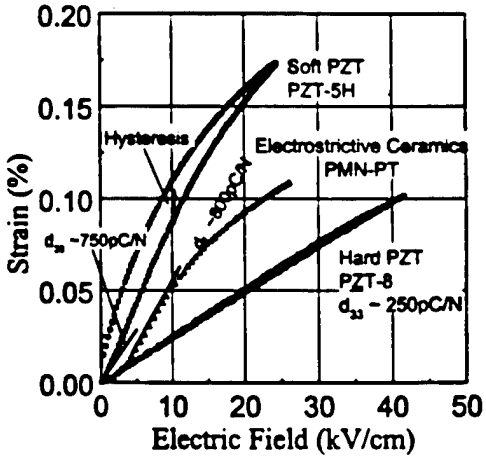

Figure 5. Strain vs. E-field behavior for various electromechanical materials.

were the same for all samples. The dicing was done on all samples with the same blade. Multiple dicing trials were done using different sample testing sequences to account for blade wear. Results were characterized by the maximum post aspect ratio essential for optimum performance (height to width) that could be achieved. Results of the dicing experiments are summarized in Table 2. A 10 MHz 1-3 composite was constructed from the fine grain material and the effective thickness coupling coefficient kt was 0.6, identical to composites made from the conventional ceramics for low frequency applications (≤ 5 MHz). The results of this study indicate that fine grain ceramic should lead to significant improvements in dicing yields without a decrease in properties.

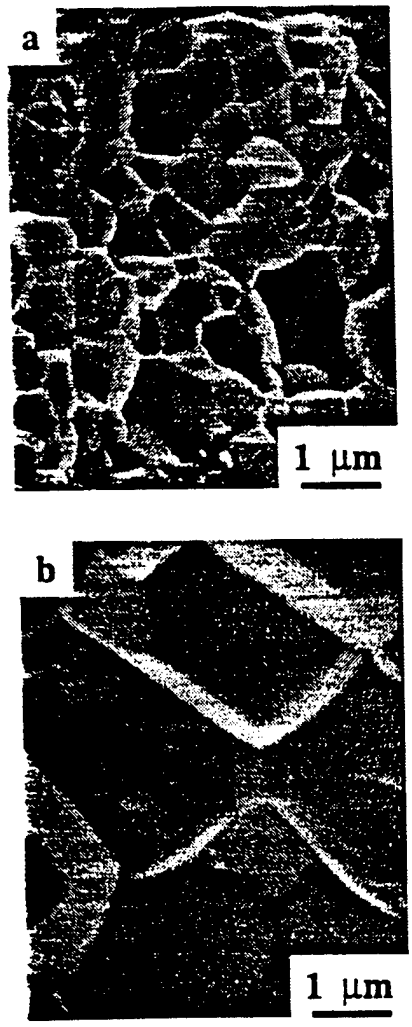

Figure 7. Microstructure comparisons for a) TRS200FG (grain size ~ 0.5 μm) and b) 3195HD (grain size ~ 3 μm).

Table 2. Summary of Dicing Study: Smallest Post Sizes.

Material	Cut Depth (μm)	Kerf (μm)	Width (μm)	Aspect Ratio
TRS200FG	380	23	18	21:1
3195HD	380	23	28	15:1
EC65	380	23	38	10:1

2.1.2 Very high frequency transducers

The ultimate benefits of fine grain ceramic were demonstrated by constructing Very High Frequency (VHF) transducers. A 2-2 composite with a resonant frequency of 50 MHz was diced using the TRS200FG material. The result is shown in Figure 8. This composite had ceramic posts approximately 15 μm wide [9]. Arrays with these dimensions could not be diced from conventional ceramics. Single element transducer plates less than 15 microns in thickness were also fabricated with corresponding thickness mode resonances ≥ 150 MHz. Such devices have potential for ultrasound backscatter microscopy.

2.2.2 Actuators

Fine grain piezoelectrics offer several potential benefits for actuator applications. PZT ceramics with grain sizes less than 1 μm are approximately 30% stronger (bending strength) than conventional materials. Thus, stacked or cofired actuators made with fine grain ceramics should be able to withstand greater tensile stresses during electric field driving. This will result in higher reliability actuators, and higher strain from a higher maximum driving field (see Figure 9). Another advantage of fine grain ceramics is thinner layers in both stacked and cofired devices allowing lower driving voltages. Finally, the improved machinability of fine grain ceramics offers potential for constructing micro-electromechanical systems (MEMS) using mechanically thinned bulk ceramic and subsequent bonding techniques.

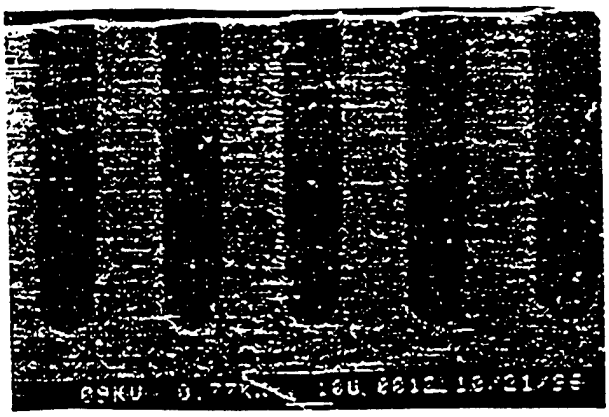

Figure 8. 50 MHz 2-2 composite fabricated from TRS200FG ceramic (grain size ~ 0.5 μm).

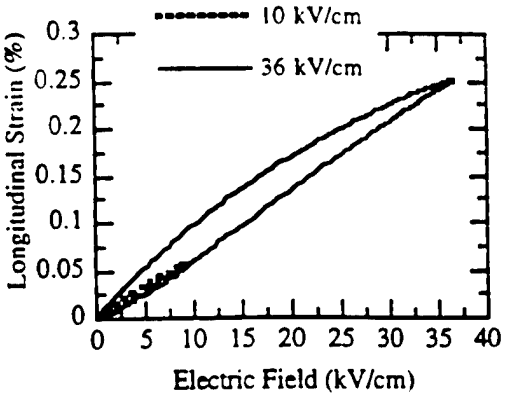

Figure 9. Increased strain available from fine grain ceramics driven at a high electric field.

3.0 SINGLE CRYSTAL PIEZOELECTRICS

In summarizing the observations presented above, the dielectric and piezoelectric properties of piezoelectric ceramics are strongly related to the transition temperature T_c. Upon direct comparison, *no one type of material*, whether PZT-based or Relaxor-PT, offers significant improvement in overall performance. Especially for actuators, soft PZTs, exhibiting piezoelectric coefficients (d_{33}) as high as 750 pC/N, are inherently limited due to hysteresis caused by domain motion. Hysteresis can be minimized with the use of hard piezoelectric ceramics, but d_{33} values of only ~ 200 to 300 pC/N are available. Even though electrostrictive ceramics offer effective d_{33}'s ~ 800 pC/N, maximum strain level is limited by its dielectric breakdown strength and polarization saturation. *The question arises, are there opportunities for new piezoelectric materials with enhanced properties?*

To answer the question above, one must look to the single crystal form of piezoelectric materials, the topic of this section.

3.1 Relaxor-PT Single crystals

Single crystal piezoelectrics such as quartz (SiO_2), lithium niobate ($LiNbO_3$), and the analogue lithium tantalate ($LiTaO_3$) are widely employed in specific applications that include oscillators, surface acoustic wave (SAW) devices, and in optics. In contrast to PZT ceramics, however, these single crystals offer inferior piezoelectric properties, with d_{33}'s < 50 pC/N.

Attempts to grow single crystals of MPB PZTs have been made by numerous researchers, resulting in crystallites too small to allow adequate property measurements [10,11,12,13,14]. In contrast to PZT crystal growth, Relaxor-PT materials can be readily grown in single crystal form. This key distinction was first realized by Soviet researchers [15,16], later by Nomura and co-workers for the PZN and PZN-PT systems [17,18] and by Shrout [19] for PMN-PT system. In

general, most $Pb(B_1B_2)O_3$-PT crystals can be grown by high temperature solution growth using Pb-based fluxes [20,21].

Although ultra high coupling and piezoelectric properties of the PZN-PT and PMN-PT systems, with d_{33} and k_{33} values greater than 1500 pC/N and 90%, respectively, have been known for several years, their potential for high performance ultrasound transducers, actuators, and related devices has only been recognized recently. Serious efforts on the development of $Pb(B_1B_2)O_3$-PT crystals for high performance transducers includes investigations at Toshiba Co. and at the Pennsylvania State University. Though the Curie temperatures (T_cs) of these materials are relatively low < 200°C, the piezoelectric property advantages become evident by directly comparing their values in relation to T_c in Figures 2–4. Although their superiority to piezoelectric ceramics is clearly evident, few systematic studies on the crystallographic aspects of these crystals have been made.

In the following section, the results based on recent investigations are presented, reporting electromechanical, dielectric/piezoelectric properties.

3.2 Electromechanical properties—low field measurements

Commonalities inherent to Relaxor-PT systems have been discussed in reviews by Shrout [22] and Randall [23]. Based on these commonalities, our presentation is limited to two representative systems, PZN-PT and PMN-PT. Though PMN-PT MPB crystals exhibit piezoelectric properties comparable with PZN-PT, more focus is given to the PZN system owing to its relatively lower PT content for MPB, allowing more uniform crystal growth of these solid solution materials. Figure 10 shows an example of oriented, cut, and polished crystals for transducer and actuator fabrication. Dielectric, piezoelectric, and electromechanical coupling coefficients for the various crystals are reported in Table 3. As reported in Table 3, large coupling coefficients (k_{33}) and large piezoelectric coefficients (d_{33}) were found for PZN-PT crystals with MPB compositions (PZN-9.5%PT), as previously reported by Kuwata [18]. Electromechanical coupling (k_{33}) equal to and larger than MPB crystal compositions were found for domain engineered rhombohedral crystals* as shown in Figure 11. Though <111> is the polar direction for rhombohedral crystals, such cuts exhibited low values in both electromechanical coupling factor and piezoelectric coefficients. Pure PZN, and PZN-8%PT crystals were found to possess high k_{33} values of ~ 85% and 94%, respectively, for (001) crystal cuts. The low values of dielectric loss < 1%, significantly less than their polycrystalline counterparts, should also be noted. Figure 12 presents the piezoelectric coefficient (d_{33}) as a function of composition, calculated based on IEEE standards. Maximum d_{33} values of ~ 2500 pC/N were determined with domain engineered rhombohedral PZN-8%PT crystals. In contrast to PZT's, d_{33} dramatically decreases at MPB to levels ~ 500 pC/N for tetragonal compositions. It should be noted that direct observation of the strain vs. E-field behavior is essential in order to investigate hysteresis and maximum levels of strain, key experiments to directly confirm actuator performance, the topic of the next section.

3.2 Electromechanical properties—high field measurements

As presented in the previous section, piezoelectric coefficients (d_{33}) as high as 2500 pC/N were determined from <001> oriented rhombohedral crystals. In relation to actuators, several questions arise: (1) How do the high d_{33} values determined using low field techniques correlate to direct measurements? (2) As for piezoelectric and electrostrictive ceramics, will the strain level saturate with increased E-field? (3) How much hysteresis accompanies the strain?

*Rhombohedral crystals oriented and poled along pseudocubic <001> direction. Crystallographically, polarization direction of rhombohedral crystal is pseudocubic <111> direction. The role of domains and their stability on the dielectric and piezoelectric properties of single crystals are investigated and reported in the article by Wada et al. [24].

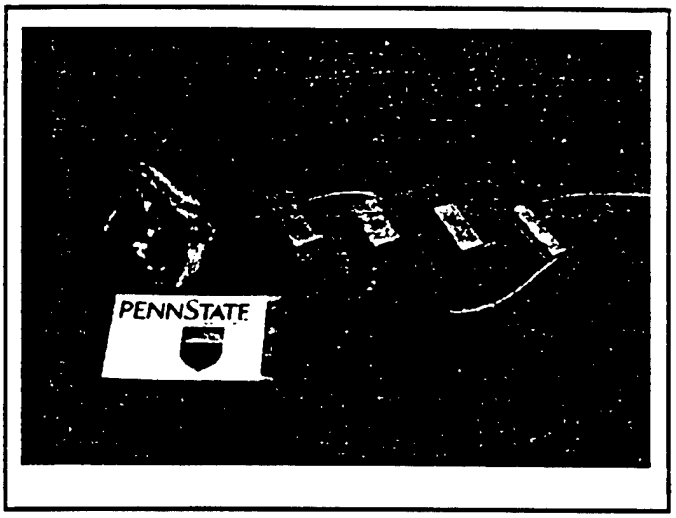

Figure 10. Oriented, cut, and polished crystals of PZN-PT.

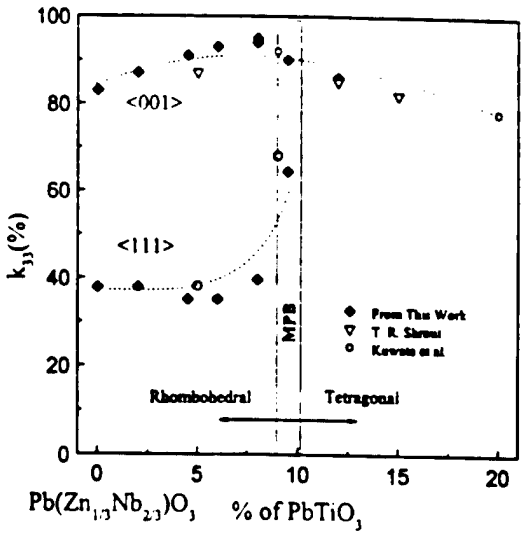

Figure 11. k_{33} as a function of composition and orientation for PZN-PT crystals.

Table 3. Dielectric and Piezoelectric Properties of $Pb(A_{1/3}B_{2/3})O_3$-$PbTiO_3$ Single Crystals ($A=Zn^{2+}$, Mg^{2+})

Composition	Orientation	K_{33}	s_{33}^E (10^{-12} m^2/N)	K_3^T	Loss	d_{33} (pC/N)
PZN	111	0.38	7.4	900	0.012	83
	001	0.85	48	3600	0.008	1100
PZN-4.5%PT	111	0.35	9.0	1500	0.004	110
	001	0.91	102	4000	0.004	2000
PZN-6%PT	111	0.33	7.3	720	0.004	74
	001	0.93	133	4800	0.012	2400
PZN-8%PT	111	0.39	74	2150	0.012	82
	001	0.95	152	5500	0.010	2600
PZN-9.5%PT	111	0.64	10.4	4300	0.007	600
	001	0.89	77	1600	0.004	1600
PZN-12%PT	001	0.86		900	0.004	500
PMN-24%PT	001			3700	0.009	900
PMN-33%PT	001	0.94	79	4500	0.012	1700
PMN-35%PT	001	0.92	67	3100	0.014	1240

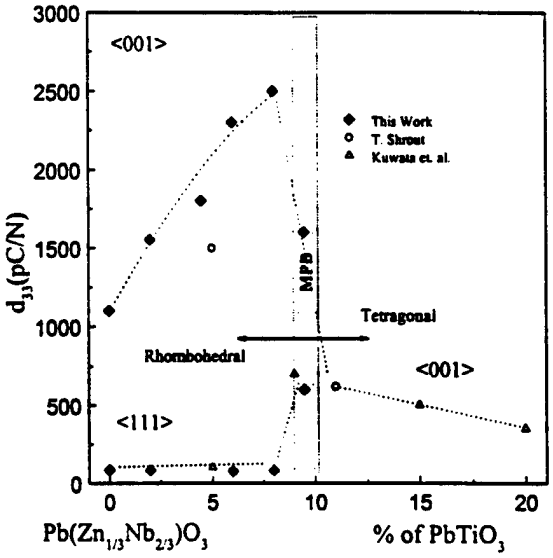

Figure 12. d_{33} as a function of composition and orientation for PZN-PT crystals.

Strain as a function of electric field for various <001> oriented rhombohedral crystals (pure PZN, PZN-4.5%PT, PZN-8%PT, and PMN-24%PT) are presented in Figure 13. Also, E-field induced strains of various electromechanical ceramics such as soft PZT (PZT-5H), hard PZT (PZT-8), and electrostrictive ceramics (PMN-PT) are compared. Piezoelectric coefficients (d_{33}) directly calculated from the slope of strain vs. electric field curves confirmed the piezoelectric coefficients determined by the low-field resonance method. Strains as high as 0.6% were observed with low hysteresis for these crystals, significantly larger than that for polycrystalline ceramics.

Strain saturation for <001> oriented rhombohedral crystals was investigated until dielectric breakdown, as presented in Figure 14. Far from saturation, the strain abruptly increased with strain levels as high as 0.8% being achieved for all crystals tested. Strain levels > 1.7%, nearly an order of magnitude larger than that achievable in present day polycrystalline ceramics, were observed for PZN-8%PT crystals as a result of higher breakdown voltage.

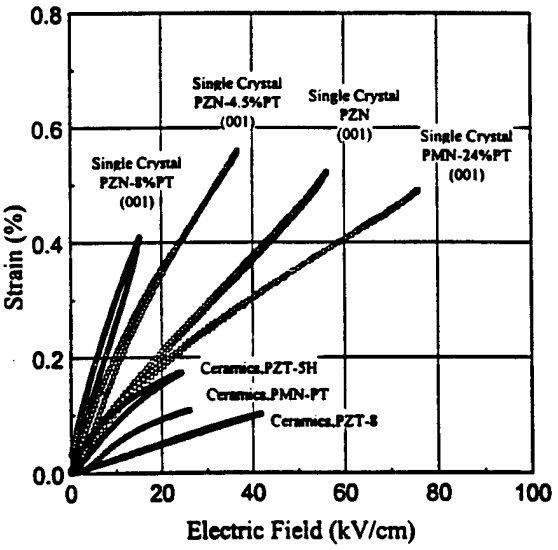

Figure 13. Strain vs. E-field behavior for <001> oriented rhombohedral crystals of PZN-PT and PMN-PT and for various electromechanical ceramics.

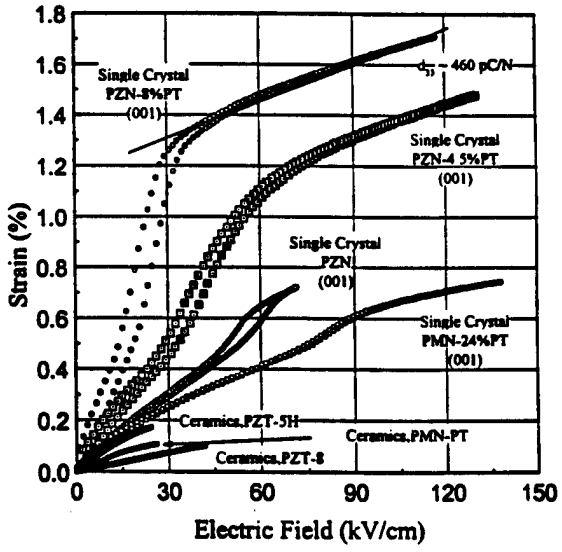

Figure 14. Strain vs. E-field behaviors for crystals of PZN-PT and PMN-PT, and for various polycrystalline ceramics. Maximum field was limited by dielectric breakdown.

4.0. MicroElectroMechanicalSystems (MEMS)

The worldwide market for MEMS (MicroElectroMechanical Systems) is predicted to grow to over $12 billion by the year 2000. MEMS which both sense and actuate are still largely in development, but are predicted to account for a substantial market share in the future [25]. While silicon will always remain the basis for MEMS, more new materials will be incorporated to enhance the performance of these devices. The large piezoelectric effect found in lead-based ferroelectrics such as PZT makes them attractive for use in both micro-actuators and sensors. Up to the present time, the integration of PLZT and MEMS has been approached through the deposition and post-processing of PZT thin films on silicon. In general, PZT films suffer from limited thickness (~ 1 μm), high internal stress, clamping by the substrate, electrode compatibility problems, and low piezoelectric coefficients. The recent developments in piezoelectric materials presented in Sections 2 and 3 offer the potential for creating hybrid MEMS from piezoelectric bulk materials:

- *Fine Grain Piezoelectrics.* Submicron piezoelectric ceramics with piezoelectric properties comparable to conventional materials have improved machinability over coarser grained ceramics with the ability to fabricate transducer elements on the order of only ~ 10 microns by precision sawing or polishing.

- *Single Crystal Piezoelectrics.* Single crystal piezoelectrics exhibit exceptional piezoelectric activity (d_{33} = 2500 pC/N and d_{31} = -1000 pC/N). Resulting strains are over 1%, which is an order of magnitude greater than the strains produced in conventional piezoceramics or thin films. Thin sections of these crystals (< 50 μm) have already been prepared.

Work is currently underway to incorporate these materials into semi-monolithic MEMS using techniques similar to those found in Epitaxial Lift-Off (ELO) processes. As schematically presented in Figure 15, micromachined silicon substrates and thin sections of the piezoelectric materials are grafted onto the substrates. It is expected that these hybrid MEMS can be used as variable positioners, optical scanners, shear force sensors, microfluidics devices, and high-torque ultrasonic motors. Preliminary calculations for a simple cantilever-type unimorph microactuator indicate that forces in the milli-Newton and displacements in the millimeter ranges can be obtained from microunimorphs ranging from micrometers to millimeters in size. It is predicted that hybrid MEMS using lead-based piezoelectrics will have several advantages over MEMS composed entirely of silicon or PZT-film MEMS. These include greater ruggedness and higher force generation in actuators and higher sensitivities in piezoelectric sensors.

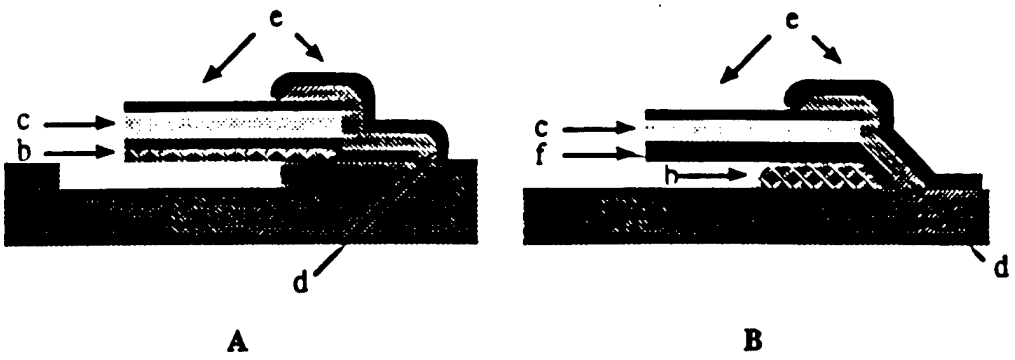

Figure 15. Schematic drawing of two microunimorph designs (not to scale): (a) silicon, (b) Si_3N_4 shim or pedestal support, (c) PZN-PT crystal, (d) insulator, (e) electrodes, and (f) metal shim. Passivation layers between the silicon and the electrodes are omitted for simplicity. A polysilicon layer that would be deposited on Si_3N_4 to promote electrode adhesion is also not shown.

5.0 SUMMARY

Recent developments in piezoelectrics include fine grain polycrystalline ceramics and single crystals. Submicron grain PZTs (< 0.5 μm) have been developed with properties comparable to conventional ceramics. Fabrication studies of ultrasonic arrays have shown that submicron grain sized PZT have superior machining characteristics to conventional ceramics. Diced or polished dimensions less than 15 μm have been achieved. Improved machinability is expected to increase array manufacturing yields and allow for the fabrication of very high frequency transducers (> 50 MHz). For actuators, the improved strength of fine grain ceramics is expected to lead to increased reliability and larger strains through high driving fields. Thinner layers in stacked and cofired actuators can also be produced with a corresponding decrease in drive voltage.

The single crystal form of Relaxor-PT materials offers the possibility of dramatic improvements in transducer performance. Electromechanical coupling coefficients greater than 90% and ultrahigh piezoelectric coefficients (d_{33}) > ~ 2500 pC/N and strain levels up to 0.6% with minimized hysteresis have been achieved. In contrast to strain saturation observed from <111> oriented rhombohedral crystals, ultrahigh strain levels up to 1.7% could be achieved for <001> oriented rhombohedral single crystals nearly an order of magnitude larger than that available in polycrystalline ceramics. Other relaxor based rhombohedral crystals are expected to exhibit similar strain vs. E-field behavior. Though clearly promising candidates for high performance transducers and actuators, further investigation in crystal growth and pre-stress testing are required for single crystal piezoelectrics to become the next generation of ultrasound and actuator materials.

The potential for the newly developed piezoelectric materials for hybrid MEMS is noted.

ACKNOWLEDGMENT

This research has been supported by Office of Naval Research and Whitaker Center for Ultrasonic Imaging. The authors would like to thank L.E. Cross for his helpful suggestions, and Patrick D. Lopath. Michael J. Zipparo, and Timothy Ritter for their help with dicing studies and property measurements, and Shi-Fang Liu and Hua Lei for their help with crystal growing and sample preparation, respectively.

REFERENCES

1. L.E. Cross, "Relaxor Ferroelectrics," *Ferroelectrics*, vol. 76, pp. 241–267, 1987.
2. Seung-Eek Park and Thomas R. Shrout, "Characteristics of Relaxor-Based Piezoelectric Single Crystals for Ultrasonic Transducers," *IEEE Trans. on UFFC*, Vol. 44, No. 5, pp. 1140–1147, 1997.
3. Y. Yamashita, "Large Electromechanical Coupling Factors in Perovskite Binary Material System," *Japanese Journal of Applied Physics*, vol. 33, Pt. 1[9B], pp. 5328–5331, 1994.
4. H. Jaffe and D.A. Berlincourt, "Piezoelectric Transducer Materials," *Proceedings of IEEE*, vol. 53 No. 10, pp. 1372–1386, 1965.
5. W.A. Smith, "New opportunities in ultrasonic transducers emerging from innovations in piezoelectric materials," 1992 SPIE International Symposium, pp. 1–24, July 1992.
6. N. Kim, Ph.D. Thesis, "Grain size effect on the dielectric and piezoelectric properties in compositions which are near the morphotropic phase boundary of lead zirconate-titanate based ceramics," The Pennsylvania State University, May 1994.
7. W. Cao and C.A. Randall, "The grain size and domain size relations in bulk ceramic ferroelectric materials," *J. Phys. Chem. Solids*, in press.
8. W.S. Hackenberger, N. Kim, C.A. Randall, T.R. Shrout, and D.J. Pickrell, "Processing and Structure-Property Relationships for Fine Grained PZT Ceramics," *Proc. 10th Intrnl. Symp. Appl. Ferroelectrics, IEEE*, East Brunswick, NJ, Aug. 18–21, pp. 903–906, 1996.

9. M. Zipparo, Ph.D. Thesis, "Very High Frequency (50 to 100 MHz) Ultrasonic Transducers for Medical Imaging," The Pennsylvania State University, Dec. 1996.
10. S. Fushimi and T. Ikeda, "Phase Equilibrium in the System PbO-TiO_2-ZrO_2, *Journal of the American Ceramic Society*, vol. 50, No. 3, pp. 129–132, March 1967.
11. V.A. Kuznetzov, "Crystallization of Titanium, Zirconium, and Hafnium Oxides and Some Titanate and Zirconate Compounds under Hydrothermal Conditions," *Journal of Crystal Growth*, vol. 34, pp. 405–410, 1968.
12. R. Clarke and R.W. Whatmore, "The Growth and Characterization of $PbZr_xTi_{1-x}O_3$ Single Crystals," *Journal of Crystal Growth*, vol. 33, pp. 29–38, 1976.
13. T. Hatanaka and H. Hasegawa, "Dielectric Properties of $Pb(Zr_xTi_{1-x}O_3$ Single Crystals Including Monoclinic Zirconia," *Japanese Journal of Applied Physics*, vol. 34, pp. 5446–5448, Sept. 1995.
14. K. Yanagiwasa, H. Kanai, and Y. Yamashita, "Hydrothermal Crystal Growth of Lanthanum-Modified Lead Zirconate Titanate, " *Japanese Journal of Applied Physics*, vol. 34, pp. 536–538 Sept. 1995.
15. V.A. Bokov and I.E. Myl'nikova, *Soviet Physics-Solid State*, Vol. 2, No. 11, pp. 2428–2432, 1961.
16. G.A. Smolenskii, V.A. Isuov, A.I. Agranovskaya, and S.N. Popov, "Ferroelectric with diffuse Phase Transitions," *Soviet Physics-Solid State*, Vol. 2, No. 11, pp. 2584–2594, 1961.
17. J. Kuwata, K. Uchino, and S. Nomura, "Phase Transitions in the $Pb(Zn_{1/3}Nb_{2/3})O_3$–$PbTiO_3$ System," *Ferroelectrics*, vol. 37, pp. 579–582, 1981.
18. J. Kuwata, K. Uchino, and S. Nomura, "Dielectric and Piezoelectric Properties of $0.91Pb(Zn_{1/3}Nb_{2/3})O_3$–$0.009PbTiO_3$ Single Crystals," *Japanese Journal of Applied Physics*, vol. 21, no. 9, pp. 1298–1302, Sept. 1982.
19. T.R. Shrout, Z.P. Chang, N. Kim, and S. Markgraf, "Dielectric Behavior of Single Crystals near the (1-x)$Pb(Mg_{1/3}Nb_{2/3})O_3$-(x)$PbTiO_3$ Morphotropic Phase Boundary," *Ferroelectric Letters*, vol. 12 pp. 63–69, 1990.
20. M.L. Mulvihill, S.-E. Park, G. Risch, Z. Li, K. Uchino, T.R. Shrout, "The Rold of Processing Variables in the Flux Growth of Lead Zinc Niobate-Lead Titanate Relaxor Ferroelectric Single Crystals," *Japanese Journal of Applied Physics*, vol. 35, no. 7, pp. 51–57, July 1996.
21. S.-E. Park, M.L. Mulvihill, G. Risch, and T.R. Shrout, "The Effect of Growth Condition on Dielectric Properties of $Pb(Zn_{1/3}Nb_{2/3})O_3$ Crystal," *Japanese Journal of Applied Physics*, Pt. 1, vol. 36, no. 3, 1154–1158, March 1997.
22. T.R. Shrout and J. Fielding, Jr., "Relaxor Ferroelectric Materials," in *Proceedings of the 1990 IEEE Ultrasonics Symposium*, 1990, pp. 711–715.
23. C.A. Randall, A.S. Bhalla, T.R. Shrout, and L.E. Cross, "Classification and Consequences of Complex Lead Perovskite Ferroelectrics with Regard to B-site Cation Order," *Journal of Materials Research*, vol. 5, no. 4, pp. 829–834, 1990.
24. S. Wada, S.-E. Park, L.E. Cross, and T.R. Shrout, "Domain Configuration and Ferroelectric Related Properties of Relaxor Based Single Crystals," *Proceedings of 8th US-Japan Seminar on Dielectric and Piezoelectric Ceramics*, in press.
25. J. Brysek, "Impact of MEMS Technology on Society," Sensors and Actuators, A56, pp. 1-9, 1996.

APPENDIX 22

Ultrahigh strain and piezoelectric behavior in relaxor based ferroelectric single crystals

Seung-Eek Park[a] and Thomas R. Shrout
Materials Research Laboratory, The Pennsylvania State University, University Park, Pennsylvania 16802

(Received 20 March 1997; accepted for publication 12 May 1997)

The piezoelectric properties of relaxor based ferroelectric single crystals, such as $Pb(Zn_{1/3}Nb_{2/3})O_3$–$PbTiO_3$ and $Pb(Mg_{1/3}Nb_{2/3})O_3$–$PbTiO_3$ were investigated for electromechanical actuators. In contrast to polycrystalline materials such as $Pb(Zr,Ti)O_3$, morphotropic phase boundary compositions were not essential for high piezoelectric strain. Piezoelectric coefficients (d_{33}'s)>2500 pC/N and subsequent strain levels up to >0.6% with minimal hysteresis were observed. Crystallographically, high strains are achieved for ⟨001⟩ oriented rhombohedral crystals, although ⟨111⟩ is the polar direction. Ultrahigh strain levels up to 1.7%, an order of magnitude larger than those available from conventional piezoelectric and electrostrictive ceramics, could be achieved being related to an E-field induced phase transformation. High electromechanical coupling (k_{33})>90% and low dielectric loss <1%, along with large strain make these crystals promising candidates for high performance solid state actuators. [S0021-8979(97)00516-1]

I. INTRODUCTION

Electromechanical actuators directly transform input electrical energy into mechanical energy. Of the many types of actuator materials including, magnetostrictive, photostrictive, and shape memory alloys, piezoelectric and electrostrictive ceramics are widely used in applications requiring high generative force, high frequency operation, accurate displacement, quick response time, or small device size.[1] Generally, among the material properties determining actuator performance, the electric field (E-field) induced strain is the most important parameter for actuators. This is demonstrated by strain energy density which is a measure of the energy per unit mass an actuator can deliver.

$$e_{max} = 1/\rho \cdot 1/4 \cdot [1/2 \cdot E(s_{max})^2], \quad (1)$$

where e_{max} is the strain energy density, E is the actuator's elastic modulus, s_{max} is the maximum field induced strain, and ρ is the actuator's density.[1] 1/4 is a factor appropriate for an actuator with its impedance matching to that of its surroundings. In designing an actuator, the maximum strain energy density should be as high as possible. In electroactive ceramics, density and elastic modulus vary little from material to material, therefore the level of strain and maximum strain achievable with a reasonable electric field (<50 kV/cm) dominates the energy density. The piezoelectric coefficient (d_{ij}), determining the level of induced strain at a given electric field, is the most widely used parameter describing actuator performance.

It is the objective of this article to report ultrahigh piezoelectric coefficients (d_{33}) and ultrahigh strain levels with low hysteresis observed for single crystals of relaxor perovskite $Pb(Zn_{1/3}Nb_{2/3})O_3$–$PbTiO_3$ (PZN-PT) and $Pb(Mg_{1/3}Nb_{2/3})O_3$–$PbTiO_3$ (PMN-PT). Strain behavior as a function of E-field will be discussed with respect to crystal structure, orientation, domain configuration, and anticipated actuator performance.

II. BACKGROUND

A. Morphotropic phase boundary and electrostrictive ceramics

$Pb(Zr_{1-x},Ti_x)O_3$ (PZT) ceramics have been the mainstay for high performance actuator applications. Compositionally, PZT ceramics lie near the morphotropic phase boundary (MPB) between the tetragonal and rhombohedral phases as shown in Fig. 1. MPB compositions exhibit anomalously high dielectric and piezoelectric properties as a result of enhanced polarizability arising from the coupling between two equivalent energy states, i.e., the tetragonal and rhombohedral phases, allowing optimum domain reorientation during the poling process. Alternate MPB systems can be found in Relaxor-$PbTiO_3$, also as shown in Fig. 1. Lead based relaxor materials are complex perovskites with the general formula $Pb(B_1B_2)O_3$, (B_1=Mg^{2+},Zn^{2+},Ni^{2+}, Sc^{3+}.... B_2=Nb^{5+},Ta^{5+},W^{6+}...). It is characteristic of relaxors to have a broad and frequency dispersive dielectric maxima.[2]

To achieve a high piezoelectric coefficient, MPB-based ceramics are further engineered by compositionally adjusting the Curie temperature (T_c) downward relative to room temperature. The effect of transition temperature (T_c) on the piezoelectric properties is clearly evident in Fig. 2. As shown, the room temperature values of d_{33} are plotted as a function of T_c for a variety of modified PZT ceramics, including Relaxor-PT systems. Enhanced piezoelectric activity of MPB-based ceramics, achieved by compositionally adjusting T_c downward relative to room temperature, results in "soft" piezoelectric ceramics. This enhanced piezoelectric effect, therefore, comes with the expense of more temperature dependent properties, and less polarization stability, i.e., aging and loss of piezoelectric activity. Further details on the

[a]Electronic mail: sxp37@email.psu.edu

 0021-8979/97/82(4)/1804/8/$10.00

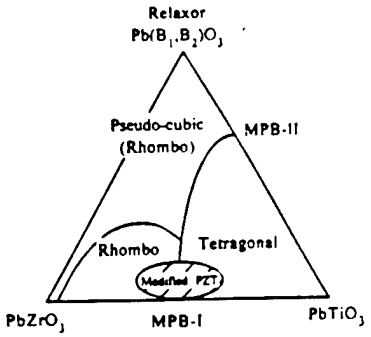

FIG. 1. Ternary diagram depicting MPBs in PZT and Relaxor-PT systems for piezoelectric ceramic (Ref. 19).

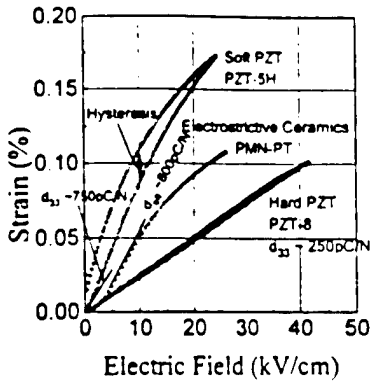

FIG. 3. Strain vs E-field behavior for various electromechanical ceramics.

relationship between dielectric/piezoelectric properties and Curie temperature (T_c) of piezoelectric ceramics can be found in the article by Park *et al.*[3]

Most importantly, a consequence of increased piezoelectric activity for these "soft" ceramics is large hysteresis in the strain versus E-field behavior as a result of domain motion. Strain versus E-field behavior for PZT-5H (Navy type-VI) is shown in Fig. 3 as an example. Although the piezoelectric coefficient (d_{33}) of PZT-5H ceramics is in the range of ~600–700 pC/N[4] (implying ~0.06%–0.07% strain at 10 kV/cm), strain as high as 0.1% can be observed at 10 kV/cm. This enhanced nonlinear strain is the result of domain motion, and therefore, accompanied by significant hysteresis, results in poor positioning accuracy. The area within the strain versus E-field curve, or dielectric loss, also results in significant heat generation during operation. Heat generation combined with a decreased temperature usage range results in poor temperature stability and limits these ceramics to low frequency applications.

Strain versus E-field hysteresis can be minimized with the use of the "hard" piezoelectric ceramics. Hard piezoelectric ceramics such as PZT-8 (Navy type III) offer very low hysteresis as shown in Fig. 3. However, the reduction in hysteresis and loss comes at the expense of d_{33} and subsequent strain level. Typically d_{33} values, for hard PZTs range from ~200 to 300 pC/N.[4]

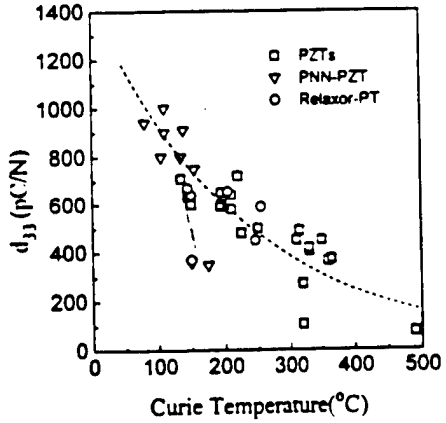

FIG. 2. Piezoelectric coefficient (d_{33}) as a function of transition temperature (T_c) for piezoelectric ceramics, including PZT, modified PZTs, and Relaxor-PT systems. Data were compiled from references, commercial brochures, and internal investigations.

Another category of ceramic materials used in commercial actuators are electrostrictors. Electrostrictive strain is proportional to the square of polarization. A few materials such as PMN and its solid solution with PT exhibit significant electrostrictive strain (>0.1%) with virtually no hysteresis as shown in Fig. 3. Effective d_{33}'s>~800 pC/N calculated directly from the strain versus E-field curve can be achieved, but only over a very narrow range of E field and temperature. For hard piezoelectric and electrostrictive ceramics, strain level with low hysteresis does not exceed 0.15%. This limitation originates from the material's dielectric breakdown strength and polarization saturation.

In summary, piezoelectric and electrostrictive ceramics offer strain levels up to ~0.15%. Soft PZTs, exhibiting piezoelectric coefficients (d_{33}) as high as 750 pC/N, are inherently limited due to hysteresis caused by domain motion. Hysteresis can be minimized with the use of hard piezoelectric ceramics, but d_{33} values of only ~200–300 pC/N are available. Even though electrostrictive ceramics offer effective d_{33}'s~800 pC/N, maximum strain level is limited by its dielectric breakdown strength and polarization saturation. To achieve E-field induced strain levels >0.15%, electroactive materials should possess high piezoelectric coefficients (d_{33} >1000 pC/N) and high dielectric breakdown strength.

B. Single crystal piezoelectrics

Single crystal piezoelectrics such as quartz (SiO_2), lithium niobate ($LiNbO_3$), and the analogue lithium tantalate ($LiTaO_3$) are widely employed in specific applications that include oscillators, surface acoustic wave (SAW) devices, and in optics. In contrast to PZT ceramics, however, these single crystals offer inferior piezoelectric properties, with d_{33}'s<50 pC/N.

Attempts to grow single crystals of MPB PZTs have been made by numerous researchers, resulting in crystallites too small to allow adequate property measurements.[5–9] In contrast to PZT crystal growth, relaxor-PT materials can be readily grown in single crystal form. This key distinction was realized by Nomura and co-workers for the PZN and PZN-PT systems[10,11] and later by Shrout for the PMN-PT.[12] In general, most $Pb(B_1,B_2)O_3$-PT crystals can be grown by high temperature solution growth using Pb-based fluxes.[13,14]

Piezoelectric coefficients as high as ~1500 pC/N have been reported[11,12] for MPB Relaxor-PT crystals. However, it should be noted that piezoelectric coefficients are generally determined using low-field (<0.1 kV/cm) techniques such as the resonance method (IEEE standard).[15] Therefore, direct observation of the strain versus E-field behavior is essential in order to investigate hysteresis and maximum levels of strain, key experiments to directly confirm actuator performance. In relation to actuators, several questions arise:

(1) How do the high d_{33} values determined using low field techniques correlate to direct measurements? As for piezoelectric and electrostrictive ceramics, will the strain level saturate with increased E field?
(2) How much hysteresis accompanies the strain?
(3) Is morphotrophy essential for enhanced piezoelectric properties?
(4) Are there optimum crystallographic cuts as in the case of the other piezoelectric crystals?

In the following sections, we will attempt to answer these questions, reporting piezoelectric properties and direct observation of strain behavior as a function of crystallographic orientation and electric field for Relaxor-PT single crystals.

Commonalties inherent to Relaxor-PT systems have been discussed in reviews by Shrout[16] and Randall.[17] Based on these commonalties, our research was limited to two representative systems, PZN-PT and PMN-PT. Although PMN-PT MPB crystals exhibit piezoelectric properties comparable with PZN-PT, more focus was given to the PZN system owing to its relatively lower PT content for MPB, allowing more uniform crystal growth of these solid solution materials.

III. EXPERIMENTAL PROCEDURE

A. Crystal growth

Crystals of PZN, PMN, and their solid solutions with PT were grown using the high temperature flux technique. High purity (>99.9%) powders of Pb_3O_4 (Aldrich, WI), ZnO (Johnson Matthey, MA), $MgCO_3$ (Johnson Matthey, MA), Nb_2O_5 (Aldrich, WI), and TiO_2 (Aldrich, WI) were used. Raw powders were weighed with desired molar ratio with excess Pb_3O_4 as a flux. The powders were dry mixed for a desired period of time using a tumbling mill. The mixed powders were loaded into a Platinum crucible, which was placed in an alumina crucible sealed with an alumina lid and alumina cement to minimize PbO volatilization. The crucible and powder were placed in a tube furnace and held at soak temperatures (1100–1200 °C), followed by slow cooling (1–5 °C/h). The crucible was then furnace-cooled to room temperature. Hot HNO_3 is used to separate the crystals out of the rest of the melt. Typically crystal size ranged from 3 to 20 mm. Further details on the flux growth technique of these crystals can be found in Refs. 13 and 14.

B. X-ray diffraction (XRD) analysis

Single crystals were ground into a fine powder for XRD analysis ranging from 20° to 80° 2θ with a step size of 0.01 and a counting time of 3 s, in order to confirm phase pure perovskite and to calculate lattice parameter. Individual crystals were oriented along various crystallographic directions such as their pseudocubic ⟨001⟩ and the ⟨111⟩ axis using a Laue back reflection camera.

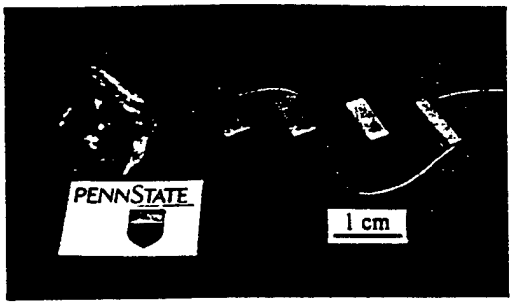

FIG. 4. An as grown crystal, an aligned sample using the Laue camera, a cut and polished sample, an electroded sample for direct strain observation as well as for low field planar mode resonant sample, and a low field longitudinal mode resonant sample, for PZN-9.5%PT, respectively (from left to right).

C. Electrical characterization

Dielectric and piezoelectric properties were measured using direct observation of strain as a function of electric field as well as low-field property measurements using the IEEE resonance technique.[15] For electrical characterization, samples were prepared by polishing with silicon carbide and alumina polishing powders to achieve flat and parallel surfaces onto which gold electrodes were sputtered. High-field measurements included polarization and strain hysteresis using a modified Sawyer–Tower circuit and linear variable differential transducer (LVDT) driven by a lock-in amplifier (Stanford Research Systems, Model SR830). Plate shape samples with thickness ranging from 0.2 to 0.5 mm were used. Electric fields as high as ~140 kV/cm were applied using an amplified unipolar wave form at 0.2 Hz, using a Trek 609C-6 high voltage dc amplifier. During testing the samples were submerged in Flourinert (FC-40, 3M, St. Paul, MN), an insulating liquid, to prevent arcing. For piezoelectric coefficient (d_{33}) determination, bar shape samples with lengths ranging from 3 to 5 mm were tested. Samples were poled either by field cooling (10 kV/cm) from temperatures above the dielectric maximum temperature (T_{max}) or by applying 40 kV/cm at room temperature. Figure 4 presents, from left to right, a representative of an as grown crystal, an aligned sample using the Laue camera, a cut and polished sample, an electroded sample for direct strain observation as well as for low field planar mode resonant sample, and a low field longitudinal mode resonant sample, for PZN-9.5% PT, respectively.

IV. RESULTS AND DISCUSSION

A. Low field measurements

Piezoelectric coefficients as a function of composition and crystal orientation for PZN-PT, calculated based on IEEE standards, are presented in Fig. 5. As shown, large piezoelectric coefficients (d_{33}~1600 pC/N) were found for

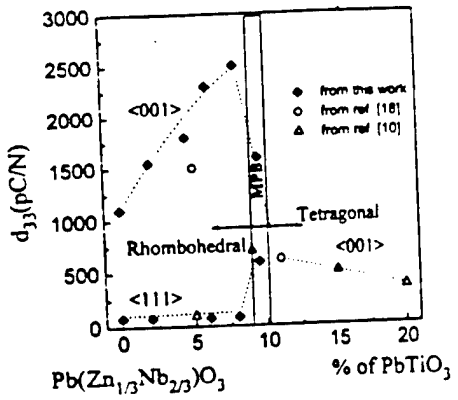

FIG. 5. d_{33} as a function of crystal composition and orientation.

PZN-PT with MPB compositions (9.5% PT), as previously reported by Kuwata.[11] PMN-PT crystals with MPB compositions (PMN-35% PT) also exhibited large piezoelectric coefficients ($d_{33}\sim 1500$ pC/N).[3] It should be noted, however, that all rhombohedral crystals oriented along their pseudocubic ⟨001⟩ direction exhibited large piezoelectric coefficients. As shown in Fig. 5, d_{33} increased with increased amount of $PbTiO_3$ for ⟨001⟩ oriented rhombohedral crystal. Maximum d_{33} values of $\sim$2500 pC/N were determined with rhombohedral PZN-8% PT crystals oriented along ⟨001⟩. In contrast to PZTs, d_{33} dramatically decreases at MPB to levels $\sim$500 pC/N for tetragonal composition. Although ⟨111⟩ is the polar direction for rhombohedral crystals, such cuts exhibited a low piezoelectric coefficient as shown in Fig. 5. In the following section the origin of apparent anisotropy will be discussed by direct strain observation as a function of electric field.

B. Domain (in)stability and associated anisotropy

Table I presents dielectric and piezoelectric properties for two rhombohedral crystals, pure PZN and PZN-8% PT, as a function of crystallographic orientation. Dielectric loss values $\leq 1\%$ and electromechanical coupling constant values (k_{33})$>90\%$, attractive for transducer applications and essential for high performance solid state actuators, could be achieved with ⟨001⟩ oriented crystals, with further details found in Ref. 3. ⟨001⟩ oriented rhombohedral crystals exhibited ultrahigh piezoelectric coefficients (d_{33}) of $\sim$1100 pC/N (PZN) up to 2500 pC/N (PZN-8% PT), and d_{33} values increased with increased $PbTiO_3$ content as presented in Fig. 5. However, electromechanical couplings

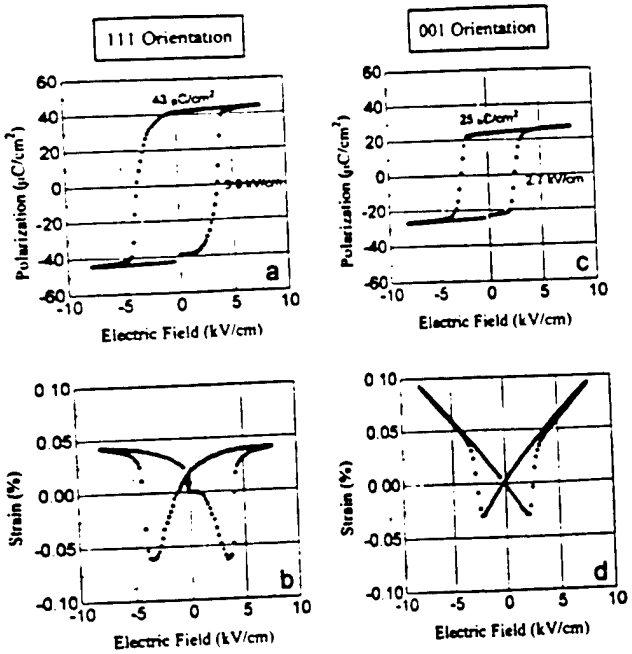

FIG. 6. Polarization and strain vs E-field (bipolar) curves for PZN crystals oriented along ⟨111⟩ (a), (b) and ⟨001⟩ (c), (d).

(k_{33}) and piezoelectric coefficients (d_{33}) of ⟨111⟩ oriented rhombohedral crystals are only $\sim$35% and $\sim$80 pC/N, respectively, regardless of composition. This composition independence of piezoelectric properties must have origins other than the inherent crystallographic anisotropy.

Polarization and strain as a function of E field (bipolar) for ⟨111⟩ oriented PZN crystal are presented in Figs. 6(a) and 6(b), respectively. Subsequent unipolar strain behavior after poling (field cooling under 20 kV/cm from 200 °C to room temperature) is shown in Fig. 7(a). As ⟨111⟩ is polar direction, complete poling results in a single domain state and piezoelectric strain behavior is expected to be hysteresis free for ⟨111⟩ poled PZN crystals. However, as shown in Fig. 7(a) significant hysteresis together with abnormally high strain values (0.1% at 10 kV/cm) indicates domain reorientation under bias, as discussed in Sec. II A. Domain motion along with increased strain must include 109° or 71° domain reorientation, starting at $E\sim 2$ kV/cm in this case [Fig. 7(a)], followed by strain saturation. It should be noted that remnant strain values of $\sim$0.04% after E field is removed and, original sample dimension recovered its zero strain point a few seconds after E field is removed, as presented in Fig. 7(a). This behavior obviously reflects domain motion, including depoling as well as reorientation. As in case of "soft" ce-

TABLE I. Dielectric and piezoelectric properties as a function of crystallographic orientation for rhombohedral $Pb(Zn_{1/3}Nb_{2/3})O_3$(PZN) and $Pb(Zn_{1/3}Nb_{2/3})O_3$-8% $PbTiO_3$(PZN-8%PT).

Crystal orientation	Composition	Mode	Coupling	S_{33}^E (10^{-12} m²/N)	Dielectric constant	Loss	d_{33} (pC/N)
111	PZN	k_{33}	0.38	7.4	900	0.012	83
	PZN-8%PT	k_{33}	0.39	7.4	1000	0.012	84
001	PZN	k_{33}	0.85	48	3600	0.008	1100
	PZN-8%PT	k_{33}	0.94	130	5000	0.010	2500

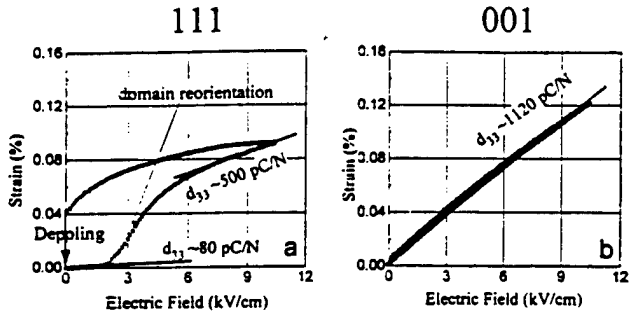

FIG. 7. Strain vs E-field (unipolar) curves for PZN crystals oriented along ⟨111⟩ (a) and ⟨001⟩ (b).

ramics, this domain motion is the origin of abnormally high strain values and hysteresis. Piezoelectric coefficient (d_{33}) values ~80 pC/N determined by low-field resonance technique could be explained by the slope of strain versus E field at low field region, as given in Fig. 7(a). Various d_{33}'s calculated by the slope of strain versus E field are given, too. Therefore, the inferior piezoelectric properties of ⟨111⟩ oriented rhombohedral crystals detected by the low-field resonance method are strongly related to domain instability. Complete domain orientation and single domain configuration under bias may cause elastic energy in crystals to increase, however, resulting in depoling after removing E field.

In contrast, the domain configuration of ⟨001⟩ oriented rhombohedral crystals was found to be stable. Polarization and strain versus E-field (bipolar) curves of ⟨001⟩ oriented PZN crystals are presented in Figs. 6(c) and 6(d), respectively. Domain switching by bipolar field abruptly occurs at E_c (~3 kV/cm), similar behavior found with single domain ferroelectric crystals. Schematics of domain configurations for ⟨001⟩ poled rhombohedral crystals are shown in Fig. 8. Since ⟨111⟩ is the polar direction, ⟨001⟩ poled crystals must have the configuration that each domain has one of four possible polar directions - ⟨111⟩, ⟨-111⟩, ⟨1-11⟩, and ⟨-1-11⟩. Remnant polarization (P_r~25 μC/cm^2) of ⟨001⟩ oriented rhombohedral PZN crystal must be $1/\sqrt{3}$ of ⟨111⟩ oriented crystal's according to Fig. 8, which explains ~25 μC/cm^2 for $P_{r,\langle 001\rangle}$ out of $P_{r,\langle 111\rangle}$~43 μC/cm^2. Therefore, abrupt domain switching at E_c (~3 kV/cm) is expected to be 71° domain switching, as shown in Fig. 8. In Fig. 7(b), ⟨001⟩ poled PZN crystals exhibit almost hysteresis-free strain behavior, a consequence of engineered-domain stability. From the slope of strain versus E-field curve revealed a d_{33} value

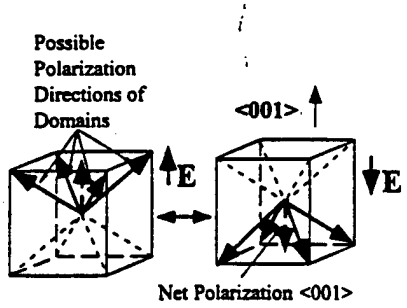

FIG. 8. Schematics of engineered domain configuration for ⟨001⟩ poled rhombohedral crystals.

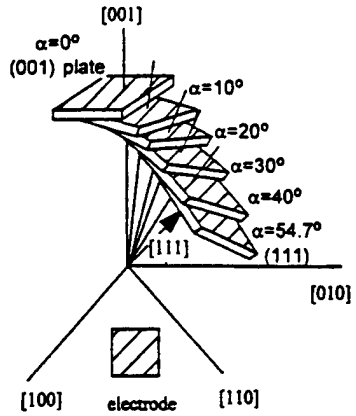

FIG. 9. Schematic diagram of sample preparation for investigating optimum crystallographic orientation.

of ~1100 pC/N, as determined by low-field resonance technique. This behavior for ⟨001⟩ oriented rhombohedral crystals will be discussed in Sec. IV C.

The observed domain (in)stability as a function of crystallographic orientation holds for all rhombohedral crystals of PZN-PT and PMN-PT. Owing to low hysteresis as well as ultrahigh piezoelectric coefficient (d_{33}), ⟨001⟩ oriented rhombohedral crystals may be attractive candidates for actuators. Although domain (in)stability is clearly a function of crystallographic orientation, *in situ* domain observation using optical microscopy is necessary and will be reported elsewhere.[18]

C. Optimum crystallographic orientation

As discussed in Sec. II B, optimum crystallographic cuts was one of the merits uniquely utilized with single crystals. For conventional piezoelectric single crystals, however, an "optimum cut" was determined from a single domain crystal, whereas engineered multidomain state is being utilized in this study. The term "optimum orientation" includes crystallographic direction not only for poling but for actuator driving to obtain hysteresis (strain) values as low (high) as possible, respectively.

Although it was determined that ⟨001⟩ is superior to ⟨111⟩, multidomain rhombohedral crystals may allow other crystallographic directions as optimum for higher strain values with comparably low hysteresis. To investigate this possibility, piezoelectric samples oriented along ⟨001⟩ + α were made, where α is the degree of deviation from ⟨001⟩ toward ⟨111⟩, as shown in Fig. 9, using PZN-4.5% PT crystal. In Fig. 10 remnant polarization (P_r) approaches the $P_{r\langle 111\rangle}$ value (~43 μC/cm^2) as orientation (α) approaches ⟨111⟩ (54.7°), respectively. The E_c value also increases with increased α. Figure 11 presents unipolar strain behavior as a function of α for ⟨001⟩ poled PZN-4.5% PT crystals. At low field, strain values do not vary significantly as a function of α, attributed to strain induced by domain reorientation when $\alpha \neq 0$. For example, the strain value of a sample ($\alpha = 10°$) is higher than that for a ⟨001⟩ oriented sample ($\alpha = 0°$). This increased domain motion with increased α is presented in

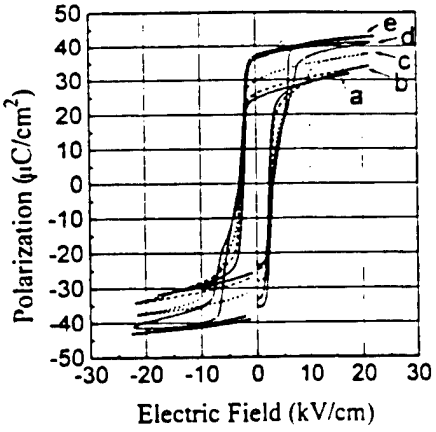

FIG. 10. Ferroelectric hysteresis for PZN-4.5%PT crystals oriented along ⟨001⟩+α, where α is the degree of deviation from ⟨001⟩ toward ⟨111⟩. (a) α=0°, (b) α=10°, (c) α=20°, (d) α=30°, (e) α=40°.

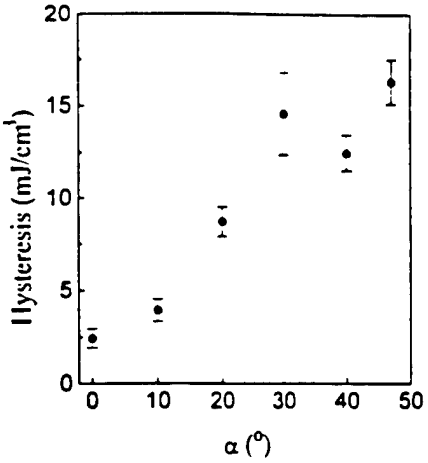

FIG. 12. Hysteresis as a function of α, where α is the degree of deviation from ⟨001⟩ toward ⟨111⟩. Hysteresis values are calculated from the area of unipolar polarization curve when maximum E field is 20 kV/cm.

Fig. 12, with hysteresis versus α calculated from the area of polarization versus unipolar E-field curves (20 kV/cm). The amount of hysteresis can be translated into degree of depoling, because more depoling consequently involves more domain reorientation, resulting in increased hysteresis. Therefore, domain becomes more unstable with the increased α. From these observations, the closer to ⟨001⟩ the rhombohedral crystal orientation is, the more stable the domain configuration and the higher the strain value are achieved. Therefore the optimum crystallographic orientation is ⟨001⟩.

High-field strain behavior is shown in Fig. 13 for ⟨001⟩ oriented PZN–4.5%PT crystals. Strain saturation becomes more significant as α increases (orientation approaches ⟨111⟩). At high fields, strain level decreases with increased α, the result of polarization saturation and subsequent strain saturation. However crystals oriented close to ⟨001⟩ (α <20°) exhibit no saturation, and furthermore, an apparent jump in strain to values over 1%. The question arises, does this strain-jump originated from domain reorientation? This question is addressed in Sec. IVD.

D. Strain versus *E*-field behaviors for ⟨001⟩ oriented rhombohedral crystals

Strain as a function of electric field for various ⟨001⟩ oriented rhombohedral crystals (pure PZN, PZN-4.5%PT, PZN-8%PT, and PMN-24%PT) are presented in Fig. 14. Also, E-field induced strains of various electromechanical ceramics such as soft PZT (PZT-5H), hard PZT (PZT-8) and electrostrictive ceramics (PMN-PT) are compared. Piezoelectric coefficients (d_{33}) directly calculated from the slope of strain versus electric field curves confirmed the piezoelectric coefficients determined by the low-field resonance method. Strains as high as 0.6% were observed with low hysteresis for these crystals, significantly larger than that for polycrystalline ceramics. The limitation of achievable strain for polycrystalline ceramics is the result of low piezoelectric coefficient, polarization saturation, and subsequent saturation on strain and breakdown strength.

Figure 15 schematically presents engineered domain states and their piezoelectric response under bias for rhombohedral crystals oriented and poled along ⟨001⟩. When ac-

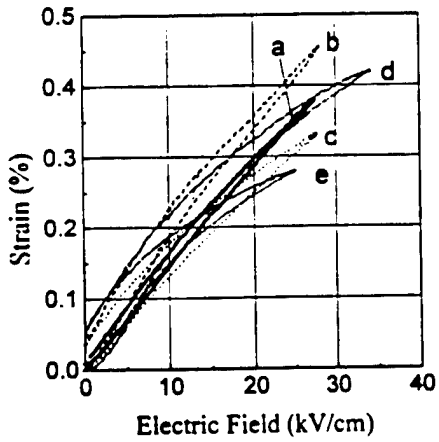

FIG. 11. Strain vs E-field (unipolar) PZN–4.5%PT crystals oriented along ⟨001⟩+α, where α is the degree of deviation from ⟨001⟩ toward ⟨111⟩. (a) α=0°, (b) α=10°, (c) α=20°, (d) α=30°, (e) α=40°.

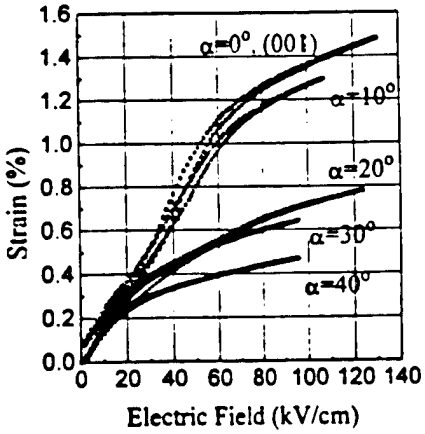

FIG. 13. Strain vs E-field (unipolar) PZN–4.5%PT crystals oriented along ⟨001⟩+α, where α is the degree of deviation from ⟨001⟩ toward ⟨111⟩. Maximum field is limited either by dielectric breakdown or by voltage limit of the apparatus.

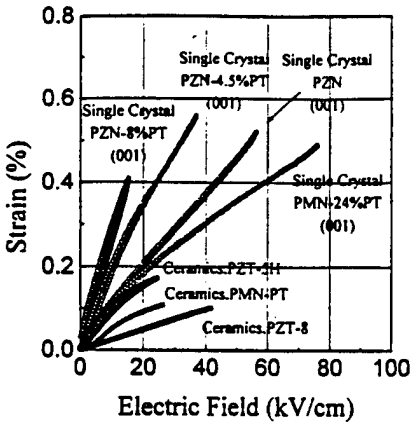

FIG. 14. Strain vs E-field behavior for ⟨001⟩ oriented rhombohedral crystals of PZN-PT and PMN-PT and for various electromechanical ceramics.

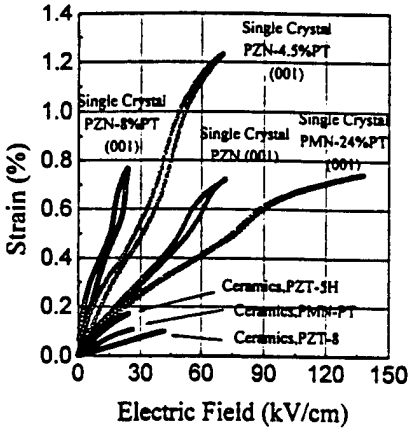

FIG. 16. Strain vs E-field behavior for ⟨001⟩ oriented rhombohedral crystals of PZN-PT and PMN-PT and for various electromechanical ceramics. Maximum field was limited either by dielectric breakdown or by voltage limit of the apparatus.

tuation is induced by an E field along ⟨001⟩, the polar direction is expected to incline close to the E-field direction in each domain (step A in Fig. 15), possibly resulting in increased rhombohedral lattice distortion. Domain reorientation is not necessary during this step because neighboring domains must involve equal amount of induced distortion, nullifying all strains in individual domains, the reason of stable domain configuration and, therefore, the origin of hysteresis-free or low-hysteresis strain behavior for ⟨001⟩ oriented rhombohedral crystals.

Strain saturation for ⟨001⟩ oriented rhombohedral crystals was investigated until dielectric breakdown, as presented in Fig. 16. Far from saturation, the strain abruptly increased with strain levels as high as 0.8% being achieved for all crystals tested. Strain levels $>1.2\%$ for the PZN-4.5%PT crystal were the result of higher breakdown voltage (compared with Fig. 13). The observed strain behavior is believed to be associated with an E-field induced rhombohedral–tetragonal phase transition. Polarization inclination towards ⟨001⟩ finally result in collapse of all polarizations into the ⟨001⟩ direction, step B in Fig. 15. This E-field induced phase transition is more apparent in Fig. 17, presenting the E-field induced strain behavior of the ⟨001⟩ oriented PZN-8%PT crystal. At ~ 120 kV/cm, the induced strain along with high dielectric breakdown strength resulted in a strain levels as high as 1.7%. The piezoelectric coefficient (d_{33}) ~ 480 pC/N calculated directly from the slope of strain versus E field in the high field region (between 40 and 120 kV/cm in Fig. 17) corresponded to values determined for tetragonal phase with a d_{33} value (~ 500 pC/N, in Fig. 5). Individual steps of piezoelectricity (step A) and phase transition (step B) shown in Fig. 15 are given in Fig. 17. Although phase transition is a likely explanation for the ultrahigh strain level, direct observation of phase transition using *in situ* XRD is required.

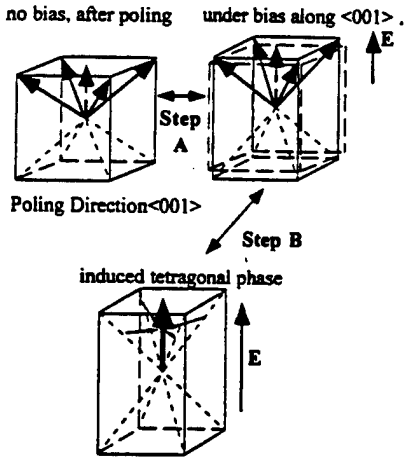

FIG. 15. Schematic diagram of domain configurations in ⟨001⟩ oriented rhombohedral crystals under bias (step A-piezoelectricity, step B-induced phase transition).

V. CONCLUSION

Pseudocubic ⟨001⟩ oriented relaxor based rhombohedral crystals such as $(1-x)$PZN-xPT ($x<0.09$) and $(1-x)$PMN-xPT ($x<0.35$) exhibited actuation levels not available with current piezoelectric ceramics. Ultrahigh piezoelectric coefficients (d_{33})$>\sim 2500$ pC/N and strain levels up to 0.6% with low hysteresis were observed. Optimum crystallographic orientation was found to be pseudocubic ⟨001⟩ for rhombohedral crystals, exhibiting high-strain and

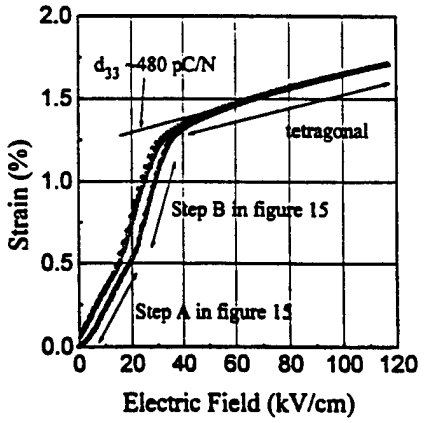

FIG. 17. Strain vs E-field behavior for ⟨001⟩ oriented PZN-8%PT crystal. Maximum field is limited by voltage limit of the apparatus.

low-hysteresis behavior. Domain instability could explain the composition independently inferior piezoelectric properties for ⟨111⟩ oriented rhombohedral crystals. Ultrahigh strain levels up to 1.7% could be achieved for ⟨001⟩ oriented rhombohedral single crystals as a result of E-field induced rhombohedral–tetragonal phase transition. Other relaxor based rhombohedral crystals are expected to exhibit similar strain versus E-field behavior. (⟨001⟩ textured polycrystalline thin films and bulk ceramics are also expected to exhibit high strain behaviors.) Although clearly promising candidates for high performance actuators, further investigation into crystal growth and prestress testing are required for single crystal piezoelectrics to become the next generation material of actuators.

ACKNOWLEDGMENTS

This research has been supported by the Office of Naval Research and Whitaker Center for Ultrasonic Imaging. The authors would like to thank L. E. Cross and C. Randall for their helpful suggestions, and Wesley Hackenberger, Patrick D. Lopath, Michael J. Zipparo for their help with the property measurements, and Shi-Fang Liu and Hua Lei for their help with crystal growing and sample preparation, respectively.

[1] V. Giurgiutiu, Z. Chaudhry, and C. A. Rogers, "Energy-based Comparison of Solid-State Actuators," Report No. CIMSS 95-101, Virginia Polytechnic Institute and State University, September 1995.
[2] L. E. Cross, Ferroelectrics **76**, 241 (1987).
[3] S.-E. Park and T. R. Shrout, IEEE Trans. Ultras., Ferroelectric and Freq. Cont. Special Issue on Ultrasonic Transducers, (1997, in press).
[4] H. Jaffe and D. A. Berlincourt, "*Piezoelectric Transducer Materials*," *Proceedings of IEEE*, (IEEE, Bellingham, WA, 1965), Vol. **53**, pp. 1372–1386.
[5] S. Fushimi and T. Ikeda, J. Am. Ceram. Soc. **50**, 129 (1967).
[6] V. A. Kuznetzov, J. Cryst. Growth **34**, 405 (1968).
[7] R. Clarke and R. W. Whatmore, J. Cryst. Growth **33**, 29 (1976).
[8] T. Hatanaka and H. Hasegawa, Jpn. J. Appl. Phys. 1 **34**, 5446 (1995).
[9] K. Yanagisawa, H. Kanai, and Y. Yamashita, Jpn. J. Appl. Phys. 1 **34**, 536 (1995).
[10] J. Kuwata, K. Uchino, and S. Nomura, Ferroelectrics **37**, 579 (1981).
[11] J. Kuwata, K. Uchino, and S. Nomura, Jpn. J. Appl. Phys. **21**, 1298 (1982).
[12] T. R. Shrout, Z. P. Chang, N. Kim, and S. Markgraf, Ferroelectr. Lett. Sect. **12**, 63 (1990).
[13] M. L. Mulvihill, S.-E. Park, G. Risch, Z. Li, K. Uchino, and T. R. Shrout, Jpn. J. Appl. Phys. 1 **35**, 51 (1996).
[14] S.-E. Park, M. L. Mulvihill, G. Risch, and T. R. Shrout, Jpn. J. Appl. Phys. 1 **36**, 1154 (1997).
[15] *IEEE Standard on Piezoelectricity* (American National Standards Institute, Washington, DC, 1976).
[16] T. R. Shrout and J. Fielding Jr., "Relaxor Ferroelectric Materials," in *Proceedings of the 1990 IEEE Ultrasonics Symposium*, (1990), pp. 711–715.
[17] C. A. Randall, A. S. Bhalla, T. R. Shrout, and L. E. Cross, J. Mater. Res. **5**, 829 (1990).
[18] S. Wada, S.-E. Park, L. E. Cross, and T. R. Shrout, presented at 9th International Meeting on Ferroelectricity, Seoul, Korea, 24–27 August, 1997.
[19] Y. Yamashita, Jpn. J. Appl. Phys. 1 **33**, 5323 (1994).

APPENDIX 23

Characteristics of Relaxor-Based Piezoelectric Single Crystals for Ultrasonic Transducers

Seung-Eek Park and Thomas R. Shrout

Abstract—For ultrasonic transducers, piezoelectric ceramics offer a range of dielectric constants ($K \sim$ 1000–5000), large piezoelectric coefficients ($d_{ij} \sim$ 200–700 pC/N), and high electromechanical coupling ($k_T \cong$ 50%, $k_{33} \cong$ 75%). For several decades, the material of choice has been polycrystalline ceramics based on the solid solution $Pb(Zr_{1-x},Ti_x)O_3$ (PZT), compositionally engineered near the morphotropic phase boundary (MPB). The search for alternative MPB systems has led researchers to revisit relaxor-based materials with the general formula, $Pb(B_1,B_2)O_3$ (B_1:Zn^{2+}, Mg^{2+}, Sc^{3+}, Ni^{2+}..., B_2:Nb^{5+}, Ta^{5+}...). There are some claims of superior dielectric and piezoelectric performance compared to that of PZT materials. However, when the properties are examined relative to transition temperature (T_c), these differences are not significant. In the single crystal form, however, Relaxor-PT materials, represented by $Pb(Zn_{1/3}Nb_{2/3})O_3$—$PbTiO_3$ (PZN-PT), $Pb(Mg_{1/3}Nb_{2/3})O_3$—$PbTiO_3$ (PMN-PT) have been found to exhibit longitudinal coupling coefficients (k_{33}) > 90%, thickness coupling (k_T) > 63%, dielectric constants ranging from 1000 to 5000 with low dielectric loss < 1%, and exceptional piezoelectric coefficients d_{33} > 2000 pC/N, the later promising for high energy density actuators. For single crystal piezoelectrics to become the next generation material of ultrasonic transducers, further investigation in crystal growth, device fabrication and testing are required.

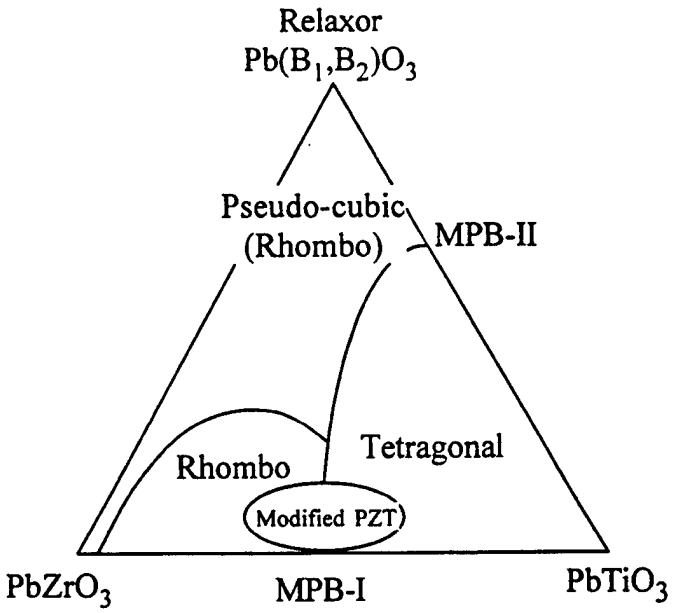

Fig. 1. Ternary diagram depicting MPBs in PZT and Relaxor-PT systems for piezoelectric ceramics [27].

I. Introduction

Innovations in transducer design continues to be the driving force for the development of new piezoelectric materials. Electromechanical coupling (k_{ij}), dielectric constant (K) and acoustic impedance (Z) are the most important parameters which determine the performance of an ultrasonic imaging system. Material characteristics associated with the design of imaging devices have been reviewed by Gururaja [1] and Smith [2]. Piezoelectric ceramics are currently the material of choice offering relatively high coupling, a wide range of dielectric constants, and low dielectric loss. These merits translate into transducer performance in the form of relatively high sensitivity, broad bandwidth, and minimal thermal heating. Two approaches have been taken to couple acoustic energy from high acoustic impedance (Z = 30 to 36 MRayls) piezoelectric ceramics to the human body (Z = 1.5 MRayls); multiple quarter wavelength matching layers and/or lower impedance composite comprised of piezoelectric ceramic with a passive polymer. Although the properties can be tailored to meet various device requirements, it is the volume ratio of the piezoelectric ceramic and its inherent properties that are critical to transducer performance.

$Pb(Zr_{1-x},Ti_x)O_3$ (PZT) ceramics have been the mainstay for high performance transducer applications. Compositionally, PZT ceramics lie near the morphotropic phase boundary (MPB) between the tetragonal and rhombohedral phases, as depicted in Fig. 1. MPB compositions have anomalously high dielectric and piezoelectric properties as a result of enhanced polarizability arising from the coupling between two equivalent energy states, i.e., the tetragonal and rhombohedral phases, allowing optimum domain reorientation during the poling process. Further modifications using acceptor and donor dopants give us the wide range of piezoelectric compositions we have today. An excellent review on piezoelectric ceramics, including both modified and undoped PZT ceramics, is given by Jaffe *et al.* [3], published in 1971.

Manuscript received July 9, 1996; accepted January 13, 1997. This research has been supported by Office of Naval Research and Whitaker Center for Ultrasonic Imaging.

The authors are with the Whitaker Center for Ultrasonic Imaging, The Pennsylvania State University, University Park, PA 16802 (e-mail: sxp37@psu.edu).

II. Relaxor-Based Piezoelectrics

The search for alternative MPB systems other than that found in PZT have led researchers to investigate relaxor-

based ferroelectrics and their solid solution with $PbTiO_3$ (PT). Lead-based relaxor materials, discovered by Soviet researchers [4], [5] in the 1950s, are complex perovskites with the general formula $Pb(B_1B_2)O_3$, ($B_1 = Mg^{2+}, Zn^{2+}, Ni^{2+}, Sc^{3+} \ldots$, $B_2 = Nb^{5+}, Ta^{5+}, W^{6+} \ldots$). Characteristic of relaxors is a broad and frequency dispersive dielectric maxima [6]. These relaxor materials and their solid solutions with $PbTiO_3$ have been compiled by Landolt-Börnstein [7] with numerous MPB systems reported.

Early investigations of Relaxor-PT ceramics in the 60s and 70s were plagued with inadequate process controls, resulting in piezoelectric ceramics of marginal interest. With the advent of the columbite precursor method and an overall better understanding of perovskite-pyrochlore phase relationship and corresponding structure-property relationships, a renewed interest in the Relaxor-PT MPB systems came about. The wide range of Relaxor-PT MPB systems have been recently reviewed, including relevant dielectric and piezoelectric properties [8].

Several of the Relaxor-PT systems are summarized in Table I and schematically shown in the $PbZrO_3$-$PbTiO_3$-$Pb(B_1B_2)O_3$ ternary system in Fig. 1. In contrast to the PZT system, the amount of PT associated with Relaxor-PT MPB is in general less than that for PZT, varying from 7% for PFN-PT to 50 mole% for PYbN-PT. In PZT, the MPB is relatively insensitive to temperature. However, in Relaxor-PT systems, the MPB compositions are strongly temperature dependent.

In recent articles on Relaxor-PT compositions, including new MPB systems, e.g., PYbN-PT [8], modified PSN-PT [9], and materials processed using hot pressing [10], there are claims of compositions with superior dielectric and piezoelectric properties compared to that of PZT ceramics. As reported in Table II, these claims appear to be valid, with Relaxor-PT ceramics[1] offering relatively high dielectric constants (K), large piezoelectric coefficients (d_{ij}), and superior electromechanical coupling coefficients (k_{ij}). In the following section, however, it will be shown that such claims are misleading and must be analyzed with respect to the ferroelectric materials transition temperature. This temperature, designated by T_c, is the temperature at which the material transforms from the prototypical nonferroelectric to ferroelectric phase being associated with a spontaneous polarization and large dielectric anomaly. The importance of this transition temperature with respect to transducer fabrication, piezoelectric activity, etc., will also be discussed.

[1]The term "relaxor ferroelectric" is used herein to represent all complex perskovite $Pb(B_1B_2)O_3$ systems. In actuality, relaxor dielectric behavior only occurs for those systems which possess short range chemical ordering as classified by Randall *et al.* [24]. In general, however, classical relaxor behavior occurs within certain compositional limits for all $Pb(B_1B_2)O_3$-PT systems.

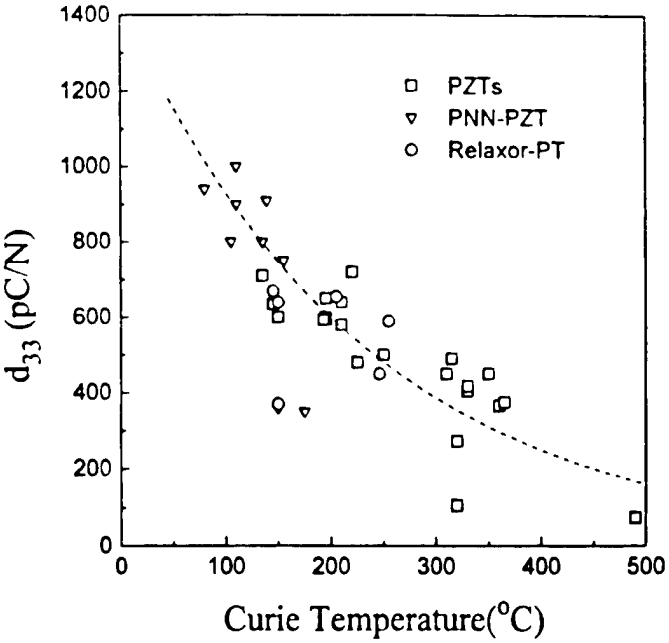

Fig. 2. Piezoelectric coefficient (d_{33}) as a function of transition temperature (T_c) for piezoelectric ceramics, including PZT, modified PZTs, and Relaxor-PT systems. Data were compiled from references, commercial brochures, and internal investigations.

III. Compositional Engineering of Piezoelectric Ceramics

Among the important material parameters mentioned previously, electromechanical coupling (k_{ij}), dielectric constant (K), and associated piezoelectric coefficient (d_{ij}) are the key parameters to be compositionally engineered. In general, the piezoelectric properties of a ferroelectric ceramic can be expressed using the simplistic term,

$$d_{ij} \sim 2Q_{ij}K\epsilon_o P_r \qquad (1)$$

where d_{ij} is the piezoelectric coefficient, P_r the remnant polarization on poling, K the dielectric constant, ϵ_o the permittivity of free space, and Q_{ij} the electrostriction coefficient. Since both Q_{ij} and P_r exhibit little dependence on composition or temperature below T_c in ferroelectric ceramics such as PZT, the piezoelectric coefficient d_{ij} and dielectric constant K are interrelated (i.e., a ceramic with high piezoelectric coefficient also exhibits a large dielectric constant). To achieve a high dielectric constant or piezoelectric coefficient, MPB-based ceramics are further engineered by compositionally adjusting the Curie temperature (T_c) downward relative to room temperature. The effect of transition temperature (T_c) on the dielectric and piezoelectric properties is clearly evident in Figs. 2 and 3. As shown, the room temperature values of both d_{ij} and K are plotted as a function of T_c for a variety of modified PZT ceramics, including Relaxor-PT systems, rather than a tabulation of properties, the methodology frequently available in company brochures, review articles, etc. To achieve both high dielectric constant and corresponding piezoelectrically "soft" materials generally used in ultrasonic imaging, requires materials with relatively low T_c.

TABLE I

MORPHOTROPIC PHASE BOUNDARIES IN PEROVSKITE $Pb(B_1B_2)O_3$-PT SYSTEMS.

Binary System	PT content on MPB	T_c (T_cs of end compounds)	Ref.
$(1-x)$ $Pb(Zn_{1/3}Nb_{2/3})O_3$ - x $PbTiO_3$ (PZN-PT)	$x \cong 0.09$	$\sim 180°C(140°C - 490°C)$	28
$(1-x)$ $Pb(Mg_{1/3}Nb_{2/3})O_3$ - x $PbTiO_3$ (PMN-PT)	$x \cong 0.33$	$\sim 150°C(-10°C - 490°C)$	29
$(1-x)$ $Pb(Mg_{1/3}Ta_{2/3})O_3$ - x $PbTiO_3$ (PMT-PT)	$x \cong 0.38$	$\sim 80°C(-98°C - 490°C)$	8
$(1-x)$ $Pb(Ni_{1/3}Nb_{2/3})O_3$ - x $PbTiO_3$ (PNN-PT)	$x \cong 0.40$	$\sim 170°C(-120°C - 490°C)$	30
$(1-x)$ $Pb(Co_{1/3}Nb_{2/3})O_3$ - x $PbTiO_3$ (PCoN-PT)	$x \cong 0.38$	$\sim 250°C(-98°C - 490°C)$	31
$(1-x)$ $Pb(Sc_{1/2}Ta_{1/2})O_3$ - x $PbTiO_3$ (PST-PT)	$x \cong 0.45$	$\sim 205°C(26°C - 490°C)$	32
$(1-x)$ $Pb(Sc_{1/2}Nb_{1/2})O_3$ - x $PbTiO_3$ (PSN-PT)	$x \cong 0.43$	$\sim 250°C(90°C - 490°C)$	33, 34
$(1-x)$ $Pb(Fe_{1/2}Nb_{1/2})O_3$ - x $PbTiO_3$ (PFN-PT)	$x \cong 0.07$	$\sim 140°C(110°C - 490°C)$	8
$(1-x)$ $Pb(Yb_{1/2}Nb_{1/2})O_3$ - x $PbTiO_3$ (PYbN-PT)	$x \cong 0.50$	$\sim 360°C(280°C - 490°C)$	8
$(1-x)$ $Pb(In_{1/2}Nb_{1/2})O_3$ - x $PbTiO_3$ (PIN-PT)	$x \cong 0.37$	$\sim 320°C(90°C - 490°C)$	35
$(1-x)$ $Pb(Mg_{1/2}W_{1/2})O_3$ - x $PbTiO_3$ (PMW-PT)	$x \cong 0.55$	$\sim 60°C(39°C - 490°C)$	36
$(1-x)$ $Pb(Co_{1/2}W_{1/2})O_3$ - x $PbTiO_3$ (PCoW-PT)	$x \cong 0.45$	$\sim 310°C(32°C - 490°C)$	37
$(1-x)$ $PbZrO_3$ - x $PbTiO_3$ (PZT)	$x \cong 0.48$	$\sim 360°C(230°C - 490°C)$	3

TABLE II

REPORTED DIELECTRIC AND PIEZOELECTRIC PROPERTIES FOR SELECTED PZT AND RELAXOR BINARY SYSTEMS.

Form	Materials	k_P	k_t*	k_{33}	d_{33} (pC/N)	K_3^T	T_c (°C)	Ref.
	PZT-MPB Composition							
Ceramics (poly-crystalline)	PZT 53/47	0.52		0.67	220	~ 800	360	38
	Modified PZTs							
	PZT-4 (Navy I)	0.58	0.51	0.70	289	1200	330	39
	PZT-8 (Navy III)	0.50	0.44	0.70	220	1000	300	39
	PZT-5 (Navy II)	0.60	0.49	0.70	400	2000	360	39
	PZT 5H (Navy VI)	0.65	0.50	0.75	590	3500	190	39
	Relaxor-PT MPB Compositions							
	0.7PMN-0.3PT	0.50			670	5000	145	29
	0.67PMN-0.33PT	0.63		0.73	690	5000	160	29
	0.60PMN-0.40PZT(40/60)	0.50			—	2370	170	40
	0.55PST-0.45PT	0.61		0.73	655	4000	205	32
	0.575PSN-0.425PT	0.66	0.55	0.74	389	1550	260	9
	0.575PSN-0.425PT (1%Nb doped)	0.69	0.52	0.76	504	2540	248	9
	0.575PSN-0.425PT (2% Sc doped)	0.63	0.53	0.72	359	1480	260	9
	0.58PSN-0.42PT	0.71	0.56	0.77	450	2200	260	41
	0.5PNN-0.5PZT(35/65)	0.45	—		370		150	42
	0.87PZN-0.05BT-0.08PT	0.52	0.49		640	5200	150	43
Single Crystals	95PZN-5PT			0.86	~ 1500	4000	160	†
	91PZN-9PT			0.92	~ 1500	2200	190	18, 19
	89PZN-11PT			0.92	620	1000	200	†
	70PMN-30PT				~ 1500	4000	150	20
	60PMN-40PT				~ 1500		170	20

* Reported coupling factors often do not follow the simplistic equation, $k_{33}^2 \sim k_p^2 + k_T^2 - k_p^2 * k_T^2$. Based on the difficulties in accurately determining k_T, the confirmation of values should be made.

† T. R. Shrout, unpublished information.

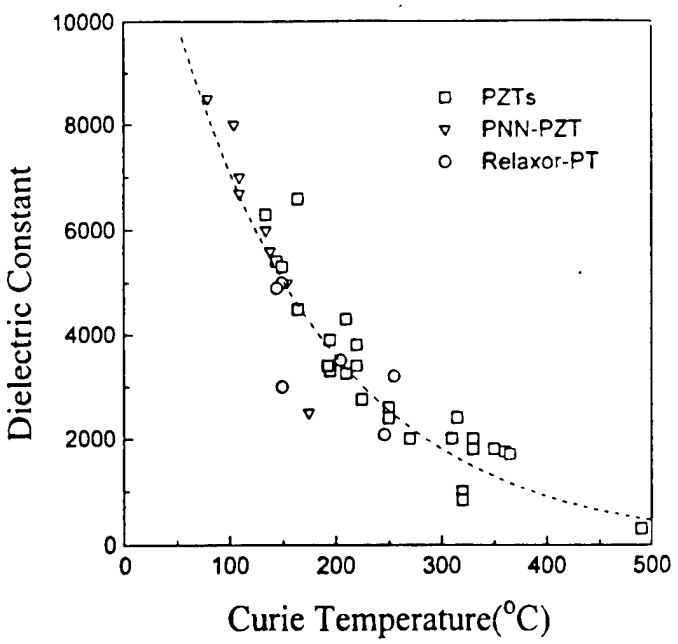

Fig. 3. Dielectric constant (K) as a function of transition temperature (T_c) for piezoelectric ceramics, including PZT, modified PZTs, and Relaxor-PT systems. Data were compiled from references, commercial brochures, and internal investigations.

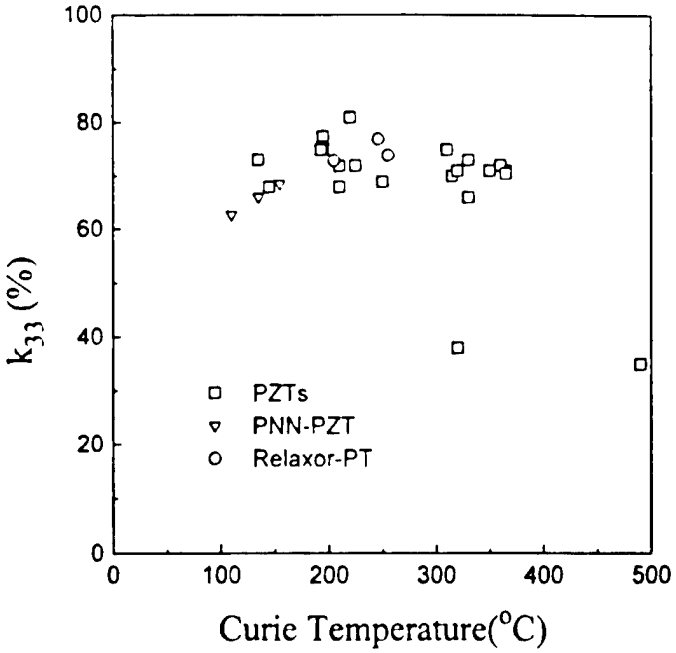

Fig. 4 Longitudinal coupling coefficient (k_{33}) as a function of transition temperature (T_c) for piezoelectric ceramics, including PZT, modified PZTs, and Relaxor-PT systems. Data were compiled from references, commercial brochures, and internal investigations.

However, high piezoelectric coefficients and dielectric constants with correspondingly low T_cs come with the expense of more temperature dependent properties and less polarization stability (i.e., aging and loss of piezoelectric activity). As a general rule of thumb, piezoelectric materials can be safely used to approximately $1/2\ T_c$, without significant reduction in piezoelectric activity. This can restrict the working range of the device or limit fabrication techniques. During the fabrication process of transducers, the piezoelectric material may experience excessive temperature due to cutting/dicing, polymer curing, or the attachment of acoustic matching/backing materials. Therefore, not only must the dielectric and piezoelectric properties of a transducer material be considered, but also their T_c.

Electromechanical coupling factor (k_{ij}) is often referred to as the key material parameter for transducer design because it measures the true strength of the piezoelectric interaction once the elastic and dielectric response of the medium are normalized [11], [12]. In addition, high coupling factor corresponds to a broad bandwidth response, which offers better axial resolution, deeper penetration, and, most importantly, a degree of engineering freedom with the potential of operating the transducer at a narrow frequency regime for enhanced sensitivity.

Electromechanical coupling factor, piezoelectric coefficient, and dielectric constant are interrelated by the following equation:

$$k_{ij}^2 = \frac{d_{ij}^2}{K\varepsilon_0 s_{ij}} \tag{2}$$

where d_{ij} is the piezoelectric coefficient, K is the dielectric constant, ε_0 is the permittivity of free space, and s_{ij} is the elastic compliance. The question arises, since both d_{ij} and K are strongly dependent on T_c, what is the dependence of coupling k_{ij}? Fig. 4 presents room temperature values of k_{33} (longitudinal coupling) as a function of T_c. Important for high frequency ultrasound back-scattered microscopy (UBM) and single element transducers, k_T (thickness) coupling values are given in Fig. 5. As observed for both coupling coefficients, no relationship with T_c was evident. It is noted that the most widely used material in the ultrasonic imaging industry has a $T_c \sim 210$°C owing to the materials relatively high dielectric constant and coupling coefficient while providing good temperature stability.

In summarizing the observations presented above, the dielectric and piezoelectric properties of piezoelectric ceramics are strongly related to the transition temperature T_c. Upon direct comparison, no one type of material, whether PZT-based or Relaxor-PT, offer significant advantages in overall transducer performance. The question arises, are there opportunities for new piezoelectric materials with enhanced properties? To answer this question, one must look to the single crystal form of piezoelectric materials, the topic of the following section.

IV. Single Crystal Piezoelectric Materials

Single crystal piezoelectrics such as quartz (SiO_2), lithium niobate ($LiNbO_3$), and the analogue lithium tantalate ($LiTaO_3$) are widely employed in specific applications that include oscillators, surface acoustic wave (SAW) devices, and in optics. In contrast to PZT ceramics, these single crystals offer inferior dielectric and piezoelectric prop-

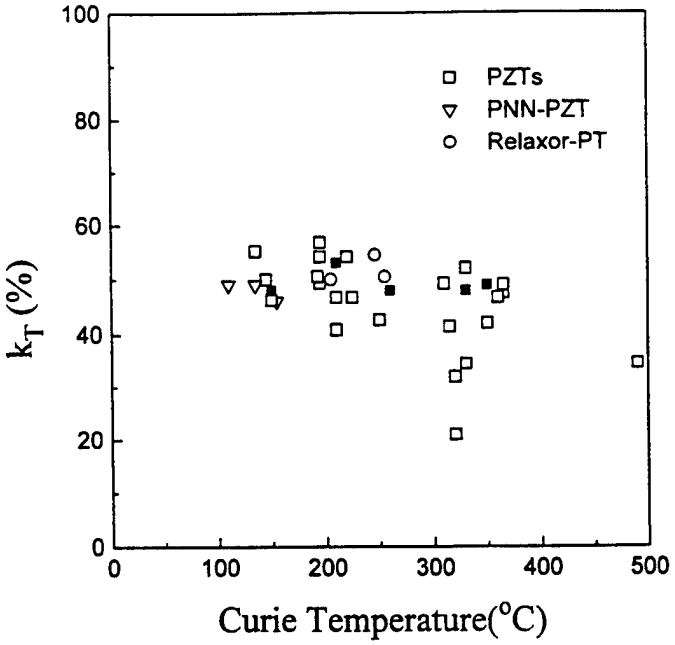

Fig. 5. Thickness coupling coefficient (k_T) as a function of transition temperature (T_c) for piezoelectric ceramics, including PZT, modified PZTs, and Relaxor-PT systems. Data were compiled from references, commercial brochures, and internal investigations.

erties. The single crystal form of high performance PZTs has been the research interest for many materials scientists. Attempts to grow single crystals of PZTs have been made by numerous researchers, resulting in crystallites too small to allow adequate property measurements [13]–[17]. Though Relaxor-PT ceramics were not shown to offer enhanced dielectric and piezoelectric properties comparable to PZT ceramics of similar T_cs, they can be readily grown in single crystal form. This key distinction was realized by Kuwata *et al.* [18], [19] for the PZN and PZN-PT systems. Following this work, single crystal growth of PMN-PT [20] and PSN-PT [21], etc., followed. In general, most $Pb(B_1,B_2)O_3$-PT crystals can be grown by high temperature solution growth using Pb-based fluxes.

Dielectric and piezoelectric properties for several $Pb(B_1B_2)O_3$-PT crystals are reported and compared to their polycrystalline counterparts in Table II. As presented, piezoelectric coefficients and coupling coefficients are significantly higher, with d_{33} and k_{33} values greater than 1500 pC/N and 90%, respectively, found for MPB compositions in both the PZN-PT ($x - 0.09$) and PMN-PT ($x = 0.35$) systems. Though the Curie temperature (T_c) of these materials are relatively low < 200°C, the significance of these values becomes evident by directly comparing their values in relation to T_c in Figs. 2–5.

Although ultra high coupling and piezoelectric properties of the PZN-PT system, first reported in 1981 and later in the PMN-PT system (1989), have been known for several years; their potential for high performance bio-medical ultrasound transducer and related devices has only been recognized recently. Serious efforts on the development of $Pb(B_1B_2)O_3$-PT crystals for high performance transducers includes investigations at Toshiba Co. and at the Pennsylvania State University.

Merits of the single crystal form itself include the possibility of "optimum" crystallographic cuts as analogous in AT and BT cuts in quartz crystals for a zero temperature coefficient of resonance, and X-cut in $LiTaO_3$ or 128° rotated Y cut in $LiNbO_3$ crystals for optimum conditions including surface acoustic speed and coupling [22]. Another advantage of the single crystal form lies in terms of microstructural issues associated with polycrystalline ceramics, including grain size, porosity, etc. These also can be ignored removing scaling limitations, particularly relevant to high frequency transducers.

As stated above, the merits of using single crystals for high performance transducers is clearly evident, but few systematic studies have yet to be made. In the following section, preliminary results based on the author's ongoing investigation are presented.

V. Crystal Structural Property Relationships

Commonalties inherent to Relaxor-PT systems have been discussed in reviews by Shrout and Fielding [23] and Randall *et al.* [24]. Based on these commonalties, our research was limited to two representative systems of PZN-PT and PMN-PT. Though PMN-PT MPB crystals exhibit piezoelectric properties comparable with PZN-PT, more focus was given to the PZN system owing to its relatively lower PT content for MPB. This allows more uniform crystal growth of these solid solution materials. Details of crystal growth for these systems are given in [25] and [26]. Compositions investigated include the rhombohedral PZN end member, MPB compositions (PT $\cong$ 9%) and tetragonal phases (> 10% PT).

High quality crystals (maximum size $1 \times 1 \times 1$ cm) grown using PbO-based fluxes were characterized and samples prepared in accordance with IEEE standards. Fig. 6 shows an example of the sequence of sample preparation starting with an as-grown PZN-9.5%PT crystal.

Dielectric, piezoelectric, and electromechanical coupling coefficients for the various crystals are reported in Tables III and IV. Parameters relevant to transducer designs, including dielectric loss, frequency constant (N), elastic compliance (s_{ij}), mechanical Q, etc., are also reported.

As reported in Table III, large coupling coefficients (k_{33}) and large piezoelectric coefficients (d_{33}) were found for PZN-PT crystals with MPB compositions, as previously reported by Kuwata *et al.* [19]. Electromechanical coupling (k_{ij}) and piezoelectric coefficients (d_{ij}) equal to and larger than MPB crystal compositions were found for domain engineered rhombohedral crystals[2] as shown in Fig. 7. Both pure PZN and PZN-8% PT crystals were found to possess high k_{33} values of $\sim$ 85% and 94%, respectively, for (001)

[2]Rhombohedral crystals oriented and poled along pseudocubic ⟨001⟩ direction. Crystallographically, polarization direction of rhombohedral crystal is pseudocubic ⟨111⟩ direction.

TABLE III

DIELECTRIC AND PIEZOELECTRIC PROPERTIES OF $Pb(A_{1/3}Nb_{2/3})O_3$-$PbTiO_3$ CRYSTALS (A = Zn, Mg) FROM THIS WORK—LONGITUDINAL MODE

Crystal	Cut	Tmax (°C)	Dielectric Constant (Loss)	Coupling(k_{33})	s_{33}^D($\times 10^{-12}$ m^2/N)	d_{33}($\times 10^{-12}$ C/N)	Nt^* (Hz m)
PZN	111	~ 140	900 (0.012)	0.377	7.2	83	2058
	001		3600 (0.008)	0.852	13.2	1100	1521
PZN-	111	~ 165	2150 (0.012)	0.395	6.3	82	2205
8%PT	001		4200 (0.012)	0.938	15.5	2070	1401
PZN-	111	~ 176	4300 (0.007)	0.644	6.1	405 (600**)	2240
9.5%PT	001		1400 (0.004)	0.894	15.5	880 (1600**)	1403
PMN-30%PT	001	~ 150	2890 (0.014)	0.808	11.6	730	1608
PMN-35%PT	001	~ 160	3100 (0.014)	0.923	10.2	1240	1730

- The sample shape of longitudinal mode measurements was bar with $z > 5x$, $z > 5y$, where x, y are widths and z is length. Typically, z ranged from 3 mm to 5 mm.
- $k_{33} = \sqrt{(\pi/2 \cdot f_s/f_p \cdot \tan(\pi/2 \cdot (f_p - f_s)/f_p))}$, f_p and f_s are parallel resonance frequency and series resonance frequency, respectively.
- $d_{33} = k_{33}\sqrt{(\varepsilon_{33}^T s_{33}^E)}$, where ε_{33}^T is free permittivity, and $s_{33}^E = s_{33}^D/(1 - k_{33}^2)$.
* $N \cdot t = f_p \cdot z$, where f_p and z are parallel resonance frequency and length of the bar, respectively.
** values determined by Berlincourt d_{33} meter.

TABLE IV

DIELECTRIC AND PIEZOELECTRIC PROPERTIES OF $Pb(A_{1/3}Nb_{2/3})O_3$-$PbTiO_3$ CRYSTALS (A = Zn, Mg) FROM THIS WORK—THICKNESS MODE

Crystal	Cut	Coupling (k_T)	K_3^T	Loss	Qm	Nt^* (Hz m)
PZN	001	0.493	2732	0.013	40	2056
PZN- 8%PT	001	0.481	4450	0.017	39.5	1831
PZN- 9.5%PT	001	0.541	1553	0.024	31.3	1967
PZN-11%PT**	001	0.638	890	0.024	16.6	1576
PMN-30% PT	001	0.568	4739	0.014	43.7	2368
PMN-35%PT	001	0.541	4540	0.031	35.3	2305

- The sample shape of longitudinal mode measurements was bar with $x > 20z$, $y > 20z$, where x, y are widths and z is thickness. Typically, z ranged from 70 to 150 μm.
- $k_T = \sqrt{(\pi/2 \cdot f_s/f_p \cdot \tan(\pi/2 \cdot (f_p - f_s)/f_p))}$, f_p and f_s are parallel resonance frequency and series resonance frequency, respectively.
* $N \cdot t = f_p \cdot z$, where f_p and z are parallel resonance frequency and sample thickness, respectively.
** Sample size was 3.32 × 3.81 × 0.145 mm.

crystal cuts. Low values of dielectric loss < 1%, significantly less than their polycrystalline counterparts, should also be noted. The role of domains and their stability on the dielectric and piezoelectric properties of single crystals is the topic of further investigation, and further details are beyond the scope of this work.

As previously reported and given in Fig. 7, large values of k_{33} are also found in the tetragonal region (PT > 10%) and, as reported in Table IV, a value of 63% k_T was detected for the PZN-11% PT. High thickness coupling may be associated with the large anisotropy of the tetragonal crystals.

The dielectric constant was also found to be dependent on the crystal symmetry. Tetragonal crystals exhibited dielectric constants on the order of less than 1000 being significantly lower than rhombohedral crystals (3000 ~ 5000). Lower dielectric constants are also associated with both increased anisotropy and T_c. With similar coupling coefficients, the range of dielectric constants found in the PZN-PT system offer the flexibility in designing transducers with equivalent electrical impedance for a wide range of frequency and geometry.

VI. SUMMARY

The single crystal form of Relaxor-PT materials offers the possibility of dramatic improvements in transducer performance. Electromechanical coupling coefficients greater than 90% with non-MPB compositions as well as MPB compositions enable degree of freedom in designing transducers with broad bandwidth and/or improved sensitivity. A range of dielectric constants from

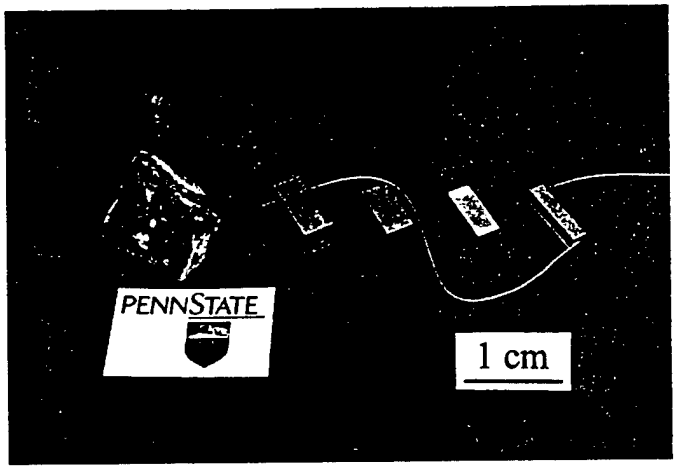

Fig. 6. Sequence of sample preparation based on IEEE standards (PZN-9.5%PT (001) cuts). From left, as grown crystal, oriented sample using Laue back reflection camera, cut and polished sample, lateral mode sample, and longitudinal mode sample (electroded gold sputtering).

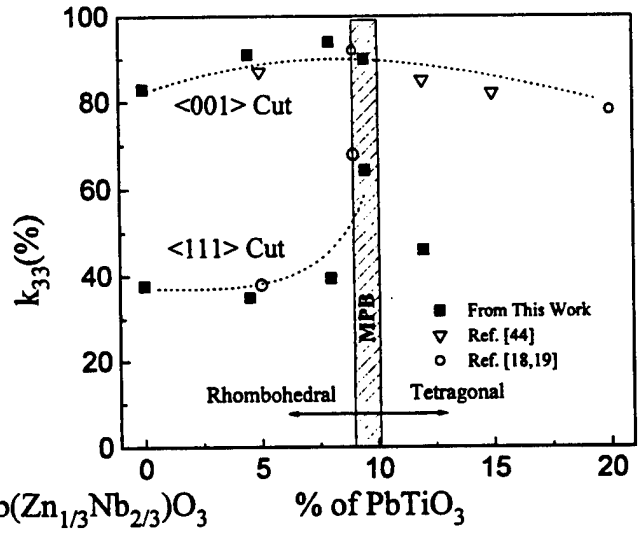

Fig. 7. k_{33} as a function of composition and orientation in crystals of PZN-PT.

$\sim$ 1000 to 5000 in the PZN-PT system offers designers dielectrics for optimum electrical impedance matching. Ultrahigh piezoelectric strain coefficient $d_{33} > 2000$ pC/N clearly warrants further investigations in relation to high energy density actuators. Microstructurally, single crystal transducers are not limited by grain size or porosity, offering high performance at very high frequencies.

Though clearly promising, the commercialization and growth of single crystals must be demonstrated; and anticipated difficulties in fabrication and processing such as dicing, attaching matching layers, etc., must be overcome if single crystal piezoelectrics are to become piezoelectric materials for the next generation of ultrasound transducers.

ACKNOWLEDGMENT

The authors would like to thank Patric D. Lapath and Michael J. Zipparo for their help with the property measurements, and Hua Lei for her help with the preparation of samples.

REFERENCES

[1] T. R. Gururaja, "Piezoelectrics for medical ultrasonic imaging," *Amer. Ceram. Soc. Bull.*, vol. 73, pp. 50–55, May 1994.

[2] W. A. Smith, "New opportunities in ultrasonic transducers emerging from innovations in piezoelectric materials," *Proc. SPIE Int. Symp.*, July 21–22, 1992.

[3] B. Jaffe, W. R. Cook, Jr., and H. Jaffe, *Piezoelectric Ceramics*, New York: Academic, 1971.

[4] G. A. Smolenskii, V. A. Isupov, A. I. Agranovskaya, and N. N. Kainik, "New ferroelectrics of complex composition, IV," *Sov. Phys.—Solid State*, vol. 2, pp. 2651–2654, May 1961.

[5] G. A. Smolenskii, V. A. Isupov, A. I. Agranovskaya, and S. B. Popov, "Ferroelectrics with diffuse phase transitions," *Sov. Phys.—Solid State*, vol. 2, pp. 2584–2594, May 1961.

[6] L. E. Cross, "Relaxor ferroelectrics," *Ferroelectrics*, vol. 76, pp. 241–267, 1987.

[7] Landolt-Börnstein, *Ferroelectric and Antiferro-electric Substances*, vol. 19, Group III. Berlin: Springer Verlag, 1981.

[8] Y. Yamashita, "$Pb(B'B'')O_3$-$PbTiO_3$ Materials," *The 7th US-Japan Study Seminar on Dielectric and Piezoelectric Ceramics*, Tukuba, 1995, pp. 181–185.

[9] Y. Yamashita, "Improved ferroelectric properties of niobium-doped $Pb[(Sc_{1/2}Nb_{1/2})Ti]O_3$ ceramics material," *Jpn. J. Appl. Phys.*, vol. 32, pp. 5036–5040, Nov. 1993.

[10] N. Kim, Grain size effect on the dielectric and piezoelectric properties in compositions which are near the morphotropic phase boundary of lead zirconate-titanate based ceramics, Ph.D. dissertation, Pennsylvania State University, University Park, 1994.

[11] J. F. Nye, *Physical Properties of Crystals, Oxford University Press*, Oxford: Clarendon Press, 1957.

[12] D. A. Berlincourt, D. R. Curran, and H. Jaffe, "Piezoelectric and peizomagnetic materials and their function in transducers," in *Physical Acoustics*, vol. 1A. W. P. Mason, Ed. New York: Academic, 1964, p. 169.

[13] S. Fushimi and T. Ikeda, "Phase equilibrium in the system PbO-TiO_2-ZrO_2," *J. Amer. Ceram. Soc.*, vol. 50, pp. 129–132, Mar. 1967.

[14] V. A. Kuznetzov, "Crystallization of titanium, zirconium and hafnium oxies and some titanate and zirconate compounds under hydrothermal conditions," *J. Crystal Growth*, vol. 34, pp. 405–410, 1968.

[15] R. Clarke and R. W. Whatmore, "The growth and characterization of $PbZr_xTi_{1-x}O_3$ single crystals," *J. Crystal Growth*, vol. 33, pp. 29–38, 1976.

[16] T. Hatanaka and H. Hasegawa, "Dielectric properties of $PbZr_xTi_{1-x}O_3$ single crystals including monoclinic zirconia," *Jpn. J. Appl. Phys.*, vol. 34, pp. 5446–5448, Sept. 1995.

[17] K. Yanagisawa, H. Kanai, and Y. Yamashita, "Hydrothermal crystal growth of lanthanum-modified lead zirconate titanate," *Jpn. J. Appl. Phys.*, vol. 34, pp. 536–538 Sept. 1995.

[18] J. Kuwata, K. Uchino, and S. Nomura, "Phase transitions in the $Pb(Zn_{1/3}Nb_{2/3})O_3$-$PbTiO_3$ system," *Ferroelectrics*, vol. 37, pp. 579–582, 1981.

[19] J. Kuwata, K. Uchino, and S. Nomura, "Dielectric and piezoelectric properties of $0.91Pb(Zn_{1/3}Nb_{2/3})O_3$-$0.09PbTiO_3$ single crystals," *Jpn. J. Appl. Phys.*, vol. 21, pp. 1298–1302, Sept. 1982.

[20] T. R. Shrout, Z. P. Chang, N. Kim, and S. Markgraf, "Dielectric behavior of single crystals near the $(1-x)Pb(Mg_{1/3}Nb_{2/3})O_3$-$(x)$ $PbTiO_3$ morphotropic phase boundary," *Ferroelect. Lett.*, vol. 12, pp. 63–69, 1990.

[21] Y. Yamashita and S. Shimanuki, "Synthesis of lead scandium niobate—lead titanate pseudo binary single crystals," to be published.

[22] J. M. Herbert, *Ferroelectric Transducers and Sensors*. New York: Gordon and Breach, 1982.

[23] T. R. Shrout and J. Fielding, Jr., "Relaxor ferroelectric materials," *Proc. IEEE Ultrason. Symp.*, 1990, pp. 711–715.
[24] C. A. Randall, A. S. Bhalla, T. R. Shrout, and L. E. Cross, "Classification and consequences of complex lead perovskite ferroelectrics with regard to B-site cation order," *J. Mater. Res.*, vol. 5, no. 4, pp. 829–834, 1990.
[25] M. L. Mulvihill, S.-E. Park, G. Risch, Z. Li, K. Uchino, and T. R. Shrout, "The role of processing variables in the flux growth of lead zinc niobate-lead titanate relaxor ferroelectric single crystals," *Jpn. J. Appl. Phys.*, vol. 35, pp. 51–57, July 1996.
[26] S.-E. Park, M. L. Mulvihill, G. Risch, and T. R. Shrout, "The effect of growth condition on dielectric properties of $Pb(Zn_{1/3}Nb_{2/3})O_3$ crystal," submitted for publication.
[27] Y. Yamashita, "Large electromechanical coupling factors in perovskite binary material system," *Jpn. J. Appl. Phys.*, vol. 33, Pt. 1[9B], pp. 5328–5331, 1994.
[28] S. Nomura, "Ferroelectric properties in the system $Pb(Zn_{1/3}Nb_{2/3})O_3$-$PbTiO_3$," *J. Phys. Soc. Jpn.*, vol. 27, p. 262, 1969.
[29] S. W. Choi, T. R. Shrout, S. J. Jang, and A. S. Bhalla, "Dielectric and pyroelectric properties in the $Pb(Mg_{1/3}Nb_{2/3})O_3$-$PbTiO_3$ system," *Ferroelectrics*, vol. 100, pp. 29–38, 1989.
[30] H. Banno, T. Tsunooka, and I. Shimano, "Phase diagram and piezoelectric properties of $Pb(Ni_{1/3}Nb_{2/3})O_3$-$PbTiO_3$-$PbZrO_3$ and an application to ceramic wave filter," *Proc. 1st meeting on Ferroelect. Mater. Their Applications*, 1975, F-14, pp. 339–344.
[31] T. Kudo, T. Yazaski, F. Naito, and S. Sugaya, "Dielectric and piezoelectric properties of $Pb(Co_{1/3}Nb_{2/3})O_3$-$PbTiO_3$-$PbZrO_3$ solid solution ceramics," *J. Amer. Ceram. Soc.*, vol. 53, pp. 326–328, June 1970.
[32] J. F. Wang, J. R. Giniewicz, and A. S. Bhalla, "Soft piezoelectric $(1-x)Pb(Sc_{1/2}Ta_{1/2})O_3$-$xPbTiO_3$ ceramics with high coupling factors and low Qm," *Ferroelect. Lett.*, vol. 16, pp. 113–118, 1993.
[33] V. J. Jonson, M. W. Valenta, J. E. Dougherty, R. M. Douglass, and J. W. Meadows, "$Pb(Sc_{0.5}Nb_{0.5})_xO_3$, perovskite-type ferroelectric solid solutions possessing relatively large spontaneous polarizations," *J. Phys. Chem. Solids*, vol. 24, pp. 85–93, 1963.
[34] V. J. Tennery, K. W. Hang, and R. E. Novak, "Ferroelectric and structural properties of the $Pb(Sc_{1/2}Nb_{1/2})_{1-x}Ti_xO_3$ System," *J. Amer. Ceram. Soc.*, vol. 51, pp. 671–674, Dec. 1968.
[35] U. Kodama, M. Osada, O. Kumon, and T. Nishimoto, "Piezoelectric properties and phase transition of $PbIn_{1/2}Nb_{1/2}O_3$-$PbTiO_3$ solid solution ceramics," *Amer. Ceram. Soc. Bull.*, vol. 48, no. 12, pp. 1122–1124, 1969.
[36] A. I. Zaslavskii and M. F. Bryzhina, "An X-ray structural investigation of the antiferroelectric Pb_2MgWO_6 and the system of solid solutions Pb_2MgWO_6-$PbTiO_3$," *Sov. Phys.—Crystallogr.*, vol. 7, no. 5, pp. 577–583, 1963.
[37] V. A. Isupov and L. P. Belous, "Phase transition in the antiferroelectric $PbCo_{0.5}W_{0.5}O_3$ and $PbCo_{0.5}W_{0.5}O_3$-$PbTiO_3$ solid solutions," *Sov. Phys.—Crystallogr.*, vol. 16, no. 1, pp. 129–133, 1971.
[38] D. A. Berlincourt, C. Cmolik, and H. Jaffe, "Piezoelectric properties of polycrystalline lead titanate zirconate compositions," *Proc. IRE*, vol. 48, pp. 220–229, 1960.
[39] H. Jaffe and D. A. Berlincourt, "Piezoelectric transducer materials," *Proc. IEEE*, vol. 53, no. 10, pp. 1372–1386, 1965.
[40] H. Ouchi, K. Nagano, and S. Hayakawa, "Piezoelectric properties of $Pb(Mg_{1/3}Nb_{2/3})O_3$-$PbTiO_3$-$PbZrO_3$ solid solution ceramics," *J. Amer. Ceram. Soc.*, vol. 48, no. 12, pp. 630–635, 1965.
[41] Y. Yamashita, "Piezoelectric properties of niobium-doped $[Pb(Sc_{1/2}Nb_{1/2})_{1-x}Ti_x]O_3$ ceramics material near the morphotropic phase boundary," *Jpn. J. Appl. Phys.*, vol. 33, pp. 4562–4656, Aug. 1994.
[42] S. T. Chung, K. Nagata, and H. Igarashi, "Piezoelectric and dielectric properties of $Pb(Ni_{1/3}Nb_{2/3})O_3$-$Pb(Zn_{1/3}Nb_{2/3})O_3$-$PbTiO_3$," *Ferroelectrics*, vol. 94, pp. 243–247, 1989.
[43] S. Baumler, "The dielectric and piezoelectric properties of PZN:PT:BT ceramics," M.S. thesis, The Pennsylvania State University, University Park, 1986.

Seung-Eek Park was born in Seoul, Korea, in 1965. He received the B.S. and M.S. degrees in 1987 and 1989, respectively, and the Ph.D. degree in 1994, all from Seoul National University, Seoul, Korea, in inorganic materials engineering.

From 1994 to 1996, he was a Postdoctoral Scholar and has been a Research Associate at Materials Research Laboratory of the Pennsylvania State University, continuing his work on ferroelectric materials.

His current research interests include the development of piezoelectric materials for transducer and actuator applications.

Thomas R. Shrout is Professor of Materials and Senior Scientist at the Pennsylvania State University. He received a B.S. and Ph.D in ceramic science from Pennsylvania State University in 1976 and 1981, respectively.

Prior to joining the faculty at Penn State, Dr. Shrout was with Sprague Electric Co. and AVX Co. He holds five patents and has coauthored more than 100 papers in the area of electronic ceramics with an emphasis on processing property relationship.

APPENDIX 24

Mat Res Innovat (1997) 1:20–25

ORIGINAL ARTICLE

Seung-Eek Park · Thomas R. Shrout

Relaxor based ferroelectric single crystals for electro-mechanical actuators

Received: 2 January 1997 / Accepted: 27 March 1997

Abstract The piezoelectric properties of relaxor based ferroelectric single crystals, such as $Pb(Zn_{1/3}Nb_{2/3})O3$–$PbTiO_3$ (PZN-PT) and $Pb(Mg_{1/3}Nb_{2/3})O_3$–$PbTiO_3$ (PMN-PT) were investigated for electromechanical actuators. In contrast to polycrystalline materials such as $Pb(Zr,Ti)O_3$ (PZTs), morphotropic phase boundary (MPB) compositions were not essential for high piezoelectric strain. Piezoelectric coefficients (d_{33}'s) >2200 pC/N and subsequent strain levels up to >0.5% with minimal hysteresis were observed. Crystallographically, high strains are achieved for <001> oriented rhombohedral crystals, though <111> is the polar direction. Ultrahigh strain levels up to 1.7%, an order of magnitude larger than those available from conventional piezoelectric and electrostrictive ceramics could be achieved, possibly being related to an E-field induced phase transformation. High electromechanical coupling (k_{33}) >90% and low dielectric loss <1%, along with large strain make these crystals promising candidates for high performance solid state actuators.

Key words Relaxor ferroelectrics · Single crystal · Actuator · Piezoelectrics · Hysteresis

Introduction

Electromechanical actuators directly input electrical energy into mechanical energy. Of the many types of actuator materials including, magnetostrictive, photostrictive, and shape memory alloys, piezoelectric and electrostrictive ceramics are widely used in applications requiring high generative force, high frequency operation, accurate displacement, quick response time, or small device size [1]. Generally, among the material properties determining actuator performance, the electric field (E-field) induced strain is the most important parameter for actuators. This is demonstrated by strain energy density which is a measure of the energy per unit mass an actuator can deliver.

$$e_{max}=1/\rho\ (1/4\cdot(1/2\cdot E(s_{max})^2) \quad (1)$$

where e_{max} is the strain energy density, E is the actuator's elastic modulus, s_{max} is the maximum field induced strain, and ρ is the actuator's density [1]. 1/4 is the appropriate factor for an actuator impedance related to its surroundings. In designing an actuator, the maximum strain energy density should be as high as possible. In electroactive ceramics, density and elastic modulus vary little from material to material; therefore, the level of strain and maximum strain achievable with a reasonable electric field (<50 kV/cm) dominates the energy density. The piezoelectric coefficient (d_{ij}), determining the level of induced strain at a given electric field, is the most widely used parameter describing actuator performance. Currently, $Pb(Zr,Ti)O_3$ (PZT) polycrystalline ceramics are used with piezoelectric coefficients (d_{33}) ranging from 200 to 750 pC/N, the later limited by hysteresis. Electrostrictive ceramics such as $Pb(Mg_{1/3}Nb_{2/3})O_3$ offer effective d_{33}'s >700 pC/N, but only over a narrow range of E-field.

It is objective of this paper to report ultrahigh piezoelectric coefficients (d_{33}) and remarkably high strain levels with low hysteresis observed for single crystals of $Pb(Zn_{1/3}Nb_{2/3})O_3$–$PbTiO_3$ (PZN-PT) and $Pb(Mg_{1/3}Nb_{2/3})O_3$–$PbTiO_3$ (PMN-PT). Strain behavior as a function of E-field will be discussed with respect to crystal structure, orientation, and anticipated actuator performance.

S.-E. Park (✉)
259 Materials Research Laboratory,
The Pennsylvania State University, University Park,
PA 16802, USA
e-mail: sxp37@psu.edu

T.R. Shrout
150 Materials Research Laboratory,
The Pennsylvania State University,
University Park, PA 16802, USA

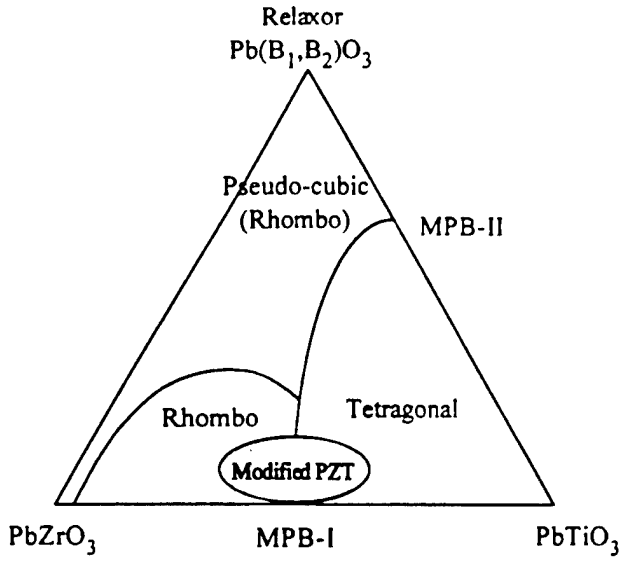

Fig. 1 Ternary diagram depicting MPBs in PZT and relaxor-PT systems for piezoelectric ceramic

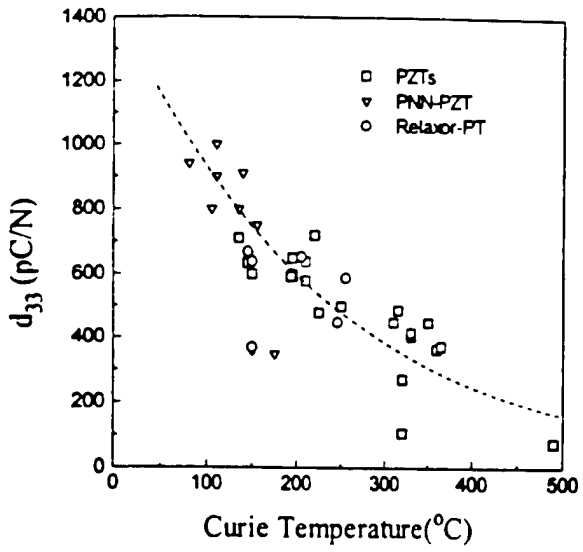

Fig. 2 Piezoelectric coefficient d_{33} as a function of transition temperature (Tc) for piezoelectric ceramics, including PZT, modified PTZs, and relaxor-PT systems

Morphotropic phase boundary ceramics

$Pb(Zr_{1-x},Ti_x)O_3$ (PZT) ceramics have been the mainstay for high performance actuator applications. Compositionally, PZT ceramics lie near the morphotropic phase boundary (MPB) between the tetragonal and rhombohedral phases as shown in Fig. 1. MPB compositions exhibit anomalously high dielectric and piezoelectric properties as a result of enhanced polarizability arising from the coupling between two equivalent energy states, i.e. the tetragonal and rhombohedral phases, allowing optimum domain reorientation during the poling process. Alternate MPB systems can be found in relaxor-$PbTiO_3$, also as shown in Fig. 1. Lead based relaxor materials are complex perovskites with the general formula $Pb(B_1B_2)O_3$, (B_1=Mg^{2+}, Zn^{2+}, Ni^{2+}, Sc^{3+} ..., B_2=Nb^{5+}, Ta^{5+}, W^{6+} ...). Characteristic of relaxors is a broad and frequency dispersive dielectric maxima [2].

To achieve a high piezoelectric coefficient, MPB-based ceramics are further engineered by compositionaly adjusting the Curie temperature (T_c) downward relative to room temperature. The effect of transition temperature (T_c) on the piezoelectric properties is clearly evident in Fig. 2. As shown, the room temperature values of d_{33} are plotted as a function of T_c for a variety of modified PZT ceramics, including relaxor-PT systems. Enhanced piezoelectric activity of MPB-based ceramics is achieved by compositionaly adjusting Tc downward relative to room temperature resulting in "soft" piezoelectric ceramics. This enhanced piezoelectric effect, therefore, comes with the expense of more temperature dependent properties, and less polarization stability, i.e. aging and loss of piezoelectric activity. Further details on the relationship between dielectric/piezoelectric properties and T_c of piezoelectric ceramics can be found in [3].

Most importantly, a consequence of increased piezoelectric activity for these "soft" ceramics is large hysteresis in the strain vs. E-field behavior as a result of domain motion. Strain vs. E-field behavior for PZT-5H (Navy type-VI) is shown in Fig. 3 as an example. Though the piezoelectric coefficient (d_{33}) of PZT-5H ceramics is in the range of ~600 to 700 pC/N [4] (implying ~0.06 to 0.07% strain at 10 kV/cm), strain as high as 0.1% can be observed at 10 kV/cm. This enhanced nonlinear strain is the result of domain motion, and therefore, accompanied by significant hysteresis, resulting in poor positioning accuracy. Area within the strain vs. E-field curve or dielectric loss results in significant heat generation during operation. Heat generation combined with a decreased temperature usage range, results in poor temperature stability and limits these ceramics to low frequency applications.

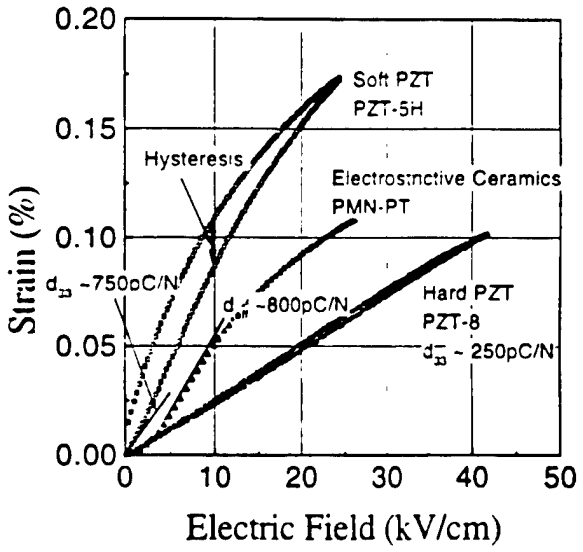

Fig. 3 Strain vs. E-field behaviors for various electromechanical ceramics

Strain vs. E-field hysteresis can be minimized with the use of the "hard" piezoelectric ceramics. Hard piezoelectric ceramics such as PZT-8 (Navy type III) offer very low hysteresis as shown in Fig. 3. However, the reduction in hysteresis and loss comes at the expense of d_{33} and subsequent strain level. Typically d_{33} values. for "hard" PZTs range from ~200 to 300 pC/N [4].

Another category of ceramic materials used in commercial actuators are electrostrictors. Electrostrictive strain is proportional to the square of polarization. A few materials such as PMN and its solid solution with PT exhibit significant electrostrictive strain (>0.1%) with virtually no hysteresis as shown in Fig. 3. Effective d_{33}'s >~800 pC/N calculated directly from the strain vs. E-field curve can be achieved, but only over a very narrow range of E-field. For hard piezoelectric and electrostrictive ceramics, strain level with low hysteresis does not exceed 0.15%. This limitation originates from the material's dielectric breakdown strength and polarization saturation.

In summary, piezoelectric and electrostrictive ceramics offer strain levels up to ~0.15%. Soft PZTs, exhibiting piezoelectric coefficients (d_{33}) as high as 750 pC/N. are inherently limited due to hysteresis caused by domain motion. Hysteresis can be minimized with the use of hard piezoelectric ceramics. but d_{33} values of only ~200–300 pC/N are available. Even though electrostrictive ceramics offer effective d_{33}'s ~800 pC/N, maximum strain level is limited by its dielectric breakdown strength and polarization saturation. To achieve E-field induced strain levels >0.15%. electroactive materials should possess high piezoelectric coefficients (d_{33} >1000 pC/N) and high dielectric breakdown strength.

Single crystal piezoelectrics

Single crystal piezoelectrics such as quartz (SiO_2), lithium niobate ($LiNbO_3$), and the analogue lithium tantalate ($LiTaO_3$) are widely employed in specific applications that include oscillators, surface acoustic wave (SAW) devices. and in optics. In contrast to PZT ceramics, however. these single crystals offer inferior piezoelectric properties, with d_{33}'s <50 pC/N.

Attempts to grow single crystals of MPB PZTs have been made by numerous researchers, resulting in crystallites too small to allow adequate property measurements [5–9]. In contrast to PZT crystal growth, relaxor-PT materials can be readily grown in single crystal form. This key distinction was first realized by Nomura and coworkers for the PZN and PZN-PT systems [10, 11] and later by Shrout for the PMN-PT [12]. In general, most $Pb(B_1,B_2)O_3$–PT crystals can be grown by high temperature solution growth using Pb-based fluxes [13, 14].

Piezoelectric coefficients as high as ~1500 pC/N have been reported [11, 12] for MPB Relaxor-PT crystals. However. it should be noted that piezoelectric coefficients are generally determined using low field (<0.1 kV/cm) techniques such as the resonance method (IEEE standard) [15]. Therefore, direct observation of the strain vs. E-field behavior is essential in order to investigate hysteresis and maximum levels of strain, key experiments to directly confirm actuator performance. In relation to actuators, several questions arise: (1) How do the high d_{33} values determined using low field techniques correlate to direct measurements? As for piezoelectric and electrostrictive ceramics, will the strain level saturate with increased E-field? (2) How much hysteresis accompanies the strain? (3) Is morphotrophy essential for enhanced piezoelectric properties? (4) Are there optimum crystallographic cuts as in the case of the other piezoelectric crystals? In the following sections, we will attempt to answer many of these questions, reporting piezoelectric properties and direct observation of strain behavior as a function of crystallographic orientation and electric field for relaxor-PT single crystals.

Dielectric and piezoelectric properties of relaxor based single crystals

In this section, the dielectric and piezoelectric properties of relaxor-PT systems as a function of crystal composition and orientation are summarized. Commonalties inherent to relaxor-PT systems have been discussed in reviews by Shrout [16] and Randall [17]. Based on these commonalties, our research was limited to two representative systems, PZN-PT and PMN-PT. Though PMN-PT MPB crystals exhibit piezoelectric properties comparable with PZN-PT, more focus was given to the PZN system owing to its relatively lower PT content for MPB, allowing more uniform crystal growth of these solid solution materials. Experimental procedures are briefly summarized including crystal growth, crystal alignment, dielectric and piezoelectric measurements using direct observation of strain as a function of electric field as well as low field property measurements using the IEEE resonance technique [15].

Crystal growth, sample preparation and property measurements

High purity (>99.9%) powders of Pb_3O_4, ZnO. $MgCO_3$, Nb_2O_5 and TiO_2 were used as starting material. Raw powders were weighed with desired molar ratio with excess Pb_3O_4 as a flux. The powders were dry mixed for a desired period of time using a tumbling mill. The mixed powders were loaded into a platinum crucible, which was placed in an alumina crucible sealed with an alumina lid and alumina cement to minimize PbO volatilization. The crucible and powder were placed in a tube furnace and held at soak temperatures (1100–1200° C), followed by slow cooling (1–5° C/h). The crucible was then furnace-cooled to room temperature. Hot HNO_3 is used to separate the crystals out of the rest of the melt. Typically crystal size ranged from 3 to 20 mm. Further details on the flux growth technique of these crystals can be found in [13, 14].

Individual crystals were oriented along their pseudocubic <001> and the <111> axis using a Laue back re-

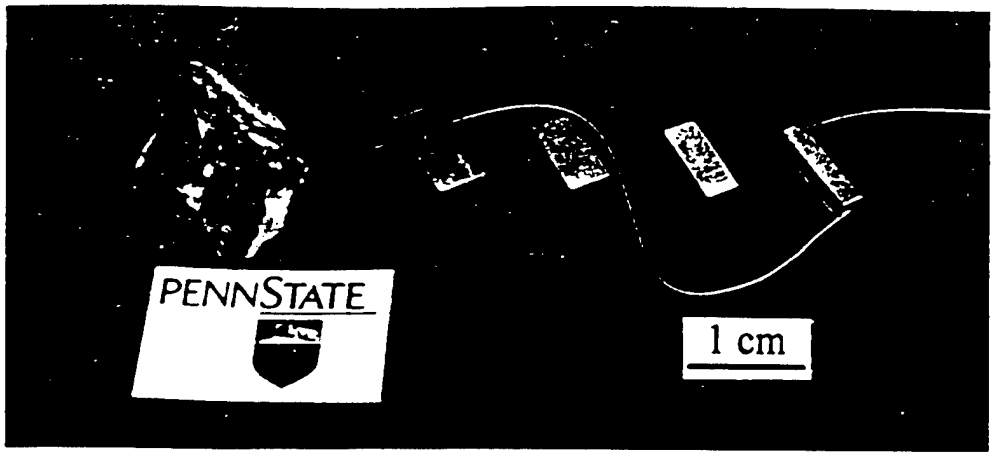

Fig. 4 As grown crystal, an aligned sample using the Laue camera, a cut and polished sample, an electroded sample for direct strain observation as well as for low field planar mode resonant sample, and a low field longitudinal mode resonant sample, for PZN-9.5%PT (from *left* to *right*)

flection camera. For electrical characterization, samples were prepared by polishing with silicon carbide and alumina polishing powders to achieve flat and parallel surfaces onto which gold electrodes were sputtered. High-field measurements included polarization and strain hysteresis using a modified Sawyer-Tower circuit and linear variable differential transducer (LVDT) driven by a lock-in amplifier (Stanford Research Systems, Model SR830). Plate shape samples with thickness ranging from 0.2 mm to 0.5 mm were used. Electric fields as high as ~140 kV/cm were applied using an amplified unipolar wave form at 0.2 Hz, using a Trek 609C-6 high voltage DC amplifier. During testing the samples were submerged in Fluorinert (FC-40, 3M, St. Paul, Minn.), an insulating liquid, to prevent arcing. For piezoelectric coefficient(d_{33}) determination, bar shape samples with lengths ranging from 3 mm to 5 mm were tested. Samples were poled either by field cooling (10 kV/cm) from temperatures above the dielectric maximum temperature (T_{max}) or by applying 40 kV/cm at room temperature. Figure 4 presents, from left to right, a representative of an as grown crystal, an aligned sample using the Laue camera, a cut and polished sample, an electroded sample for direct strain observation as well as for low field planar mode resonant sample, and a low field longitudinal mode resonant sample, for PZN-9.5%PT, respectively.

Low field measurements

Piezoelectric coefficients as a function of composition and crystal orientation for PZN-PT, calculated based on IEEE standards, are presented in Fig. 5. As shown, large piezoelectric coefficients (d_{33}~1600 pC/N) were found for PZN-PT with MPB compositions (9.5% PT), as previously reported by Kuwata [11]. PMN-PT crystals with MPB compositions (PMN-35% PT) also exhibited large piezoelectric coefficients (d_{33}~1500 pC/N) [3]. It should be noted, however, that all rhombohedral crystals oriented along also their pseudocubic <001> direction exhibited large piezoelectric coefficients. As shown in Fig. 5, d_{33} increased with increased amount of $PbTiO_3$ for <001> oriented rhombohedral crystal. Maximum d_{33} values of ~2200 pC/N were determined with domain engineered rhombohedral crystals.[1] In contrast to PZT's, d_{33} dramatically decreases at MPB to levels ~500 pC/N for tetragonal composition. Though <111> is the polar direction in rhombohedral crystals, such cuts exhibited low piezoelectric coefficient, believed to be associated with domain instability. Further details on domain motion and crystal anisotropy are reported elsewhere [18]. Dielectric loss value <1% and electromechanical coupling constant values (k_{33}) >90% can be found in ref. [3].

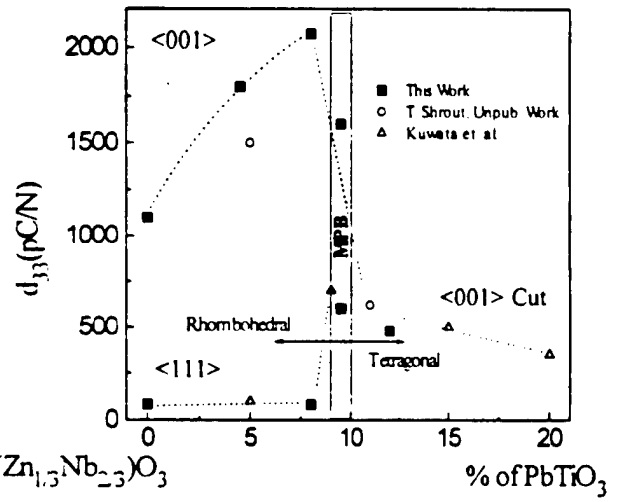

Fig. 5 d_{33} as a function of composition and crystallographic orientation in crystals of PZN-PT

Strain vs. E-field behaviors for relaxor based single crystals

Though high piezoelectric coefficients (d_{33}) were determined, high field measurements are more indicative of actuator performance. The following observations will

[1] Rhombohedral crystals oriented and poled along pseudocubic <001> direction. Crystallographically, polar direction of rhombohedral crystal is pseudocubic <111> direction.

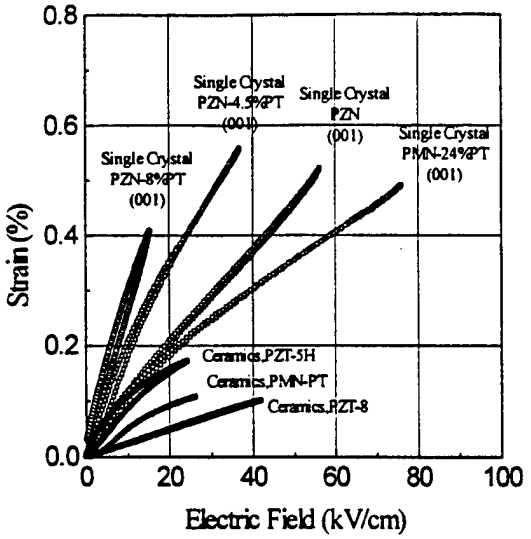

Fig. 6 Strain vs. E-field behaviors for crystals of PZN-PT and PMN-PT. and for various electromechanical ceramics

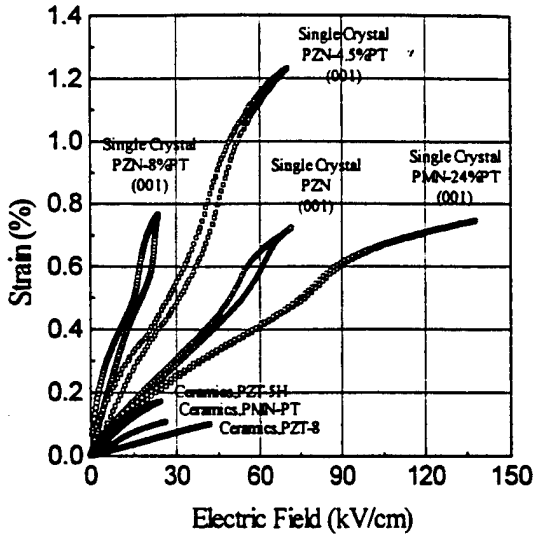

Fig. 7 Strain vs. E-field behaviors for crystals of PZN-PTand PMN-PT. and for various electromechanical ceramics (high fields)

clearly show the potential of relaxor based ferroelectric single crystals, for applications as actuators.

Strain as a function of electric field for various <001> oriented rhombohedral crystals (pure PZN, PZN-4.5%PT. PZN-8%PT, and PMN-24%PT) are presented in Fig. 6. Also E-field induced strains of various electromechanical ceramics such as soft PZT (PZT-5H), hard PZT (PZT-8) and electrostrictive ceramics (PMN-PT) are compared. Piezoelectric coefficients (d_{33}) directly calculated from the slope of strain vs. electric field curves confirmed the piezoelectric coefficients determined by the low field resonance method. Strains as high as 0.58% were observed with low hysteresis for these crystals, significantly larger than that for polycrystalline ceramics. The limitation of achievable strain for polycrystalline ceramics is the result of polarization saturation and subsequent saturation on strain and breakdown strength. However, as shown in Fig. 6, strain did not saturate with increased E-field for <001> oriented rhombohedral crystals. This remarkable strain vs. E-field behavior with low hysteresis is believed to be related to the engineered domain state. Although crystallographically <111> is the polar direction, low piezoelectric coefficients (d_{33}) <100 pC/N were determined as shown in Fig. 5. This inferior piezoelectric activity was found to be related to domain instability after poling. Details on mechanisms are presented elsewhere [18].

Saturation of E-field induced strain behavior for <001> oriented rhombohedral crystals was investigated until dielectric breakdownas presented in Fig. 7. Far from saturation, the strain abruptly increased with strain levels as high as 0.8% being achieved for all crystals tested. Strain levels >1.2% for the PZN-4.5%PT crystal were the result of higher breakdown voltage. The E-field induced strain behavior observed is believed to be associated with an E-field induced rhombohedral-tetragonal

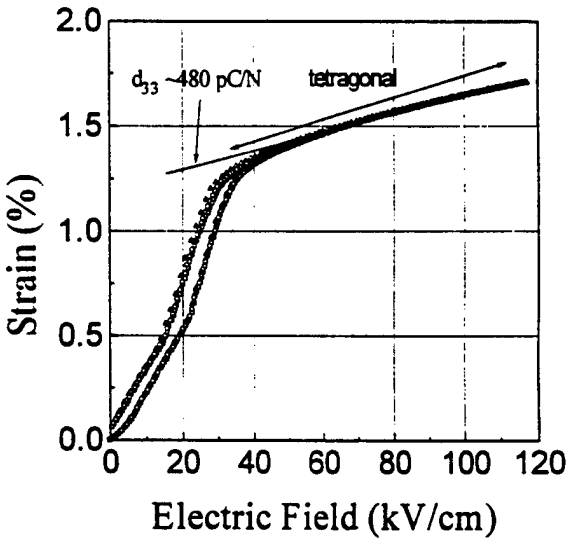

Fig. 8 Strain vs. E-field behaviors for <001> oriented PZN-8%PT crystal

phase transition. This phase transition behavior is more apparent in Fig. 8 presenting the E-field induced strain behavior of the <001> oriented PZN-8%PT crystal. At ~120 kV/cm, the induced strain along with high dielectric breakdown strength resulted in a strain level as high as 1.7%. The piezoelectric coefficient (d_{33}) ~480 pC/N calculated directly from the slope of strain vs. E-field in the high field region corresponded to the tetragonal phase (between 40 and 120 kV/cm in Fig. 8) coincides with a d_{33} value (~500 pC/N) of tetragonal PZN-12%PT crystal. Although phase transition is a likely explanation for the ultrahigh strain level, direct observation of phase transition using in situ XRD is required.

Conclusion

Pseudocubic <001> oriented relaxor based rhombohedral crystals such as (1-x) PZN-x PT (x<0.09) and (1–x), PMN- xPT (x<0.35) exhibited actuation levels not available with current piezoelectric ceramics. Ultrahigh piezoelectric coefficients (d_{33}) >~2200 pC/N and strain levels up to 0.58% with low hysteresis were observed. Ultrahigh strain levels up to 1.7% could be achieved for relaxor based ferroelectric single crystals as a result of E-field induced rhombohedral-tetragonal phase transition. Other relaxor based rhombohedral crystals are expected to exhibit similar strain vs. E-field behavior. Textured polycrystalline ceramics is also believed to exhibit high strain behaviors. Though clearly promising candidates for high performance actuators, further investigations in crystal growth and prestress testing are required for single crystal piezoelectrics to become the next generation material of actuators.

Acknowledgements This research has been supported by Office of Naval Research and Whitaker Center for Ultrasonic Imaging. The authors would like to thank L.E. Cross and C. Randall for their helpful suggestions, and Wesley Hackenberger, Patrick D. Lopath and Michael J. Zipparo for their helps with the property measurements, and ShiFang Liu and Hua Lei with crystal growth and preparation of samples.

References

1. Giurgiutiu V, Chaudhry Z, Rogers CA (Sept 1995) Energy-based comparison of solid-state actuators, report no CIMSS 95-101, Virginia Polytechnic Institute and State University
2. Cross LE (1987) Ferroelectrics 76:241
3. Park S-E, Shrout TR (1997) IEEE Trans UFFC special issue on ultrasonic transducers (in press)
4. Jaffe H, Berlincourt DA (1965) Proc IEEE 53:1372
5. Fushimi S, Ikeda T (1967) J Am Ceram Soc 50:129
6. Kuznetzov VA (1968) J Cryst Growth 34:405
7. Clarke R, Whatmore RW (1976) J Cryst Growth 33:29
8. Hatanaka T, Hasegawa H (1995) Jp J Appl Phys 34:5446
9. Yanagisawa K, Kanai H, Yamashita Y (1995) Jpn J Appl Phys 34:536
10. Kuwata J, Uchino K, Nomura S (1981) Ferroelectrics 37:579
11. Kuwata J, Uchino K, Nomura S (1982) Jpn J Appl Phys 21:1298
12. Shrout TR, Chang ZP, Kim N, Markgraf S (1990) Ferroelectric Lett 12:63
13. Mulvihill ML, Park S-E, Risch G, Li Z, Uchino K, Shrout TR (1996) Jpn J Appl Phys 35:51
14. Park S-E, Mulvihill ML, Risch G, Shrout TR (1997) Jpn J Appl Phys 36:1154
15. IEEE standard on piezoelectricity (1976) American National Standards Institute
16. Shrout TR, Fielding J jr (1990) Proc IEEE Ultra Symp 711–715
17. Randall CA, Bhalla AS, Shrout TR, Cross LE (1990) J Mater Res 5:829
18. Park S-E, Shrout TR (unpublished work)

APPENDIX 25

Jpn. J. Appl. Phys. Vol. 36 (1997) pp. 1154–1158
Part 1. No. 3A, March 1997

The Effect of Growth Conditions on the Dielectric Properties of $Pb(Zn_{1/3}Nb_{2/3})O_3$ Single Crystals

Seung-Eek PARK, Maureen L. MULVIHILL, George RISCH and Thomas R. SHROUT
Materials Research Laboratory, The Pennsylvania State University, University Park, PA 16801, USA

(Received September 17, 1996; accepted for publication December 24, 1996)

The effect of growth conditions on the dielectric properties and ferroelectric transition of perovskite $Pb(Zn_{1/3}Nb_{2/3})O_3$ single crystals was examined. Crystals were grown by the flux technique using PbO as a self flux. Increased cooling rate and soaking temperature resulted in a decreased Zn/Nb ratio, and corresponding increased temperature of the maximum dielectric constant (T_{max}), and decreased room temperature values of the dielectric constant and loss. Different crystal colors and quality were also associated with the various growing conditions. Although dielectric properties, domain stability after poling, and associated piezoelectric properties are a function of T_{max}, it was shown that crystal quality was critical for the observed variation in these properties.

KEYWORDS: relaxor ferroelectrics, crystal growth, $Pb(Zn_{1/3}Nb_{2/3})O_3$, nonstoichimetry, phase transition

1. Introduction

$Pb(Zn_{1/3}Nb_{2/3})O_3$ (PZN) is a prototypical relaxor ferroelectric which undergoes a diffuse phase transition around 140°C.[1] Macroscopic lattice distortion with rhombohedral symmetry can be observed at room temperature due to the high transition temperature of PZN.[2,3] In spite of the observed lattice anisotropy, as-grown PZN crystals do not show ferroelectric macrodomains.[4] However PZN switches into a stable ferroelectric macrodomain state with the application of an E-field, and effectively exhibits piezoelectric characteristics.[5] High dielectric and piezoelectric properties were reported for PZN[6] and $Pb(Zn_{1/3}Nb_{2/3})O_3$–$PbTiO_3$ (PZN–PT)[7,8] single crystals, making them promising candidates for various transducer applications.

It is known that perovskite PZN or PZN–PT with low PT content can not be prepared by conventional solid state reaction. The reason for this phase instability has been investigated from both the viewpoints of crystal chemistry[9] and thermodynamics.[10] However, crystals of PZN and PZN–PT can be readily grown using the high temperature flux. To date, however, few studies correlating the dielectric and piezoelectric properties as a function of growth conditions for the materials have been reported, particularly with respect to nonstoichimetric variations.

It is the purpose of this study to report the variation of chemical composition, dielectric and ferroelectric properties as a function of growth conditions. PZN rather than PZN–PT was selected to eliminate the possibility of property and compositional variations caused by the change in solute concentration and ionic valence of Ti^{4+}.

2. Experimental Procedure

2.1 *Crystal growth*

PZN crystals were grown using the high temperature flux technique. High purity (>99.9%) powders of Pb_3O_4 (Aldrich, WI), ZnO (Johnson Matthey, MA), and Nb_2O_5 (Aldrich, WI) were used. Raw powders were mixed and loaded into a 30 cm^3 Pt crucible. The Pt crucible was then placed in an alumina crucible which was sealed with an alumina lid and alumina cement to minimize PbO volatilization. The crucible and powder were then placed in a furnace and held at a soak temperature of 1150 to 1200°C for 10 h, followed by cooling at a rate of 1°C/h to 5°C/h down to 900°C. The crucible was then furnace-cooled to room temperature. The flux was leached out with hot HNO_3 (20%) and the crystals removed for characterization. These growing conditions were determined based on several preliminary experiments including differential thermal analysis. Further details concerning the crystal growth can be found in ref. 11.

2.2 *X-ray diffraction (XRD) and chemical analysis*

Single crystals were ground into a fine powder for XRD analysis ranging from 20°–80° 2θ with a step size of 0.01 and a counting time of 3 s. Individual crystals were oriented along their polar axis (111) using a Laue back reflection camera. Crystals were chemically analyzed using inductively coupled plasma spectrophotometer (ICP, Leeman Labs PS30000UV). To determine reproducibility, chemical analysis was performed at least twice with different crystals from the same batch. The detection limit was ~80 ppm due to the low solute concentration caused by the inherent difficulty in dissolving niobate crystals. Nonstoichiometry with the crystal growth was observed mainly associated with B-site cation variation, as crystals were grown in the PbO self flux.

2.3 *Electrical characterization-polarization and dielectric properties*

For electrical characterization, samples were then prepared by polishing with silicon carbide and alumina polishing powders to achieve flat and parallel surfaces onto which gold electrodes were sputtered. Samples were rectangular plates with the thickness ranged from 0.2 to 0.5 mm and edge to thickness ratio >10. To determine reproducibility, all dielectric and piezoelectric measurements were performed with at least three different crystals for each grown batch. Polarization vs. E-field behavior was measured at 0.2 Hz using a computer controlled Sawyer Tower system. During testing, the samples were submerged in Fluorinert (FC-40, 3 M, St. Paul, MN), an insulating liquid to prevent arcing. For piezoelectric measurements, crystals were poled by applying either 10 kV/cm at room temperature or by field (10 kV/cm) cooling from 200°C. The piezoelectric co-

efficient (d_{33}) was measured using d_{33} meter (Institute of acoustics, Academia Sinica). The dielectric properties were determined with multifrequency LCR meters (Hewlett Packard 4274 A and 4275 A) in conjunction with a computer controlled temperature chamber (Delta Design Inc., Model MK 2300) over the frequency range of 100 Hz, 1 kHz, 10 kHz and 100 kHz.

3. Results and Discussion

3.1 *Crystal growth and stoichiometry*

Table I summarizes the various conditions used for the growth of three different PZN crystals. XRD patterns of the various crystals are shown in Fig. 1. All crystals were found to be phase pure perovskite with rhombohedral symmetry ($a = 4.056(\pm 0.001)$ Å and $\alpha = 89°55'$). Rhombohedral distortion (α) was determined from the peak split observed in the {220} peaks in Fig. 2. Lattice constants of the crystals were found to be not significantly different as a function of growth condition.

As presented in Table I, growth parameters remained constant for the growth runs of PZN-A and PZN-B with the exception of the cooling rate. A flux to composition molar ratio of 70:30 and a soak temperature of 1150°C as determined by preliminary DTA analysis.[11] were employed. Cooling rates were 5°C/h and 1°C/h for run PZN-A and PZN-B, respectively. For PZN crystals obtained from growth run PZN-A and those from growth run PZN-B, crystal size was not significantly different. This indicates that the variation in cooling rate from 1 to 5°C/h does not significantly affect the nucleation behavior with a soak temperature of 1150°C. This would occur if the majority of nucleation occurred on heterogeneous sites such as the crucible wall. However, the chemical composition was found to be dependent on the cooling rate as presented in Table II. Nonstoichiometry in Pb-based compounds is usually the result of Pb volatiliza-

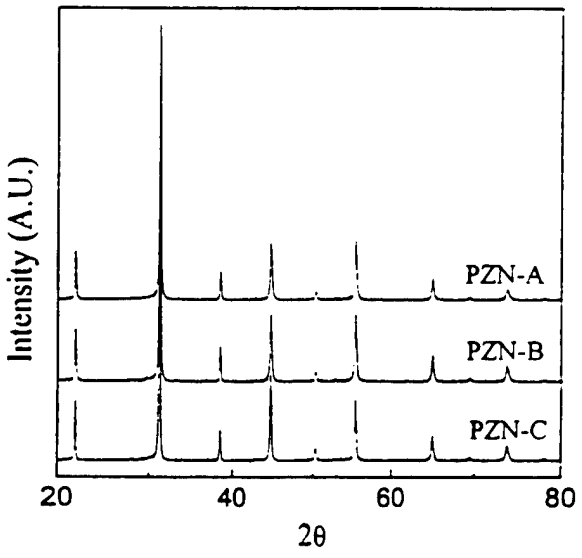

Fig. 1. XRD patterns of $Pb(Zn_{1/3}Nb_{2/3})O_3$ crystals.

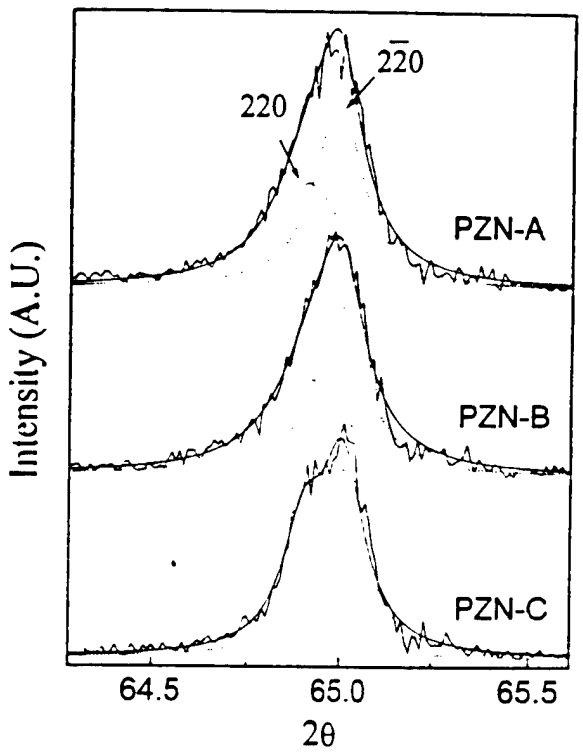

Fig. 2. {220} reflections in XRD patterns of $Pb(Zn_{1/3}Nb_{2/3})O_3$ crystals.

Table II. Composition analysis of PZN crystals using ICP (wt%).

	PZN-A	PZN-B	PZN-C	PZN[a)]
Pb	59.5	59.9	59.9	61.1
Zn	5.5	5.8	5.7	6.4
Nb	20.2	19.3	20.7	18.3
Zn/Nb	0.27	0.30	0.28	0.35
Pt	n.d.[b)]	n.d.	n.d.	

a) expected for $Pb(Zn_{1/3}Nb_{2/3})O_3$.
b) not detected, detection limit 80 ppm.

Table I. Growth condition of flux grown PZN crystals.

Growth run	PZN-A	PZN-B	PZN-C
Flux	PbO (Pb_3O_4)	PbO (Pb_3O_4)	PbO (Pb_3O_4)
Flux: composition	7:3	7:3	6:4
Soaking temperature (°C)	1150	1150	1200
Soaking time (h)	10	10	10
Cooling rate (°C/h)	5	1	1
Crystal color	Colorless	Light Yellow	Brown
Maximum crystal size (cm)	0.5	0.5	1

tion. which results in Pb vacancies on the A-site.[12,13] In this study, crystals were grown under a Pb-rich condition using PbO as a self flux. Therefore, it was expected that the observed nonstoichiometry, if any, would be caused by the compositional variation of the B-site cations. In Table II, the Pb content did not change significantly with growth conditions whereas the variation in the Zn/Nb ratio was observed. Increased cooling rate resulted in a decreased Zn/Nb ratio to decrease (PZN-A and PZN-B in Table II). The different cooling rate and subsequent growth rate changes may have affected the composition at the boundary layers on the crystal. Additional investigations as to the actual origin of the compositional variation are required.

Crystals grown with the flux to composition ratio of 60:40 (designated PZN-C (Table II)) required an increase in soak temperature to 1200°C. As can be seen in Table I, the decreased flux: composition ratio resulted in relatively increased size of the PZN crystals. This could be ascribed to the increased temperature range of crystallization for PZN (PZN+liquid). In contrast with the PZN-B crystals grown at a cooling rate of 1°C/h. the PZN-C crystals also showed decreased Zn/Nb ratio. In this case, the higher soaking temperature may have been responsible for a Zn-deficient composition owing to the volatilization of Zn-rich phase. The 1°C/h cooling also efficiently allows the batches to stay at a higher temperature longer inducing more volatilization of Zn-rich phase.

The color of the crystals varied significantly with respect to growing conditions. as presented in Table I. PZN-A crystals were colorless whereas PZN-B crystals were slightly yellow, and PZN-C crystals dark brown for both as-grown crystals and dielectric/piezoelectric measurement samples (thickness 0.2 to 0.5 mm). One possible explanation of coloration is the role of defects involved with oxygen vacancies or interstitials both of which are common in perovskite crystals.[14] However, direct inspection such as high temperature annealing in order to check that possibility could not be employed because perovskite PZN crystal transforms into pyrochlore.[10] Figure 3 utilizes XRD to demonstrate the decomposition of PZN crystal powder annealed for 2 h at the temperatures of 500°C. 700°C, 900°C, and 1050°C in the air. Transformation to the pyrochlore phase were initiated at only 2 h annealing at temperatures of 700°C with 100% pyrochlore phase after 2 h annealing at 1050°C. This confirmed the perovskite phase instability without the presence of the PbO flux.

Another possible explanation of coloration is the role of impurities caused by the reaction between the solution and crucible at high temperature. However, no impurities such as Pt could be found within the detection limit of ICP as presented in Table II. Additional studies are required to investigate the origin of the coloration.

3.2 *Dielectric and polarization behavior*

One of the direct effects of compositional variation on the dielectric properties of relaxor ferroelectrics is the shift of the temperature where the dielectric constant is maximum (T_{max}).[15-17] Figure 4 shows the temperature dependence of dielectric constant for the various PZN crystals. T_{max} of the PZN crystals was found to be dependent on composition as shown in Fig. 4. The decreased Zn/Nb ratio was associated with an increase in T_{max}. The opposite obervation, decreased T_{max} with decreased Zn/Nb ratio, had been reported by Matsuo.[17] This might be ascribed to the different growth conditions. Faster cooling rate (25°C/h) in ref. 17 might be associated with the second phase inclusions. All the crystals followed the quadratic law, $1/K \sim (T - T_{max})^2$ at temperatures higher than T_{max}. Table III presents the

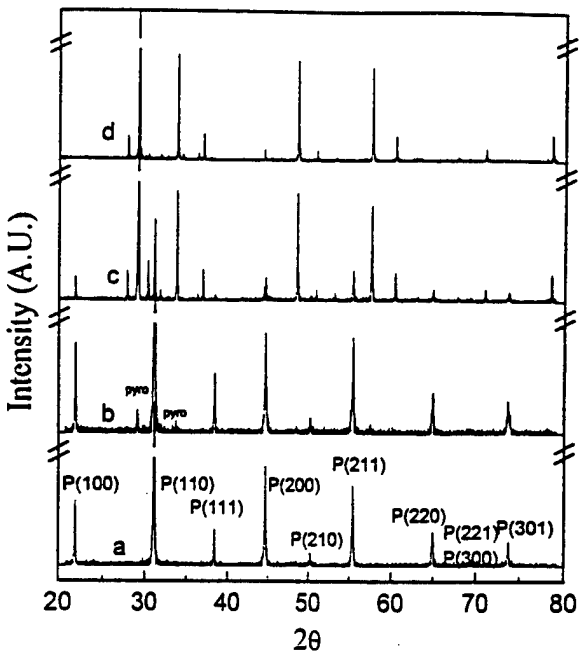

Fig. 3. XRD patterns of $Pb(Zn_{1/3}Nb_{2/3})O_3$ crystal powder after heat treatment for 2 h at (a) 500°C, (b) 700°C, (c) 900°C, (d) 1050°C.

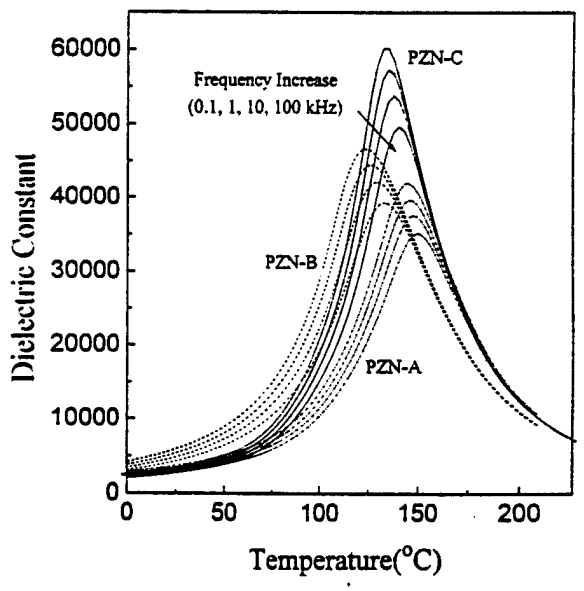

Fig. 4. Temperature dependence of dielectric constant for (111) oriented $Pb(Zn_{1/3}Nb_{2/3})O_3$ crystals.

Table III. Dielectric (1 kHz) and E-field induced properties of PZN crystals ((111) orientation) at room temperature.

	K_{RT} (virgin)	loss (virgin)	K_{RT} (poled)	loss (poled)	T_{max} (°C)	K_{max} (μC/cm^2)	P_r (kV/cm)	E_c	d_{33} (pC/N)
PZN-A	3490	0.054	2540	0.047	145	39700	18	4.6	10
PZN-B	5350	0.066	2980	0.013	126	44600	30	4.0	88
PZN-C	3140	0.052	1260	0.019	135	57000	42	3.6	86

T_{max} and dielectric constant (K, 1 kHz) at room temperature. PZN-B crystals showed the lowest T_{max} (126°C, 1 kHz), the room temperature dielectric constant being higher than both PZN-A and PZN-C crystals. For the case of as-grown crystals, higher dielectric loss was observed with PZN-B, which can be also ascribed to a low T_{max}. All the PZN crystals exhibited a linear dependency of $1/T_{max} = f(\ln\omega)$ (ω: measuring frequency) as observed for other relaxor-ferroelectrics, shown in Fig. 5. The frequency behavior of T_{max} for PZN crystal in ref. 3 is compared, ranging between those of PZN-A and PZN-C. However, growth conditions could not be directly compared due to the lack of specific conditions reported in the literature. It could be found from the slopes in Fig. 5 that T_{max} was more dependent on measurement frequency as T_{max} decreases. A decrease of T_{max} would induce the increase of frequency-dependent contributions (reorientation of polar regions) to polarization through the temperature range of the diffuse phase transition.

Figure 6 shows P vs. E behavior for the various PZN crystals at room temperature. Remnant polarization (P_r) and coercive field (E_c) are reported in Table III. An increased Curie temperature (T_c, here translated into T_{max}) corresponds to an increase in P_r at room temperature. PZN-C crystal (T_{max} = 135°C, 1 kHz) exhibited larger P_r than PZN-B (T_{max} = 126°C), but in case of PZN-A crystal (T_{max} = 145°C), small P_r was observed in spite of highest T_{max} among the crystals. This may be ascribed to the poor crystal quality of PZN-A, probably a subsequence of relatively fast cooling rate during crystal growth. It should be noted that mechanical failure happened most frequently during the sample preparation of PZN-A crystal. Therefore, it could be said that the inferior crystal quality of PZN-A is responsible for low P_r in spite of high T_{max}.

3.3 *Relaxor-ferroelectric transition*

In Table III, decreased dielectric constant (K) and loss are reported for the poled crystals. However, the ratio of K_{poled}/K_{virgin} varied from ~0.75 (PZN-A) to ~0.4 (PZN-C). The piezoelectric coefficient (d_{33}) also varied from values as low as ~10 pC/N (PZN-A) to ~80 pC/N (PZN-B, PZN-C). The low value of d_{33} for (111) oriented PZN crystals was also reported by Kuwata.[7] These observed low values of d_{33} are belived to be associated with domain instability with respect to crystal orientation, reported elsewhere.[6]

It has been suggested that as grown PZN crystals do not exhibit a macrodomain state before poling.[5] Therefore, poling of PZN crystals can be also translated into switching of the relaxor state to macrodomain state. The poled crystals transform to relaxor with the increase of temperature at T_{FR} (ferroelectric-relaxor transition temperature). The T_{FR} was reported to be ~ −60°C and ~100°C for $Pb(Mg_{1/3}Nb_{2/3})O_3$[8,19] and PZN relaxors.[20] respectively. For transducer applications, relaxor based crystals should stay in the oriented macrodomain state. Transition temperature (T_{FR}) of ferroelectric-relaxor implies the temperature limit of the oriented ferroelectric macrodomain state, and that of a given trans-

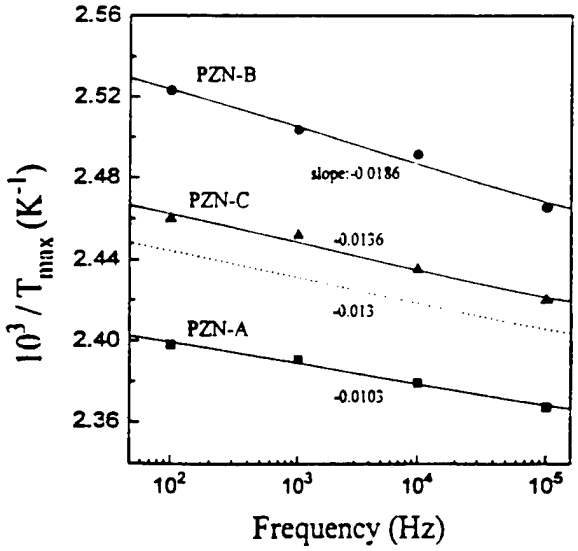

Fig. 5. $1/T_{max}$ as a function of ln f for $Pb(Zn_{1/3}Nb_{2/3})O_3$ crystals (dot line form ref. 3).

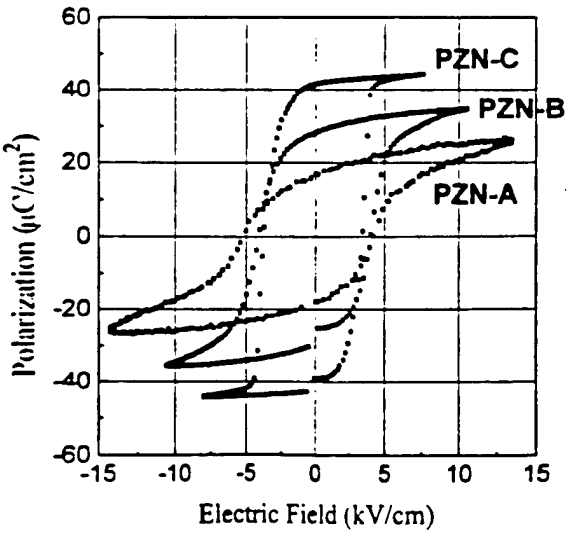

Fig. 6. Polarization as a function of electric field for (111) oriented $Pb(Zn_{1/3}Nb_{2/3})O_3$ crystals.

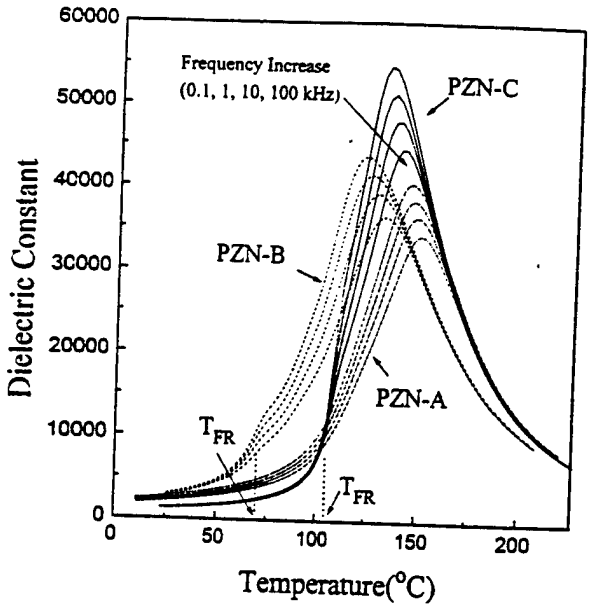

Fig. 7. Temperature dependence of dielectric constant for E-field exposed (10 kV) $Pb(Zn_{1/3}Nb_{2/3})O_3$ crystals (heating run, (111) orientation).

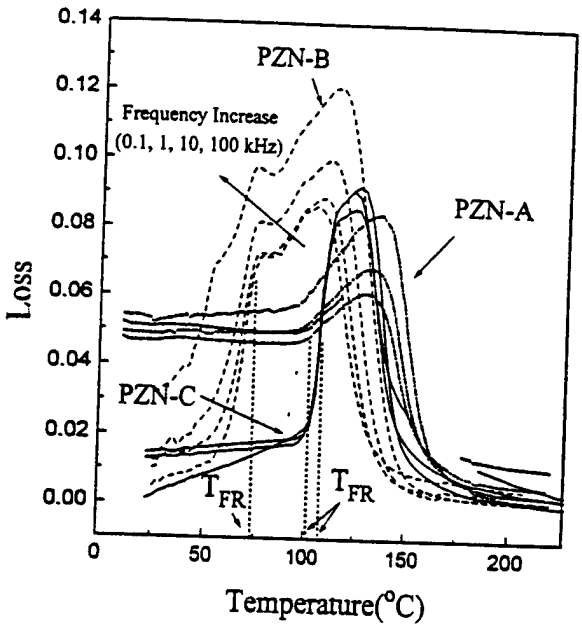

Fig. 8. Temperature dependence of dielectric loss for E-field exposed (10 kV) $Pb(Zn_{1/3}Nb_{2/3})O_3$ crystals (heating run, (111) orientation).

ducer application. Hence, the high T_{FR} is required for increased temperature stability of piezoelectric properties.

Figure 7 shows the dielectric constant as a function of temperature with heating (no-field) from room temperature to 210°C for poled crystal. An abrupt increase of the dielectric constant (indicated by arrow) can be observed for PZN-B and PZN-C crystals, indicating ferroelectric (macrodomain)-relaxor transition. T_{FR}'s of 72°C and 105°C were observed for PZN-B and PZN-C crystals, respectively. Different T_{FR} for PZN-B and PZN-C crystals is due to the free energy variation associated with the different T_{max}. This transition was not observable for PZN-A crystals in Fig. 7. However, ferroelectric-relaxor transition behavior for PZN-A crystal could be observed from the dielectric loss as a function of temperature for poled crystals (Fig. 8). Decreased dielectric loss by E-field exposure showed an abrupt jump at T_{FR} (indicated by arrow again) but T_{FR} of PZN-A crystal was almost same as that of PZN-C in spite of higher T_{max}. This behavior may be also ascribed to poor domain stability, resulted from inferior crystal quality.

4. Conclusions

The dielectric and ferroelectric behavior of PZN crystals grown by the flux technique were determined as a function of growth conditions. Increased cooling rate and soaking temperature caused the Zn/Nb ratio to decrease, which corresponded to a shift of both T_{max} and ferroelectric-relaxor transition to higher temperatures and various room temperature dielectric constant and loss.

Crystal quality and color were also as a function of the growing condition. Relatively fast cooling rate (>5°C/h) may have associated with inferior crystal quality, resulting in poor domain stability after poling, lower piezoelectric coefficient, and low ferroelectric-relaxor transition temperature.

Acknowledgement

This work has been supported by the Office of Naval Research and the Whitaker Center for ultrasound transducers.

1) V. A. Bokov and I. E. Myl'nikov: Sov. Phys.-Solid State **2** (1961) 2428.
2) S. Nomura and T. Takahashi: J. Phys. Soc. Jpn. **27** (1969) 262.
3) Y. Yokomizo, T. Takahashi and S. Nomura: J. Phys. Soc. Jpn. **28** (1970) 1278.
4) N. N. Krainik, L. S. Gokhberg and I. E. Myl'nikova: Sov. Phys.-Solid State **12** (1971) 1885.
5) M. L. Mulvihill, L. E. Cross and K. Uchino: J. Am. Ceram. Soc. **78** (1995) 3345.
6) S.-E. Park, M. Zipparo and T. R. Shrout: unpublished work.
7) J. Kuwata, K. Uchino and S. Nomura: Ferroelectrics **37** (1981) 579.
8) J. Kuwata, K. Uchino and S. Nomura: Jpn. J. Appl. Phys. **21** (1982) 1298.
9) A. Halliyal, U. Kumar, R. E. Newnham and L. E. Cross: Am. Ceram. Soc. Bull. **66** (1987) 671.
10) H. Jang, S. Oh and J. Moon: J. Am. Ceram. Soc. **73** (1992) 82.
11) M. L. Mulvihill, S.-E. Park, G. Risch, Z. Li, K. Uchino and T. R. Shrout: Jpn. J. Appl. Phys. **35** (1996) 51.
12) R. Gerson and H. Jaffe: J. Phys. & Chem. Solids **24** (1963) 979.
13) D. A. Northrop: J. Am. Ceram. Soc. **21** (1967) 441.
14) B. Jaffe, W. R. Cook, Jr. and H. Jaffe: Piezoelectric Ceramics (Academic Press, New York, 1971) Chap. 10, p. 237.
15) S. L. Swartz, T. R. Shrout, W. A. Schulze and L. E. Cross: J. Am. Ceram. Soc. **67** (1984) 311.
16) F. Chu, I. M. Reaney and N. Setter: J. Am. Ceram. Soc. **78** (1995) 1947.
17) Y. Matsuo: Yogyo-Kyokai-shi, **78** (1970) No. 7, 213.
18) V. A. Bokov and I. E. Myl'nikova: Sov. Phys.-Solid State **3** (1961) 613.
19) Z. Ye and H. Schmid: Ferroelectrics **145** (1993) 83.
20) M. Mulvihill, L. E. Cross and K. Uchino: to be published in Ferroelectrics.

APPENDIX 26

journal

Reprinted from the Journal of the American Ceramic Society, Vol. 80, No. 6, June 1997

J. Am. Ceram. Soc., 80 [6] 1462–68 (1997)

Domain-Related Phase Transitionlike Behavior in Lead Zinc Niobate Relaxor Ferroelectric Single Crystals

Maureen L. Mulvihill,* L. Eric Cross,* Wenwu Cao,* and Kenji Uchino*

International Center for Actuators and Transducers (ICAT), Materials Research Laboratory, The Pennsylvania State University, University Park, Pennsylvania 16802

The relaxor ferroelectric lead zinc niobate ($Pb(Zn_{1/3}Nb_{2/3})O_3$) has been intensively investigated, because of its large dielectric and piezoelectric properties for applications in actuators and transducers. In this study, the *in-situ* behavior of the domains in $Pb(Zn_{1/3}Nb_{2/3})O_3$ single crystals has been observed using optical microscopy in combination with a charge-coupled device (CCD) camera. The temperature of the sample has been cycled between −185°C and +200°C, while applying an electric field of up to ±10 kV/cm. Many characteristics, such as the induction of birefringence, the transition between the microdomains and macrodomains, and the "freeze-in" of the macrodomains, have been optically observed. The optical and dielectric data have been collected and plotted as a function of temperature and electric field. An electric-field–temperature diagram showing five domain-related regions has been proposed. The microdomain-to-macrodomain phase transitionlike behavior seems to be an analog of a martensitic phase transition.

I. Introduction

Lead zinc niobate, $Pb(Zn_{1/3}Nb_{2/3})O_3$ (PZN), single crystals have been studied intensively since it was suggested in 1981 that they would make good candidate materials for actuator and transducer applications, because of their large dielectric constant ($K_{RT} \approx 3000$) and piezoelectric coefficient ($d^*_{33} \approx 1050 \times 10^{-12}$ C/N).[1,2] PZN has a disordered perovskite structure in which the Zn^{2+} and Nb^{5+} ions exhibit short-range ordering on the B site, resulting in regional composition variations on the nanometer scale.[3,4] These compositional fluctuations not only broaden the phase transition but also introduce fine-scale inhomogeneities for the nucleation of microdomains.

The symmetry of PZN is cubic, $Pm3m$, above the Curie temperature and rhombohedral, $3m$, below the transition point. Because a broad phase transition occurs in PZN, a "Curie temperature range," T_m, occurs rather than a Curie temperature as in normal ferroelectrics.[3,5] In this study, the Curie temperature range correlates to the "microdomain formation temperature," T_m. K_{RT} and dielectric loss (tan δ) values are strongly dependent on the measurement frequency (dielectric relaxation). At 1 kHz, T_m occurs at ~140°C with a K_{RT} maximum of 56000 along the ⟨111⟩.[6]

The broad phase transition and frequency dispersion that are exhibited by relaxor ferroelectrics such as PZN have a strong link to the configurations of the ferroelectric microdomains. Static ferroelectric domains have been observed by several methods, such as optical microscopy on acid-etched samples[7] or transmission electron microscopy (TEM) on mechanically thinned samples.[4] However, the dynamic observation of switching domains under an applied electric field or with changing temperature has been difficult experimentally, which has resulted in limited research efforts.[8–11]

An optical technique has been used to explore the growth of macrodomains (>0.1 μm) from microdomains (~20 nm and 0.1 μm) in PZN single crystals along the ⟨111⟩ direction, as functions of temperature and applied electric field. The measured dielectric constant d^*_{33} and tan δ, as a function of temperature for a poled sample, are compared to the optically observed macrodomain motion in an attempt to develop a fundamental understanding of the relaxor behavior in PZN. The focus of this paper is to develop an electric-field–temperature diagram that describes the domain behavior in PZN. Optically and electrically measured characteristics will be used to develop the different phase fields.

II. Experimental Procedure

Single crystals of PZN were grown using a flux method with excess lead oxide.[6] The crystals were light brown, with sizes ranging from 0.5 mm to 1 cm on an edge. The Laué X-ray technique was used to precisely determine the [111] directions in the crystals. The crystals were then sliced, ground to a thickness of 100 μm, and polished with diamond paste until a near-mirror finish was obtained on both surfaces. The samples were sputtered on the top and bottom surfaces with a very thin, semitransparent gold layer, as shown in Fig. 1. Silver leads were attached to the sample with air-dry silver paste.

The domain patterns were observed by polarized light that was transmitted through the single crystal along the ⟨111⟩, the spontaneous polarization direction. A high-resolution charge-coupled device (CCD) camera was attached to a petrographic TEM microscope (Nikon, Tokyo, Japan) that was connected to a monitor and videocassette recorder (VCR), as illustrated in Mulvihill *et al.*[9] Polarizing light microscopy was used to observe the domains at magnifications of up to 1300× through the birefringence difference between the domains. The temperature-controlled sample stage, in conjunction with the long working distance of the objective lens, allowed an electric field to be applied across the sample while cycling the temperature. The electric field was applied as a triangular wave at 0.05 Hz with a maximum field level of ±10 kV/cm, and the temperature was cycled between 200°C and −185°C. The moving domain walls and domain patterns were instantaneously recorded by the VCR and observed on the monitor.

III. Results and Discussion

(1) Development of Electric-Field–Temperature Diagram

The microscope system was used to observe many characteristics of the PZN domain structure, such as the birefringence change, the microdomain-to-macrodomain transition, and the

W. H. Huebner—contributing editor

Manuscript No. 191564. Received September 3, 1996; approved December 13, 1996.

Supported by the Office of Naval Research under Grant Nos. N00014-91-J-4145 and N00014-92-J-1501.

Based in part on the thesis submitted by M. L. Mulvihill for the Ph.D. degree from the Department of Materials, The Pennsylvania State University, University Park, PA, 1996.

*Member, American Ceramic Society.

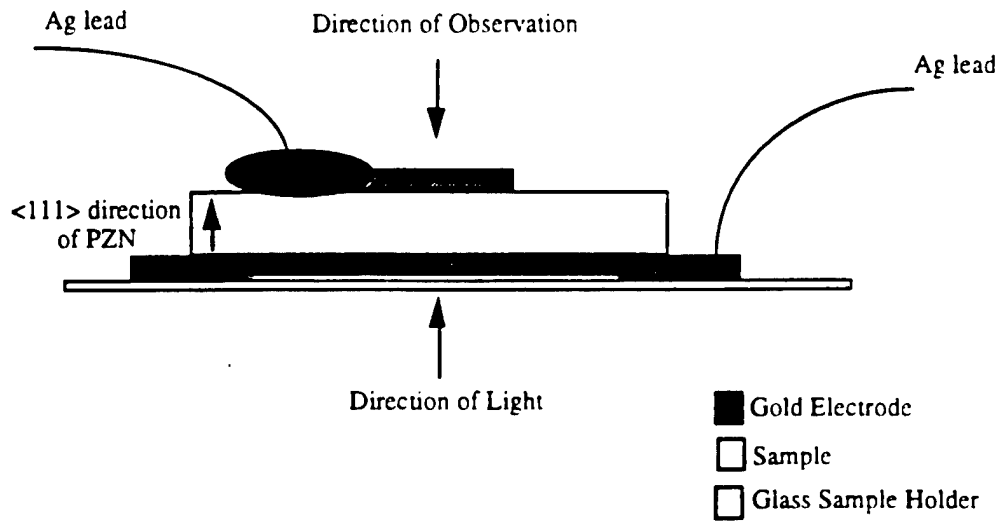

Fig. 1. Schematic of the side view of an electroded PZN sample

"freeze-in" temperature. The magnitude of the electric field has been plotted against temperature using the optically observed characteristics and measured dielectric data, as shown in Fig. 2, which identifies five domain-related regions.

Because the birefringence changes were caused by the alignment of the microdomains and the peak in the permittivity (at 0.05 Hz) was caused by the onset of microdomains, it was assumed that these two anomalies marked the first phase transition when the temperature was decreased. It is the boundary between the paraelectric and ferroelectric microdomain regions, which will be discussed in Section III*(1)(A)*.

The second transition occurs at the temperature where the macrodomains appear when field cooling is applied and disappear when field heating is applied, which will be discussed in Section III*(1)(B)*. This transition separates the ferroelectric microdomain region from the ferroelectric macrodomain region and corresponds to the shoulderlike anomaly of the permittivity curve. Section III*(1)(C)* describes the behavior of the switching macrodomains, as a function of the electric field and temperature.

The third transition occurs at the domain freeze-in temperature, which will be discussed in Section III*(1)(D)*. When the field heating is applied, the unfreezing temperature occurs at slightly higher temperatures. (The freeze-in temperature that is referenced in this study corresponds to the temperature when the electric field cannot switch the macrodomains anymore.) The transition temperature between the ferroelectric macrodomain region and the ferroelectric frozen domain region shifts to lower temperatures as the magnitude of the electric field increases. In the vicinity of this transition temperature, the dispersion of tan δ is observed.

(A) Boundary between Paraelectric Region ↔ Ferroelectric Microdomain Region: The single crystals used in this study were beige in the paraelectric region and retained this

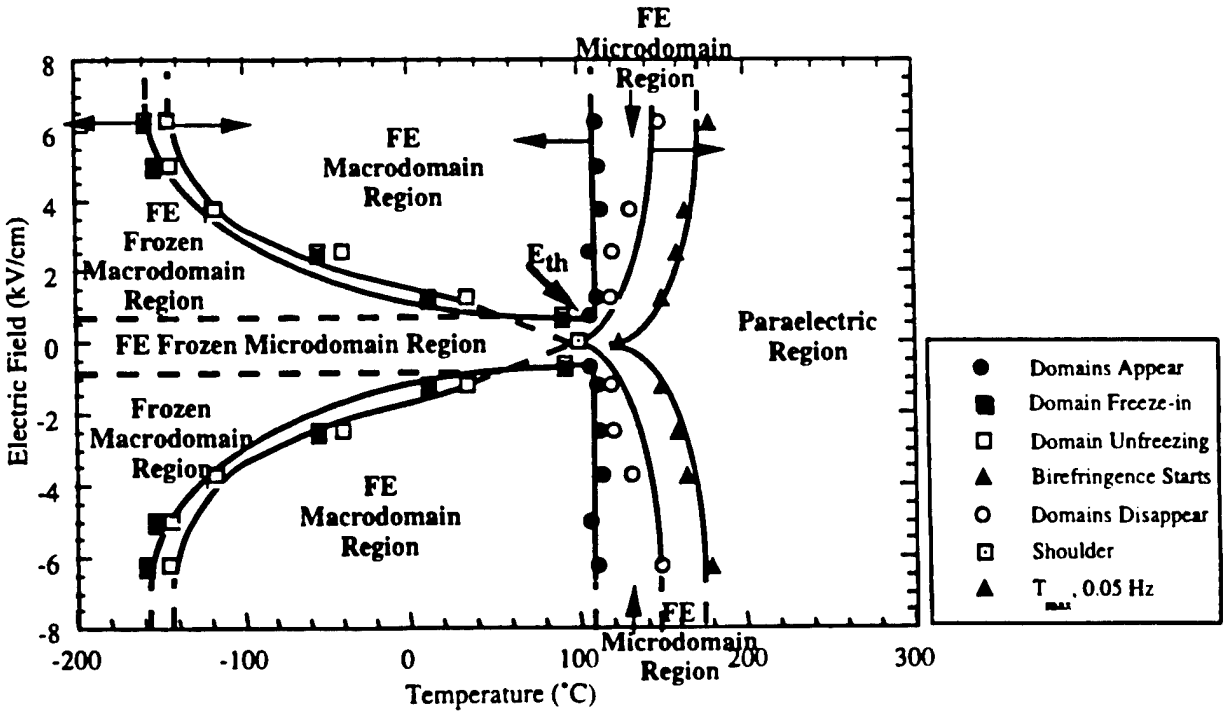

Fig. 2. Suggested five domain-related electric-field–temperature diagram, as positive and negative electric fields are plotted, as a function of temperature.

color as the temperature was cycled between 200°C and −185°C without an applied electric field. Under an applied electric field (0.05 Hz) near the microdomain formation temperature (T_m), the color of the single crystal changed to a combination of blues and browns. The macroscopic birefringence that has been detected as color changes in the crystal was caused by the microdomains orienting with the electric field. As the magnitude of the ac field increased, the microdomain formation temperature (the temperature at which the birefringence appeared) increased. The first boundary was determined by observing birefringence as a function of the electric field and temperature. No temperature hysteresis was observed at the paraelectric ↔ ferroelectric microdomain boundary, represented by solid triangles in Fig. 2.

The position of the paraelectric ↔ ferroelectric microdomain boundary was supported by the K_{RT} and tan δ behavior for an unpoled (Fig. 3) and poled (Fig. 4) PZN single crystal. The dielectric behaviors were identical for both the poled and unpoled samples at temperatures of $>T_m$. However, when T_m, as a function of frequency, for the unpoled sample was plotted and then extrapolated to a frequency of 0.05 Hz. T_m was ~124°C. The frequency-dependent transition temperature corresponded to the paraelectric ↔ ferroelectric microdomain boundary, represented by a solid triangle at 124°C (for 0.05 Hz) in Fig. 2.

(B) Boundary between Ferroelectric Microdomains ↔ Ferroelectric Macrodomains: The ferroelectric microdomain → macrodomain boundary temperature was that at which the macrodomains were first observed with an electric field, represented by solid circles in Fig. 2. This temperature (~110°C) was almost constant for all applied electric fields. Macrodomains were not observed with fields below ±0.7 kV/cm, the threshold field (E_{th}) of PZN. The threshold field is necessary to induce the microdomain-to-macrodomain transition. A threshold field also was observed in $Pb(Mg_{1/3}Nb_{2/3})O_3$ (PMN).[12]

When field heating was applied, the ferroelectric microdomain ← macrodomain boundary, which was characterized by the disappearance of the macrodomains, occurred at slightly higher temperatures, represented by the open circles in Fig. 2. The boundary increased to higher temperatures as the electric-field level increased.

The dielectric behavior that is represented in Figs. 3 and 4 also supports the ferroelectric microdomain ↔ macrodomain boundary. Frequency dispersion, which is exhibited by the unpoled sample, did not occur in the poled sample below this temperature. The temperature region (~100°−120°C) where K_{RT} had a nondispersive frequency behavior appeared as a "shoulder" in the poled sample, as shown in Fig. 4. Also, the dielectric loss (tan δ) decreased drastically in this temperature region. The decrease in tan δ and the shoulder in the poled sample were caused by the macrodomain generation by the +15 kV/cm poling field. However, in the unpoled sample, the microdomains had not aligned and the variation in the orientations of the microdomains caused frequency dispersion in the dielectric data. This temperature region, from the start of the frequency dispersion (~124°C) to 100°C, corresponds to the ferroelectric microdomain region. The shoulder corresponds to the critical temperature (100°C) that signifies the ferroelectric microdomain ↔ macrodomain boundary.

(C) Ferroelectric Macrodomain Behavior: The macrodomain region occurs at temperatures of <110°C at >0.7 kV/cm and remains until the macrodomains are not switchable with the electric field anymore. Several interesting macrodomain behaviors were observed as a function of the electric field and temperature.

Figures 5(A)–(D) are micrographs of the domain patterns of PZN single crystal at 100°C as the electric field increased. The domain wall density increased as the electric field was increased from 1.3 kV/cm to 5 kV/cm. The length of macrodomains elongated and narrowed as the electric field increased. The domain modulations were ~5 μm in size and lenticular in shape. The domain walls oriented along [011] directions. None of the samples that were examined achieved a monodomain state, even when a dc bias of up to +15 kV/cm was applied, which is similar to monodomain behavior that has been reported in PMN single crystals[12] but contrary to later PMN results.[8]

Figures 6(A)–(D) demonstrate the electric-field dependence of the domain density change during 15 s of a 20 s cycle at 60°C. In each of these figures, the direction of the electric field is normal to the micrograph. The domains seem to have equivalent numbers and structures in the region between +5 kV/cm and −5 kV/cm, as shown in Figs. 6(A) and (C), respectively. Such a result is expected from the crystallographic symmetry requirements of PZN.

(D) Boundary between Ferroelectric Macrodomains ↔ Frozen Ferroelectric Macrodomains: At temperatures that were electric-field dependent, the macrodomains became nonswitchable. This temperature is referred to as the macrodomain freeze-in temperature, represented by solid squares in Fig. 2.

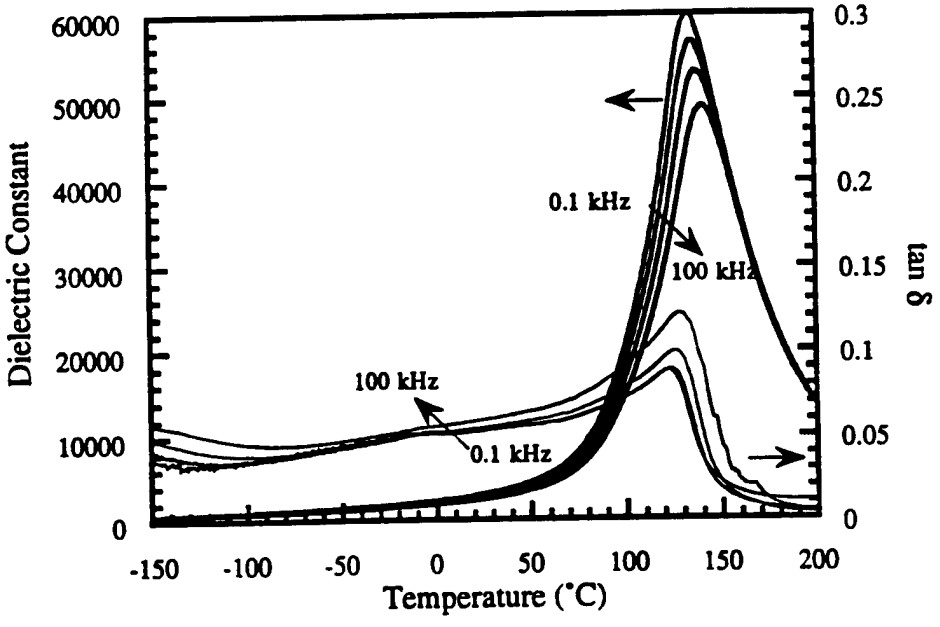

Fig. 3. Permittivity versus temperature for an unpoled PZN single crystal at 100 Hz, 1kHz, 10 kHz, and 100 kHz.

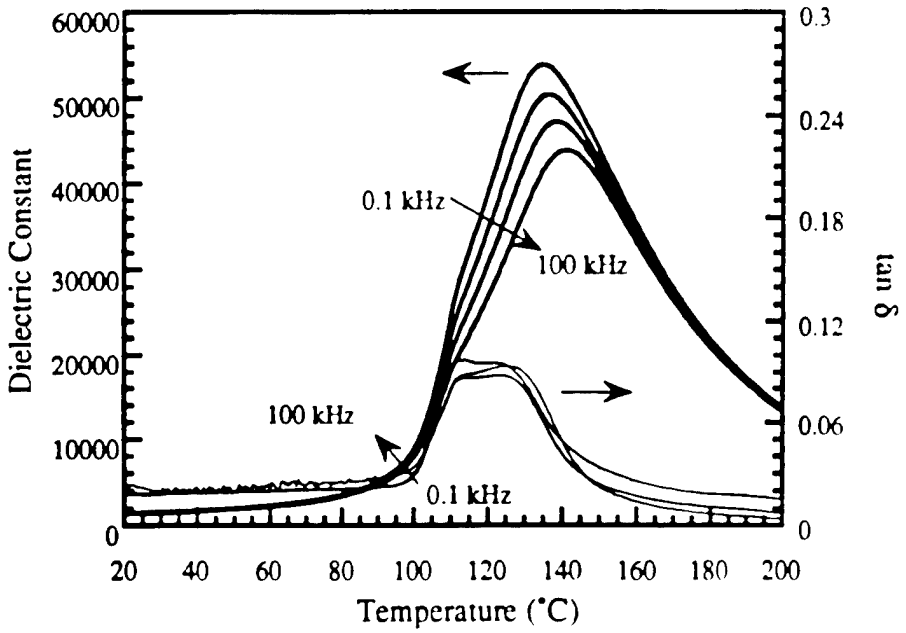

Fig. 4. Permittivity versus temperature for a poled PZN single crystal at 100 Hz, 1 kHz, 10 kHz, and 100 kHz.

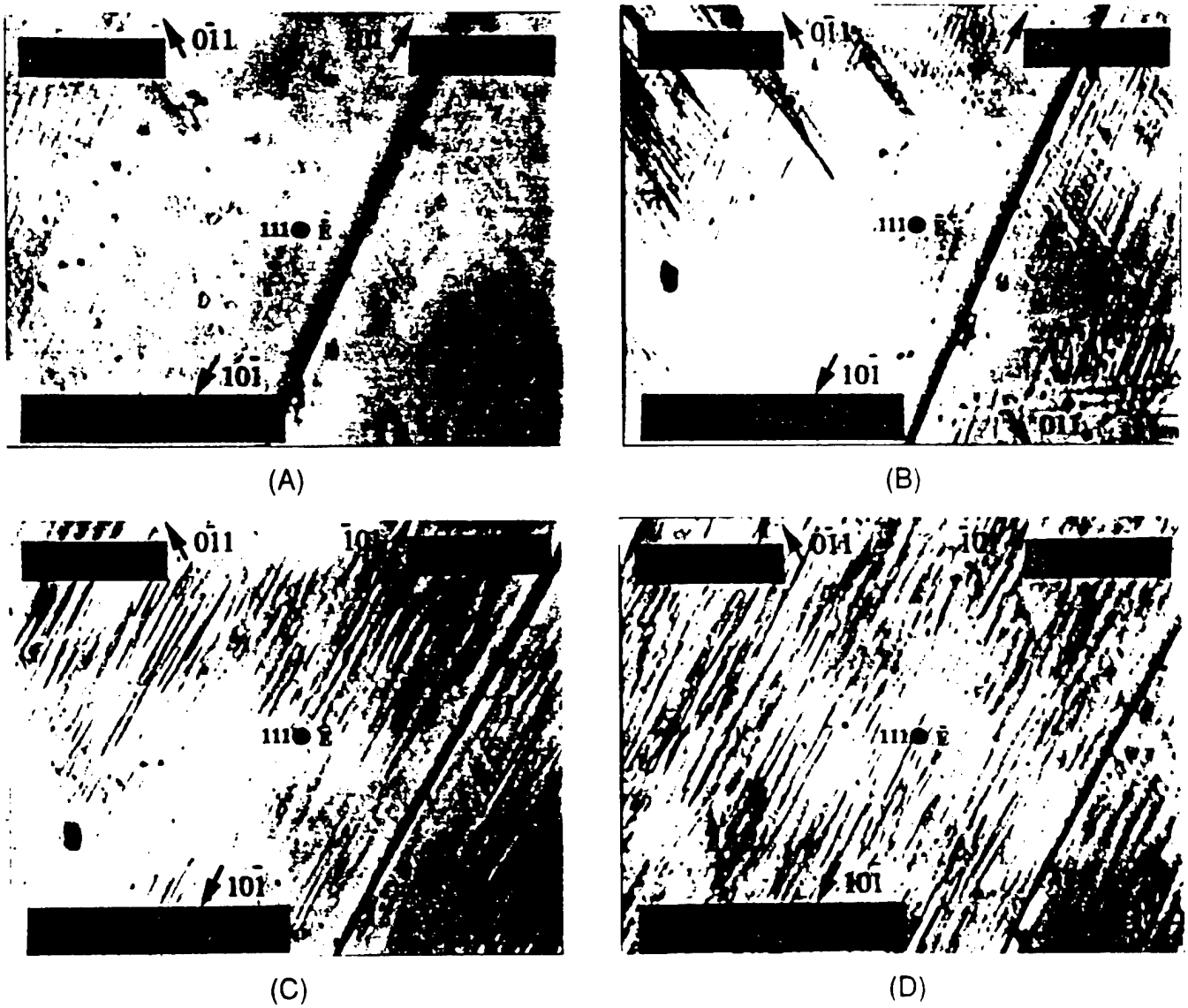

Fig. 5. Four frames from the videotape that represent changes in domain density at 100 C with increasing electric field (A) 1.3, (B) 2.5, (C) 3.8, and (D) 5.0 kV/cm.

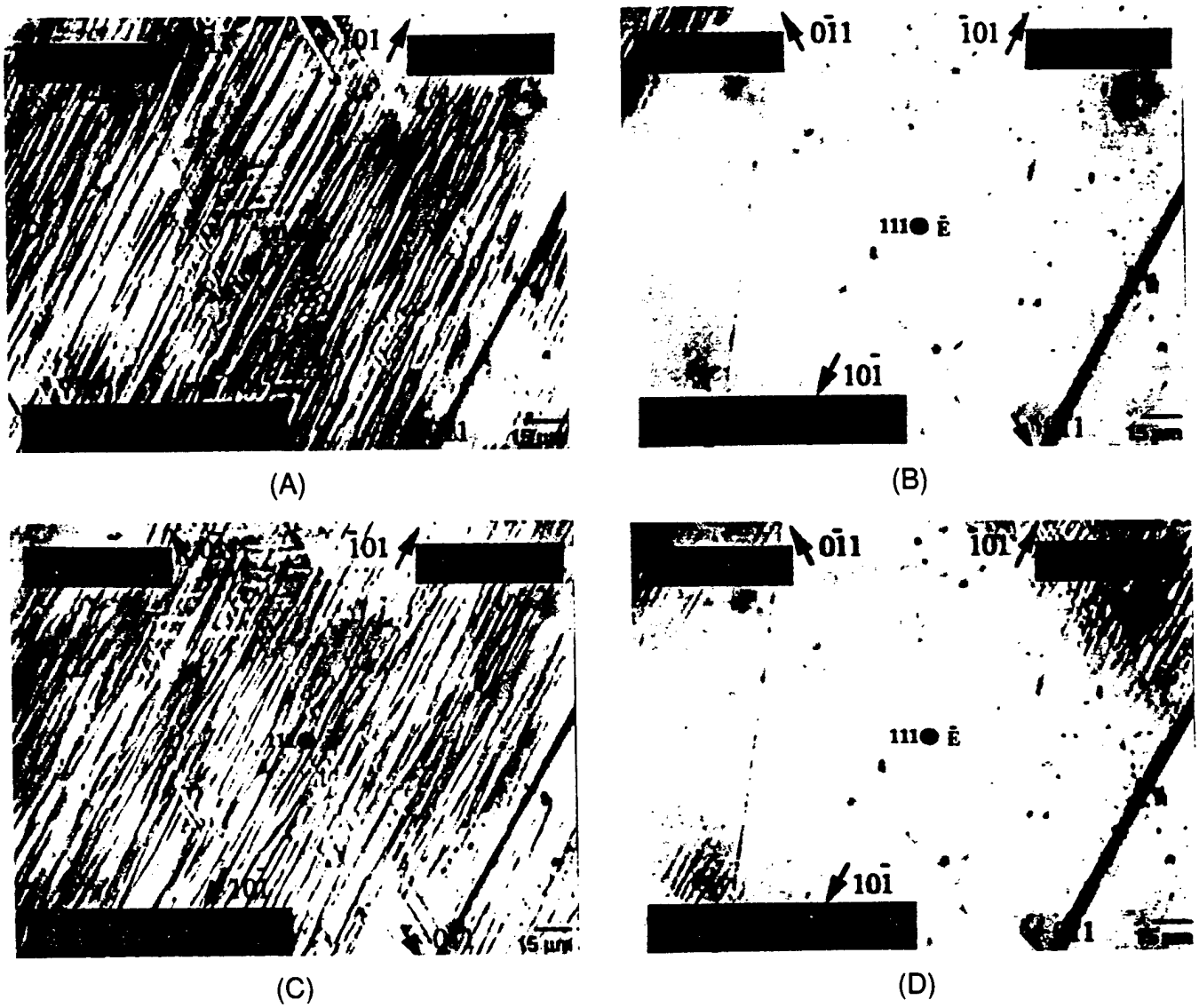

Fig. 6. PZN single crystal during 15 s of a 20 s cycle at 60°C ((A) 1 s, +5 kV/cm; (B) 5 s, 0 kV/cm; (C) 10 s, −5 kV/cm; and (D) 15 s, 0 kV/cm).

The dispersion of the tan δ value that is observed below −70°C in Fig. 3 may be attributed to the domain freeze-in phenomenon. The freeze-in temperature marked the ferroelectric macrodomain → frozen macrodomain boundary. When field heating was applied, the thawing or "unfreezing" temperature, represented by open squares in Fig. 2, occurred at temperatures slightly higher than the freeze-in temperature, indicating a slight temperature hysteresis. The unfreezing temperature represented the ferroelectric macrodomain ← frozen macrodomain boundary. The behavior of the electric-field dependence was approximately the same when field heating and cooling were applied.

At temperatures just above the freeze-in temperature, the single crystal seemed to undergo a domain structural transition. The domains split into narrower domain segments. The width of each segment decreased as the temperature decreased. The segments switched synchronistically. At ±3 kV/cm, the domain switching was "frozen in" at −50°C. However, at ±5 kV/cm, the freeze-in temperature occurred at −150°C. Figures 7(A)–(D) show the domain configuration at +5 kV/cm (ac field of ±5 kV/cm) as the temperature was decreased from 26°C down to −154°C. For this sample, as the temperature decreased, the number density of domains also decreased.

The polarization-versus-electric-field (P vs E) data, shown in Fig. 8, supported the optically observed freeze-in temperature for PZN single crystals. For a normal ferroelectric, the P vs. E curve has an "S"-shaped hysteresis. With PZN, the P vs. E curve developed a rounded rhombic loop as the temperature decreased. As the electric field increased, the rhombic loop was maintained to lower temperatures, as shown in Figs. 8(A)–(D). At the freeze-in temperature, the loop closed as spontaneous polarization vanished. From Fig. 8, it can be observed that, at ±5 kV/cm, the rhombic loop closed between −125°C and −175°C, which is in the same temperature range as the optically observed domain freeze-in temperature of −150°C plotted in Fig. 2. However, even at −175°C, the P vs. E curve for ±10 kV/cm has a slight rhombic shape, which signifies that the sample was still able to switch.

(E) Ferroelectric Frozen Microdomain Region: At temperatures of <100°C and electric fields between +0.7 kV/cm and −0.7 kV/cm, a fifth domain-related region is proposed. This region is called the ferroelectric frozen microdomain region. Because the size of the microdomains is below the resolution of the optical microscope, this region has been extrapolated: therefore, it is represented by the dashed lines in Fig. 2.

(2) Phase Transition Analogy between PZN Microdomains and Platelike Martensite Regions

The optically observed domain behavior in PZN seems to be analogous to a martensitic phase transition (MPT). This idea was suggested for the domain behavior of PMN.[12] The MPT is dispersive and initiates at a temperature M_s, which is the martensite start, and stops at a temperature M_f, which is the martensite finish.[12–14] The martensite phase begins far above the

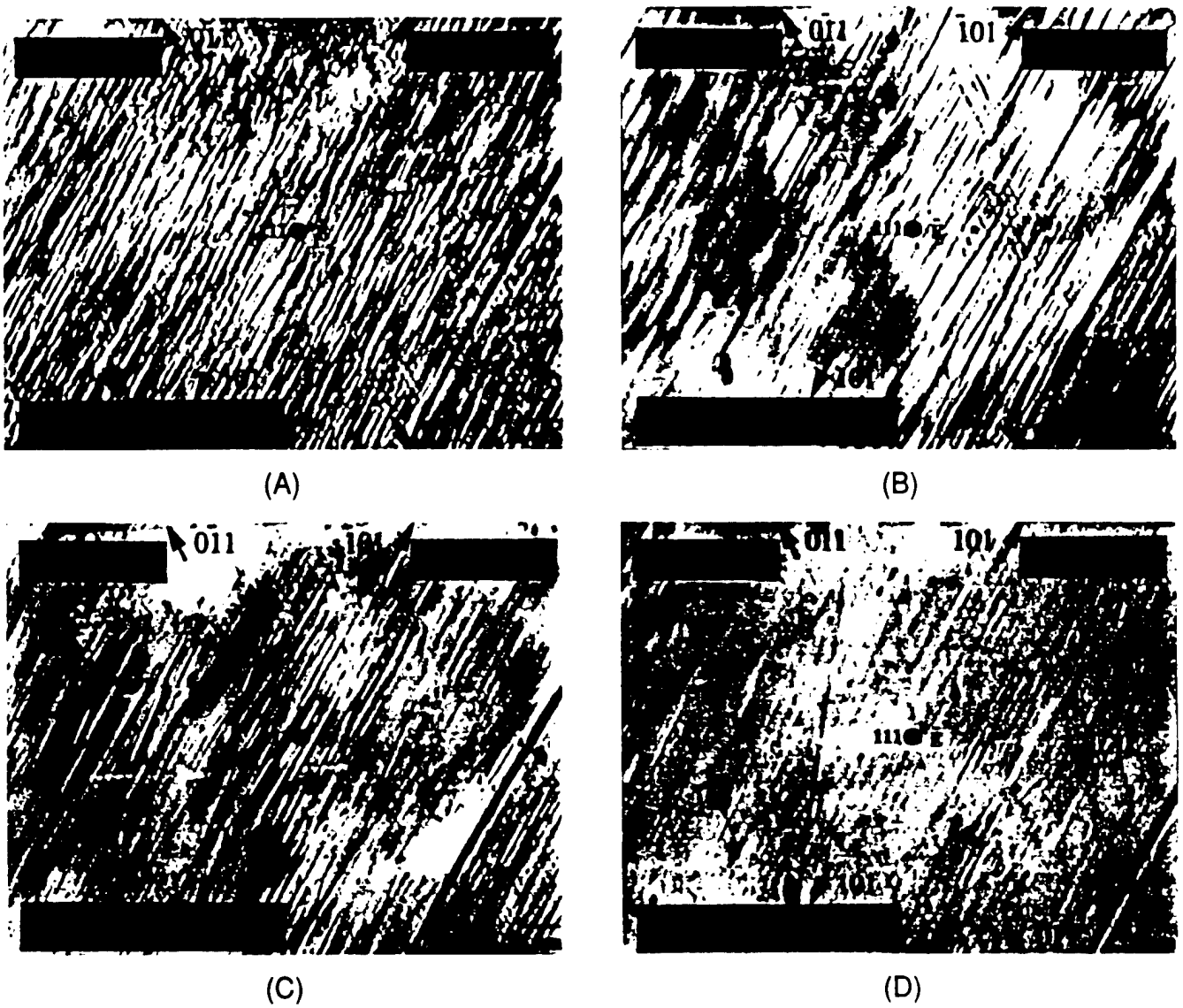

Fig. 7. Density of domains, decreased as temperature decreases at +5 kV/cm ((A) 24°, (B) −53°, (C) −116°, and (D) −154°C).

global transition temperature by the formation of platelike martensitic regions in the parent phase. The platelike martensitic regions form randomly in the structure.[13] The growth of these regions occurs by the formation of new plates as temperature decreases rather than by increasing the size of already-formed plates. The M_s temperature of a MPT can be shifted to higher temperatures with increasing stress,[13] which could be understood from the formation of the local stress concentration.[15,16] Another property of a MPT is a large temperature hysteresis between heating and cooling.

The behavior of PZN microdomains that form between the paraelectric region and macrodomain region under applied electric field seems to be an analog of the platelike martensitic regions in a MPT. In Section III(*1*)(*A*), the onset of birefringence, as well as the peak in the permittivity, were the first sign of the alignment of the microdomains in the nonpolar region. The microdomains and nonpolar regions correspond to the platelike martensite regions and parent phase, respectively. The temperature of the observed birefringence (beginning of microdomains) as a function of electric field, shown in Fig. 2, is analogous to the M_s temperature (beginning of platelike regions) in a MPT. Also, the temperature at which birefringence occurs notably increases as the electric field increases, which also is similar to a stress-induced increase of the M_s in a MPT. The temperature where the first macrodomains are observed at a particular electric field is analogous to the M_f temperature in a MPT where all the parent phase has been transformed. The transition temperature range (M_s to M_f) and the dispersion of a MPT are similar to a dispersive and broad relaxor ferroelectric transition. Figure 2 shows a temperature hysteresis between the microdomain ↔ macrodomain transition when heating and cooling is applied. A temperature hysteresis also is a property of a MPT. Short-range order exists in each microdomain; however, the microdomains are randomly distributed over the entire structure,[4] similar to the random formation of the platelike martensitic regions.

There are many observed behaviors of the microdomains in PZN that seem to be analogous to martensite regions in metal alloys. Further study is necessary to determine if this MPT modeling can be applied to the relaxor ferroelectric microdomain behavior.

IV. Summary

Five domain-related regions have been shown to exist in PZN in an electric-field–temperature diagram. The boundaries of these regions were determined by optical observations of the domain configurations. These results suggest that the temperature at which the initial birefringence occurs increases as the electric field increases. This temperature can be considered as the border between the paraelectric and ferroelectric microdomain regions. The transition from ferroelectric microdomains to ferroelectric macrodomains when field cooling is applied occurs at ~130°C and is independent of the electric field. When

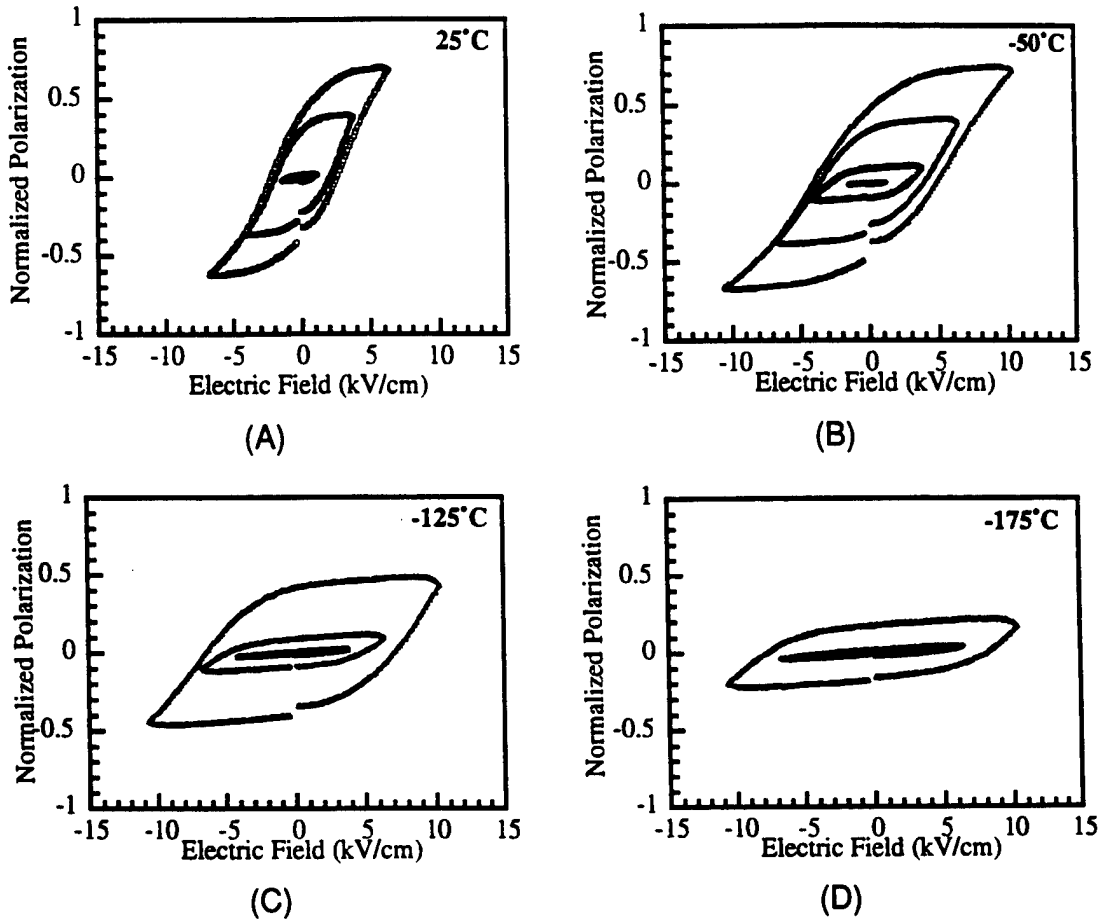

Fig. 8. Polarization as a function of electric field for several field magnitudes at decreasing temperature ((A) 25°, (B) −50°, (C) −125°, and (D) −175°C).

the dielectric constant of an unpoled PZN single crystal is compared to that of a poled sample, a shoulder occurs in the dielectric constant of the poled sample. The shoulder at 100°C for the poled sample is caused by the microdomain alignment. This temperature corresponds to the optically observed microdomain-to-macrodomain transition. The freeze-in temperature, when field cooling is applied, and the unfreezing temperature, when field heating is applied, is optically observed and decreases in temperature as the electric field increases. This observation is confirmed by the P vs. E curves at various temperatures and electric fields. As the freeze-in temperature is attained, the shape of the P vs. E curve changes from a ferroelectric "S" shape to a closed loop, which was accompanied by the disappearance of spontaneous polarization. The microdomain region behaves analogously to the platelike martensite regions; therefore, one might explore the possibility of using some of the well-documented studies on martensite to study the ferroelectrics relaxor systems.

References

[1]J. Kuwata, K. Uchino, and S. Nomura, "Phase Transitions in the $Pb(Zn_{1/3}Nb_{2/3})O_3$–$PbTiO_3$ System," *Ferroelectrics*, 37, 579–82 (1981).

[2]J. Kuwata, K. Uchino, and S. Nomura, "Dielectric and Piezoelectric Properties of 0.91PZN–0.10PT Single Crystals," *Jpn. J. Appl. Phys.*, 21, 1298–302 (1982).

[3]Y. Yokomizo, T. Takahashi, and S. Nomura, "Ferroelectric Properties of $Pb(Zn_{1/3}Nb_{2/3})O_3$," *J. Phys. Soc. Jpn.*, 28, 1278–84 (1970).

[4]C. A. Randall and A. S. Bhalla, "Nanostructure–Property Relations in Complex Lead Perovskites," *Jpn. J. Appl. Phys.*, 29, 327–33 (1990).

[5]J. Kuwata, K. Uchino, and S. Nomura, "Diffuse Phase Transition in Lead Zinc Niobate," *Ferroelectrics*, 22, 863–67 (1979).

[6]M. L. Mulvihill, S. E. Park, G. A. Risch, Z. Li, K. Uchino, and T. R. Shrout, "The Role of Processing Variables in the Flux Growth of PZN–PT Relaxor Ferroelectric Single Crystals," *Jpn. J. Appl. Phys.*, 35, 3984–90 (1996).

[7]G. Arlt and P. Sasko, "Domain Configuration and Equilibrium Size of Domains in $BaTiO_3$ Ceramics," *J. Appl. Phys.*, 51 [9] 4956–60 (1980).

[8]Z. G. Ye and H. Schmid, "Optical, Dielectric and Polarization Studies of the Electric Field-Induced Phase Transition in PMN," *Ferroelectrics*, 145, 83–108 (1993).

[9]M. L. Mulvihill, L. E. Cross, and K. Uchino, "Low-Temperature Observation of Relaxor Ferroelectric Domains in Lead Zinc Niobate," *J. Am. Ceram. Soc.*, 78 [12] 3345–51 (1995).

[10]M. L. Mulvihill, Z. Li, K. Uchino, and W. Cao, "*In-situ* Observation of the Domain Configurations During the Phase Transitions in Barium Titanate," *Philos. Mag. B*, 74, 25–36 (1996).

[11]K.-Y. Oh, K. Uchino, and L. E. Cross, "Optical Study of Domains in $Ba(Ti,Sn)O_3$ Ceramics," *J. Am. Ceram. Soc.*, 77 [11] 2809–16 (1994).

[12]G. Schmidt, "Diffusive Phase Transitions," *Ferroelectrics*, 78, 199–206 (1988).

[13]R. E. Reed-Hill, *Physical Metallurgy Principles, 2nd Ed.*; Ch. 16 ("Deformation Twinning and Martensite Reactions"). PWS Publishers, Boston, MA, 1973.

[14]D. A. Porter and K. E. Easterling, *Phase Transformations in Metals and Alloys*; Ch. 6 ("Diffusion Transformations"). TJ. Press, U.K., 1981.

[15]W. Cao and J. A. Krumhansl, "Continuum Theory of 4 mm–2 mm Proper Ferroelastic Transformation Under Inhomogeneous Stress," *Phys. Rev. B: Condens. Matter*, 42 [7] 4334–40 (1990).

[16]W. Cao, J. A. Krumhansl, and R. J. Gooding, "Defect-induced Heterogeneous Transformations and Thermal Growth in Athermal Martensite," *Phys. Rev. B: Condens. Matter*, 41, 11319–27 (1990). □

APPENDIX 27

Relaxor-based single crystal materials for ultrasonic transducer applications

Seung-Eek Park[a], Patrick D. Lopath[b], Kirk K. Shung[b], and Thomas R. Shrout[a]
[a] Materials Research Laboratory, The Pennsylvania State University, University Park, PA 16802
[b] Department of Bioengineering, The Pennsylvania State University

ABSTRACT

Relaxor ferroelectric single crystals of $Pb(Zn_{1/3}Nb_{2/3})O_3$ (PZN), $Pb(Mg_{1/3}Nb_{2/3})O_3$ (PMN) and their solid solutions with normal ferroelectric $PbTiO_3$ (PT) were investigated for ultrasonic transducer applications. Crystals offer adjustable properties not only by compositional tailoring but also by domain state engineering associated with different crystallographic orientation, which is not achievable in polycrystalline materials. Longitudinal coupling coefficients (k_{33}) as high as 94 % and dielectric constants (K_3^T) in the range of 3500-6000 were achieved with low dielectric loss (<1%) using <001> oriented rhombohedral crystals of (1-x)PZN-xPT and (1-y)PMN-yPT, where x<0. 09 and y<0. 35. Dicing direction as well as poling direction were critical for high coupling under laterally clamped condition. Dicing parallel to the (001) yields 90% of laterally clamped coupling (k_{bar}) out of 94% longitudinal coupling (k_{33}) for PZN-8%PT. On the other hand, samples diced parallel to (110) exhibited no dominant mode present. Thickness coupling (k_T) as high as 64% and low dielectric constant (K_3^T) < 600 with low loss (<1%) could be achieved using tetragonal crystals of (1-x)PZN-xPT and (1-y)PMN-yPT, where x>0. 1 and y>0. 4. The performance gains associated with these ultra-high coupling coefficients and range of dielectric constants are evident in relation to broader bandwidth and electrical impedance matching. Specifically, rhombohedral crystals offer the possibility of extremely broad bandwidth devices for transducer arrays and tetragonal crystals for single element transducers. Transducer simulation was performed using the KLM model. The pulse/echo response simulated a 124% bandwidth subdiced array element with a center frequency of 10 MHz. An optimized array design of the same geometry constructed of PZT 5H displays a 87% bandwidth.

Keywords: relaxor ferroelectrics, single crystal, crystal orientation, bandwidth, impedance matching.

1. INTRODUCTION

Piezoelectric ceramics are currently the material of choice for ultrasonic transducer applications offering relatively high coupling (kij), a wide range of dielectric constants (K), and low dielectric loss. These merits translate into transducer performance in the form of relatively high sensitivity, broad bandwidth, impedance matching and minimal thermal heating. Among piezoelectric ceramics, $Pb(Zr_{1-x},Ti_x)O_3$ (PZT) ceramics have been the mainstay for high performance transducer applications. Compositionally, PZT ceramics lie near the morphotropic phase boundary (MPB) between the tetragonal and rhombohedral phases, as depicted in Figure 1. MPB compositions have anomalously high dielectric and piezoelectric properties as a result of enhanced polarizability arising from the coupling between two equivalent energy states, i. e. the tetragonal and rhombohedral phases, allowing optimum domain reorientation during the poling process. Further modifications using acceptor and donor dopants give us the wide range of piezoelectric compositions we have today. Alternative MPB systems can be found in relaxor-based ferroelectrics and their solid solutions with $PbTiO_3$ (PT). Lead based relaxor materials are complex perovskites with the general formula $Pb(B_1B_2)O_3$, (B_1=Mg^{2+}, Zn^{2+}, Ni^{2+}, Sc^{3+} . . . , B_2=Nb^{5+}, Ta^{5+}, W^{6+} . . .). Characteristic of relaxors is a broad and frequency dispersive dielectric maxima.[1]

Dielectric and piezoelectric properties for selected PZT's and relaxors-PT systems are summarized in table 1. Some relaxor-PT compositions such as modified $Pb(Sc_{1/2}Nb_{1/2})O_3$ - $PbTiO_3$ (PSN-PT) seem to possess superior dielectric and piezoelectric properties compared to that of PZT ceramics. However, if being analyzed with respect to the ferroelectric transition temperature designated by Tc (the temperature at which the material transforms from the prototypical non-ferroelectric to ferroelectric phase being associated with a spontaneous polarization and large dielectric anomaly) no one type of ceramic offers significant advantages in overall transducer performance. Enhanced piezoelectric activity of MPB-based ceramics by compositionaly adjusting the Curie temperature (Tc) downward relative to room temperature comes with the expense of more temperature dependent properties, and less polarization stability, i.e. aging and loss of piezoelectric activity.

Park 1/3

Table 1 Reported Dielectric and Piezoelectric Properties for selected PZT and Relaxor Binary Systems

Form	*Materials*	k_p	k_t*	k_{33}	d_{33} *(pC/N)*	K_3^T	*Tc (°C)*	*Ref.*
	PZT-MPB Composition							
Ceramics (poly-crystalline)	PZT 53/47	0. 52		0. 67	220	~800	360	3
	Modified PZTs							
	PZT-4 (Navy I)	0. 58	0. 51	0. 70	289	1200	330	4
	PZT-8 (Navy III)	0. 50	0. 44	0. 70	220	1000	300	4
	PZT-5 (Navy II)	0. 60	0. 49	0. 70	400	2000	360	4
	PZT 5H (Navy VI)	0. 65	0. 50	0. 75	590	3500	190	4
	Relaxor-PT MPB Compositions							
	0. 7PMN-0. 3PT	0. 50			670	5000	145	5
	0. 67PMN-0. 33PT	0. 63		0. 73	690	5000	160	5
	0. 60PMN-0. 40PZT(40/60)	0. 50			-	2370	170	6
	0. 55PST-0. 45PT	0. 61		0. 73	655	4000	205	7
	0. 575PSN-0. 425PT	0. 66	0. 55	0. 74	389	1550	260	8
	0. 575PSN-0. 425PT (1%Nb doped)	0. 69	0. 52	0. 76	504	2540	248	8
	0. 575PSN-0. 425PT (2% Sc doped)	0. 63	0. 53	0. 72	359	1480	260	8
	0. 58PSN-0. 42PT	0. 71	0. 56	0. 77	450	2200	260	9
	0. 5PNN-0. 5PZT(35/65)	0. 45	-		370		150	10
	0. 87PZN-0. 05BT-0. 08PT	0. 52	0. 49		640	5200	150	11
Single Crystals	95PZN-5PT			0. 86	~1500	4000	160	12
	91PZN-9PT			0. 92	~1500	2200	190	13,14
	89PZN-11PT			0. 92	620	1000	200	12
	70PMN-30PT				~1500	4000	150	15
	60PMN-40PT				~1500		170	15

* Reported coupling factors often do not follow the simplistic equation, $k_{33}^2 \sim k_p^2 + k_T^2 - k_p^2 * k_T^2$. Based on the difficulties in accurately determining k_T, the confirmation of values should be made.

Further details on the relationship between dielectric/piezoelectric properties and Curie temperature (Tc) can be found in the article by S. -E. Park et al.[2]

Though Relaxor-PT ceramics do not offer enhanced dielectric and piezoelectric properties comparable to PZT ceramics of similar T_Cs, it is the single crystal form of relaxor-PT's that exhibits ultrahigh piezoelectric properties not currently available with piezoelectric MPB ceramics. This key distinction was first realized by Nomura and co-workers[13,14] for MPB compositions of $Pb(Zn_{1/3}Nb_{2/3})O_3$ - $PbTiO_3$ (PZN-PT) systems with d_{33} and k_{33} values of 1500 pC/N and 90%, respectively, followed by the crystal growth of $Pb(Mg_{1/3}Nb_{2/3})O_3$ - $PbTiO_3$ (PMN-PT)[15] and $Pb(Sc_{1/2}Nb_{1/2})O_3$ - $PbTiO_3$ (PSN-PT)[16]. In general, most $Pb(B_1,B_2)O_3$-PT crystals can be grown by high temperature solution growth using Pb-based fluxes. Distinctly increased dielectric and piezoelectric properties of $Pb(B_1,B_2)O_3$-PT crystals are compared with ceramics in table 1. Though clearly attractive, few systematic studies have followed.

Merits of the single crystal form itself include the possibility of "optimum" crystallographic cuts as analogous in AT and BT cuts in quartz crystals for a zero temperature coefficient of resonance, and X-cut in $LiTaO_3$ or 128° rotated Y cut in $LiNbO_3$ crystals for optimum conditions including surface acoustic speed and coupling[17]. Another advantage of the single crystal form lies in terms of microstructural issues associated with polycrystalline ceramics, including grain size, porosity, etc. These can be also ignored removing scaling limitations, particularly relevant to high frequency transducers.

It is the objective of this work to systematically evaluate crystal structural property relationships and to present ongoing investigation on the theoretical designs using these single crystal materials. Based on the commonalties inherent to Relaxor-

PT systems[18,19] our research was limited to two representative systems of PZN-PT and PMN-PT. Though PMN-PT MPB crystals exhibit piezoelectric properties comparable with PZN-PT, more focus was given to the PZN system owing to its relatively lower PT content for MPB. This allows more uniform crystal growth of these solid solution materials. Details of crystal growth for these systems are given in references. [20,21]

2. DIELECTRIC AND PIEZOELECTRIC PROPERTIES OF RELAXOR-BASED SINGLE CRYSTALS

Dielectric, piezoelectric, and electromechanical coupling coefficients for the various crystals are reported in table 2 and table 3. Parameters relevant to transducer designs, including dielectric loss, frequency constant (N), elastic compliance (s_{ij}), mechanical Q etc. , are also reported.

As reported in table 2, large coupling coefficients (k_{33}) and large piezoelectric coefficients (d_{33}) were found for PZN-PT crystals with MPB compositions, as previously reported by Kuwata[14]. It should be noted, however, that electromechanical coupling (k_{ij}) and piezoelectric coefficients (d_{ij}) equal to and larger than MPB crystal compositions were found for domain engineered rhombohedral crystals* as shown in Figure 2. PZN-4. 5%PT and PZN-8%PT crystals were found to possess high k_{33} values of ~92% and 94%, respectively, for (001) crystal cuts. Low values of dielectric loss < 1% should also be noted.

As previously reported and given in table 3 and figure 2, large values of k_{33} are also found in the tetragonal region (PT>10%) and, as reported in table 3, a value of 63% and 62% k_T was detected for the PZN-11%PT and PZN-12%PT, respectively. High thickness coupling may be associated with the large anisotropy of the tetragonal crystals.

The dielectric constant was also found to be dependent on the crystal symmetry. Tetragonal crystals exhibited dielectric constants on the order of less than 1000 being significantly lower than rhombohedral crystals (3000~5000). Lower dielectric constants are also associated with both increased anisotropy and T_c. With similar coupling coefficients, the range of dielectric constants found in the PZN-PT system offer the flexibility in designing transducers with equivalent electrical impedance for a wide range of frequency and geometry. In following sections, transducer simulation using these material properties will be discussed.

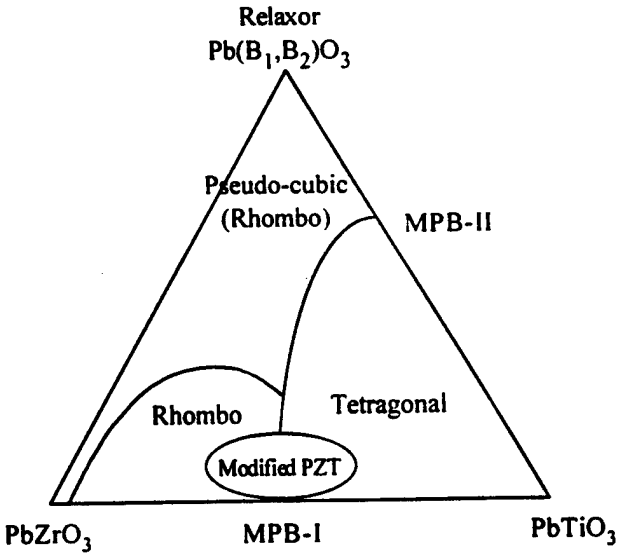

Figure 1 Ternary diagram depicting MPBs in PZT and Relaxor-PT systems for piezoelectric ceramics.

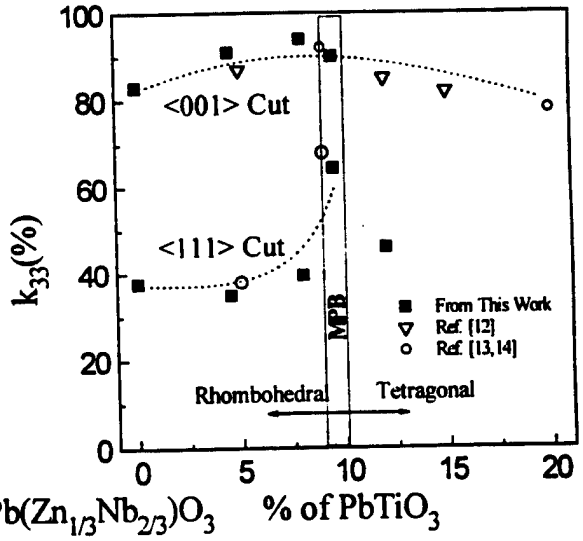

Figure 2 k_{33} as a function of composition and orientation in crystals of PZN-PT.

* Rhombohedral crystals oriented and poled along pseudocubic <001> direction. Crystallographically, polarization direction of rhombohedral crystal is pseudocubic <111> direction.

Table 2 Dielectric and piezoelectric properties of $Pb(A_{1/3}Nb_{2/3})O_3$ - $PbTiO_3$ crystals ($A=Zn^{2+}$, Mg^{2+}) - longitudinal (k_{33}) mode

Composition	T_{max} (°C)	Crystal Structure	Orient.	coupling	s_{33}^E ($10^{-12}m^2/N$)	K_3^T	loss	d_{33} (pC/N)	Nt (Hz m)
PZN	140	Rhom[1]	111	0.38	7.4	900	0.012	83	2058
			001	0.85	48	3600	0.008	1100	1521
PZN-4.5%PT	160	Rhom	111	0.35	9.0	1500	0.004	110	1961
			001	0.92	102	4000	0.004	2000	1344
PZN-8%PT	170	Rhom	111	0.39	7.4	2150	0.012	82	2205
			001	0.94	130	4200	0.012	2200	1401
PZN-9.5%PT	176	MPB[2]	111	0.64	10.4	4300	0.007	600	2240
			001	0.89	77	1600	0.004	1600	1403
PZN-12%PT	200	Tetra[3]	001	0.86		900	0.004	500	1296
PMN-24%PT	150	Rhom	001			3700	0.009	900	1608
PMN-33%PT		Rhom	001	0.94	79	4500	0.012	1700	1866
PMN-35%PT	160	MPB	001	0.92	67	3100	0.014	1240	1730

[1] Rhombohedral structure
[2] morphotrophic phase boundary composition
[3] Tetragonal structure

3. TRANSDUCER DESIGN

3.1 Arrays

Once the ideal polarization axis is defined, one must consider the geometry of the ultrasonic device to be fabricated. An acoustic array uses a different geometry, and thus a different vibrational mode, than a single element transducer or, for that matter, a k_{33} test sample. Consider first an array which consists of many tall, narrow elements. Each element utilizes a partially clamped k_{33} mode of vibration. A true k_{33} mode would be a rod poled through the long axis and driven parallel to the poling direction. The rod is not laterally clamped in any direction. An array element, however, is laterally clamped in the elevation direction. This geometry tends to reduce the coupling coefficient from the ideal k_{33}. The tall, narrow geometry also mandates a small surface area, and thus a low capacitance, which leads to a large electrical impedance and an electrical mismatch to standard 50 Ω transmit and receive electronics. The need to increase the capacitance of each element forces the designer to look for high dielectric constant materials. As discussed in the previous chapter, both a high k_{33} and a large free dielectric constant are found on the rhombohedral side of the MPB. However the large coupling coefficients leads to a low clamped, or high frequency, dielectric constants with respect to soft PZTs. The result of this lower clamped relative permittivity can be seen in the simulated pulse echo response in figure 5. While the <001> family is defined as the poling direction for an array element showing high coupling, it is now left to define a dicing direction along the surface of the crystal

Table 3 Dielectric and piezoelectric properties of $Pb(A_{1/3}Nb_{2/3})O_3$ - $PbTiO_3$ crystals ($A=Zn^{2+}$, Mg^{2+}) - thickness (k_T) mode

Crystal	Cut	Coupling	K_3^T	Loss	Qm	Nt (Hz m)
PZN	001	0.49	2732	0.013	40	2056
PZN-8%PT	001	0.48	4450	0.017	39.5	1831
PZN-9.5%PT	001	0.54	1553	0.024	31.3	1967
PZN-11%PT	001	0.64	890	0.024	16.6	1576
PZN-12%PT*	001	0.62	580	0.001	16.0	1926
PMN-30% PT	001	0.57	4739	0.014	43.7	2368
PMN-35%PT	001	0.54	4540	0.031	35.3	2305

* under bias of 100V (15kV/cm)

which will provide the optimum performance. Given crystal symmetry with the <001> family every 90 degrees, the [100] and [110] (45 degrees from <001>) directions have been investigated, as shown in Figure 3. Dicing parallel to the [100] axis yields three distinct modes, with the thickness or clamped k_{33} mode along the poling axis (at 880 KHz in the test sample of Figure 4) being the dominant mode. The low frequency mode at 228 KHz is the k_{31} mode, with the bar resonating in the length dimension perpendicular to the poling direction. The center mode has been attributed to a flexural length mode. The frequency constants (Nt measured in Hz m) of the present modes are such that it is fairly easy to move undesired modes and harmonics out of the main thickness mode to allow accurate measurement and efficient operation. The drop in k_{33} to what we call k_{bar} (for the clamped k_{33} or 'bar' mode) is minimal, from 94% to 90%. Dicing parallel to the [110] direction yields a more confusing picture. There is not a dominant mode present. The frequency constants of the various modes result in modal overlap in samples cut to approximate array dimensions, bleeding energy between modes and making accurate measurement and efficient operation impossible.

Up to this point we have defined the characteristics needed for an array element: A rhombohedral composition, poled parallel to <001> and diced, parallel to [100], to dimensions defined by the frequency constants to achieve a pure thickness vibrational mode over the final bandwidth of the transducer. It will be seen later that these single crystal materials can yield very wide bandwidth devices, so care must be taken when dimensioning the final transducer to avoid exciting unwanted modes.

3.2 Single elements

Transducer design for an application such as ultrasound backscatter microscopy (UBM) has requirements different than design for arrays. Since impedance of the piezoelectric resonator varies inversely with capacitance as in (1),

$$Z = \frac{1}{j\omega C} \qquad (1)$$

at high frequencies, large area, high frequency, single element transducers suffer from the opposite problem than array elements; low electrical impedance, offers a poor match to the 50Ω driving electronics. As before, a large coupling coefficient is desired to achieve a wide bandwidth. However, these elements operate in a true clamped thickness, or k_t, mode. Rhombohedral crystals, compositions with PT content below the MPB tend to have very efficient k_{33}, but k_t's only comparable to PZT.

Compositions above the MPB have low free dielectric constants characteristic as reported in table 3. In this tetragonal configuration, the crystal is very anisotropic with the polar axis at [001]. Evaluation of PZN-11%PT and PZN-12%PT crystals show $k_t \sim 63\%$ and 62% as reported in table 3, in comparison to PZT Navy Type VI at k_t of only 52%, potentially promising increased performance for single element transducers.

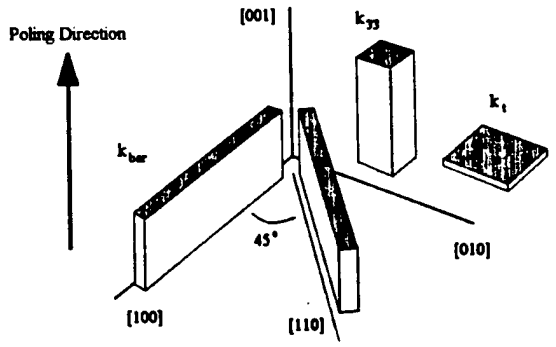

Fig 3. Resonant samples prepared. k_{33} and k_t samples were not aligned in the 1 and 2 directions.

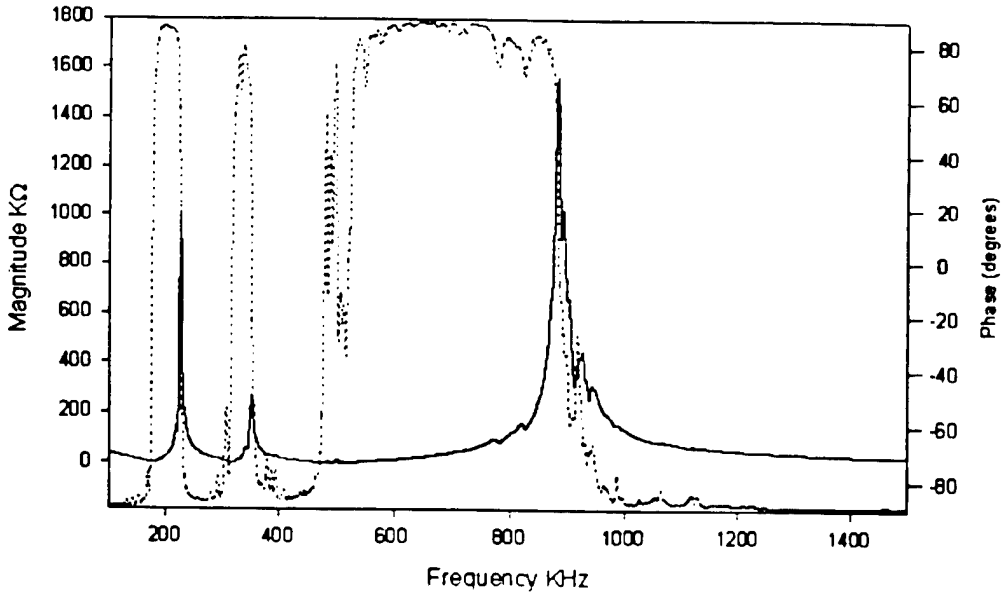

Figure 4 Impedance plot for a <001> poled and [100] aligned PZN-8%PT kbar sample. The low frequency mode is k_{31}.

4. TRANSDUCER SIMULATION

The second step in the design of a transducer is to optimize the required transducer response. For example, a Doppler transducer has different bandwidth requirements than an imaging transducer. Our goal herein is to construct very high resolution imaging transducers. Design was simulated using the KLM model[22] employed via an ABCD parameter approach encoded in MathCad[23].

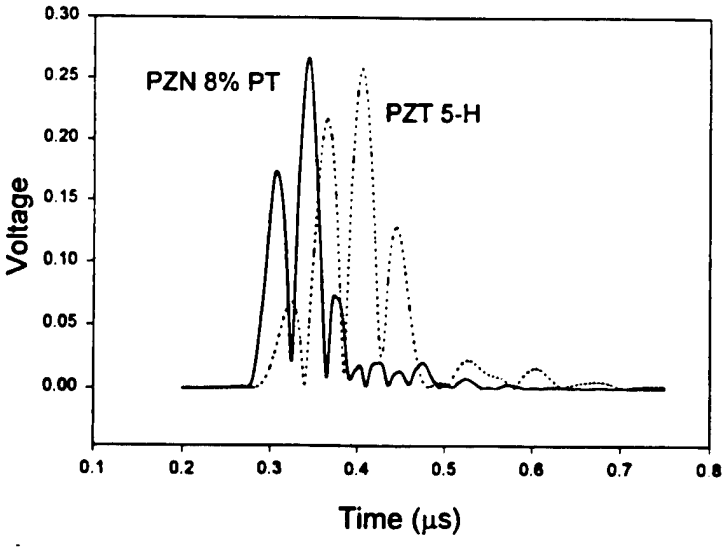

Figure 5 Simulated pulse/echo response of a 124% bandwidth PZN-8% PT array element at 10 MHz compared to 87% bandwidth PZT element of similar design.

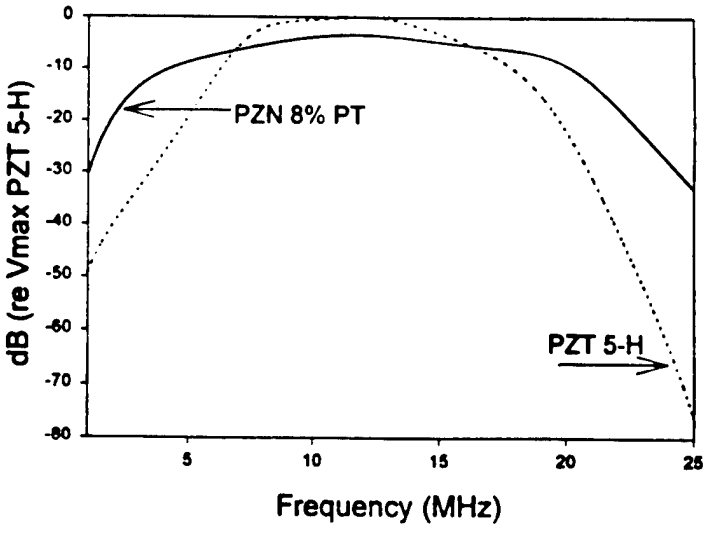

Figure 6 Bandwidth comparison between PZN-8%PT 10 MHz array element vs. PZT-5H.

The pulse/echo waveform in figures 5 simulates a 125% bandwidth array element with a center frequency of 10 MHz. The bandwidth was measured at the -6dB points in the spectrum. Figure 6 shows bandwidth comparison between PZN-8%PT vs. PZT-5H. This simulation predicts results for an array fabricated from PZN 8% PT poled in <001> and diced parallel to [001]. A 10 Mrayl impedance backing was simulated and an idealized 2 layer matching scheme as described by Desilets et al. was used to achieve a maximally flat response[24]. An optimized array design of the same geometry constructed of Navy type VI PZT 5-H displays only a 87% bandwidth.

5. SUMMARY

The single crystal form of Relaxor-PT materials offers the possibility of dramatic improvements in transducer performance. Electromechanical coupling coefficients greater than 94% with non-MPB compositions as well as MPB compositions enables degree of freedom in designing transducers with broad bandwidth and/or improved sensitivity. A range of dielectric constants from ~600 to 5000 in the PZN-PT system offers designers dielectrics for optimum electrical impedance matching.

Transducer simulation was carried out using the KLM model. The pulse/echo response simulated a 124% bandwidth subdiced array element with a center frequency of 10 MHz. An optimized array design of the same geometry constructed of Navy type VI PZT 5-H displays a 87% bandwidth.

Dicing parallel to the (001) yields 90% of laterally clamped coupling (k_{bar}) out of 94% longitudinal coupling (k_{33}). On the other hand, samples diced parallel to (110) exhibited no dominant mode present. Thickness coupling (k_T) as high as 64% and low dielectric constant (K_3^T) < 800 with low loss (<1%) could be achieved using tetragonal crystals of (1-x)PZN-xPT and (1-y)PMN-yPT, where x>0. 1 and y>0. 4.

ACKNOWLEDGMENTS

This research has been supported by Office of Naval Research and Whitaker Center for Ultrasonic Imaging. The authors would like to thank Mike Zipparo for his help with property measurements and Shi-Fang Liu, Hua Lei for their helps with the preparation of samples.

REFERENCES

1. L. E. Cross, "Relaxor Ferroelectrics," *Ferroelectrics*, vol. 76, pp. 241-267, 1987.
2. Seung-Eek Park, Thomas R. Shrout, "Characteristics of Relaxor-Based Piezoelectric Single Crystals for Ultrasonic Transducers," in press *IEEE Trans. on Ultrasonics, Ferroelectric and Frequency Control Special Issue on Ultrasonic Transducers*, 1997.
3. D. A. Berlincourt, C. Cmolik, and H. Jaffe, "Piezoelectric Properties of Polycrystalline Lead Titanate Zirconate Compositions," *Proceedings of the IRE*, vol. 48, pp. 220 -229, 1960.
4. H. Jaffe and D. A. Berlincourt, "Piezoelectric Transducer Materials," *Proceedings of IEEE*, vol. 53 no. 10, pp. 1372-1386, 1965.
5. S. W. Choi, T. R. Shrout, S. J. Jang, and A. S. Bhalla, "Dielectric and Pyroelectric Properties in the $Pb(Mg_{1/3}Nb_{2/3})O_3$ -$PbTiO_3$ system," *Ferroelectrics*, vol. 100, 29-38, 1989.
6. H. Ouchi, K. Nagano, and S. Hayakawa, "Piezoelectric Properties of $Pb(Mg_{1/3}Nb_{2/3})O_3$ -$PbTiO_3$ - $PbZrO_3$ Solid Solution Ceramics," *Journal of American Ceramic Society*, vol. 48, no. 12, pp. 630-635, 1965.
7. J. F. Wang, J. R. Giniewicz, and A. S. Bhalla, "Soft Piezoelectric (1-x)$Pb(Sc_{1/2}Ta_{1/2})O_3$ - x$PbTiO_3$ Ceramics with High Coupling Factors and Low Qm," *Ferroelectric Letters*, vol. 16, pp. 113-118, 1993.
8. Y. Yamashita, "Improved Ferroelectric Properties of Niobium-Doped $Pb[(Sc_{1/2}Nb_{1/2})Ti]O_3$ Ceramics Material," *Japanese Journal of Applied Physics*, vol. 32, pp. 5036-5040, Nov. 1993.
9. Y. Yamashita, "Piezoelectric Properties of Niobium-Doped $[Pb(Sc_{1/2}Nb_{1/2})_{1-x}Ti_x]O_3$ Ceramics Material near the Morphotropic Phase Boundary," *Japanese Journal of Applied Physics*, vol. 33, no. 8, pp. 4562 -4656, August 1994.
10. S. T. Chung, K. Nagata, and H. Igarashi, "Piezoelectric and Dielectric Properties of $Pb(Ni_{1/3}Nb_{2/3})O_3$ -$Pb(Zn_{1/3}Nb_{2/3})O_3$ -$PbTiO_3$," *Ferroelectrics*, vol. 94, pp. 243-247, 1989.

Park 7

11. S. Baumler, "The Dielectric and Piezoelectric Properties of PZN:PT:BT Ceramics," M. S. Thesis, The Pennsylvania State University, 1986.
12. T. R. Shrout, unpublished work.
13. J. Kuwata, K. Uchino, and S. Nomura, "Phase Transitions in the $Pb(Zn_{1/3}Nb_{2/3})O_3$ -$PbTiO_3$ System," *Ferroelectrics*, vol. 37, pp. 579-582, 1981.
14. J. Kuwata, K. Uchino, and S. Nomura, "Dielectric and Piezoelectric Properties of 0.91$Pb(Zn_{1/3}Nb_{2/3})O_3$ -0.09$PbTiO_3$ Single Crystals," *Japanese Journal of Applied Physics*, vol. 21, no. 9, pp. 1298-1302, Sept. 1982.
15. T. R. Shrout, Z. P. Chang, N. Kim, and S. Markgraf, "Dielectric Behavior of Single Crystals near the (1-x)$Pb(Mg_{1/3}Nb_{2/3})O_3$ - (x) $PbTiO_3$ Morphotropic Phase Boundary," *Ferroelectric Letters*, vol. 12, pp. 63-69, 1990.
16. Y. Yamashita and S. Shimanuki, "Synthesis of Lead Scandium Niobate - Lead Titanate Pseudo Binary Single Crystals," Materials Research Bulletin, in press.
17. J. M. Herbert, *Ferroelectric Transducers and Sensors*, London and New York: Gordon and Breach Science Publishers, 1982.
18. T. R. Shrout and J. Fielding, Jr. , "Relaxor Ferroelectric Materials," *in Proceedings of the 1990 IEEE Ultrasonics Symposium*, 1990, pp. 711-715.
19. C. A. Randall, A. S. Bhalla, T. R. Shrout, and L. E. Cross, "Classification and Consequences of Complex Lead Perovskite Ferroelectrics with regard to B-site Cation Order," *Journal of Materials Research*, vol. 5, no. 4, pp. 829-834, 1990.
20. M. L. Mulvihill, S. -E. Park, G. Risch, Z. Li, K. Uchino, T. R. Shrout, "The Role of Processing Variables in the Flux Growth of Lead Zinc Niobate-Lead Titanate Relaxor Ferroelectric Single Crystals," *Japanese Journal of Applied Physics*, vol. 35, no. 7, pp. 51-57, July 1996.
21. S. -E. Park, M. L. Mulvihill, G. Risch, and T. R. Shrout, "The Effect of Growth Condition on Dielectric Properties of $Pb(Zn_{1/3}Nb_{2/3})O_3$ Crystal," *Japanese Journal of Applied Physics*, Pt. 1, vol. 36, no. 3, March 1997.
22. R. Krimholtz, D. A. Leedom, and D. L. Matthaei, "New Equivalent Circuits for Elementary Piezoelectric Transducers," *Electr. Let.* ,vol. 6, pp 398-399, July 1971.
23. M. J. Zipparo, K. K. Shung, T. R. Shrout, "High Frequency Properties of Fine Grain PZT," *Proc. IEEE Ultrasonic Symposium*, vol. 1, pp. 601-604, November, 1995.
24. C. S. Desilets, J. D. Fraser, and G. S. Kino, "The Design of Efficient Broad-Band Piezoelectric Transducers," *IEEE Trans. on Sonics and Ultrasonics.* , vol. 25, no. 3, pp 115-25, May 1978.

APPENDIX 28

$Pb(Zn_{1/3}Nb_{2/3})O_3$ / $PbTiO_3$ Single Crystal Piezoelectrics for Ultrasonic Transducers

Patrick D. Lopath[1], Seung-Eek Park[2], K. Kirk Shung[1] and T.R. Shrout[2]
The Whitaker Center for Medical Ultrasonic Transducer Engineering

[1]Bioengineering Department
[2]Materials Research Laboratory
The Pennsylvania State University
University Park, Pennsylvania 16802

ABSTRACT

The $Pb(Zn_{1/3}Nb_{2/3})O_3$ (PZN) / $PbTiO_3$ (PT) solid solution has been grown in single crystal form. The dielectric and piezoelectric properties have been determined over a wide range of compositions. Longitudinal coupling constants in this system can be maintained at near 90% for a wide range of relative permittivities, allowing a 'designer dielectric' approach to ultrasonic transducer design. The piezoelectric transducer model developed by Kimholtz, Leedom and Matthaei (KLM) was employed to first optimize transducer design points, and then to study the behavior of these materials as operational transducers. Two types of transducers were modeled and contrasted to conventional materials, a 50 MHz single element designed for ultrasound backscatter microscopy and a 5 MHz phased array element. These two transducer designs are representative of the wide range of properties available in this system by carefully choosing a composition. Extremely high piezoelectric coupling coefficients (k_{33} > 94%) and a range of dielectric constants (3000-5000) have been observed in these systems on the rhombohedral side of the morphotropic phase boundary (MPB). Relatively low dielectric constants (~1000) and high thickness mode coupling (kt > 63%) were observed as typical of tetragonal formulations. A prototype single element transducer at 35 MHz was fabricated from PZN / 8% PT and compared, in pulse / echo mode, to a PZT-5H transducer similar design.

Keywords: ultrasonic transducers, single crystals, $Pb(Zn_{1/3}Nb_{2/3})O_3$ / $PbTiO_3$ (PT)

1. INTRODUCTION

Modern ultrasound diagnostics require an ever broadening range of transducer designs to cover the complete spectrum of non or minimally invasive imaging. Current technology spans from the low frequency end between 2.5 and 10 MHz for transthoracic imaging, to around 100 MHz[1] for ultrasound backscatter microscopy. With this broad frequency range comes demands on the transducer engineer to develop materials that will provide optimum properties for a specific application. Currently, many types of piezoelectrics are available for such applications. ranging from polycrystalline ceramics to piezo-polymers. Each material has its advantages as well its drawbacks in terms of the material properties offered to the designers.

In this work, a transducer material system is introduced which will avail many desirable properties over the standard frequency range. The lead zinc niobate / lead titanate, $Pb(Zn_{1/3}Nb_{2/3})O_3$ / $PbTiO_3$ (PZN / PT), single crystal system displays properties which vary both crystallographically and compositionally over the range investigated[2] (from 4% PT to 12% PT). These variations can be exploited to meet the demands of vastly different types of transducers. Single crystal forms offer several other advantages over polycrystalline ceramics; high frequency transducers can be constructed free from the grain size effects which can plague high frequency ceramic transducers and crystallographic orientation can be exploited in dicing of arrays to move undesired modes out of the pass-band.

In order to explore the desirable material properties for various transducer designs, an extensive simulation routine was undertaken utilizing the KLM transmission line model[3]. Material parameters such as the coupling coefficients and clamped relative permittivities were varied over the range available in current single crystalline materials, while transducer responses such as sensitivity and bandwidth were evaluated. Compositional selection within the PZN / PT system was based on the optimum available points derived from these simulations.

Two transducer designs were selected to illustrate the advantages of the PZN / PT system representing the extremes of medical ultrasonic imaging: a 5 MHz phased array and a 50 MHz single element transducer. Typical 5 MHz phased array elements are very small (<100 μ wide), and thus have a low capacitance presenting a large impedance (>150 Ω) to the electronics. The high frequency single element transducers have the opposite problem, presenting a very low impedance (<50 Ω). These problems were addressed in simulation for the 5 MHz phased array case by using PZN / 4.5% PT which has a longitudinal coupling constant (k_{33}) of 92% and a relative clamped dielectric permittivity (ε_r^S) of 775. For the high frequency transducer, PZN / 12% PT was chosen with a 62% thickness mode coupling constant (k_t) and a clamped dielectric permittivity of 128. Both these designs are compared, in pulse echo simulation, to standard polycrystalline ceramics currently used for such designs.

To explore operational transducer designs and fabrication demands, a 35 MHz single element transducer from PZN / 8% PT was constructed. While this choice of material is not necessarily optimum for the type of transducer displayed, material selection was based on current availability, thus the potential pitfalls of single crystal transducer design could be explored. Additional advantages of the single crystalline form in regard to fabrication will be discussed.

2. MATERIAL PROPERTIES SIMULATION

At the heart of an ultrasonic transducer is the piezoelectric material. In the past, much transducer design was done from an acoustic engineering standpoint of applying existing piezoelectric materials to a specific design need, and living with that material's shortcomings. Recently, we have been looking at the problem of ultrasonic transducer design from a materials science standpoint, where, given a particular need, we try to design the piezoelectric material itself to solve the problem. Careful consideration of the material properties needed for a specific application will lead to a more effective transducer. To aid us in our material properties evaluation, we investigated the effect of varying both the coupling constant and the permittivity at differing acoustic impedances. Because k_{33} and ε_{33} are related by the following equation[4],

$$k_{33} = \frac{d_{33}}{\sqrt{s_{33}^E \varepsilon_{33}^T}} \tag{1}$$

our manipulation of these parameters allows $d_{33} / \sqrt{s_{33}^E}$ to float. We chose to vary k_{33} and ε_{33} because these two properties are probably the most commonly quoted with respect to a material suitable to medical transducers, and within the PZN/PT system, k_{33} can be held at elevated levels while ε_{33} is very easily manipulated with composition.

2.1 High frequency transducers

For our simulation of transducer response, we chose the KLM transmission line model T matrix approach implemented in MathCad[5]. Our first objective was to isolate crystal compositions which look promising for future development. Varying the chosen parameters systematically and plotting the results is processor time intensive, however the results from our model have, in the past, been shown to match up very well with experimental transducers[5].

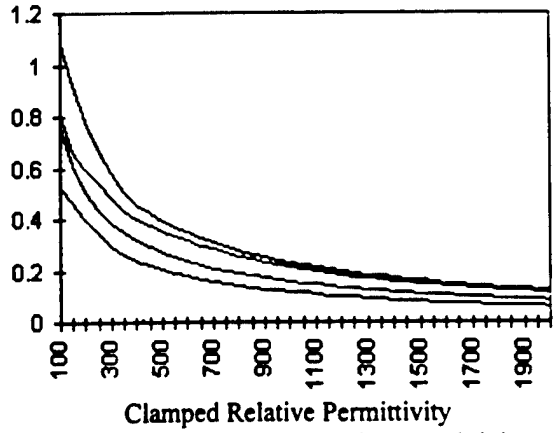

Fig. 1. Transducer sensitivity vs. relative permittivity and coupling constant for a 2 mm diameter 50 MHz transducer.

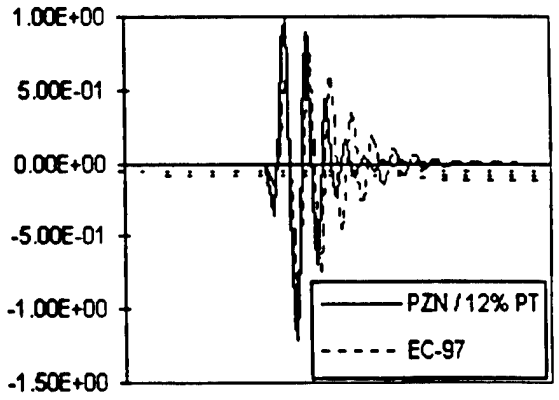

Fig. 2. Pulse / echo response comparison between PZN / 12% PT at 50 MHz and a commercial lead titanate

Figure 1 demonstrates graphically that transducers must be matched to their driving electronics. As the clamped permittivity of the active material is decreased in these high frequency transducers, the received voltage increases for a given excitation. This results from a better match to the 50 Ω driving electronics. Obviously, the sensitivity of the transducer also increases as the k_t increases. We can see the need to choose a material with as high a coupling constant as possible and a low relative permittivity. With conventional ceramics, a low dielectric constant is usually achieved with a lead titanate ceramic. Using measured values for a commercial PT material (EC-97, Edo Corporation. Salt Lake City, UT) and a single crystal of PZN / 12 % PT, the KLM simulation yields the time domain plot in Fig.2. for a set of lightly backed 50 MHz resonators One can immediately see the increased sensitivity and bandwidth due to the higher k_t of the PZN/PT (0.62 vs. 0.47) and the lower relative dielectric constant (128 vs. 200).

2.2. Array transducers

The use of low dielectric constant materials is a must for large area high frequency transducers, but the tiny elements of modern phased array imaging systems require materials with much higher dielectric constants in order to match into the 50 Ω electronics. The example of a 5MHz phased array is illustrative. In order to avoid grating lobes in the steered acoustic pattern of a 5MHz array, the elements of the sampled aperture must be placed no more than λ/2 apart, or 150 μm on center. Now, if this transducer has broad bandwidth (as is the goal), it will have significant energy carried in frequency components above 5MHz, which means that the elements should be placed even closer than 150 μm to avoid grating lobes at these frequencies. Assuming we space the elements 120 μm apart and dice a 20 μm kerf between elements, our array elements are 100 μm wide. Each element may be 5-10 mm long, leaving a very small capacitor, as capacitance varies with the following equation,

$$C = \frac{A\varepsilon_r\varepsilon_o}{t} \tag{2}$$

where C is capacitance, A is the area of the dielectric material, ε_r is the relative permittivity, ε_o is the permittivity of free space, and t is the thickness of the dielectric. Since impedance varies inversely with C, array elements tend to be very high impedance devices to drive with 50 Ω electronics. This problem is currently tackled by the use of high permittivity, soft PZTs such as 5H. The PZN/PT system aids the transducer engineer designing for 50 Ω electronics in two ways. First, the relative clamped dielectric constants are near those of soft PZTs (775 for PZN/4.5% PT vs 1100 for PZT-5H) and second, the extremely high coupling constants combined with a slow longitudinal sound velocity (2790 mm/μm vs. 4520 mm/μs for PZT-5H) mandate that the active material in a transducer be thinner than a material with a lower coupling constant and a higher sound velocity. The thinner material and relatively high clamped dielectric constant correlate to an overall higher capacitance element than PZT.

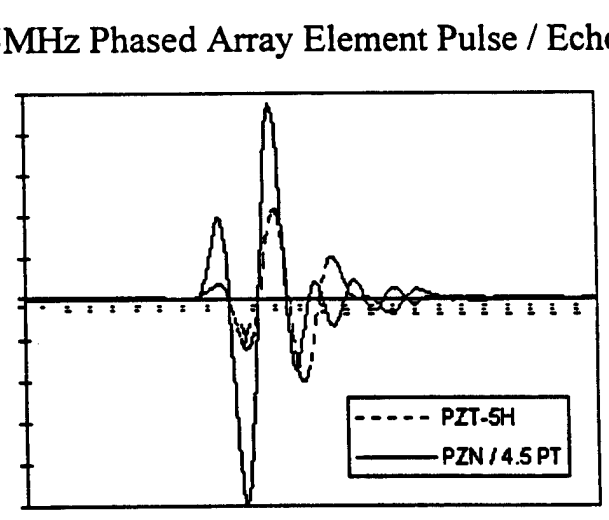

Fig. 3. Pulse / Echo of a 5MHz phased array element. Each element is moderately backed and a two layer maximally flat response matching scheme[6] is simulated. Note not only the increased signal amplitude afford by the PZN 4.5 % PT element, but also its shorter pulse ringdown time which corresponds to better axial resolution.

Figure 3 displays theoretically predicted responses of two different types of elements. The first simulation uses the industry standard PZT-5H parameters and the second uses measured values from PZN 4.5% PT. The increased signal amplitude arises from a number of sources. Most obviously, the bar mode coupling of this composition is approximately 87%, vs. 69% for the PZT 5H. Also, as mentioned earlier, the higher capacitance of the 4.5% PT element leads to an impedance which is less than half of that of the PZT element. Also, the single crystal material has a much lower acoustic impedance than the PZT due to the much slower longitudinal wave velocity. This provides an easier match to the simulated water load via the quarter wave transformers.

3. TRANSDUCER FABRICATION

In our previous work (Lopath, Park et. al)[2] we investigated the mechanical properties of some of these single crystal materials in regard to operational transducers. Most notably, we tediously optimized the poling and dicing procedures necessary to construct operational transducers. It was found that not only does the poling direction play a major role[7] in the measured properties, but, for an array geometry element, the surface dicing orientation with respect to the crystallographic axes can have a significant influence on modal interference. For this work we concentrated on easier to fabricate single element transducers. While the simulation results pointed our high frequency single element endeavors toward the 12% tetragonal crystals, current crystal availability forced us to design and fabricate a 35 MHz element from PZN 8% PT. As is characteristic of the rhomohedral side of the MPB in this system, 8% PT crystals display k_t only comparable to PZT; however the lower relative dielectric constant allows for a fairly well matched transducer at 2 mm in diameter.

Fabrication begins as the crystal is sliced parallel to the (001) plane and then lapped to the desired thickness. The pieces are then sputter coated with gold and backed with conductive epoxy. Following Lookwood et al.[8], the samples are turned at high speed in a lathe to the proper diameter and mounted in a SMA connector for evaluation. Gold is then sputtered onto the front face as a ground electrode and the piece is poled at 20 kV/cm for 10 minutes. Care must be taken to pole the ceramic using the same polarity field as the driving pulser, as the high voltage broadband spike can depole thin transducers if fabricated improperly. As a final step, a quarter wave transform can be applied with a parylene deposition system (Specialty Coating Systems, Indianapolis, In). Some compositions in this system must be poled before they are backed, as the unusually high strain levels (1.5% in the poling field, or orthogonal to it) can be damaging.

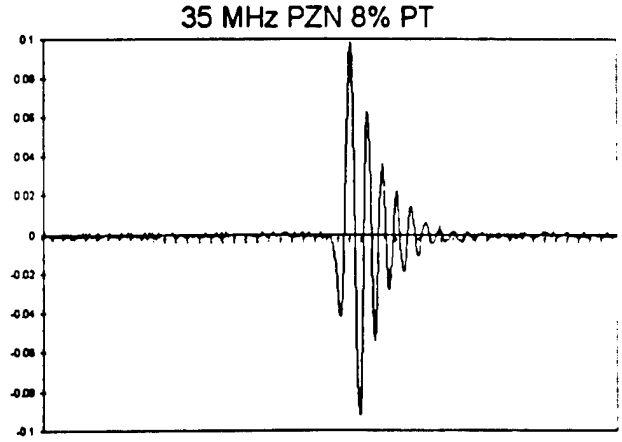

Fig 4. 35 MHz PZN 8% PT transducer pulse / echo response, unmatched into a water load. Target distance 11.7 mm.

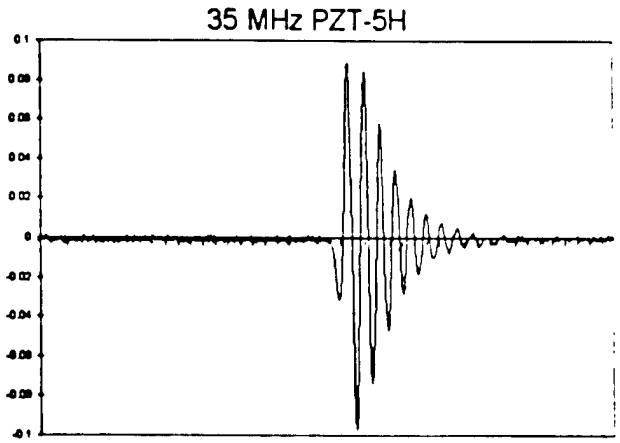

Fig. 5. 35 MHz PZT-5H transducer pulse / echo response, unmatched into a water load. Target distance 11.7 mm.

The pulses above were generated and received by 2 mm diameter single element transducers. On the left (fig. 4), is the pulse / echo from a 57% 6 dB bandwidth PZN 8% PT element operating at 35 MHz. Figure 5 is a comparable PZT-5H single element at 35 MHz. The bandwidth for the PZT is only 32%. Both responses could be improved by the addition of a quarter wave transformer matching layer, which is usually accomplished in our laboratory for high frequency samples by the application of an appropriate thickness paralene layer. The transducers were excited with a broadband pulse from a Panametrics 5900PR.

4. CONCLUSION

We have demonstrated in simulation that the PZN / PT single crystal system offers a wide variety of advantages to the ultrasonic transducer engineer. The variability in the clamped relative permittivity from 775 to 128, over the compositional range from 4.5% to 12% PT allows the fabrication of the entire spectrum of medical ultrasound devices. Other advantages of this family of piezoelectric materials include a lower acoustic impedance than most conventional materials, and, of course, high coupling constants. approaching 95% for some k_{33} samples. In the low frequency regime, the crystallographic direction can be exploited to assist properties of diced arrays while high frequency transducers are aided by a lack of grain size effects. From a fabrication standpoint, these materials have different requirements than ceramic transducers, in fact, transducer fabrication can be more time consuming. However we believe that potential rewards of a device using single crystal transducers may out weigh any difficulties in processing.

ACKNOWLEDGMENTS

This work was supported by the Whitaker Center for Medical Ultrasonic Transducer Engineering and by the Office of Naval Research.

REFERENCES

[1] F. Stuart Foster, et al., "Principles and Applications of Ultrasound Backscatter Microscopy," *IEEE Trans. on Ultrasonic. Ferroelectrics and Frequency Control*, vol. 40, no. 5, pp. 608-616, September, 1993.

[2] P.D.Lopath, Seung-Eek Park, K. K. Shung, T. R. Shrout, "Ultrasonic Transducers Using Single Crystal Perovskites," to be published in *Proc. ISAF*, August, 1996.

[3] R. Krimholtz, D. A. Leedom, and D. L. Matthaei, "New Equivalent Circuits for Elementary Piezoelectric Transducers, *Electr. Let.*,vol. 6, pp 398-399, July 1971.

[4] Bernard Jaffe, William R. Cook, Jr., and Hans Jaffe, Piezoelectric Ceramics, R.A.N. Publishers (1971).

[5] M.J. Zipparo. K. K. Shung, T. R. Shrout, "High Frequency Properties of Fine Grain PZT," *Proc. IEEE Ultrasonic Symposium*, vol. 1, pp. 601-604, November, 1995.

[6] C. S. Desilets, J. D. Fraser, and G. S. Kino, "The Design of Efficient Broad-Band Piezoelectric Transducers," *IEEE Trans. on Sonics and Ultrasonics.*, vol. 25, no. 3, pp 115-25, May 1978.

[7] Seung-Eek Park, Thomas R. Shrout, "Characteristics of Relaxor-Based Piezoelectric Materials for Ultrasonic Transducers," in press *IEEE Trans. on Ultrasonics, Ferroelectric and Frequency Control Special Issue on Ultrasonic Transducers*, 1996.

[8] G.R.Lockwood, D.H. Turnbull, and F.S. Foster, "Fabrication of High-Frequency Spherically Shaped Ceramic Transducers", *IEEE Trans. Ultrason., Ferroelect., Freq. Contr.*, vol. 41, no 2, pp.231-235, March 1994.

[9] Jun Kuwata. Kenji Uchino, and Shoichiro Nomura, "Phase Transitions in the $Pb(Zn_{1/3}Nb_{2/3})O_3$-$PbTiO_3$ System". *Ferroelectrics*, vol. 37, pp. 579-582, 1981.

[10] Jun Kuwata. Kenji Uchino, and Shoichiro Nomura, "Dielectric and Piezoelectric Properties of $0.91Pb(Zn_{1/3}Nb_{2/3})O_3$ - 0.09PbTiO3 Single Crystals," *Japanese Journal of Applied Physics*, vol. 21, no. 9, pp. 1298-1302, September, 1982.

[11] U.S. Patent Number 5402791, "Piezoelectric Single Crystal, Ultrasonic Probe, and Array-Type Ultrasonic Probe" Toshiba. April, 1995.

[12] Shoichiro Nomura, Takashi Takahashi, Yuji Yokomizo, "Ferroelectric Properties in the System $Pb(Zn_{1/3}Nb_{2/3})O_3$-$PbTiO_3$," *J. Phys. Soc. Japan*, vol. 27, pp. 262, 1969.

[13] T. R. Shrout, J. Fielding, "Relaxor Ferroelectric Materials", *Proc. IEEE Ultrasonics Symposium* ,1990.

[14] K. K. Shung, "General Engineering Principles In Diagnostic Ultrasound," *IEEE Eng. Med. Biol. Magazine*, pp 7-13, Dec 1987.

[15] W. A. Smith, "Piezocomposite Materials for Acoustical Imaging Transducers", *Proc. International Symposium on Acoustical Imaging*, 1994.

APPENDIX 29

Single Crystal $Pb(Zn_{1/3}Nb_{2/3})O_3$ / $PbTiO_3$ (PZN/PT) in Medical Ultrasonic Transducers

Patrick D. Lopath[1], Seung-Eek Park[2], K. Kirk Shung[1] and T.R. Shrout[2]

[1]Bioengineering Department, [2]Materials Research Laboratory
The Pennsylvania State University, University Park, Pennsylvania 16802

Abstract- Solid solutions of $Pb(Zn_{1/3}Nb_{2/3})O_3$ (PZN) and $PbTiO_3$ (PT) have been grown in single crystal form to sizes large enough to permit the fabrication of a 5MHz phased array. Transducer construction techniques employed differ from standard ceramic arrays. Crystallographic alignment is found to be a significant contributor to piezoelectric performance. The crystal structure and phase diagram play a major role in processing steps requiring heating such as poling and electroding. A complex composite structure is utilized to allow for efficient operation while maintaining structural integrity. The pulse-echo performance and insertion loss of this array are found to be superior to a similarly constructed PZT 5H array.

I. INTRODUCTION

With the state of the art in the ultrasound systems advancing rapidly with electronic technology there has recently been great interest in the transducer as a source of increased resolution for medical diagnostic imaging. The newly emerging single crystal piezoelectrics offer material properties to the transducer engineer which vastly exceed PZT. Extremely high coupling constants, low acoustic impedances and a wide range of dielectric constants promise to see single crystal solid solutions such as lead zinc niobate/lead titante (PZN/PT) and lead magnesium niobate/lead titanate (PMN/PT) completely replace PZT for most applications within the coming decade. Currently, crystal growth and transducer fabrication issues are limiting the advance of these materials in the ultrasound community.

High piezoelectric activity was reported in single crystal relaxor based materials as early as 1969 by Yonezawa et al. [1], followed by Kuwata et al. [2], and in 1990 by Shrout et al. [3] for a morphotropic phase boundary (MPB) compositions of the PZN/PT and PMN/PT systems respectively. We have previously investigated the use of high PT content tetragonal compositions in the construction of very high frequency single element transducers for ultrasound backscatter microscopy [4]. This current work involves the application of rhombohedral compositions (fig.1), [2], for phased array transducers, taking advantage of a compositionally independent elevated coupling coefficient and a high clamped dielectric constant. The ability of the PZN/PT system to maintain coupling constants over 80% for a wide range of compositionally controlled dielectric constants will allow the introduction of this material to many far reaching medical ultrasonic applications.

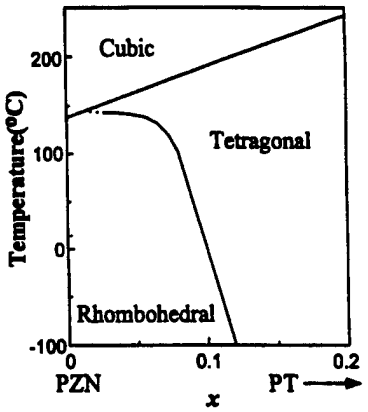

Fig 1. The $(1-x)Pb(Zn_{1/3}Nb_{2/3})O_3$ - $(x)PbTiO_3$ Phase diagram showing the MPB.

II. CRYSTAL STRUCTURE

Transducer applications requiring small array elements demand high dielectric constant rhombohedral crystals with low PT contents, such as the PZN / 8%PT used in this work.

Unlike polycrystalline ceramic materials which display ∞mm symetry after poling, single crystal piezoelectrics demand that the crystallographic

orientation be considered for processes such as poling and dicing. Kuwata et al. found optimal piezoelectric performance is achieved by poling along the <001> direction for MPB compositions of PZN/PT. Park and Shrout showed elevated piezoelectric properties with only slight compositional variance in rhombohedral crystals poled along <001>. Once the polar direction is defined, the surface orientation of a plate to be diced into array elements must be considered, as well as the final aspect ratio of the elements. While complete tensor characterization of the PZN/PT rhombohedral systems remains a goal of single crystal research, we have investigated the effect of a number of aspect ratios along two crystallographic orientations. Test samples along the <001> and <110> were diced to aspect ratios from 1:1 to 2.5:1.

Although the coupling constant in this laterally clamped k_{33} mode (k_{33}') was found to increase only slightly from 85.4 % to 86.4% from aspect ratios of 1.5:1 to 2.5:1, the thickness resonance peaks were more prominent in the high aspect ratio samples. Orientation was found to have a more drastic effect on the observable resonances within a sample. Resonances existed within the <110> test samples which did not correspond to thickness or length extentional modes or associated harmonics [6]. These modes were most likely due to internal domain structures strongly resonant in samples cut parallel to <110>. Samples cut along <001> did exhibit a fairly clean thickness mode with a frequency constant near 1.3 MHz*mm. Non-dimensionally controlled modes of vibration did exist within the <001> oriented samples; however, the thickness mode in these samples was very prominent. For these reasons high aspect ratio, <001> diced elements were chosen for this array.

III. PHASED ARRAY DESIGN

Array Layout

A 5MHz phased array design was chosen to test the feasibility of the PZN/PT system in medical transducers. At 5MHz, greater than 100% bandwidths theoretically achievable with these transducers make it possible to cover the entire medical diagnostic range of traditional clinical ultrasound, from 2.5 MHz to 7.5 MHz, with a single transducer [6]. Other applications include the recent introduction of harmonic imaging. A single broad bandwidth transducer has the potential to transmit a low frequency signal and receive the higher harmonic produced by an introduced contrast agent, permitting B-scan overlay of harmonic imaging data [7].

Phased arrays demand an inter-element spacing of 1/2 of an acoustic wavelength, or less, to prevent the introduction of grating lobes as the beam is steered to the extremes of the imaged sector. At 5MHz in water this corresponds to a pitch of 150μm. It is at this point that the design for a PZT phased array differs from a single crystal array. The sound velocity in PZT permits elements spaced at 150μm to achieve an acceptable aspect ratio with standard kerf dimensions. The slow speed of sound in the PZN / 8%PT (3451 m/sec vs. appox. 4100 m/s for k_{33}' mode PZT) combined with the wide separation between series and parallel resonances brought about by the extremely high electromechanical coupling, demand a k_{33}' mode transducer operating at 5MHz to be approximately 200μm thick. With standard kerfs, the individual elements become almost square in cross section, introducing lateral mode problems confirmed with the 1:1 aspect ratio test samples. The solution to this problem is subdicing. In our design, a 30μm kerf defines the major elements and a 25μm kerf separates the two subelements of each major element. The larger kerf takes advantage of the greater blade exposure available with larger blade. The larger exposure allows kerfs deeper than necessary to be cut into the crystal to accommodate any potential bending of the composite due to polymer fill shrinkage upon curing. A smaller kerf was used in the subdices to maximize the amount of high dielectric material remaining in each element.

Forty eight (48) active elements were diced into the crystal plate. Two additional elements on each end of the array were included; one as a spacer and the outermost one as a ground element.

Future arrays centered at 5MHz may be designed to more effectively take advantage of the bandwidths possible with these materials. A 100% bandwidth 5MHz transducer mandates that the array layout be sufficiently fine to prevent grating lobes at the upper end of the passband (7.5 MHz). The 100μm pitch required at 7.5 MHz will allow high aspect ratio elements without subdicing. The current design is a compromise for ease of interconnection.

Transducer Fabrication

The two kerf sizes were filled with two different polymers. A hard epoxy (Insulcast 502, American Safety Technologies, Roseland, NJ) was used in the subelement kerfs, while a soft urethane (EN-4/EN-7, Conap Inc., Olean, NY) was used in the major kerfs. We have learned that 2-2 composites fabricated from rhombohedral PZN/PT and a hard polymer fill do not display the high coupling characteristic of isolated test samples. We theorize that it is the low stiffness of these crystals which prevents efficient operation when clamped with rigid polymers. The ferroelastic nature of these crystal mandates repoling after stressful processes such as polishing and dicing. We have found that 1-3 composites (a processing intensive structure) composed of PZN / 8% PT and a hard polymer can be repoled to a k_{33} of only 79%. While this is superior than PZT composites with coupling near 70%, it is far from the k_{33} potential of PZN / 8% PT of 95%. 1-3 composites of PZN / 8% PT filled with urethane are able to be repoled to 87%. It is for this reason that we have chosen a soft urethane between the major elements. The soft polymer has the added benefit of more effectively decoupling adjacent elements for phase steering.

Two additional issues were addressed with the inclusion of the hard polymer fill in the subkerfs. The kerf width of 25μm is less than 1/4 of a shear wavelength (λ_s) in the polymer ($\lambda_s/4 \sim 65\mu m$). Under these conditions, the entire major element should operate as one unit [8]. The other advantage of the hard polymer is structural integrity. At only 200μm thick, the entire array would be extremely fragile with only a soft polymer fill.

The procedure for the complex composite construction is that of standard dice and fill applied twice, [9]. The second fill is with the hard polymer leaving a 1 mm border of polymer surrounding the array once it is diced to size. This border provides rigidity and protection during the polishing stages.

Once the composite is polished to thickness with a 5μm finish, electrodes are applied. Here, one must be conscious of the phase diagram of the PZN/PT system (fig. 1). Many electroding processes require heating of the sample. This rhombohedral 8% PT material undergoes a phase change at 100 C. For our array, electroless nickel electrodes were applied at Sound Technology Inc. of State College, PA. This process does not involve heating above the phase change. As it is an immersion technique, the electroding process completely encases the composite in nickel. The polymer border at the elevational ends of the array and each of the individual elements are isolated by scoring on the dicing saw.

Soldering of leads to each of the elements is another potential source of damaging heat. Here, a low temperature reflow solder technique was used. An NTK 68 pin ceramic pin grid array (PGA) was used as a generic interconnect between the ultrasound system and the array. A rectangular hole was cut through the center of the PGA with an ultrasonic mill, and the array, mounted on a piece of wafer handling tape, was placed in the center of the hole, positively poled side down. Leads were attached to the PGA and then individually attached to the 120μm wide elements (fig. 2). With no way to quantify the temperature to which the elements were raised, the minimum temperature and reflow time were used with the pre-tinned 50μm lead wires. Ground connections were made by connecting to the outermost elements, employing the nickel electrode wrapped around from the front of the array. This technique should allow the application of non-conductive matching layers in the future to improve bandwidth and bandshape.

Once all the electrical connections were made, each element was repoled to recover any processing damage to the domain alignment.

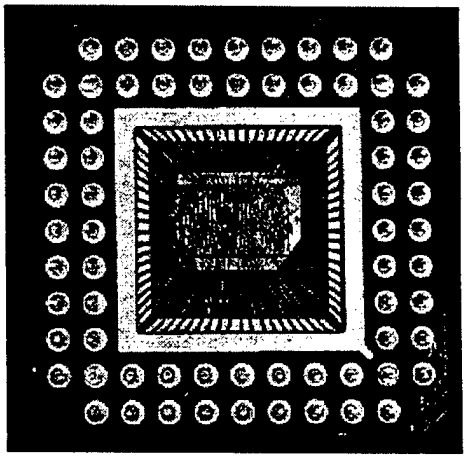

Fig 2. PGA with array connected, before backing.

A 10kV/cm field was put across each element for one minute.

An additional plastic PGA was added behind the ceramic chip carrier to provide room for sufficient backing. A tungsten and alumina loaded polymer (Za = 4.3 Mrayls) was degassed and poured into the back of the array.

IV. RESULTS

The array was designed to allow the use of an Ultramark 9, 48 element phased array scanner (ATL, Inc.) for future imaging tests. Presently, a Panametrics model 5900PR was used to drive individual elements from the single crystal and PZT-5H arrays to assess their pulse-echo responses. A cylindrically focused steel reflector was used to minimize diffraction losses. Figure 3 shows the pulse-echo responses and received spectrums of the two transducers. One potential problem for the single crystal array is the extended low level ringdown which appears to be a spurious composite resonance; however the PZT array, utilizing the same composite structure, does not display this effect. This low level ringing may attributed to the previously observed weak spurious resonances in the <001> test samples interacting with the composite structure. Only future complete tensor characterization of the single crystal and finite element analysis (FEA) of the array will reveal the true nature of the extended ringdown.

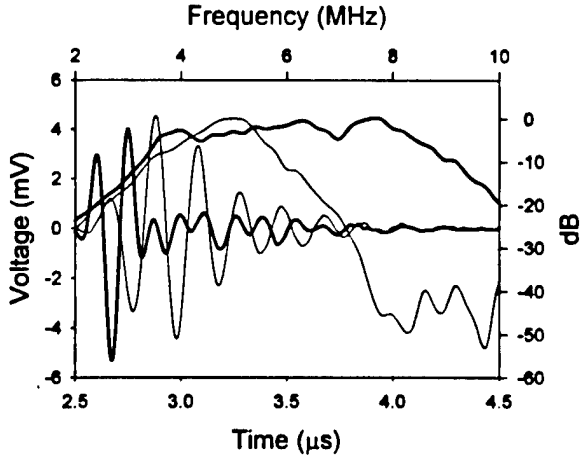

Fig. 3. Measured echo waveforms and spectra for PZN / 8%PT array element (bold) and PZT 5H array element.

The PZN/PT elements operate at a slightly higher center frequency (6MHz) than designed, again possibly a contribution of the spurious modes not allowing complete polarization along the thickness direction. These issues aside, the single crystal elements displayed a significantly broader fractional bandwidth (85%) than the PZT (32%). This bandwidth will improve in arrays which are matched. The insertion loss was measured at 58dB for the PZT array. The single crystal array had an insertion loss of 48dB.

VI. ACKNOWLEDGMENTS

This work was supported by the Whitaker Foundation and the Office of Naval Research. The authors would also like to thank Sound Technology Inc. of State College, PA.

VI. REFERENCES

[1] M. Yonezawa, K. Doi, S. Nanamatsu, N. Tsubouchi, M. Takahashi, and S. Nomura, "The Crystal Stucture and Piezoelectricity of the System Pb(Zn1/3Nb2/3)O3 - PbTiO3", *Journ. of Jap. Soc. on Powder. Metallurgy*, 16, 253, 1969.

[2] Jun Kuwata, Kenji Uchino, and Shoichiro Nomura, "Phase Transitions in the $Pb(Zn_{1/3}Nb_{2/3})O_3$-$PbTiO_3$ System," *Ferroelectrics*, vol. 37, pp. 579-582, 1981.

[3] T. R. Shrout, Z.P. Chang, N. Kim and S. Markgraf, "Dielectric Behavior of single Crystals Near the (1-x)Pb(Mg1/3Nb2/3)O3 (x)PbTiO3 Morphotropic Phase Boundary", *Ferroelectr. Let.*, vol. 12, pp. 63-69, 1990.

[4] P.D.Lopath, Seung-Eek Park, K. K. Shung, T. R. Shrout, "$Pb(Zn_{1/3}Nb_{2/3})O_3$ / $PbTiO_3$ Single Crystal Piezoelectrics for Ultrasonic Transducers, *Proc. SPIE Symp. on Medical Imaging*, vol. 3037, 170, 1997.

[5] S.-E. Park and T. R. Shrout, "Ultrahigh Strain and Piezoelectric Behavior in Relaxor based Ferroelectric Single Crystals" *Journ. of Appl. Phys.*, 82 [4], (1997).

[6] P.D.Lopath, Seung-Eek Park, K. K. Shung, T. R. Shrout, "Ultrasonic Transducers Using Single Crystal Perovskites", *Proc. Intern. Symp. Applicat. Ferroelet.*, pp.543, 1996.

[7] M. Spigelmyer, personal communication.

[8] Oakley, Clyde G., "Analysis and Development of Piezoelectric Composites for Medical Ultrasound Transducer Applications", Ph.D. Thesis, Acoustics Department, The Pennsylvania State University, May 1991.

[9] Savakus, H. P., K. A. Klicker and R. E. Newnham, PZT-Epoxy Piezoelectric Transducers: A Simplified Fabrication Procedure", *Materials Research Bulletin*, vol. 16, pp. 677-680, 1981.

New High Strain Polymer Materials

APPENDIX 30

Effects of Transitional Phenomena on the Electric Field Induced Strain–Electrostrictive Response of a Segmented Polyurethane Elastomer

J. SU,[1] Q. M. ZHANG,[1] C. H. KIM,[1]* R. Y. TING,[2] R. CAPPS[2]

[1] Intercollege Materials Research Laboratory, The Pennsylvania State University, University Park, Pennsylvania 16802

[2] Naval Undersea Warfare Center, USRD, Materials Research Division, Orlando, Florida 32856

Received 25 November 1996; accepted 20 January 1997

ABSTRACT: The electromechanical properties of a segmented polyurethane elastomer were investigated as functions of temperature and frequency. Two transitional phenomena were observed in the temperature range from −50 to 85°C. In these transition regions, the electric field induced strain coefficient exhibits large increases, which indicate that the effect of the transition processes is significant. The experimental analysis suggests that the transitional processes in the polyurethane are related to the chain-segment motions. From the elastic compliance and the dielectric constant data, the contribution of the uniform Maxwell stress was determined. It was found that the contribution of the Maxwell stress effect to the measured strain coefficient increased from about 10% below the glass transition temperature (T_g) (~ −25°C) to about 50 and 35% for the frequencies of 10 and 100 Hz, respectively, at ~ 40°C, which is above T_g. The large difference between the measured strain response and the calculated Maxwell stress effect indicates a significant contribution to the field-induced strain from other mechanisms, such as electrostriction. © 1997 John Wiley & Sons, Inc. J Appl Polym Sci 65: 1363–1370, 1997

Key words: polyurethane elastomer; electric field induced strain; Maxwell stress; electrostriction; transitional phenomena

INTRODUCTION

Electromechanical coupling effects such as piezoelectricity and electrostriction have been widely utilized in transducer, sensor, and actuator technologies.[1,2] During the last three decades, electromechanical polymers, especially piezoelectric poly(vinylidene fluoride) (PVDF) and its copolymers with trifluoroethylene (TrFE), have drawn much attention because of their low acoustic impedance, mechanical flexibility, and good processing properties as well as low manufacturing cost.[3,4] However, their applications have been limited because of the lower electromechanical activity when compared with that of piezoceramic lead zirconate titanate (PZT).[5,6] The recent development in electromechanical properties of polymers showed that some thermoplastic polymer elastomers, especially segmented polyurethane elastomers, can exhibit very high electric field induced strain response. These electromechanically active polyurethane elastomers have drawn more and more attention and many experimental investigations have been conducted[7–9] since the large electric field induced strain of this class of polyurethane elastomers was reported.[10]

Correspondence to: J. Su.

Permanent address: Department of Chemistry, Chongju University, Chongju City, 360-764, Korea.

Contract grant sponsor: Office of Naval Research; contract grant numbers: N00014-95-1-1225 and N00014-96-1-0418.

 CCC 0021-8995/97/071363-08

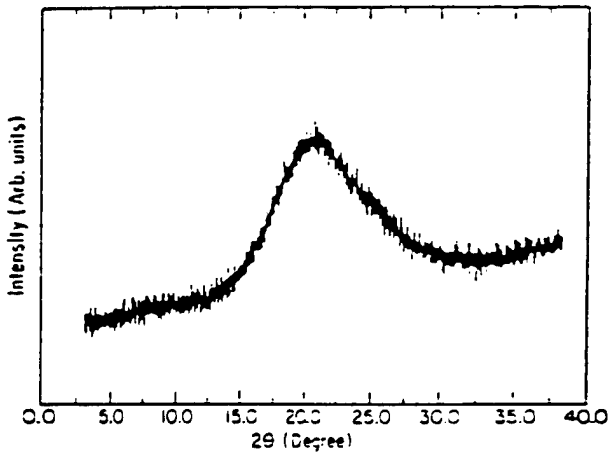

Figure 1 X-ray diffraction data of the polyurethane elastomer at room temperature where the broad halo near 20 degree (2θ) is the reflection of the amorphous phase. No crystalline phase was observed within the data resolution.

The objective of this study is to provide understanding of the possible mechanisms for the observed large electric field induced strain in this class of polyurethane elastomers through investigations of the temperature–frequency dependence of the field induced strain and the dielectric and the elastic properties. In addition, the temperature dependence of the molecular motions in the material were also examined using differential scanning calorimetry (DSC), Fourier transform infrared (FTIR) spectroscopy, and thermal expansion (TE) techniques to elucidate the property–molecular motion relationship.

EXPERIMENTAL

Sample Preparation

The material used in this investigation was produced by Deerfield Urethane, Inc. using a Dow polyurethane (Dow 2103-80AE). The polyurethane is a segmented elastomer consisting of poly(tetramethylene glycol) (PTMEG) as the soft segment and methylenedi-*p*-phenyl diisocyanate (MDI) as the hard segment with 1,4-butanediol (Bdiol) acting as the extender. The molar ratio of the components in the polyurethane is 1.8 mol MDI/0.8 mol. Bdiol/1.0 mol. PTMEG. The samples for experimental measurements were prepared by solution casting followed by vacuumdrying for 24 h. The thickness of the sample in this investigation was 2 mm. The gold electrodes were vacuum-evaporated onto the opposing surfaces of the cast samples.

The result of X-ray diffraction shown in Figure 1, which was obtained by a Philips APD1700 diffractometer, indicates that there is no detectable crystalline phase in the samples investigated within the experimental resolution, or it can be said that the sample is amorphous.

Electric Field-Induced Strain Measurement

A double-beam laser interferometer was employed to measure the strain induced by the applied electrical field at frequencies of 10 and 100 Hz in the temperature range from −30 to 80°C. A detailed description of the technique, including the basic principle, the setup and the sample mounting for the strain measurements was reported with schematic representation in a previous publication.[8]

Dielectric and Elastic Measurements

The temperature–frequency dependence of the dielectric constant of the polyurethane was measured in a temperature-controlled chamber by a lock-in amplifier. The temperature range for the measurement was from −40 to 80°C and the heating rate was 2°C/min. The measurement frequencies were 10 and 100 Hz.[5]

The temperature–frequency dependence of the elastic compliance of the polyurethane was investigated using a Seiko Instruments SDM/5600 dynamic mechanical analyzer (DMTA), from −40 to 80°C with a heating rate of 2°C/min. The measurement frequencies were also 10 and 100 Hz. The sample dimension was 25 mm (length) × 5 mm (width) × 2 mm (thickness).

DSC, FTIR, and TE Measurements

To understand how the observed macroscopic properties are related to the molecular structures, molecular motions, and transitional phenomena, DSC, FTIR spectroscopy, and TE measurements of the polyurethane were examined as functions of temperature. A Perkin–Elmer DSC-7 was employed to obtain the DSC curves and a Digilab Model FTS-45 at a resolution of 2 cm^{-1} was used to acquire the FTIR spectra, for which a minimum of 64 scans were signal-averaged. The film used for FTIR examination was sufficiently thin to be within an absorbance range wherein the Beer–Lambert law is obeyed. The temperature range for DSC and FTIR measurement was from 25 to

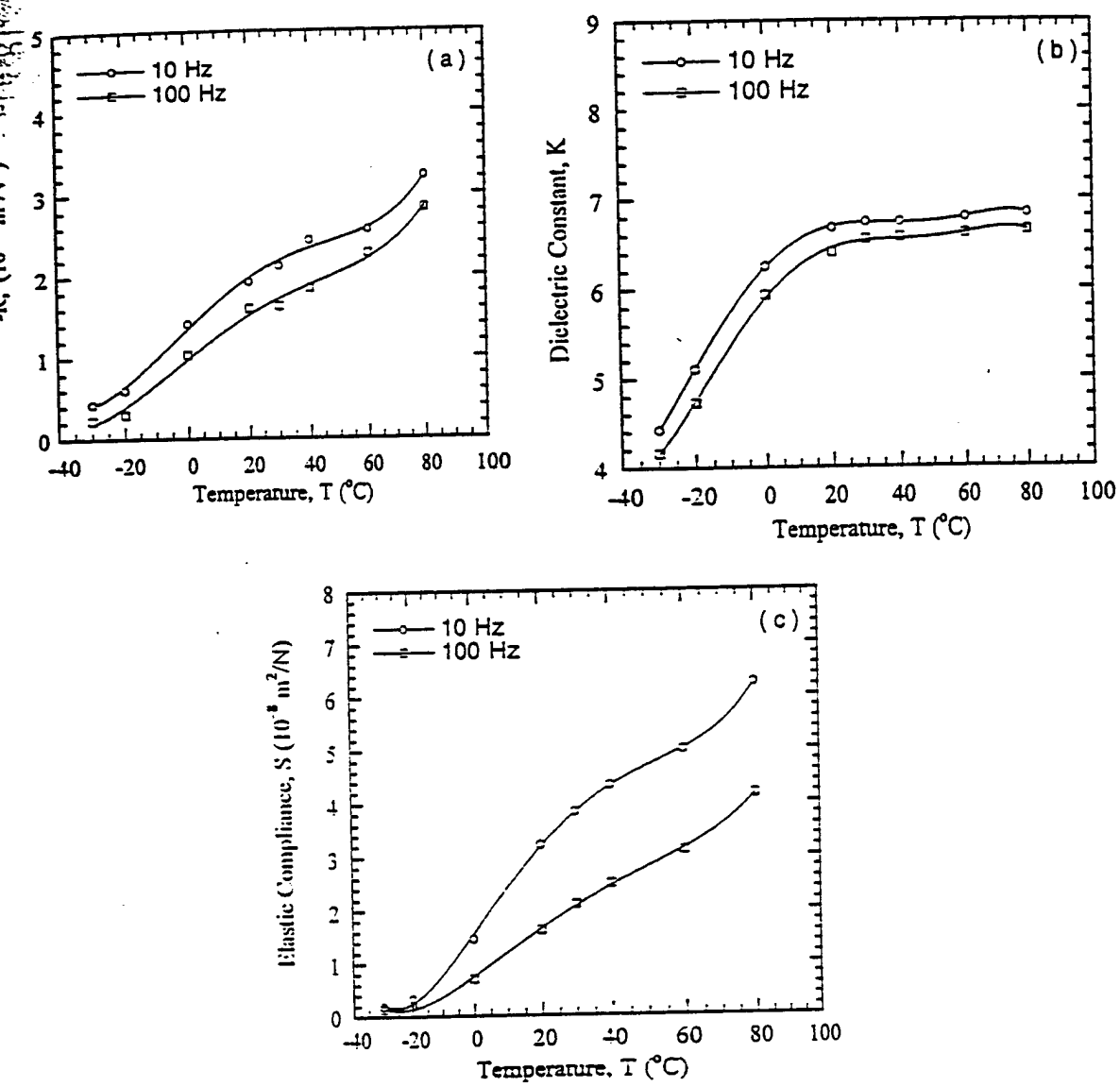

Figure 2 Temperature dependence of (a) the electric field induced strain coefficient, R; (b) the dielectric constant, K; and (c) the elastic compliance, s, of the polyurethane elastomer (Dow 2105-80AE) at 10 Hz and 100 Hz. The solid lines are drawn to guide the eye.

°C and from 25 to 180°C, respectively, whereas or TE the temperature range was from 40 to 00°C. The heating rate was 10°C/min for the SC and TE measurements.

RESULTS AND DISCUSSION

Temperature and Frequency Dependence nd Transitions

The experimental results of the electric field induced strain are presented in Figure 2(a). The strain coefficient, R_{33} ($S_3 = R_{33}E_3^2$, *where* S is the strain, E is the applied electric field, and the subscript 3 represents the direction perpendicular to the sample surface), increases with temperature and decreases with frequency. In the temperature range from −30 to 60°C, two relatively sharp increments are observed: one starts at about −20°C and the other at about 50°C. Similar trends are also observed in the dielectric and elastic data shown in Figure 2(b,c), respectively. The dielectric constant, K, shows a rapid increase at about −20°C but a relatively small change at about 60°C, while the temperature dependence of the elastic compliance shows two rapid increases starting at about −25 and 60°C, respectively. The

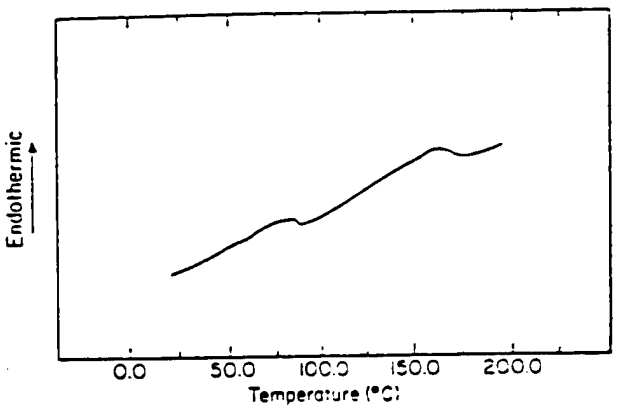

Figure 3 DSC trace of the segmented polyurethane elastomer (Dow 2105-80AE), from 25 to 190°C.

sharp change in the material properties at the lower temperature, observed in these measurements, is related to the glass transition of the polyurethane due to large-scale molecular motions of the soft segments, PTMEG.[11] In order to understand the change at higher temperature transition, DSC, FTIR, and TE investigations, which are employed extensively in studies of structures and molecular motions of segmented polyurethane elastomers,[11-13] were carried out. The DSC curve, shown in Figure 3, exhibits an endothermic peak at about 75°C, starting at about 50°C and ending at about 90°C, which is much higher than the glass transition temperature (T_g) (about −20°C) and much lower than the melting temperature (about 170°C), which is reflected by another endothermic peak starting at about 100°C and ending at about 185°C. From the DSC results, the enthalpy change associated with the transition between 50 and 100°C was calculated by assuming the change is associated with the dissociation of the hydrogen bonding in hard segments since previous publications suggested the endothermic peak might be associated with hydrogen bonding dissociation. However, the value obtained (3.71 kcal/mol) is obviously lower than the previously reported enthalpy change due to hydrogen-bond dissociation in segmented polyurethanes having similar chemical structure.[14] The thermal expansion measurement of the segmented polyurethane elastomer also exhibits a characteristic transitional change in the temperature range between 50 and 100°C. As can be seen in Figure 4, the material exhibits a rapid thermal expansion in the temperature range from about 50°C to about 90°C.

The temperature dependence of the absorbency spectroscopy of the FTIR study on the polyurethane is shown in Figures 5(a–d). The change in the infrared absorption related to the —NH- and —C=O-related hydrogen bonding was investigated at 60, 100, 140, and 180°C. As the temperature is increased from 60 to 100°C, the absorption of bonded —NH (3327 cm^{-1}) associated with the absorption of bonded —C=O (1714 cm^{-1}) shows only a minor decrease. The absorption of unbonded, or free, —NH (3448 cm^{-1}) and the unbonded —C=O (1730 cm^{-1}) shows very little increase in the same temperature range, which indicates that the transitional change observed in the DSC and TE measurements is not associated mainly with the dissociation of the hydrogen bonding in the MDI segments. However, when the temperature is increased from 100 to 140°C, a relatively large change (i.e., a large drop) in the absorption of the H-bonded groups and an increase in the absorption of the unbonded groups can be observed. Further increase of the temperature to 180°C results in a significant dissociation of the hydrogen bonding, which is reflected by the disappearance of the bonded —NH (3327 cm^{-1}) and —C=O (1714 cm^{-1}) absorption peaks, and the large increase of the absorption peak due to the unbonded —NH (3448 cm^{-1}) and —C=O (1730 cm^{-1}). This observation corresponds to the endothermic peak observed in the temperature region from 100 to 180°C in the DSC measurement, which is associated with the hard-segment dissolution (melting) as a consequence of the dissociation of the hydrogen bonding in MDI segments.

The experimental results obtained from the DSC, TE, and FTIR investigations show that the transition between 50 and 100°C, which might be

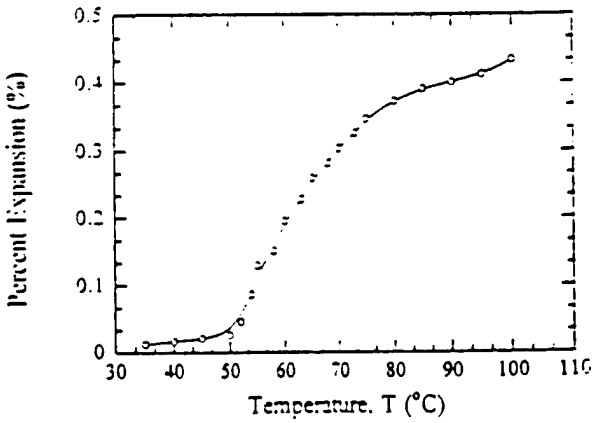

Figure 4 TE measurement of the segmented polyurethane elastomer exhibits a characteristic transitional change in the temperature region from 50 to 100°C.

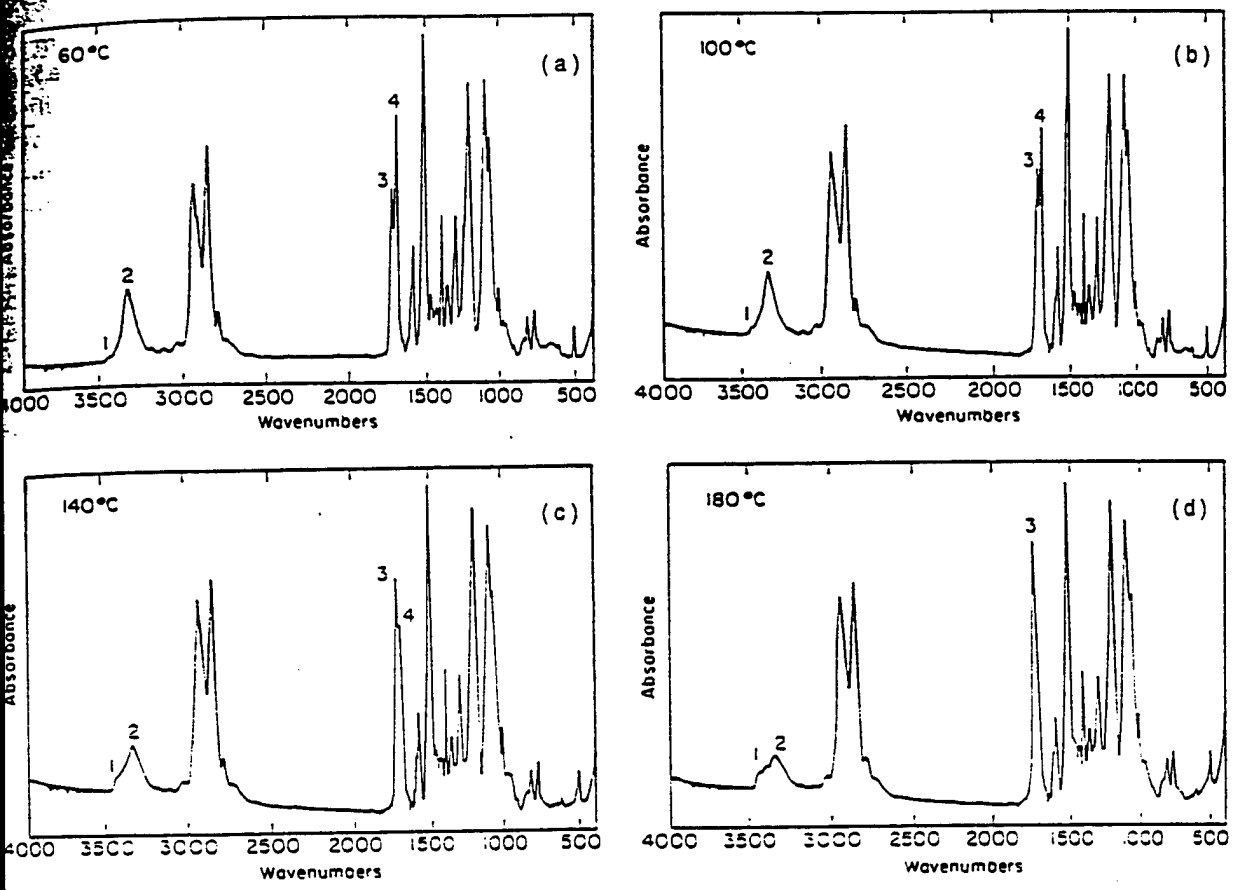

Figure 5 FTIR spectroscopy of the polyurethane elastomer (Dow 2105-80AE) at (a) 60°C, (b) 100°C, (c) 140°C, and (d) 180°C. (Absorbency wave number: 1: 3,448 cm^{-1}; 2: 3,327 cm^{-1}; 3: 1,730 cm^{-1}; and 4: 1,714 cm^{-1}).

the key factor resulting in the increased field-induced strain response of the segmented polyurethane in the temperature region, is neither the glass transition nor the melting if the glass transition reflects the molecular motion of the soft segments and the melting reflects the molecular flow of whole polymer chains when the hydrogen-bond dissociation occurs. The molecular origin of the transition might be related to the molecular motion of the extenders within the hard segments, which might occur without destroying the hydrogen bonding sheet structure,[12] and result in expanding in the direction perpendicular to the hydrogen bonding sheets and increasing free volume. When this happens, it should lead to transitional changes in elastic and thermal expansion properties, as observed in Figures 2(c) and 4, respectively. A similar transition has been observed for similar types of materials and assigned to the glass transition of the amorphous hard-segment domain.[15-17] The asymmetric endothermic peak [i.e., slow increase before the peak position (about 75°C) and rapid decrease after the peak observed in the DSC curve] could be a result of the restraining of the hydrogen bonding in MDI segments to the extender (Bdiol)-related molecular motion. This restraint can limit the molecular motion of extenders between MDI segments, which results in the slow increase. When the temperature is high enough to cause the motion of or dissociation of the hydrogen bonds in the hard segments to a significant level, the limited molecular motion of the extenders can be accelerated, which results in the rapid decrease.

Contributions from the Maxwell Stress Effect and Non-Maxwell Stress Effects

In general, the electric field induced strain in a nonpiezoelectric material can be from the electrostrictive effect and also from the Maxwell stress effects. The electrostrictive effect is a direct coupling between the polarization and mechanical response in the material. It can be expressed as

the strain change induced by a change in the polarization level in the material:

$$S_E = QP^2 \tag{1}$$

where S is the strain, P is the polarization level, and Q is the electrostrictive coefficient of the material. For a linear dielectric, $P = \varepsilon_0(K - 1)E$, so eq. (1) can be rewritten as

$$S_E = Q\varepsilon_0^2(K - 1)^2E^2 \tag{2}$$

where K is the dielectric constant of the material, ε_0 is the vacuum dielectric permittivity, and E is the applied electric field. On the other hand, Maxwell stress, T, which is due to the interaction between the free charges on the electrode (Coulomb interaction), can also contribute to the electric field induced strain response. For the situation considered here, it is also proportional to the square of the applied electric field and can be expressed as

$$T = -\varepsilon_0 K E^2/2 \tag{3}$$

Therefore, the dimensional change due to the Maxwell stress is obtained as

$$S_M = -s\varepsilon_0 K E^2/2 \tag{4}$$

where s is the compliance of the material. As can be seen, the strain induced by the Maxwell stress can be quite substantial for a soft, or high-compliance, material such as the polyurethane elastomer investigated.

From the temperature dependence of the dielectric constant and elastic compliance measurements, the electric field induced strain due to the Maxwell stress effect and the percentage of this contribution to the total strain response were determined, which are shown in Figure 6(a,b), respectively. When the temperature is lower than the T_g, the contribution of the Maxwell stress is relatively small—only about 10%—because the elastic compliance is low. During the glass transition period, which is approximately from −20 to 30°C, the Maxwell stress contribution increases from about 10% to about 35% and 50% for 100 and 10 Hz, respectively, while the elastic compliance, s, increases about one order of magnitude and the dielectric constant, K, increases from 4 to 6.5. From 50 to 80°C, the temperature region for the observed second transition from DSC analysis, increased strain is also observed. Associated with this increase, the elastic compliance shows a corresponding increase while the dielectric constant does not show a significant change.

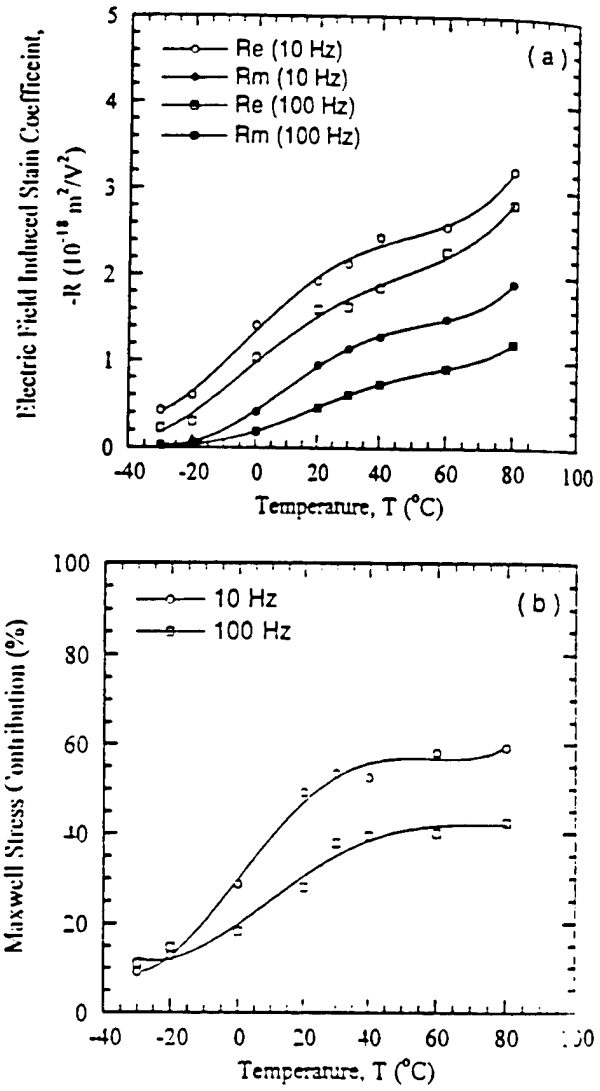

Figure 6 Comparison of the temperature dependence of (a) the total electric field induced strain coefficient, R_t (●, 10 Hz; ■, 100 Hz), and the Maxwell stress-contributed strain coefficient, R_m (○, 10 Hz; □, 100 Hz), and (b) the percentage of Maxwell stress contribution to the total strain coefficient, at 10 and 100 Hz. The solid lines are drawn to guide the eye.

From the discussion above, it can be seen that the Maxwell stress contribution is important for the electric field induced strain, especially when the temperature is higher than the T_g of the polyurethane. On the other hand, the non-Maxwell contribution, which is assumed to be electrostrictive strain, is also very significant. As can be seen in Figure 7(a,b), the non-Maxwell stress part of

the field-induced strain coefficient (represented as $R_e - R_m$, where R_e is the total measured strain coefficient and R_m is the Maxwell stress contribution) shows significant values in the whole temperature region where the measurement was conducted; and when the temperature is lower than the T_g, the electrostrictive contribution dominates (at about 90%). Even though the Maxwell stress contribution is significantly increased when the temperature is raised above 60°C, which is higher than T_g, the electrostrictive strain is still contributing to the total field induced strain of about 40% at 10 Hz and about 60% at 100 Hz.

Temperature and Frequency Dependence of the Electrostrictive Coefficient

The experimental results show that the glass transition plays an important role in the observed large electric field induced strain of the polyurethane investigated. During the transition, both the dielectric and elastic properties show transitional change; therefore the contribution of Maxwell stress effect shows similar characteristics, as discussed. Based on eq. (2), the electrostrictive coefficient Q can be evaluated. The temperature dependence of the coefficient Q at 10 Hz and 100 Hz is presented in Figure 8. As can be seen, when the electrostrictive coefficient Q is examined over the temperature range of the glass transition, it does not show the same temperature dependence as that observed in the Maxwell stress effect, which depends directly on the elastic compliance. However, when the temperature is raised to the second transitional region, the coefficient Q exhibits increase with temperature. Considering the fact that the electromechanical response of a polymer material is contributed by the molecular motions which participate in both the polarization and elastic processes,[3] the increase in the electrostrictive coefficient Q is a result of the increased elasticity per unit polarization change, which can be caused by lowering the energy barrier for the mechanically related segment motion as reflected by the increase in the elastic compliance in this temperature range, where the dielectric constant does not show much change. On the other hand, when the electrostrictive coefficient Q is examined as a function of the frequency, it is observed that Q measured at 100 Hz is about 25% lower than that measured at 10 Hz. The decrease of the Q with frequency indicates that the component of the polarization motions of high frequency (short relaxation time) does not generate

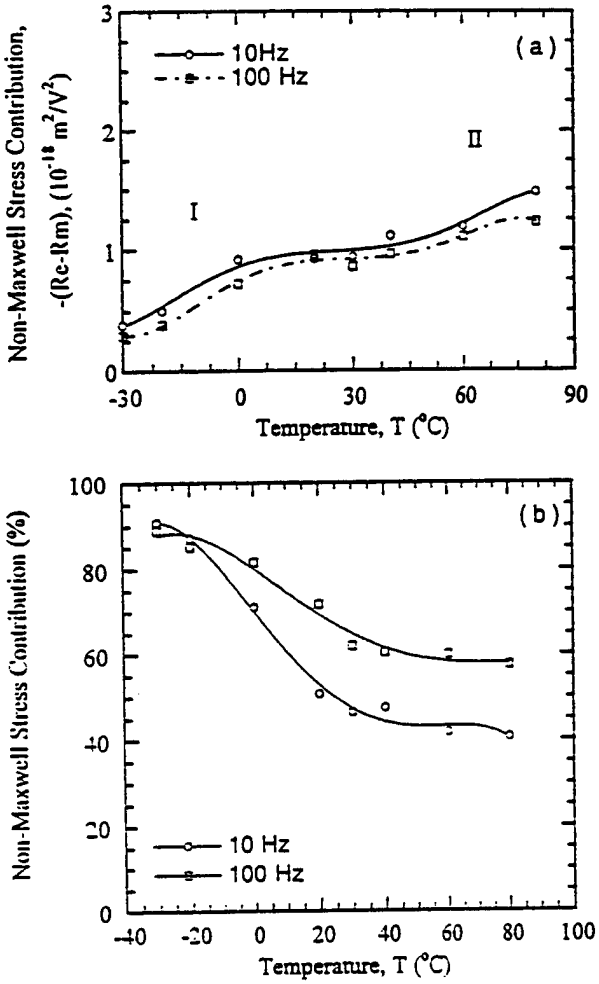

Figure 7 Temperature dependence (a) of non-Maxwell contribution to the electric field induced strain response ($R_e - R_m$) and (b) of the percentage of the non-Maxwell contribution. The solid and dashed lines are drawn to guide the eye.

as much strain in the material and therefore is more like pure dielectric. It should be mentioned that the relatively large data scatter in Figure 8 is due to the fact that the calculated results are obtained from three sets of experimental data (the dielectric constant, the elastic compliance, and the electric field induced strain measurements).

CONCLUSIONS

The temperature and frequency dependence of the electric field induced strain and the dielectric and elastic properties show that both the Maxwell stress effect and electrostriction are important to the electric field induced strain of the polyure-

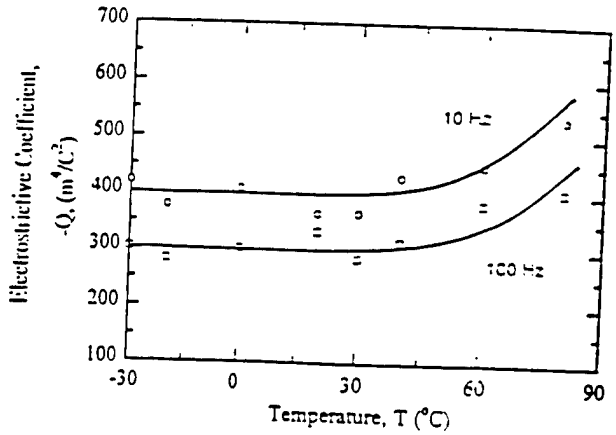

Figure 8 The electrostrictive coefficient Q as a function of temperature at the measurement frequencies of 10 and 100 Hz. The open circles and open squares are data points, and the solid lines are drawn to guide the eye.

thane elastomer investigated. The Maxwell stress contribution increases markedly during the glass transition, along with the sharp increase in the elastic compliance and dielectric constant. In spite of these large changes, the non-Maxwell contribution, such as the electrostrictive coefficient Q, seems to be independent of temperature in the glass transition region. In addition to the glass transition, another transitional change at about 75°C was also observed in the experimental temperature range. The thermal and chemical structural analysis, such as the DSC, TE, and FTIR studies, indicates that the transition might be related to the molecular motion of the extenders in the hard segments. Interestingly, the electrostrictive coefficient Q exhibits an increase with temperature along with the elastic compliance, while there is only a small change in the dielectric constant in the same temperature range. The experimental results show that the two transitional phenomena, which are reflections of the molecular motions of the soft segment and the extender in hard segment, are important for the observed electric field induced strain of the polyurethane elastomer. Even though these transitional phenomena can significantly increase the Maxwell stress contribution, the non-Maxwell stress contribution, such as the electrostrictive coefficient (which seems unchanging with temperature in the glass transition region), is also important for the field-induced strain of the segmented polyurethane elastomer. The different behaviors, observed in the two transitional regions, of the electrostrictive coefficient, the elastic constant, and the dielectric constant suggest that in this class of the material, the chain-segment motions can be grouped into those related to polarization, those related to the elastic process, and those related to both. The change in the relative activation energies related to these motions with temperature results in the different behaviors in the dielectric and elastic properties and the electrostrictive coefficient.

The authors are grateful for stimulating discussions with Professor L. E. Cross. The technical assistance of Drs. M. M. Coleman, M. Sobkowiak, and V. Kugel is greatly appreciated. This work was supported by the Office of Naval Research through Grant Nos. N00014-95-1-1225 and N00014-96-1-0418.

REFERENCES

1. W. G. Cady, *Piezoelectricity*, Dover Publications, Inc., New York, 1964.
2. J. M. Herbert, *Ferroelectric Transducers and Sensors*, Gordon and Breach Science Publishers, New York, 1982.
3. A. J. Lovinger, *Science*, **220**, 1115 (1983).
4. H. R. Gallantree, *IEE Proceedings*, **130**, 219 (1983).
5. H. Wang, Ph.D. thesis, The Pennsylvania State University, 1994.
6. B. Jaffe, W. R. Cook, and H. Jaffe, *Piezoelectric Ceramics*, Academic Press, New York, 1971.
7. H. Wang, Q. M. Zhang, L. E. Cross, R. Ting, C. Coughlin, and K. Rittenmyer, *Proc. Int. Symp. Appl. Ferro.*, **9**, 182 (1994).
8. Q. M. Zhang, J. Su, C. H. Kim, R. Ting, and R. Capps, *J. Appl. Phys.*, to appear.
9. S. Tasaka, T. Shouko, K. Asami, and N. Inagaki, *Jpn. J. Appl. Phys.*, **33**, L1376 (1994).
10. M. Zhenyi, J. I. Scheinbeim, J. W. Lee, and B. A. Newman, *J. Polym. Sci., Part B: Polym. Phys. Ed.*, **32**, 2721 (1994).
11. V. W. Srichatrapimuk and S. L. Cooper, *J. Macromol. Sci., Phys.*, **B15**(2), 267 (1978).
12. N. R. Legge, G. Holden, and H. E. Schreoder, *Thermoplastic Elastomers: A Comprehensive Review*, Hanser Publishers, New York, 1993.
13. W. J. Macknight and M. Yang, *J. Polym. Sci.: Symposium*, **42**, 817 (1973).
14. R. W. Seymour and S. L. Cooper, *Macromolecules*, **6**, 48 (1973).
15. J. T. Koberstein, A. F. Galambos, and L. M. Leung, *Macromolecules*, **25**, 6195 (1992).
16. Y. Li, T. Gao, J. Liu, K. Linliu, C. R. Desper, and B. Chu, *Macromolecules*, **25**, 7365 (1992).
17. A. J. Ryan, C. W. Macosko, and W. Bras, *Macromolecules*, **25**, 6277 (1992).

APPENDIX 31

Space-charge-enhanced electromechanical response in thin-film polyurethane elastomers

J. Su and Q. M. Zhang[a)]
Materials Research Laboratory, The Pennsylvania State University, University Park, Pennsylvania 16802

R. Y. Ting
Naval Undersea Warfare Center, Naval Research Laboratory, Orlando, Florida 32856

(Received 9 April 1997; accepted for publication 20 May 1997)

We show that the large electrical-field-induced strain response observed in certain polyurethane elastomers is a thin-film effect. Based on the frequency dispersion of the strain response in samples with different thicknesses and the thermally stimulated discharge current on samples with different processing conditions, we suggest that the charge injection, an interface effect, which results in a nonuniform space-charge distribution and, hence, a nonuniform electric-field distribution across the sample thickness, is responsible for the enhanced electromechanical response in thin polyurethane samples. © *1997 American Institute of Physics.* [S0003-6951(97)03329-9]

Due to many advantages of polymeric materials, there is a constant effort to develop high performance electroactive polymers for electromechanical applications.[1] Recently, it has been observed that in certain polyurethane elastomers, a large electric-field-induced strain can be achieved with a moderate external field, hence, in the electric-field biased state, the material exhibits a large effective piezoelectric response, comparable to that in lead zirconate titanate piezoceramics.[2] This makes the material very attractive for a wide range of electromechanical applications. In earlier publications, we have shown that both the electrostriction and Maxwell stress effect (Coulomb force) contribute to the electromechanical response in the material.[3,4]

It was found recently, however, that the electric-field-induced strain response of the material exhibits a marked dependence on the sample thickness. As shown in Fig. 1(a), with a fixed field, the strain S_3, which is measured in the direction parallel to the applied electric-field E, of a 0.1 mm thin film is much higher than that in a 2 mm thick sample although the strain-field relationship in both samples follows $S_3 = RE^2$, where R is the strain coefficient. Data presented in Fig. 1(b) summarize this thickness dependence behavior. Since the elastic compliance of the polymer is much higher than that of the gold electrode, the electrodes impose mechanical clamping on the polymer and reduce the measured strain response, especially in thin-film samples.[5] In Fig. 1(b), the data for the corrected strain response, which takes the electrode clamping effect into consideration, are also shown. Apparently, the high strain sensitivity of the material reported is a thin-film effect, and in thick samples the strain sensitivity of the material is not very high. In addition, the frequency dispersion of a 0.1 mm film is also much stronger than that from a 2 mm thick sample, as presented in Fig. 2.

All the samples used in this investigation were made by the solution casting method from Dow 2103-80AE polyurethane. The electrodes were sputtered gold film of 300 Å thick. The strain measurement was made with a high sensitivity bimorph cantilever based dilatometer specially designed for characterizing the strain response in soft and thin polymer films.[6]

In searching for possible mechanisms for the large strain response in thin polyurethane films, we note that the dielectric constant and elastic compliance of the material do not show much change with thickness, and their frequency dispersions are also much weaker than the strain dispersion from a 0.1 mm thick film.[3] The observed thickness and frequency dependence of the strain response, hence, indicate the existence of other factors contributing to the high strain sensitivity in thin films and it is likely to be related to the electrode–polymer interface effects. In insulating polymers,

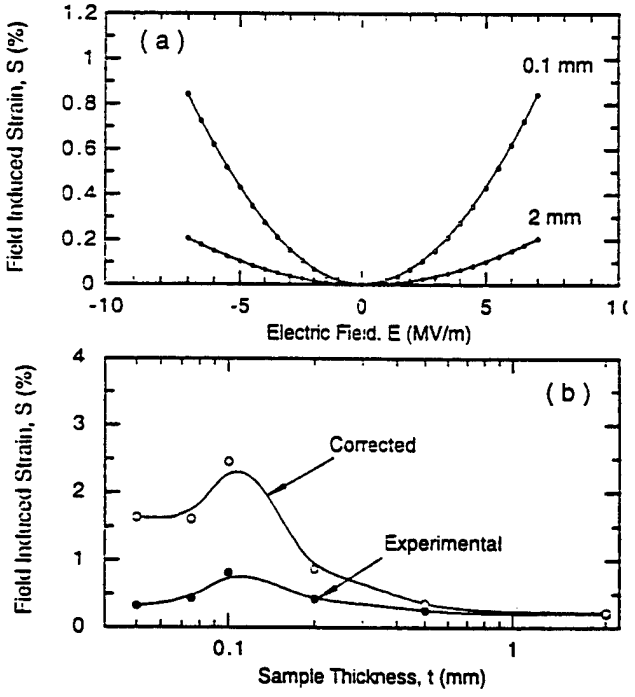

FIG. 1. (a) Comparison of the strain response, measured at 2 Hz, from a 0.1 mm thick and 2 mm polyurethane samples (Dow 2103-80AE). (b) The thickness dependence of the strain response in polyurethane elastomers (measured at 2 Hz). The black dots are the measured data and the open circles are those after the correction for the gold electrode mechanical clamping effect. Solid lines are drawn to guide the eyes.

a)Corresponding author. Electronic mail: Qxz1@psu.edu

 0003-6951/97/71(3)/386/3/$10.00

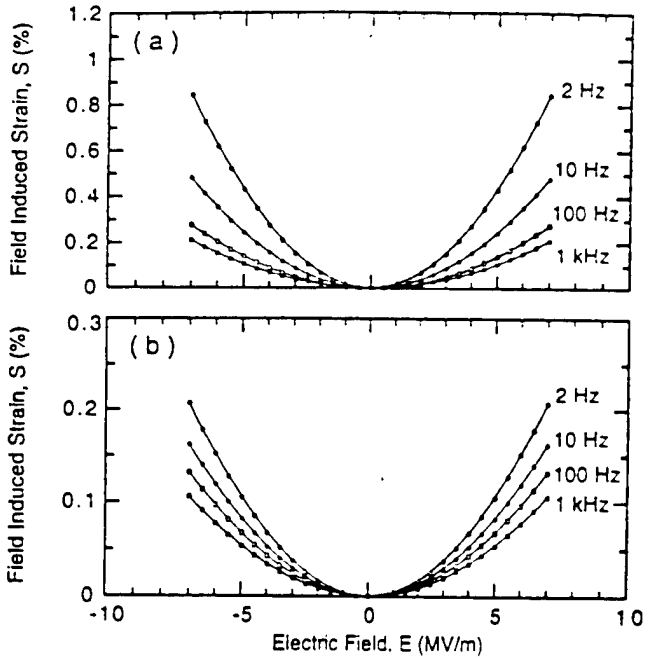

FIG. 2. Frequency dispersion of the strain response of (a) a 0.1 mm thick sample, and (b) a 2 mm thick sample, respectively. The frequency dispersion of the 2 mm thick sample is much smaller than that of the 0.1 mm thick sample.

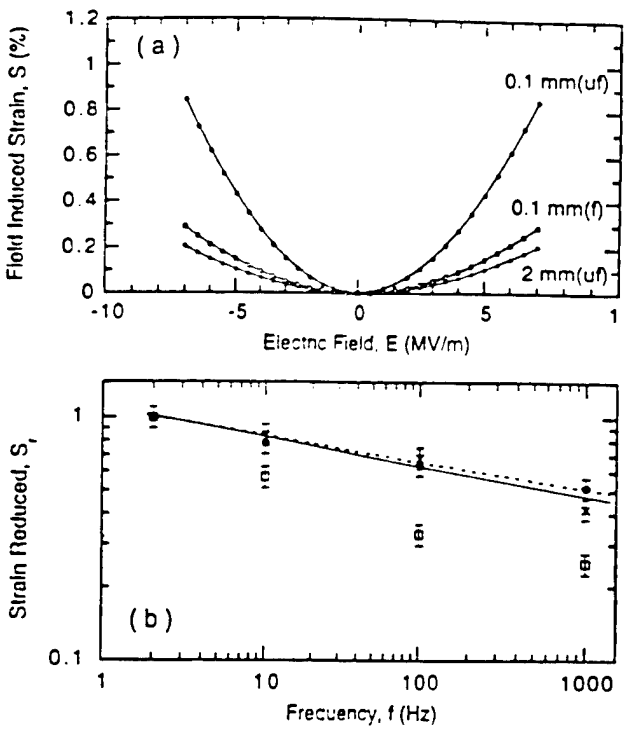

FIG. 3. (a) Comparison of the strain response of an unfiltered sample (uf) 0.1 mm thick, a filtered sample 0.1 mm thick (f), and a sample 2 mm thick. For the 2 mm thick sample, there is very little difference in the strain responses between the filtered and unfiltered samples. (b) Comparison of the frequency dispersion of the unfiltered sample 0.1 mm thick (open squares), the filtered sample 0.1 mm thick (crosses), and the 2 mm thick sample (black dots). The solid lines are drawn to guide the eyes.

one of the most commonly observed interface effects is the charge injection under external fields.[7,8] These charges can be from electrons and holes injected from the electrodes and/or impurity ions in the samples, and can be trapped in the interface and interphase regions, as well as other defect sites, resulting in a nonuniform space-charge distribution, which usually has a strong thickness and frequency dependence.

In order to investigate this possibility, samples were made from filtered solution (using a Fisher-P5 filter) in an attempt to remove some of the impurities from the original material. As shown in Fig. 3(a), there is a significant reduction in the strain response in the filtered films, where the data were from films of 0.1 mm thickness. In thick samples there is not much difference in the strain response in filtered and nonfiltered samples. Correspondingly, the thickness dependence of the strain response in the filtered samples is significantly reduced. Accompanying the strain reduction, the frequency dispersion of the stain response in filtered samples of 0.1 mm thickness also becomes nearly the same as that of a 2 mm thick sample, as illustrated in Fig. 3(b).

The thermally stimulated discharge current (TSDC) method, a technique widely used to characterize the charge injection in polymeric materials, was employed to study the charge injection in these samples.[9] In this method, a sample was subjected a high dc electric field ($E=4$ MV/m) at a high temperature (here, at 80 °C) for 5 min, and then cooled down under the field to a low temperature (here, at −70 °C). TSDC data were collected for both nonfiltered and filtered films where the samples were heated at 4 °C/min without external bias field.

As presented in Fig. 4, for the nonfiltered sample, there are four significant peaks in the temperature range measured. By comparison with the dielectric constant data, it can be identified that peak 1 (at −35 °C) and peak 3 (at 45 °C) are related to the glass transition of the soft segments and "glass transition" in the hard segments, respectively.[3,4] Both peaks are followed by a discharge peak, i.e., peak 2 (near 10 °C) and peak 4 (near 70 °C).[10,11] In analogy to other polymer systems, these discharge peaks can be identified as related to the nonuniformly distributed space charges in the soft segment region and the hard segment region, respectively. Hence, TSDC data confirm the existence of the nonuniform space-charge formation due to charge injection.

When the curve of the filtered film is examined, it is clear that there are marked changes in the TSDC data between the nonfiltered and filtered samples. Although the peak

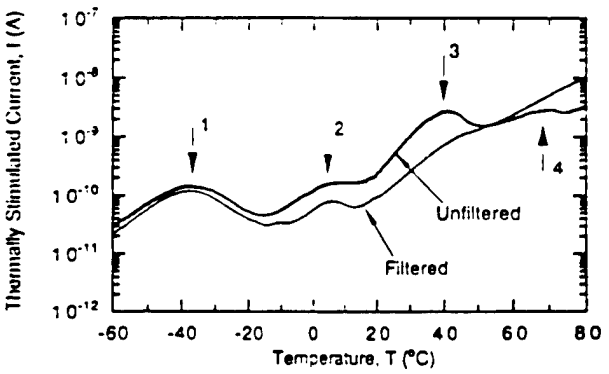

FIG. 4. Thermally stimulated current data for both unfiltered and filtered samples. The thickness of the samples is 0.1 mm and the area is about 1.2 cm^2.

related to the glass transition of the soft segments does not show much change, the peak area underneath peak 2 is reduced by about half, indicating a reduction of the trapped space charges in the filtered sample in the interface region. In addition, peak 3 is significantly reduced while the following discharging peak becomes barely visible. These results imply that the contributors, which can trap the space charges to form a nonuniform space-charge distribution in the sample, have been significantly reduced by filtering.[12,13] Since the mesoscopic morphology of a polyurethane elastomer consists of hard segments embedded in a soft segment matrix, the interfaces between the soft segment and hard segment will act as space-charge trapping sites. The change in the hard segments as revealed by the change in peak 3 due to the filtering will likely change the energy levels at these trap sites and, hence, the trap modulated space-charge mobility and charge injection process.[11,14,15]

Based on these results, we suggest that the enhanced strain response in thin polyurethane films is a consequence of the change injection, which results in a nonuniform space-charge distribution across the thickness direction. From the Poisson's equation, it can be deduced that such a charge distribution will produce a nonuniform local electric field across the thickness direction, especially in the electrode–polymer interface.[12] Hence, the effect is not significant in thick samples. For the polymer studied here, the electric-field-induced strain locally $S(x)$ is proportional to the square of the local field $E(x)$ and, hence, the total strain response S of the sample is equal to

$$S=\frac{1}{t}\int_0^t S(x)dx=\frac{R}{t}\int_0^t E^2(x)dx,$$

where we have assumed the strain coefficient R is nearly a constant in the sample, and t is the sample thickness. It can be shown that for a fixed applied voltage $V=\int_0^t E(x)dx$, $\int_0^t E^2(x)dx>(\int_0^t E(x)dx)^2/t$. That is, any nonuniform field distribution across the thickness direction will enhance the strain response if the coupling between the strain and the electric field is through a square relationship, such as the electrostriction and Maxwell stress effect. In fact, such an enhancement mechanism can also be generalized to other effects, such as the Kerr electro-optical effect, to improve the sensitivity. In this scenario, in thick samples, the local electric field is not very different from the average field and there is no enhancement effect due to the interface space charge. As the film thickness is reduced, the local field becomes much higher than the average field, resulting in an enhanced electromechanical response. In even thinner films, where the two interface regions near the two electrodes start to overlap, which reduces the nonuniform charge distribution, this enhancement effect is reduced, as shown in Fig. 1.

The authors appreciate the financial support of this work from the Office of Naval Research through Grant Nos. N00014-96-1-0418 and N00014-95-1-1225.

[1] *Ferroelectric Polymer*, edited by H. S. Nalwa (Marcel Dekker, New York, 1994).
[2] M. Zhenyi, J. I. Scheinbeim, J. W. Lee, and B. A. Newman, J. Polym. Sci. Part B: Polym. Phys. 32, 2721 (1994).
[3] Q. M. Zhang, J. Su, C. H. Kim, and R. Ting, J. Appl. Phys. 81, 2770 (1997).
[4] J. Su, Q. M. Zhang, C. H. Kim, and R. Ting, J. Appl. Polym. Sci. (to be published).
[5] H. Wang, Q. M. Zhang, L. E. Cross, and A. O. Sykes, Ferroelectrics 150, 255 (1993).
[6] J. Su, P. Moses, and Q. M. Zhang, Rev. Sci. Instrum. (submitted).
[7] *Electrets*, edited by G. M. Sessler, Topics in Applied Physics, Vol. 33 (Springer-Verlag, Berlin, 1980), Chap. 2.
[8] W. Suzuoki, H. Muto, T. Mizutami, and M. Ieda, J. Phys. D 18, 2293 (1985).
[9] J. van Turnhout, *Thermally Stimulated Discharge of Polymer Electrets* (Elsevier Science, Amsterdam, 1975).
[10] E. J. Kim and Y. Ohki, IEEE Trans. Dielectr. Electr. Insul. 2, 74 (1995).
[11] A. Thielen, E. Hendrick, J. Niezette, J. Vanderschueren, and G. Feyder, J. Appl. Phys. 75, 4069 (1994).
[12] K. S. Suh, D. Damon, and J. Tanaka, IEEE Trans. Dielectr. Electr. Insul. 2, 1 (1995).
[13] Y. Li, T. Takada, H. Miyata, and T. Niwa, J. Appl. Phys. 74, 2725 (1993).
[14] M. M. Perlman and A. Kumar, J. Appl. Phys. 72, 5265 (1992).
[15] A. Hirao, H. Nishizawa, and M. Sugiuchi, J. Appl. Phys. 74, 1083 (1993).

Shape-Changing Crystals Get Shiftier

talented family of materials has gained me even more gifted members. So-called iezoelectric crystals have the unique ability o swell or shrink when zapped with electricy, as well as give off a jolt of juice themlves when compressed or pulled apart. Enineers have exploited this trait for decades convert mechanical energy to electricity nd back again in applications ranging from honograph needles to telephone speakers.

Now, a pair of researchers from Pennsylvaa State University has bred new piezoelectric underkinds, some of which display an effect 0 times greater than that of current family embers. A paper by the researchers, materials ientists Thomas Shrout and Seung-Eek Park, scheduled to appear this spring in the inaugul issue of the journal *Materials Research Innotions*, but early word of the new work is aldy turning a few heads. "It's an exciting eakthrough," says Eric Cross, another piezoectric materials expert at Penn State, who is ot affiliated with the project. "Improvements a factor of 10 are not easy to come by in a ld that's 50 years old and considered mature."

The materials are commercialed, as Cross and others believe ey will be, they could usher in new generation of piezoelectric vices that would improve evthing from the resolution of rasound machines to the range sonar listening devices.

Piezoelectric materials owe eir abilities largely to the asymtrical arrangement of positely and negatively charged oms in their crystal structure. The positive and negative charges balance out in each of the crystal's unit cells—its basic repeating units—but the positive charges, for instance, may be weighted toward the top of each cell. An electric field can displace the charges even farther, which distorts the overall shape of the unit cell and of the crystal as a whole. The process can also run in reverse: Squeezing or stretching the material shifts the charges relative to each other, redistributing electric charge around the surface of the crystal, which can produce a small electric current.

The usual showcase for these properties is a cheap ceramic material called PZT, containing millions of crystalline grains in different orientations. PZT, which is composed primarily of lead, zirconium, titanium, and oxygen, can deform by as much as 0.17% in a strong applied field. To boost this shape-shifting ability, researchers have tried to grow single crystals of PZT, in which all the unit cells would line up in the same direction. Their contributions to the piezoelectric effect would also line up, enhancing it. But because PZT's components tend to separate during processing, the ceramic is extremely difficult to grow as a single crystal, says Shrout.

To coax the material into forming single crystals, Shrout and Park tried varying its composition. They settled on a couple of different mixtures, such as a combination of lead, zinc, and niobium spiked with varying amounts of lead-titanate (PT). The researchers found that a small admixture of PT—less than 9%—yielded materials that not only grew into single crystals, but also ended up with piezoelectric abilities that are enhanced more than they expected.

Just why that is, "we still don't know for sure," says Shrout. But he and Park believe that at least part of the enhancement is due to the fact that an electric field applied to the new materials does more than just shift a few atoms around in the unit cell, as in PZT: "We think it causes the whole crystalline lattice structure to change from one form to another," says Shrout. The changed crystal structure, in turn, frees individual atoms to respond more strongly to the field, increasing the overall distortion of the material. Likewise, a mechanical distortion probably produces a similar lattice shift, enabling the material to generate more current than standard PZT.

Whatever the reason for the effect, it's likely to be very useful, says Robert Newnham, another piezoelectricity expert at Penn State. The new crystals will undoubtedly cost more than ceramics like PZT, says Park, because growing single crystals is a slow and painstaking process. But he adds that he and Shrout are working on ways to speed it up. If they succeed, the new piezoelectric wunderkinds could grow up to live expansive lives indeed.

–Robert F. Service

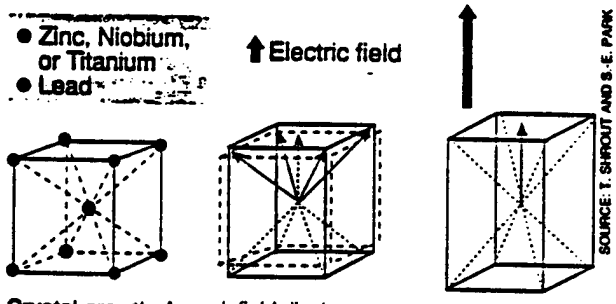

Crystal growth. A weak field displaces atoms toward the corners of the unit cells, but a stronger field rearranges the lattice.